UNIVERSITY OF Southampton

University of Southampton Research Repository
ePrints Soton

Copyright © and Moral Rights for this thesis are retained by the author and/or other copyright owners. A copy can be downloaded for personal non-commercial research or study, without prior permission or charge. This thesis cannot be reproduced or quoted extensively from without first obtaining permission in writing from the copyright holder/s. The content must not be changed in any way or sold commercially in any format or medium without the formal permission of the copyright holders.

When referring to this work, full bibliographic details including the author, title, awarding institution and date of the thesis must be given e.g.

AUTHOR (year of submission) "Full thesis title", University of Southampton, name of the University School or Department, PhD Thesis, pagination

http://eprints.soton.ac.uk

UNIVERSITY OF SOUTHAMPTON

FACULTY OF ENGINEERING, SCIENCE AND MATHEMATICS

Institute of Sound and Vibration Research

Analysis of Very Low Frequency Oscillations in Electromagnetic Brain Signal Recordings

by

Charmaine Demanuele

Thesis for the degree of Doctor of Philosophy

March 2010

Abstract

Spontaneous very low frequency oscillations (<0.5 Hz), previously regarded as *physiological noise*, have of late been increasingly analysed in neuroimaging studies. These slow oscillations, which occur within widely distributed neuroanatomical systems and are unrelated to cardiac and respiratory events, are thought to arise from variations in metabolic demands in the resting brain. However, they also persist during active goal-directed processing, where they predict inter-trial variability in evoked responses and may present a potential source of attention deficit during task performance. This work presents a series of new approaches for investigating: (i) the slow waves in electromagnetic (EM) brain signal recordings, (ii) their contribution in brain function, and (iii) the changes that the slow wave mechanisms undergo during cognitive processing versus resting states. State-of-the-art blind source separation methodologies, including single-channel and space-time independent component analysis (SC-ICA and ST-ICA), are employed for denoising and dimensionality reduction of multi-channel EM data, and to extract neurophysiologically meaningful brain sources from the recordings. Particularly, magnetoencephalographic (MEG) data of attention-deficit/hyperactivity disorder (ADHD) and control children, and electroencephalographic (EEG) data recorded from healthy adult controls, are analysed. The key analytical challenges and techniques available for the analysis of the slow waves in EM brain signal recordings are discussed, and specific solutions proposed.

Core results demonstrate that the inter-trial variability in the amplitude and latency of the event-related fields sensory component, the M100 (in MEG), exhibits a slow wave pattern, which is indicative of the intrinsic slow waves modulating underlying brain processes. In a separate study, phase synchronisation in the slow wave band was observed between fronto-central, central and parietal brain regions, and the level of synchrony varied between rest and task conditions, and as a function of ADHD. Furthermore, a new EEG experimental framework and a multistage signal processing methodology have been designed and implemented in order to investigate brain activity during task performance in contrast with that during rest. Here, the brain has been envisaged as an oscillatory system onto which a graded load was imposed to yield a variable output response – the P300. Specifically, results show that the amplitude and phase of the brain sources in the slow wave band share essential similarities during rest and task conditions, but are distinct enough to be classified separately. This is in keeping with the view that the intrinsic slow waves are continuously influencing active brain sources and they are in turn affected by external stimulation. These slow wave variations are also significantly correlated with the level of cognitive attention

assessed by performance measures (such as reaction time and error rates). Moreover, the power of the sources in the slow wave band is attenuated during task, and the level of attenuation drops as the task difficulty level is increased, whilst their phase undergoes a change in structure (measured through entropy).

These new methodologies, developed for gaining insight into the neurophysiological role of the slow waves, could be used for assessing changes in the brain electrical oscillators as a function of various psychiatric and/or neurobehavioural disorders such as ADHD. This could ultimately lead towards a more scientific (and accurate) approach for the prognosis and diagnosis of these disorders.

Declaration of Authorship

I, Charmaine Demanuele, declare that this thesis entitled ANALYSIS OF VERY LOW FREQUENCY OSCILLATIONS IN ELECTROMAGNETIC BRAIN SIGNAL RECORDINGS and the work presented in it are my own, and have been generated by me as a result of my own original research.

I confirm that:

1. This work was done wholly while in candidature for a research degree at this University;
2. Where I have consulted the published work of others, this is always clearly attributed;
3. Where I have quoted from the work of others, the source is always given. With the exception of such quotations, this thesis is entirely my own work;
4. I have acknowledged all main sources of help;
5. Where the thesis is based on work done by myself jointly with others, I have made clear exactly what was done by others and what I have contributed myself;
6. Parts of this work have been published in peer-reviewed papers as listed in Chapter 1.

……

Charmaine Demanuele

…….

Date

Acknowledgements

It is a great pleasure to express my gratitude to all those who have made this thesis possible. First of all, thanks to my sponsors: the Lord Rayleigh Scholarship from the ISVR and funding from the School of Psychology at the University of Southampton, which supported my research and living expenses. Next, my main supervisor, Prof Christopher James – it is so hard not to be inspired by his amazing dedication towards this work. His methodical way of looking at every problem we've encountered along the way, his constant support and optimism, and his genuine care for the person behind the PhD have been crucial for me throughout these three and a half years. I am also very grateful to his wife Antoinette for being my other mum in England. Many thanks to my secondary supervisor, Prof Edmund Sonuga-Barke, whose input has always been very constructive and encouraging. Thanks to Prof Paul While for providing invaluable insight into the work, and to Dr Samantha Broyd for her help in the design and setting-up of the experiments. Here, I also wish to acknowledge my colleagues from the ISVR and the School of Psychology who eagerly volunteered to take part in my experiments, let me wire them up, followed strict instructions on performing the tasks, and left the lab with kilograms of abrasive gel stuck into their hair – all in the name of science – and friendship of course! Particularly, Aída Jiménez-González, Dr Disha Gupta, Dr Norma Castañeda-Villa and Dr Suogang Wang have been fantastic colleagues from the very start; our discussions on ICA and related algorithms have been very beneficial to my work. Thanks also to my Maths students for giving me the opportunity to revise Maths with them, and for being ever so inquisitive.

Einstein once said: "*Most people say that it is the intellect which makes a great scientist. They are wrong: it is character.*" And I think this is very true (though the '*great*' bit is of course subjective) – that is why I feel very lucky to be enriched with so many friends and relatives, who all in their own way leave their mark on whatever I accomplish. My most sincere thanks to my wonderful parents, Raymond and Emma, my sister Antoinette and my brother Joseph for their unfailing belief they have in me, which I find comforting … and at times a bit amusing too.

My immense gratitude to my partner Toby for his love and patience, but most of all for his terrific sense of humour which added fun to all aspects of my research. Our endless (and timeless) discussions (and quarrels) about *scientific* concepts brightly coloured every bit of problem solving throughout this research.

Finally, I dedicate this work to the loving memory of my *Nannu Nenu*, the most beautiful person I know. His life will forever be my source of joy and inspiration – his determination to carry out whatever he set out to do; his eagerness to learn and to share his knowledge with us; his inquisitive, brave yet humble nature; his amazing love for every form of life; his incessant dedication, kindness and altruism, have moulded my way of working, my way of living. In the words of W. H. Auden:

"*He was my North, my South, my East and West,*
My working week and my Sunday rest,
My noon, my midnight, my talk, my song;"

… All that I am, I owe to him.

Contents

Acronyms

ADHD	Attention-Deficit/Hyperactivity Disorder
AR	Autoregressive
BASC	Behaviour Assessment Scale for Children
BCI	Brain Computer Interfacing
BOLD	Blood Oxygenation Level Dependent
BSMSS	Barratt Simplified Measure of Social Status
BSS	Blind Source Separation
CT	Computerized X-ray Tomography
DC	Direct Current
DMI	Default Mode Interference
DMN	Default Mode Network
DSM	Diagnostic and Statistical Manual of Mental Disorders
EEG	Electroencephalography
E-ICA	Ensemble Independent Component Analysis
EM	Electromagnetic
EMD	Empirical Mode Decomposition
ER	Event Related
ERF	Event Related Fields
ERP	Event Related Potentials
EOG	Electroculogram
FIR	Finite Impulse Response
FFT	Fast Fourier Transform
fMRI	functional Magnetic Resonance Imaging
GMM	Gaussian Mixture Models
HC	Hierarchical Clustering
HOS	Higher Order Statistics
IC	Independent Component
ICA	Independent Component Analysis
ID	Itakura-Saito Distance
IIR	Infinite Impulse Response
ISO	Infraslow Oscillations

MA	Moving Average
MEG	Magnetoencephalography
MICA	Multi-dimensional Independent Component Analysis
MRI	Magnetic Resonance Imaging
PCA	Principal Component Analysis
PET	Positron Emission Tomography
PLS	Phase Locking Statistics
PLV	Phase Locking Value
PRS	Parent Rating Scales
PS	Phase Synchrony
PSD	Power Spectral Density
RBF	Radial Basis Function
RMS	Root Mean Square
RT	Reaction Time
SART	Sustained Attention to Response Task
SC-ICA	Single Channel Independent Component Analysis
SDH	Structured Developmental History
SES	Socio-Economic Status
SPECT	Single Photon Emission Computed Tomography
ST-ICA	Space Time Independent Component Analysis
STFT	Short Time Fourier Transform
SNR	Signal to Noise Ratio
SRP	Self-Report of Personality
SVD	Singular Value Decomposition
TDSEP	Temporal Decorrelation Source Separation
TRS	Teacher Rating Scales
VLF	Very Low Frequency
VLFO	Very Low Frequency Oscillations
WT	Wavelet Transform

List of Figures

List of Tables

Chapter 1

INTRODUCTION

1.1. Project Aim

"Men ought to know that from the human brain and from the brain only, arise our pleasures, joys, laughter and jests, as well as our sorrows, pain, griefs and fears. Through it, in particular, we think, see, hear and distinguish the ugly from the beautiful, the bad from the good, the pleasant from the unpleasant.'

Hippocrates (460-370 BCE), the "Father of Medicine" in his book "The Sacred Disease".

This amazing living organ that is the brain comprises billions of neurons in constant communication, which elaborate into a surpassingly complex structure at the centre of our nervous system. Humans have tried to gain insight into its anatomy and performance, with the earliest record of brain function dating back as far as 4000 BC (Bear *et al.*, 2001). Although the road to discovery of how the human brain generates the vast range of functions that determine our lives and shape our ever-vibrant world, is long and intricate, it is nonetheless achievable, since as the Nobel Prize winner for Medicine (1981), Prof. Dr. David H. Hubel, affirmed:

"The brain is a tissue. It is a complicated, intricately woven tissue, like nothing else we know of in the universe, but it is composed of cells, as any tissue is. They are, to be sure, highly specialized cells, but they function according to the laws that govern any other cells. Their electrical and chemical signals can be detected, recorded and interpreted and their chemicals can be identified; the connections that constitute the brain's woven felt-work can be mapped. In short, the brain can be studied, just as the kidney can."

Such propositions have driven researchers from a wide range of disciplines – philosophers and physicians, physiologist and psychologist, physicists, engineers and mathematicians – to explore ways of enhancing our understanding of how cognition and behaviour emerge from this human central processing unit. The last century has seen a vast body of systems, techniques and

methodologies developed by biomedical engineers, medical physicists, signal processors and computer scientists to provide windows into the human brain. Neuroimaging systems yield detailed spatial mappings of the brain for the prognosis, diagnosis, and treatment of numerous neurological and psychiatric pathologies (Al-Chalabi *et al*., 2006). Electrophysiology then provides a direct, non-invasive neuronal probe that captures the electrical activity of the neurons during perception, action and thought (Fisch, 1999). The human electroencephalogram (EEG), first recorded by Hans Berger in 1929, reveals oscillations of varying frequencies, each having different spatial distributions and associated with different neural states such as waking and sleep. These oscillations, which represent the synchronized activity of thousands of neurons, interact to form a number of dynamic, functional networks which vary according to the absence or presence of stimulation (Buzsáki and Draguhn, 2004; Fox *et al*., 2005). For instance, functional magnetic resonance imaging (fMRI) studies show that the brain remains active in an organised manner during periods of 'apparent' rest (when no cognitive task is being performed) and displays (amongst others) a neuro-anatomically robust default network of activity (Fox *et al*., 2005).

Recently, it has been suggested that the brain oscillators span frequency bands from as low as 0.025 and up to 600 Hz (Buzsáki and Draguhn, 2004). Of particular interest are spontaneous neuronal very low frequency oscillations (VLFO, <0.5 Hz) a.k.a. slow waves, previously regarded as *physiological noise* (Vanhatalo *et al*., 2005). These VLFOs, which appear to be intrinsically generated by the brain and occur within widely distributed neuroanatomical systems, have been consistently reported and analysed in fMRI blood oxygenation level dependent (BOLD) imaging studies. They are more prominent in the resting brain and may be used to promote synchronisation between diverse neuronal networks. When they persist into task sessions, they are thought to contribute to inter-trial variability in evoked responses and behaviour (Fox *et al*., 2006; Fox and Raichle, 2007), and may present a potential source of interference during task performance leading to periodic lapses in attention (Sonuga-Barke and Castellanos, 2007). These VLFOs have also been observed in electrophysiological signal recordings linked with specific pathologies such as epileptic seizures, and in sleep studies (Vanhatalo *et al*., 2004:2005).

EEG and magnetoencephalographic (MEG) data (the latter captures the magnetic fields generated by the electrical activity of the neurons) are obtained from an inherently noisy recording process and typically contain a mixture of physiological (for example, ocular and muscular) and ambient artifacts, along with active brain sources. For this reason, blind source separation (BSS) techniques are often employed to efficiently isolate neurophysiologically

meaningful sources from the recorded signals (James and Hesse, 2005). Independent component analysis (ICA) is one BSS technique that has been extensively used in the literature for decomposing the signals into a number of statistically independent components (ICs) with a *distinct spatial* profile. Single channel ICA (SC-ICA) is a variant of ICA which can be applied to extract underlying processes from a single recording sensor by using *only* temporal information inherent in the signal dynamics. Expansion of this technique has led to the development of Space-time ICA (ST-ICA), whereby SC-ICA is applied to a number of recording channels, hence providing *both* temporal and spatial information to inform the standard ICA algorithm. This presents a specific form of BSS that exploits the rich, dynamical time structure of EEG/MEG data as well as the multi-channel (spatial) nature of the recordings (James, 2008).

The main aim of this work has been to investigate the slow wave mechanisms and their functional contribution in the human brain through the analysis of electromagnetic (EM) signal recordings. First, the use of the aforementioned BSS techniques was explored for investigating slow waves in MEG data recorded from control children and from children with attention-deficit/hyperactivity disorder (ADHD), where the involvement of VLFOs in the periodic attention lapses experienced by individuals suffering from this neurobehavioural disorder has been implicated (Sonuga-Barke and Castellanos, 2007). Second, an experimental framework was designed to test the functional significance of the slow waves, in contrast to other brain oscillators, namely delta ($0.5<f<4$ Hz), theta ($4<f<8$ Hz) and alpha ($8<f<12$ Hz), during various experimental conditions. EEG data was collected from healthy adult controls and a BSS methodology, coupled with a neural network feature extraction and classification method, was developed in order to assess variations in the slow wave characteristics during periods of quiet wakefulness (termed as "rest"), and during the performance of visual tasks of various difficulty levels. This thesis is organised as follows.

1.2. Thesis Organisation

A review of the literature surrounding the aim of this thesis is presented in Chapters 2 and 3. The psychological and physiological background for this work; the notion of differing brain networks activation patterns during default mode, i.e. when the brain is apparently at rest, and during cognitive tasks is described in Chapter 2. In addition, the putative role of the slow waves in brain function as understood from the literature to date is discussed. Chapter 3 then focuses on the key analytical challenges in analysing VLF brain activity in EM brain signal recordings, and gives an account of the signal processing techniques available for the extraction of spatial, temporal and spectral information from the data. The brain recording systems are discussed in Chapter 4, with

special emphasis on the mechanisms of EEG and MEG. Chapter 5 then provides a detailed description of the ICA techniques used, particularly SC-ICA and ST-ICA; these techniques are applied to epileptic seizure data as an illustration and for better understanding of this recently-introduced source analysis framework, whereby data decomposition is undertaken through the use of temporal/spatio-temporal information.

Chapter 6 gives an account of the methodologies employed for the analysis of VLFOs in EM brain signals. This chapter is divided into two sections:

(i) It has been acknowledged that the frequency spectrum of measured EM brain signals shows a decrease in power with increasing frequency (Buzsáki and Draguhn, 2004). This spectral behaviour may lead to difficulty in distinguishing task- or condition-related peaks from ongoing brain activity in the EEG and MEG signals spectra. In this work a simple method that can be used to compensate for this $1/f^{\gamma}$ $(0<\gamma\leq 2)$ trend is proposed in order to achieve spectral normalisation (as this can become an issue in the analysis of VLFOs).

(ii) The methodologies employed and the results obtained from two separate studies on MEG recordings of children with ADHD and controls during selective attention and perception tasks are described. These include:

a. *Low frequency phase synchronisation analysis using SC-ICA.*
In this section, a preliminary investigation on the level of connectivity in the brain during task segments separated by resting periods is presented. SC-ICA is used to isolate low frequency brain activity within the data in the presence of higher frequency activity and artifacts. Phase synchrony analysis, which is a vital mechanism for assessing the functional connectivity of neuronal networks (Lachaux *et al*., 1999), is then carried out between the underlying sources extracted from selected channels of interest in order to quantify any interaction between distant brain regions in the slow wave band.

b. *Trial-to-trial Variability in Evoked Neural Responses.*
As explained earlier, fMRI BOLD imaging studies have shown that when VLFOs persist into task sessions they can predict trial-to-trial variability in both evoked behaviour and brain responses by providing a baseline onto which deterministic responses elicited by the task are superimposed (Fox *et al*., 2006). Moreover, evidence in the literature tentatively suggests that this VLF activity may not be present in the data as distinct, independent source(s) *per se* but rather as a mechanism that modulates and perhaps even governs underlying brain processes (Monto *et al*., 2008). This section investigates the inter-trial variability observed in MEG event-related field (ERF)

components, and examines whether this variability exhibits a VLF time signature in order to indirectly infer information about the underlying slow waves. The focus is on the visual component, the M100, understood to be regulated by attention. The notion of whether individual differences in the M100 VLF pattern vary as a function of ADHD is also explored by comparing 11 cases against 11 controls. The M100 component is extracted from the data using ST-ICA, which allows trial-by-trial analysis to be performed on the M100 for proper assessment of VLF modulation.

It is important to note here that the MEG data used for these studies has been supplied by the Complutense, University of Madrid (UCM) in Spain, and was not recorded with the specific aim of analysing VLF brain activity *or* for comparing brain activity during cognitive function and rest conditions, which are both central to this work. For this reason, EEG experiments were designed and carried out to specifically investigate the functional role of the slow waves in the EEG during rest sessions (when participants were relaxed), and whilst performing stimulus-based tasks, on a sample of 23 healthy adult controls. The tasks have been based on the Go No-go paradigm (Datta *et al*., 2007) and the three-stimulus oddball paradigm with graded difficultly levels (Comerchero and Polich, 1999), both are known to elicit a standard P300 response. This event-related potential (ERP) component (occurring about 300 ms after stimulus onset) has been extensively studied in the last forty years because of its relation to attention and memory operations, and its sensitivity to task environments (Polich, 2007). The motivation behind and the design of the experimental protocols are presented in Chapter 7.

Chapter 8 describes the multistage signal processing system that has been developed for the analysis of this EEG data, namely: (i) the application of BSS for denoising the data and extracting the underlying brain sources (ICs), (ii) subspace analysis of the task ICs based on hierarchical clustering (Everitt, 1993), (iii) the extraction of features from the amplitude and phase of the ICs in different frequency bands and, (iv) classification of these features based on a neural network approach for pattern recognition using the Neuroscale algorithm (Lowe and Tipping, 1997) and Gaussian Mixture Models (Bishop, 1995). This was done in order to quantify the changes that the brain oscillators, particularly the slow waves, undergo in different experimental conditions. The second section of this chapter shows specific and combined results and further analysis carried out on the output of this multistage system.

At the end of the thesis in Chapter 9, the conclusions drawn from this work are summarised and prospective future work is outlined. The thesis organisation is illustrated in Figure 1-1.

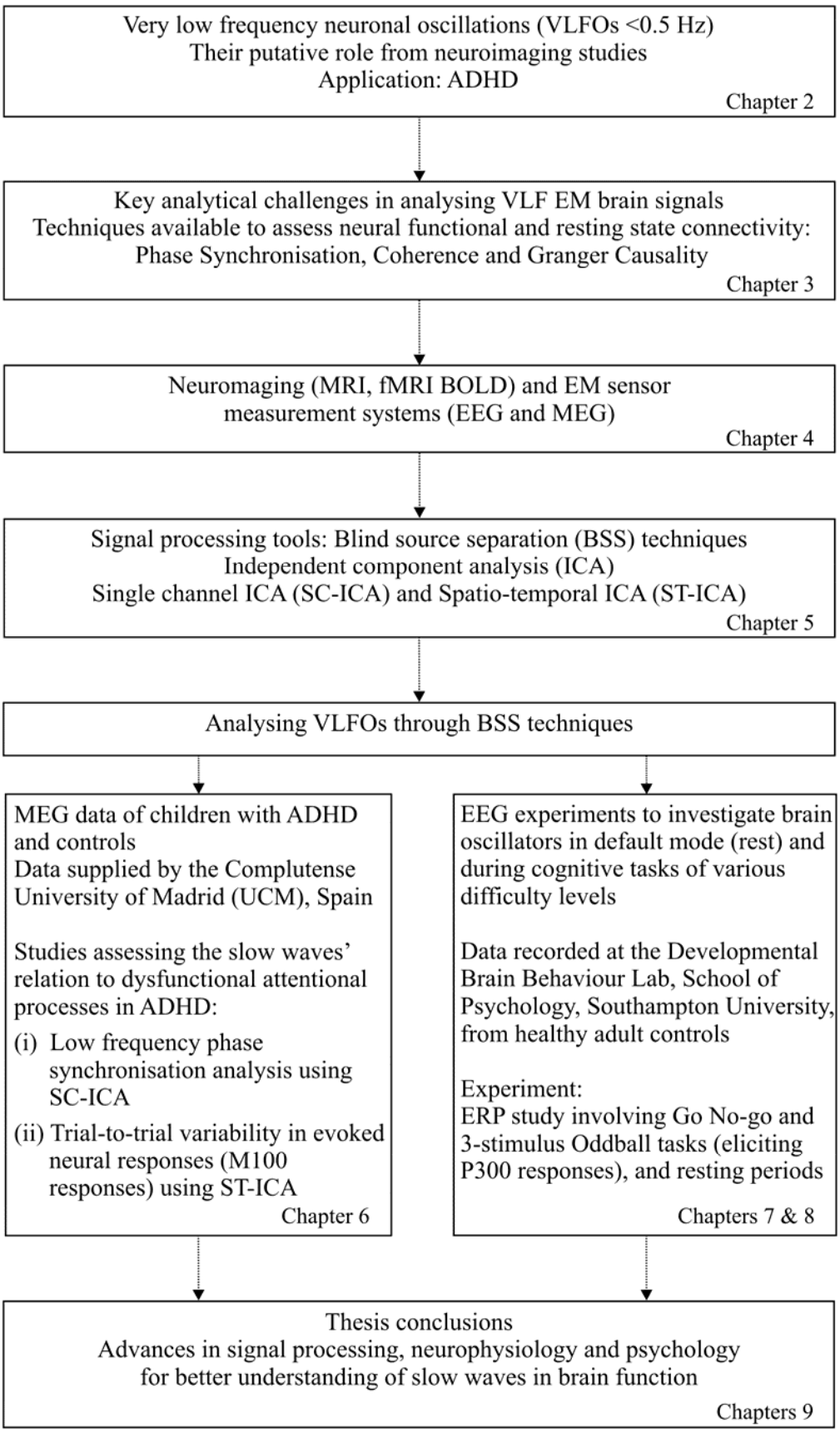

Figure 1-1. Thesis Organisation highlighting the main aspects of each chapter.

1.3. Original Contributions

Due to the interdisciplinary nature of this work, the research problem has been tackled from a signal processing and engineering, as well as from a neuroscience and psychological perspective; this led to several contributions in both domains, namely:

- Identification of the key analytical challenges for the analysis of the slow waves in EM brain signal recordings, (Chapter 3). This was followed by the development of a technique for normalising the intrinsic $1/f^{\gamma}$ power spectrum of EEG and MEG signals, which is useful for highlighting peaks of interest in the data as well as for comparing the power in the very low and higher frequency bands, (Chapter 6).

- Novel application of SC-ICA for the analysis of phase synchronisation in multi-channel MEG recordings. Phase synchronisation estimation between two channels requires the signals to be narrowband (Pikovsky *et al*., 2002). SC-ICA is an adaptive method that extracts band-limited sources from the data, hence adhering to this requirement without the need for band-pass filtering in the desired frequency band. For this reason, it has been used for the first time as an optimal technique for phase synchrony analysis between processes extracted from distinct brain regions, (Chapter 6).

- Detailed explanation of the recently-introduced ST-ICA as an extension of SC-ICA for the analysis of biomedical signals (Chapter 5). Novel application of ST-ICA for de-noising of event-related data (M100 and P300) recorded from highly-dense multi-channel EEG and MEG systems (Chapters 6 and 8).

- Development of a new methodology for investigating the inter-trial variability of event-related responses in EM brain signals. This was done in order to indirectly infer information about the underlying VLFOs, posited to be modulating/affecting/governing underlying brain processes, (Chapter 6).

- Design of a new experimental procedure which renders three task-rest environments with graded difficulty levels (Chapter 7). Design and implementation of a multistage signal processing system for investigating the activity of the brain electrical oscillators during different experimental conditions (Chapter 8, Section 1). The results obtained from this system provide evidence that the slow wave features (such as their amplitude and phase structure, and power) vary with mental load and behaviour. This indicates that the slow waves play a specific neurophysiological role and are more than just fluctuations arising from the recording process and/or the analysis procedure (Chapter 8, Section 2).

Some of these contributions are highlighted in publications which resulted from this work, as listed next.

1.4. Original Publications

1.4.1. Refereed Journal Articles

- Demanuele, C., Capilla A., Pérez Hernández, E., Sonuga-Barke, E.J.S. and James, C.J. (in press). Trial-to-trial variability in evoked neural responses exhibit a very low frequency temporal signature; A Magnetoencephalography study. *Journal of Psychophysiology*.

- Broyd, S. J., Demanuele, C., Debener, S., Helps, S.K., James, C.J. and Sonuga-Barke, E. J. S. (2009). Default-mode brain dysfunction in mental disorders: A systematic review. *Neuroscience and Biobehavioral Reviews*, 33, 279-296.

- Demanuele C., James C.J. and Sonuga-Barke E.J.S. (2007). Distinguishing low frequency oscillations within the 1/*f* spectral behaviour of electromagnetic brain signals. *Behavioural and Brain Functions Journal*, 3(62), 14 pgs.

1.4.2. Refereed Conference Papers

- Demanuele, C., Sonuga-Barke, E.J.S. and James, C.J. (2010). Slow neuronal oscillations in the resting brain vs task execution: A BSS-based investigation of EEG recordings. *Submitted for the 32nd IEEE Engineering in Medicine and Biology Annual International Conference*, *(EMBS'10)*, Buenos Aires, Argentina.

- James, C.J. and Demanuele, C. (2010). Space-Time Independent Component Analysis: the definitive BSS technique to use in biomedical signal processing? *Submitted for the 32nd IEEE Engineering in Medicine and Biology Annual International Conference*, *(EMBS'10)*, Buenos Aires, Argentina.

- James, C.J. and Demanuele, C. (2009). On spatio-temporal component selection in space-time Independent Component Analysis: An application to ictal EEG. (Oral presentation), *Proceedings of the 31st IEEE Engineering in Medicine and Biology Annual International Conference*, *(EMBS'09)*, Minnesota, USA.

- Demanuele, C., James, C.J. and Sonuga-Barke, E.J.S. (2009). Investigating the functional role of slow waves in brain signal recordings during rest and task conditions. (Poster presentation), *Proceedings of the 5th IEEE EMBS Postgraduate Conference on Biomedical Engineering and Medical Physics*, *(PGBIOMED'09)*, University of Oxford, UK.

- Demanuele, C., James, C.J., Capilla, A. and Sonuga-Barke, E.J.S. (2008). Extracting event-related field components through space-time ICA: A study of MEG recordings from children with ADHD and controls. (Oral presentation), *Proceedings of the 4th European Congress for Medical and Biomedical Engineering*, *(EMBEC'08)*, Antwerp, Belgium.

- Demanuele, C., James, C.J., Sonuga-Barke, E.J.S. and Capilla, A. (2008). Low frequency phase synchronisation analysis of MEG recordings from children with ADHD and controls using single channel ICA. (Oral presentation), *Proceedings of the 4th International Conference on Advances in Medical, Signal and Information Processing*, *(MEDSIP'08)*, Sta. Margherita Ligure, Italy.
  Awarded the Best Student Paper at the conference.

- Demanuele, C., James, C.J. and Sonuga-Barke, E.J.S. (2007). Analysis of low frequency oscillations in brain signal recordings of children with ADHD and controls. (Poster presentation), *Proceedings of the 3rd Life Sciences Interface Conference*, University of Southampton, UK.

1.4.3. Other Oral and Poster Presentations

- Demanuele, C., James, C.J. and Sonuga-Barke, E.J.S. Very low frequency oscillations in brain signal recordings: Are these of relevance in ADHD? (Poster Presentation), Set for Britain Event 2010, Westminster, London, 8th March 2010.

- Demanuele, C. and James, C.J. On the analysis of very low frequency neuronal oscillations in electromagnetic brain signal recordings: A blind source separation approach. (Public Lecture), University of Malta, 2nd June 2009.

- Three one-hour oral presentations of the PhD work and results given in the School of Psychology at the University of Southampton, (June 2007, December 2008, April 2010).

- Three 15-minute oral presentations of the PhD work for the signal processing and control group (SPCG), ISVR at the University of Southampton, (2007 till 2009).

Chapter 2

SLOW WAVES IN BRAIN SIGNALS: A REVIEW OF THE LITERATURE I

This chapter provides a psychological and physiological basis for the analyses carried out in this work. First, neural activity manifested in the EEG as a series of band-limited oscillators engaged in dynamic functional networks is discussed. This is followed by an explanation of the current understanding (through fMRI BOLD imaging) of the brain networks activation patterns during rest as opposed to externally imposed cognitive tasks. Special emphasis is given to existing theoretical models, hypotheses and evidence of VLF activity, derived from neuroimaging as well as from electro- and magneto-physiological studies. Lastly, ADHD is introduced as a bio-behavioural neurological disorder with implications in the slow wave band.

2.1. Networks of Brain Activity

The brain is believed to be a highly-distributed, self-organising system with different modules linked dynamically by synchronous oscillations (Varela *et al*., 2001; Buzsáki and Draguhn, 2004; Penttonen and Buzsáki, 2003). Transient assemblies, comprising many neurons, act in parallel in order to produce coherent perceptions, evaluation and behaviour depending on the task to resolve. These assemblies have a dynamic topography emerging as structures oscillating at multiple frequencies, (infraslow oscillations <0.1 Hz; slow oscillations <0.5 Hz; delta waves 0.5–4 Hz; theta 4–8 Hz; alpha 8–12 Hz; beta 13–20 Hz and gamma 25-100 Hz), each associated with different aspects of cognition and different brain states (Bear *et al*., 2001; Buzsáki and Draguhn, 2004). Large amplitude delta rhythms are observed in the human EEG during deep, dreamless and non-rapid eye movement sleep, and during waking states with low levels of arousal. Theta rhythms also occur during sleep and often represent a slowing of the alpha frequency, as in phases of drowsiness (Levin and Lüders, 2000). The alpha rhythm is most prominent during periods of non-agitation and tranquil relaxation, and is thought to reflect cortical idling (Ben-Simon *et al*., 2008). Relaxed yet focused states involving mental activity

(such as thinking) yield prominent beta waves, whilst high-level, information-rich task processing results in prominent gamma activity (Lachaux *et al*., 1999). Interestingly, these oscillators interact with each other and work together at various levels of synchrony; they can temporally co-exist in the same or different neural structures, and slower oscillators appear to group and modulate faster ones (Buzsáki and Draguhn, 2004; Balduzzi *et al*., 2008; He *et al*., 2008).

Three main classes of neural activity have been identified in the literature, namely (i) oscillatory activity of the brain independent of stimulation (spontaneous), (ii) activity tightly correlated in phase with the time of stimulus onset (evoked), and (iii) activity elicited by a stimulus but which is not tightly phase-locked to it (induced) (Karakas *et al*., 2000). The notion is that spontaneous ongoing activity represents the *ready* mode of the brain, i.e. the basic continuous activity in the absence of stimulation. In contrast, the *go* mode is characterised by acute neuronal firing for short periods of time (ii and iii), whereby distinct neuronal assemblies signal the presence of a preferred stimulus and respond to a subset of features. Both modes of neural activity are vital for specifying different cognitive states (Balduzzi *et al*., 2008). Furthermore, the empirically based theory of oscillatory neural assemblies formulated by Basar suggests that oscillations reflect the brain's information processing (Karakas *et al*., 2000); it posits that each oscillator represents multiple functions (like parallel processing systems) selectively distributed in the brain. These oscillators interact and their activity is coordinated during cognitive processing. Accordingly, the genesis of event-related (ER) morphology is a compound resulting from the superposition of oscillatory responses, the characteristics of which vary with task conditions; for instance, the P300 is the result of the additive effects of delta and theta oscillations, adhering to the principle of superposition (Karakas *et al*., 2000; Yordanova *et al*., 2000). Another proposition is that *all* cognitive functions can indeed be represented by a set of multiple oscillations, each responding to changes in task conditions by varying the amplitude, latency, duration and strength of stimulus-locking (Karakas *et al*., 2000). Such ER activity has been extensively used as a basic, non-invasive method of neurophysiological investigation, providing sensory and cognitive information for the evaluation of neural pathologies such as schizophrenia (Campanella *et al*., 2006) and occipital epilepsies (Gokcay *et al*., 2003).

Buzsáki and Draguhn (2004) suggest that neuronal oscillators go above and beyond the conventional EEG band ($0.5<f<50$ Hz) and potentially span frequencies from approximately 0.025 Hz to 600 Hz, (Figure 2-1). These frequency bands form a linear progression on a natural log scale (Penttonen and Buzsáki, 2003). Ultrafast activity is likely to be apparent in the electrophysiology of neurocognition and motor initiation ($150<f<500$ Hz) (Niedermeyer, 2005),

whereas infraslow oscillations ($0.01<f<0.1$ Hz) have been recorded in the EEG of preterm neonates, during epileptic seizure activity (Vanhatalo *et al*., 2005), and during sleep stages (Steriade *et al*., 1993; Vanhatalo *et al*., 2004). Furthermore, it is suggested that for meaningful classification of these brain oscillations the individual oscillatory classes must be generated by distinct physiological entities. This leads to the prediction that such oscillatory patterns are supported not only by different mechanisms but also by different networks. These network oscillations are responsible for biasing input selection, temporally linking neurons into assemblies, and facilitating synaptic plasticity in order to support long-term consolidation of information (Buzsáki and Draguhn, 2004).

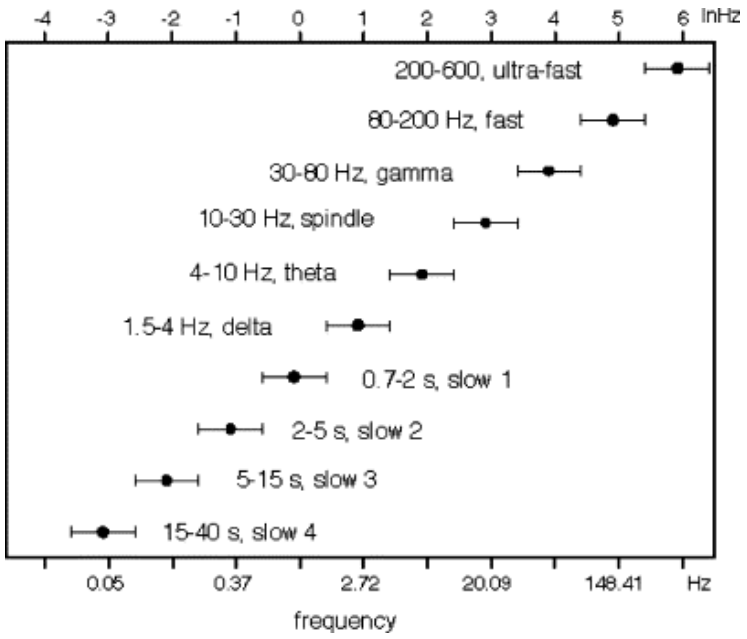

Figure 2-1. Frequency bands of the oscillators in the rat cortex (Penttonen and Buzsáki, 2003).

This is in keeping with fMRI BOLD imaging findings which suggest that "*the human brain is intrinsically organised into dynamic, anti-correlated functional networks*", as illustrated in Figure 2-2 (Fox *et al*., 2005). In this study the authors identified two diametrically opposed, widely distributed brain networks spanning regions that routinely experience task-related activations or deactivations respectively. Both networks demonstrate patterns of spontaneous low frequency correlations within their regions and anticorrelations with respect to the other network. Similarly, studies on the classification of neuronal oscillations in the mammalian cortex in various frequency bands indicate that spontaneous coherent low frequency neuronal oscillations are present within a neuro-anatomically robust default network of brain activity (Buzsáki and Draguhn, 2004; Fransson 2005:2006; Fox and Raichle, 2007). This has been reinforced by the earlier works of Penttonen and Buzsáki (2003), and Steriade *et al.* (1993) which attempted to link

neuronal activity to behaviour. These findings suggest that the basic rhythms of the EEG (delta, theta, alpha, beta and gamma) represent only a part of the measured neuronal activity. Very low frequency oscillations are a salient feature of this activity and can give access to new insight into brain function.

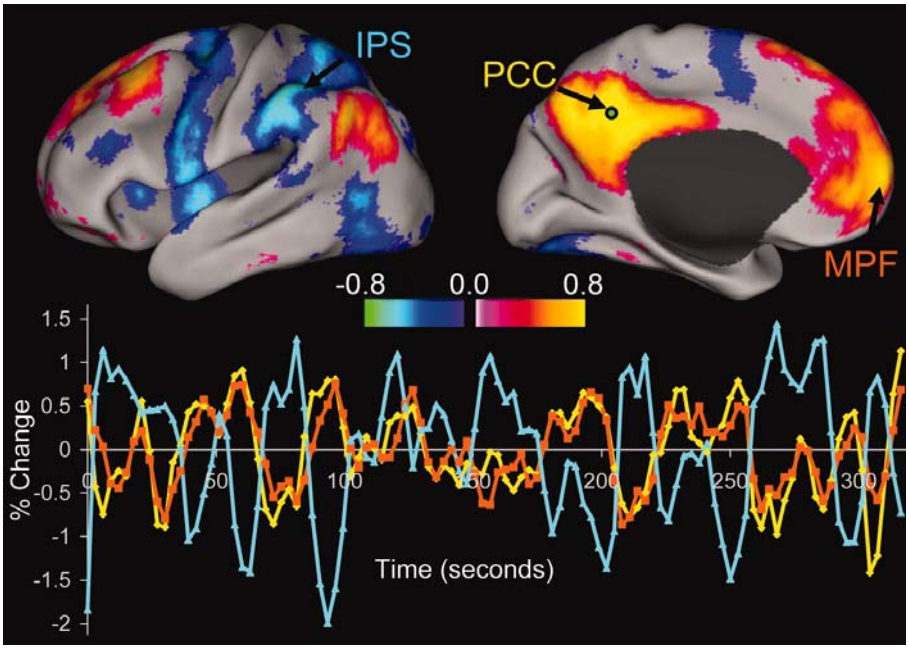

Figure 2-2. Two diametrically opposed, widely distributed brain networks and their intrinsic correlations between a seed region in the posterior cingulate/precuneus (PCC) and all the other voxels in the brain (for a single subject during rest). Colour bars indicate the spatial distribution of the correlation coefficients. The time series for the PCC (marked in yellow) shows that a region in the medial prefrontal cortex (MPF; orange) is positively correlated with the PCC, whereas a region within the intraparietal sulcus (IPS; blue) is negatively correlated with this seed region (Fox *et al*., 2005).

2.2. Cognitive Processing versus Resting States

Comparisons of brain activation patterns during periods of rest (i.e. when the individual is undertaking no externally imposed cognitive task), and during task-oriented activity have led to the hypothesis that the brain remains active in an organised manner during rest, in a way that implicates multiple coherent networks which differ in their anatomical components, their temporal signature and their phase relationships (Fransson, 2006; Sonuga-Barke and Castellanos, 2007). Neuronal activity during rest consumes approximately two-thirds of the brain's energy resources, which may be used to keep the brain's synapses exercised or to maintain a kind of "metastability" that allows the cortex to be ready to enter any required states or firing patterns (Balduzzi *et al*., 2008). One of the networks that is active when the brain is apparently at rest is known as the default mode network (DMN). The DMN incorporates the medial pre-frontal

cortex, posterior cingulate/precuneus and lateral parietal cortex, and has been termed the "task-negative" network as it is attenuated when one engages in task-specific, attention-demanding activities. This is one of the two networks identified in Figure 2-2 as being temporally anti-correlated with a second "task-positive" network, which is associated with task-related active processing (Figure 2-3). As shown in this work (Fox *et al*, 2005) and in other related works including (Fransson, 2005:2006; Sonuga-Barke and Castellanos, 2007) coherent VLFOs appear to play a particularly important role in brain function during rest and seem to be crucial for synchronising activity across these two networks. Moreover, Fox *et al*. (2005) suggest that the DMN, although attenuated during tasks, provides a potential source of interference that could contribute to lapses in attention during task performance, characterised by a low frequency time-signature ($0.01<f<0.1$ Hz).

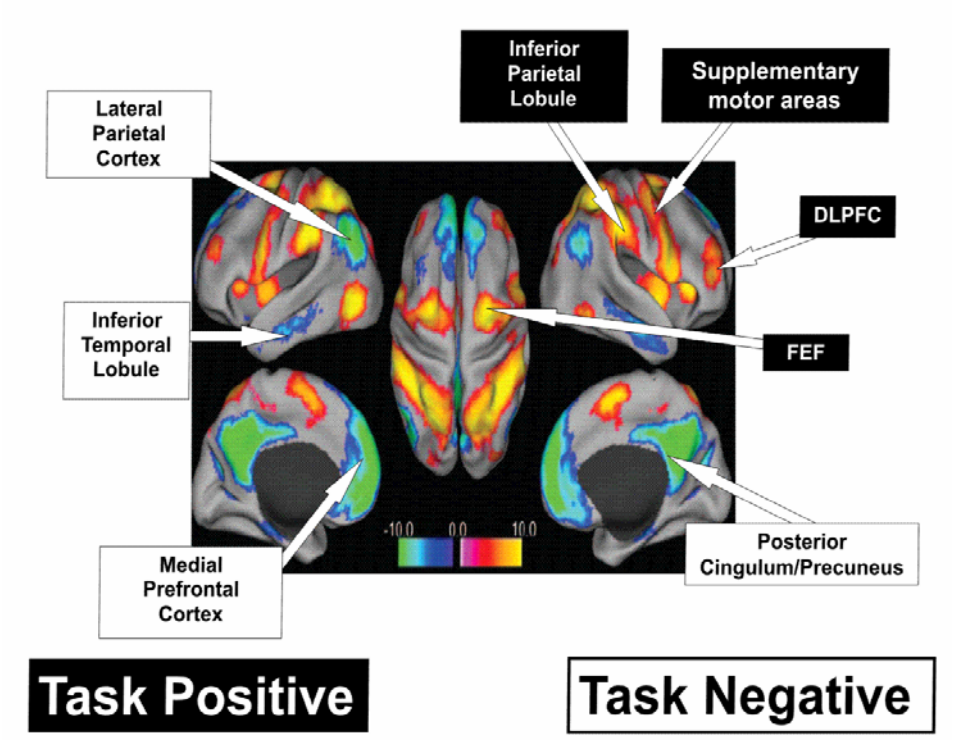

Figure 2-3. Neuroanatomical components of anti-correlated task positive and task negative components of the resting brain default network. This is shown as spontaneous fluctuations in the BOLD signal at rest. (FEF: frontal eye fields, DLPFC: Dorsolateral prefrontal cortex), (Fox *et al*., 2005; Sonuga-Barke and Castellanos, 2007).

Sonuga-Barke and Castellanos (2007) specify this interference as the Default Mode Interference (DMI) hypothesis and describe it as follows:

> *"Spontaneous low frequency activity in the task-negative component of the default-mode network which is routinely attenuated during goal directed tasks, can under*

certain circumstances (e.g. suboptimal motivational states or in individuals with attention disorders) persist into or remerge during periods of task-related active processing to such an extent that it competes with task-specific neural processing and creates the context for periodic attentional intrusions/lapses and cyclical deficits in performance; the temporal signatures of task-negative fluctuations being mirrored in patterns of attention and performance." (pp. 981).

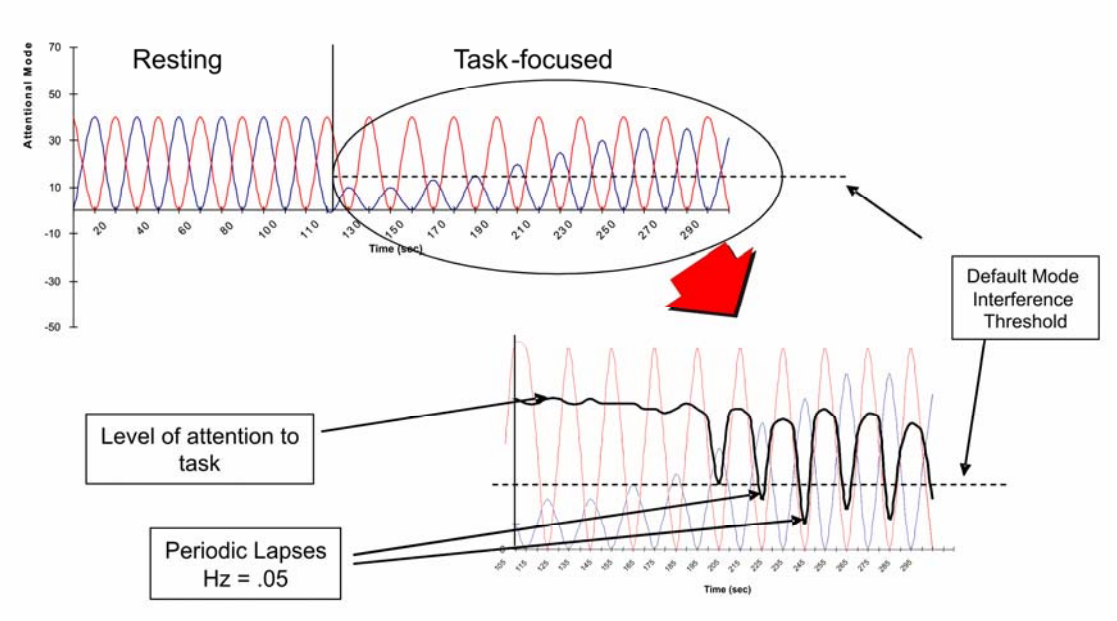

Figure 2-4. Illustration of the Default Mode Interference Hypothesis. The attenuation of the task negative component at the onset of the task results in a high level of attention. Its re-emergence throughout the course of the task leads to periodic attention lapses of a low frequency temporal signature (Sonuga-Barke and Castellanos, 2007).

This theoretical model postulates that during the course of the task there is spontaneous low frequency toggling between the task positive component (reflecting extroceptive, attentional orientation with respect to the task at hand), and the task negative component (which reflects the introspective state, related to mentalising and emotional processing, and is task-independent), which could affect task performance (Figure 2-4).

2.3. Very Low Frequency Oscillations

Coherent spontaneous VLF neuronal oscillations (<0.1 Hz) have been first observed by Biswal *et al*. (1995), within the motor cortex in fMRI signals during rest. Since then, oscillations in this frequency band, which are not attributable to specific inputs or outputs and span widely distributed neuroanatomical systems, have attracted a lot of attention in neuroscience (for a

review see Fox and Raichle, 2007). These appear to be intrinsically generated by the brain, are most prominent during rest and may allow temporal synchronisation to promote communication across diverse brain networks (Buzsáki and Draguhn, 2004; Fransson, 2005:2006). All evidence in the literature promotes the view that such slow waves, spontaneous or evoked, are not a passive electrical phenomenon but real responses in the functioning brain.

Fox *et al*. (2006) demonstrated that VLFOs in human brain activity persist throughout the course of the task and account for significant trial-to-trial variability in evoked BOLD responses. In fact, the authors suggest that the measured neuronal responses consist of the task-evoked response *superimposed on* the ongoing spontaneous VLF activity. Specifically, they showed that intrinsic activity measured in the right somatomotor cortex, contributes to variability in the left somatomotor cortex BOLD response evoked by right-hand button presses. Animal studies have also provided experimental evidence supporting these conclusions (Azouz and Gray, 1999; Fiser *et al*., 2004). Particularly, Arieli *et al*. (1996) suggest that dynamically changing ongoing activity reflects variations in brain states and is involved in the processing of sensory input in the visual cortex. Moreover, Fox *et al*. (2007) found that VLF fluctuations in the human somatomotor system are negatively correlated with trial-to-trial variability in the force of a button press, suggesting a direct correspondence between spontaneous brain activity and performance.

Both the origin and function of these VLFOs in brain activity are as yet unclear but several promising hypotheses have been proposed in recent literature. These oscillations may arise from periodic increasing and decreasing of the neurons' firing (say every 10 seconds) in the midbrain reticular formation. Another possibility is that neurons slowly modulate their level of activity because of intrinsic variations in ionic pumps, neurotransmitter transporters and glial cells (Balduzzi *et al*., 2008; He *et al*., 2008). Meanwhile, these oscillations may be essential for the development and organization of neuronal systems (Fox *et al*., 2006); alternatively they could be emerging from the network(s) itself rather than from the individual neurons (He *et al*., 2008). Furthermore, VLFOs may represent dynamic modulations in the internal brain representation, providing a basis onto which perception and behaviour occur, and hence determining our response to the outside world. Since this intrinsic brain activity is observed in both goal-oriented tasks and resting periods, it may represent continuous processes which are vital for maintaining a coherent neuronal representation of the 'self' (Fransson, 2006).

Existing evidence of spontaneous VLF activity in the brain during rest comes mainly from positron emission tomography (PET) and fMRI BOLD imaging studies, which offer excellent

spatial resolution. However, the fMRI BOLD signal is not a direct measure of neuronal activity since it reflects local variations in de-oxyhaemoglobin concentration determined by blood flow, blood volumes and oxygen metabolism, and it is not yet clear how these changes relate to concurrent changes in the spatial extent and magnitude of neuronal events (Debener *et al*., 2006). Moreover, the temporal resolution of fMRI is poor when compared to electro- and magneto-physiological techniques. Thus, EEG and MEG are employed to provide critical information about the spatiotemporal patterns of neural activity associated with a variety of sensory, perceptual, motor and cognitive processes, due to their real-time resolution (in the order of ms) and their reasonable spatial resolution (in the order of mm) (Hillyard and Anllo-Vento, 1998; Hillyard and Kutas, 2002). In fact, research by means of EEG and MEG can oftentimes complement studies of the spontaneous VLF neural phenomenon using these modalities.

Simultaneous BOLD and invasive EEG has been employed by Shmuel and Leopold (2008) who found a correlation between slow neuronal fluctuations and the low frequency BOLD signal in anesthetized monkeys. Laufs *et al*. (2003) correlated EEG activity with VLF BOLD signal fluctuations in the resting brain; Vanhatalo *et al*. (2005) observed VLFOs ($0.02<f<0.2$ Hz) across diverse scalp regions and provided evidence of phase-locking between these oscillations and traditional EEG bands. VLF signals during a short-term memory task were also observed in studies of EEG recordings (Ruckin *et al*., 1990; Rama *et al*., 1995). Furthermore, Leistner *et al*. (2007) observed VLF MEG oscillations (≈ 0.1 Hz) during a motor task, highlighting the use of MEG for temporal and spatial localisation of the brain activity of interest. Nakagawa *et al*. (1999) reported VLF activity in magnetic field recordings, localized in the inferior part of the occipital lobe, as a reflection of the storage process of the visual short-term memory. A recent study by Monto *et al*. (2008) examined large-amplitude ($0.01<f<0.1$ Hz) electrical fluctuations in ongoing brain activity of task-engaged humans and reported a high correlation between the participants' detection rate of the sensory stimuli and the phase of these EEG fluctuations, thus revealing a direct electrophysiological correlate with human performance. Moreover, the study found that amplitudes of the ($1<f<40$ Hz) EEG oscillations were strongly correlated with the phase of these fluctuations. These findings suggest that infraslow fluctuations reflect the excitability dynamics of cortical networks (Monto *et al*., 2008).

Finally, disturbances in VLFOs in brain activity have been reported in numerous pathologies, such as Alzheimer's disease, multiple sclerosis, depression, schizophrenia, autism, epilepsy and ADHD. These disturbances are often manifested as irregularities in the power and/or coherence pattern of the VLFOs, and have been correlated with the level of severity of the disease (Fox and Raichle, 2007; Broyd *et al*., 2009).

2.4. ADHD – An Application

ADHD is a relatively common and impairing childhood developmental disorder, afflicting 5.29 % of school-age children (Polanczyk *et al*., 2007). As a disorder characterized by patterns of inattention, hyperactivity and impulsivity which may persist throughout the lifespan, ADHD can substantially affect the normal cognitive and behavioural functioning of the individual (Mulas *et al*., 2006). A broad range of neuro-psychological, energetical and motivational processes have been implicated (Taylor and Sonuga-Barke, 2008) with deficits in response selection, motor adjustment and response inhibition characterising the cognitive phenotype (Jonkman *et al*., 2004). ADHD children perform worse than control children on a broad range of cognitive and attentional tasks (Jonkman *et al*., 1997; Johnstone *et al*., 2003). This variable cluster of symptoms leads to three subtypes of ADHD – predominantly hyperactive, predominantly inattentive and the combined type. Presence of this disorder during childhood usually occurs before the age of seven and some of these symptoms may persists throughout the lifespan – between 50% and 70% of children with ADHD continue to suffer from this disorder as adults (Clarke *et al*., 2001). Evidence suggests that ADHD is primarily a polygenic disorder involving at least 50 genes, including those encoding enzymes of neurotransmitter metabolism, neurotransmitter transporters and receptors (Sonuga-Barke, 2003). Because of its polygenic nature, ADHD is a highly comorbid disorder, often co-occurring with conduct disorder, oppositional defiant disorder, anxiety disorders, major depressive disorder and learning difficulties (Yordanova *et al*., 2006). Moreover, its strong genetic basis makes it highly heritable.

Neuropsychological studies reveal that ADHD is a disorder of prefrontal lobe function (Wienbruch *et al*., 2005; Banaschewski and Brandeis, 2007). A 'lazy' frontal lobe results in disinhibition of motor activity as well as disturbed attention. However, for some children with ADHD, especially those with learning disorders, the parietal lobes are likely to be involved (Comings *et al*., 2005). ADHD children miss stimuli more frequent (hence committing omission errors), more often provide erroneous responses to insignificant stimuli (a.k.a. commission errors), and their reaction time is slower than the general population indicating a weak or underdeveloped cerebellum (Modarres-Zadeh *et al*., 2005**)**. Increased response time variability is another common finding in ADHD research, which may be indicative of frontal cortex dysfunction and may also be related to deficits in sustained attention (Johnson *et al*., 2007).

All ADHD subtypes are generally treated by the prescription of methylphenidate and dexamphetamine. These stimulant medications appear to produce their therapeutic effect by increasing arousal to more normal levels (Clarke *et al*., 2003). This treatment is effective in 50-

75 % of children (Wienbruch *et al*., 2005). Biofeedback is currently being used for assessing and treating ADHD children as well as for increasing the attention span of children who suffer from attention deficits. EEG biofeedback utilizes feedback from a game played on a TV screen in attempt to train the brain to alter the levels of delta, alpha and beta waves (Comings *et al*., 2005). It has been suggested that such treatment leads to reductions in hyperactive, inattentive and disruptive behaviours and to improvements in academic performance and IQ scores (Cho *et al*., 2002). Recently, mindfulness meditation training has been proposed as a feasible intervention for ADHD adults and adolescents since it may improve attention and lower anxiety (Zylowska *et al*., 2000).

To date ADHD is diagnosed solely on the basis of patterns of observable behaviour, including interviews to reveal the history of the child and various types of questionnaires to healthcare professionals, parents and teachers (Nass, 2005). The most common form of diagnosis is done according to the Diagnostic and Statistical Manual of Mental Disorders, 4th Edition, Text Revision, (DSM-IV-TR) published by the American Psychiatric Association (2000). Neuroimaging and/or electrophysiological assessments have been given a great deal of attention with the aim of providing a more reliable diagnosis for this disorder (Nass, 2005; Mulas *et al*., 2006). Neuroimaging studies reveal differences in the brain anatomy of ADHD children, where a notable 4% decrease in their total brain volume from normals has been reported (Solanto, 2002). Single photon emission computed tomography (SPECT) studies found that ADHD participants have reduced blood flow in frontal regions as well as enhanced blood flow in motor areas (Wienbruch *et al*., 2005). Meanwhile, the EEG study by Clarke *et al*. (2001) suggests that for ADHD participants excess beta activity (which rarely occurs in children and should not exceed 25 μV in amplitude) located primarily in the right frontal region could be related to dysfunction in the frontal-lobe systems associated with self-regulation and inhibition control. This study also showed that ADHD children had increased lower frequency activity (particularly in the theta band) compared to normals.

Over the years, event-related studies have also been used to gain insight into brain activity during attentional, inhibitory and preparatory processing of ADHD participants, and attempts have been made to discriminate between clinical and control groups (for review see the work of Barry *et al*., 2003). There is a wide range of ER components which vary as a function of this disorder and although there are considerable consistencies within the ADHD-ER literature, there are many contradictory findings and the conceptualisation of ERP and ERF differences associated with ADHD is complex. A range of ADHD effects have been noted in the auditory oddball tasks with ADHD children having slower responses to late ERP components, such as the P300 responses

(Ozdag *et al*., 2004), and smaller N100 amplitudes as a result of auditory attention deficits (Jonkman *et al*., 2004). ADHD participants had longer occipital P100 latency during a visual stimuli-response compatibility task, whereas the visual P300 component was reported to differentiate clinical from control children (Jonkman *et al*., 1997; Barry *et al*., 2003). Jonkman *et al*. (1997) showed that ADHD patients exhibited smaller amplitude of this late positive ERP wave during visual tasks. Stimulant medication such as methylphenidate have been shown to normalize the ERP indices, suggesting that such treatment may be effective on impaired information processing components (Ozdag *et al*., 2004). However, there was not a case reported where a single ERF/ERP component has been consistently absent or abnormal in such a way as to be diagnostic (Hillyard and Kutas, 2002). Apart from ER studies, other techniques such as variable resolution electromagnetic tomography (VARETA) and quantitative EEG (QEEG) have been used to help explain the pathophysiology of this disorder (Di Michela *et al*., 2005).

2.4.1. ADHD and Slow Wave Literature

Crucially, when time-series data recorded from ADHD participants are considered, a pattern of greater trial-to-trial fluctuations in performance is generally observed, and these patterns exhibit a VLF time signature. Sonuga-Barke and Castellanos (2007) have recently hypothesized that performance fluctuations in ADHD mirror periodic (low frequency) lapses in attention caused by the intrusion of spontaneous (slow) fluctuations in brain activity within the DMN. This suggests that ADHD may be defined as a *default-mode deficit disorder* whereby sustained attention lapses stem from the continuous intrusion of the task negative component, which may also cause increased performance variability. fMRI studies have already reported DMN irregularities in ADHD, such as decreased functional connectivity both within the network and between the DMN and other brain regions, including the anterior cingulate cortex and the precuneus (Castellanos *et al*., 2008; Uddin *et al*., 2008). In addition, the DMI hypothesis predicts the notion that these spontaneous fluctuations in attention lead to a more variable performance for ADHD children in comparison to controls, and this variability has a VLF time signature.

Consistent with this, Castellanos *et al*. (2005) demonstrated that ADHD children exhibit higher reaction time (RT) variability for frequencies below 0.1 Hz (see also Johnson *et al*., 2007; Di Martino *et al*., 2008). Of relevance is a finding by Helps *et al*. (2008) which found reduced power in low frequency ($0.06<f<0.2$ Hz) resting state networks that was linked to high self-reported inattentive symptoms in young adults. Interestingly, attenuation of low frequency activity in this network following the transition from rest to a simple reaction time task was negatively correlated with inattention symptoms. Moreover, the VLF variation in reaction time

was correlated with the VLF activity in the EEG within the DMN regions – i.e. frontal and posterior midline, (Helps *et al*., in press). An extension of this study compared DC-EEG recordings of a sample of 16 clinic-referred adolescent boys with ADHD and 16 healthy age-matched controls during rest and during a two choice reaction time task, and reported a reduction in signal power in the ($0.02<f<0.2$ Hz) frequency band for ADHDs in comparison to controls. ADHD children, who also exhibited reduced attention during task (assessed through performance measures), showed less attenuation of power at these frequencies following a rest-to-task transition. Although preliminary (due to limited statistical power), these findings suggest that ADHD children may have difficulties in controlling the intrusion of the intrinsic slow waves, leading to poorer task performance, and may be less able to maintain a "resting" brain state in comparison to controls (Helps *et al*., 2010).

2.5. Summary

This chapter was aimed at providing a physiological and psychological perspective behind the main motivation of this work. Recent literature suggests that both spontaneous and event-related neural activity, which produce coherent cognitive processing and behaviour, are the result of the brain's electrical oscillators working together at various levels of synchrony. These oscillators span infraslow to ultrahigh ($0.025<f<600$ Hz) frequency bands and form specific networks of activity depending on the level and type of input simulation (for instance, apparent rest a.k.a. default mode activity versus stimulus-triggered active processing). Of particular interest, are very low frequency oscillations first observed in fMRI BOLD imaging studies. These VLFOs, particularly evident in the DMN during rest, are attenuated but not extinguished following a transition from rest to task, indicating that they are modulated rather than interrupted by the presence of stimulation. It is posited that when this intrinsic slow wave activity persists during task, it competes and interferes with goal-directed processing hence compromising task performance – this forms the basis of the DMI hypothesis. ADHD is a perfect candidate for exploring the DMI given the impairments in sustained attention for its diagnosis and the vast body of emergent literature investigating slow wave variations in this bio-behavioural disorder. The putative role of the slow waves in brain function has been discussed. In the next chapter, the key methodical challenges in analysing VLF EM brain activity are discussed, followed by a review of selected signal processing techniques available in the literature.

Chapter 3

ANALYSIS OF VERY LOW FREQUENCY BRAIN ACTIVITY: A REVIEW OF THE LITERATURE II

This chapter tackles the specific issues that arise when analyzing VLF activity in multichannel electrophysiological recordings. An account of the 1/f spectral behaviour of EM brain signals is presented, followed by an introduction to the BSS techniques required to achieve denoising and dimensionality reduction of the data. Works in the literature demonstrate the ability of these techniques to efficiently isolate neurophysiologically meaningful brain sources from the recordings for a vast range of biomedical applications. Methods for the extraction of spatial, temporal and spectral information from the EM brain signals are then discussed. Particularly, coherence, phase synchrony and Granger causality are reviewed as tools for the investigation of brain networks.

3.1. Issues on Analysing VLF Brain Activity

Very low frequency brain activity is notoriously difficult to study. Interference to the VLF fluctuations in the fMRI BOLD signal may arise from low frequency cycles in respiration and cardiac activity; for instance, Birn *et al*. (2006) showed that variations in respiration (≈ 0.03 Hz) correlate highly with fluctuations in the DMN (<0.1 Hz). Meanwhile, the analysis of slow waves in electromagnetic systems (EEG and MEG) below the conventional frequency range (i.e. <0.5 Hz) has several implications. Longer time recordings (in the order of tens of minutes) may be required to be able to accurately extract these VLFOs. This may compromise the compliance of participants when given a repetitive task in an experiment. Technically, it also leads to loss of stationarity and to drifts in the recordings – although these can be mediated by careful recording of the data.

VLF EM signal recordings require genuine DC-coupled amplifiers with high input impedance, high DC stability and a wide dynamic range. Sufficiently stable electrodes and gels should be used to provide a faithful EEG recording at such low frequencies (Vanhatalo *et al*., 2005). DC drift, which is superimposed on any meaningful slow activity, can be an issue unless amplifiers are reset every three minutes (Hennighausen *et al*., 1993) to ensure that the signal is kept in the optimal range of the amplifier throughout the recording. The chosen sampling rate needs to be set according to the Nyquist criterion; however, in most studies, it is better to ensure that it is high enough to allow for comparison of the slow waves with activity in higher frequencies bands. EM brain signals exhibit power spectra with high power at low frequencies; normalisation of this $1/f$ trend is required to render a flat base spectrum when no extra low frequency activity is present and to reveal distinct peaks related to specific cognitive tasks or mental conditions (such as resting states). This is particularly important in the analysis of slow oscillations and for comparison of activity in this band versus the traditional (delta, theta, alpha, beta and gamma) frequency bands.

Moreover, the EM recording process is inherently noisy and yields data that comprises a mixture of artifacts from a variety of sources (such as muscular and ocular components), along with activity from various active, if not all superficial brain regions. This implies that denoising techniques need to be used for proper network analysis. Modern EM systems have large sensor arrays which result in a data deluge problem that entails practical considerations, including long computational times and large memory requirements for the application of various signal processing techniques. Large multi-dimensional datasets also bring with them issues related to the appropriate choice of the analysis procedure.

Finally, it is crucial to explore the role that slow waves have in forming and maintaining coherent and synchronised neuronal interactions between functional areas widely distributed across the brain. Techniques such as cross correlation in the time domain and coherence in the frequency domain (Shen *et al*., 2002), phase synchrony (Lachaux *et al*., 1999) and Granger causality (Hesse *et al*., 2003) can be used to investigate how the VLF activity measured from different brain regions is linked together and information exchanged.

3.2. $1/f$ Spectral Trend

Electrophysiological activity belongs to a broad class of physical signals which arise from a so-called $1/f$ process. Such signals have a power law relationship of the form

$$S_x(f) = \frac{\text{constant}}{f^{\gamma}}, \tag{3.1}$$

where $S_x(f)$ is the power spectral density, f is the frequency and γ is a spectral parameter which is usually close to 1 but can lie in the range $0 < \gamma \leq 2$ (Keshner, 1982). Taking logs on both sides of equation (3.1) and rearranging renders

$$\ln S_x(f) = \ln(\text{constant}) - \gamma \ln(f) \tag{3.2}$$

where γ is the slope of the power spectrum.

Various works in the literature have acknowledged this intrinsic $1/f$ trend in the neuronal system, and showed that the power-law scaling in the brain exhibits a decrease in log power with increasing frequency, as illustrated in Figure 3-1. This was observed in the temporal and spatial power spectral densities (PSDs) of EEG recorded both intracranially and on the scalp (Freeman *et al*., 2003; Yamaguchi, 2003; Hermann and Demiralp, 2005), as well as in the PSDs of MEG recordings (Mäkinen *et al*., 2004).

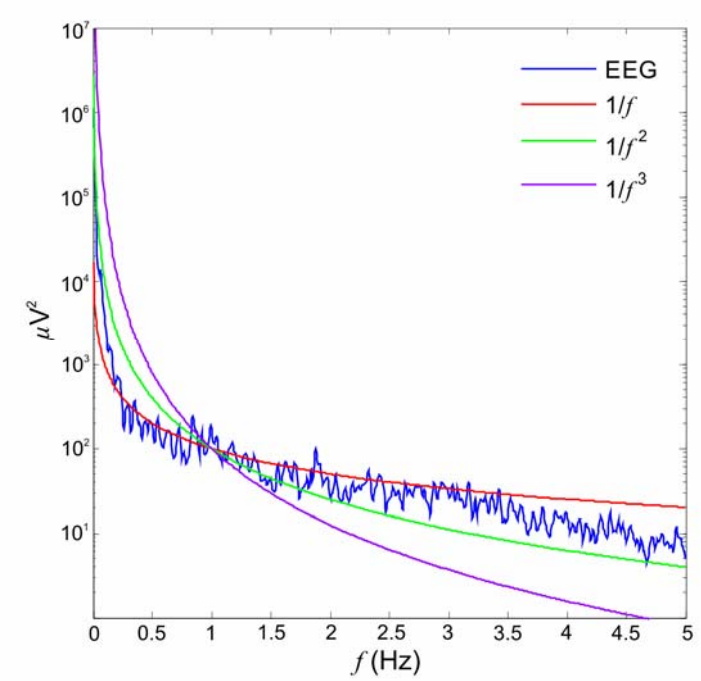

Figure 3-1. The PSD of a typical EEG channel with superimposed $1/f^{\gamma}$ curves.

The $1/f$ spectral behaviour of signals and systems was first reported in 1925 in an electric current passing through a vacuum tube (Johnson, 1925). It also appears in economic and communication systems, in electronic transistors and diodes, in the annual amount of rainfall and in the rate of traffic flow (Keshner, 1982). Biological data such as the potential measured across nerves and

physiological systems such as the cardiovascular and respiratory mammalian systems also exhibit this kind of behaviour (Wornell, 1993). The work by Kobayashi and Musha (1982) demonstrated that the human heartbeat period fluctuation exhibits this PSD trend for frequencies below 0.02 Hz but the reason for this behaviour is unknown. This $1/f$ fluctuation has also been observed in the body sway motion and in eyeball motion (Kobayashi and Musha, 1982).

The inverse relation of the PSD of EM signals with frequency in the mammalian cortex may be the result of the physical structure of neural networks and the limited speed of neuronal communication arising from axon conduction and synaptic delays (Freeman *et al*., 2003; Hermann and Demiralp, 2005). A large cluster of neurons, each generating a unit activity, forms a functional network which is held together by the neurons' synchronisation that ensures activity control (Poupard *et al*., 1996). Such synchronised behaviour seems to attract further neurons and causes the oscillation amplitude to increase. Moreover, the period of the oscillation is determined by the size of this neuronal cluster that constitutes a given cycle. Thus, large neuronal areas are associated with slow, high amplitude oscillations whereas a small, localised concentration of neurons gives rise to higher frequency, low amplitude signals (Penttonen and Buzsáki, 2003; Buzsáki and Draguhn, 2004). This explains why most of the power of the EEG signals is concentrated in the low frequency spectrum. MEG recorded data, which is sometimes preferred over EEG recordings due to its high spatial resolution and the extremely high temporal resolution, also exhibits this $1/f$ behaviour inherent in its power spectrum. This is to be expected since these two systems share the same underlying model – MEG measures the minute magnetic field generated by the electrical activity of neurons; this activity corresponds to that detected by the EEG electrodes.

In order to be able to correctly identify any spectral activity superimposed on the $1/f$, the EEG/MEG power spectrum can be normalised by removing this trend (Buzsáki and Draguhn, 2004). Mäkinen *et al*. (2004) employ a technique called Partition-Referenced Moment together with wavelet transforms to obtain a level base spectrum; this method is then used for examining ongoing oscillations and auditory ER brain responses in MEG recordings. This proposed method, based in the frequency domain, is an involved approach. As will be shown in Chapter 6, spectral normalisation can be achieved in the frequency domain by dividing any EEG/MEG spectrum by an established background $1/f^{\gamma}$ spectrum, or in the time domain by passing the raw data through a filter (such as a $\sqrt{f}$ filter: assuming γ=1, or a differentiator: assuming γ=2) prior to further data analysis. The latter approach provides a linear phase response hence preserving the phase structure of the input signal.

3.3. Denoising and Dimensionality Reduction

Through electrophysiology one aims to obtain a detailed representation of the brain electrical activity with a limited number of sensors attached to the scalp. Freeman *et al*. (2003) describe the cortex as being "*a mosaic of quasi-autonomous areas*", each area contributing its signal to the scalp EEG; however, it overlaps with other signals both spatially and temporally by volume conduction. This implies that scalp recordings represent a summation of electrical activity from various brain regions, and can be considered as unknown mixtures of a number of underlying sources that cannot be separately accessed and measured. The nature of artifactual and multi-source recordings coupled with the data-deluge problem, make these ideal candidates for the use of BSS strategies in order to remove artifacts, reduce dimensionality and single out actual brain sources.

The fundamental aim of BSS techniques in electrophysiology is to extract information from a set of EM measurements made over time without using *any* additional information about the time series or spectra of the unknown sources (Belouchrani *et al*., 1997). These techniques provide an automated methodology that (James and Hesse, 2005):

- Unmixes and isolates distinct sources given only sensor observations,
- Provides information on the number of sources underlying the measurements,
- Provides the spatial distribution and time-series of each brain source, and
- Tracks changes in the number, spatial distribution and morphology of the sources over time.

Over the years, numerous BSS methodologies have been developed. Neuroimaging methods combined with source localization algorithms have been used to obtain a picture of spatiotemporal patterns of event-related brain activity (Hillyard and Kutas, 2002). Wavelet filtering has also been used to extract ER signals from ongoing background EEG, and to obtain information about the temporal dynamics of auditory/visual processing (Heinrich *et al*., 2001). Particularly, the application of ICA to EEG and MEG recordings, and to ER data has been well documented in the literature (Makeig *et al*., 1997; Makeig *et al*., 1999a; Vigario *et al*. 2000; Jung *et al*., 2001a; Muller *et al*., 2004). ICA is a linear BSS technique that can be used to decompose EM datasets consisting of many scalp channels, stimulus types and task conditions into a sum of temporally independent, spatially fixed and physiologically plausible independent components (ICs). Hence it can separate out artifactual, stimulus-locked and ongoing brain activity (Vigario *et al*., 1998; James and Hesse, 2005).

ICA in its basic form achieves the separation of *spatially* distinct sources from a set of biosignals; the measured signals are assumed to be a mixture of underlying brain sources which are statistically independent and non-Gaussian (Comon, 1994). It is also generally assumed that the sources are mixed in a linear, square and invertible manner, and that the mixing process is stationary. In essence, since EM brain signals are linear time invariant mixtures of source components, the sensor measurements can be represented as

$$\boldsymbol{x} = \boldsymbol{A}\boldsymbol{s}\,, \tag{3.3}$$

where $\boldsymbol{x}$ is a matrix containing n sensor measurements, $\boldsymbol{A}$ is an $[n \times b]$ mixing matrix and $\boldsymbol{s}$ is the source matrix consisting of b underlying sources ($b \leq n$) (Hyvärinen *et al*., 2001).
Depending on the algorithm used, ICA provides *estimates* of brain sources, somewhere in between the actual brain sources and the scalp signals, such that the recovered components are maximally independent. Generally, separate ICs are grouped together to form subspaces representing brain sources of interest (Hyvärinen *et al*., 2001).

As explained in Chapter 1, SC-ICA (James and Lowe, 2001; Davies and James, 2007) is an ICA-BSS technique that has been recently introduced to isolate underlying processes within the data from *single channel* recordings. This ICA algorithm learns a set of band-limited, adaptive filters from the measured signal in order to extract underlying sources with disjoint spectra. An augmentation of this algorithm comes in the form of ST-ICA, whereby SC-ICA is applied to a number of channels, thus providing both temporal *and* spatial information to inform the standard ICA process (Davies *et al*., 2007; James *et al*., 2007). These two algorithms are explained in more detail in Chapter 5 of this work.

3.3.1. Other BSS Algorithms

Some researchers argue that the mixing model assumed by ICA (as in equation (3.3)) is not ideal since although it is perfectly correct to assume that brain sources and artifacts are independent, it is not as justifiable to assume that the brain sources themselves are mutually independent (Li *et al*., 2003 and 2006). Physiologically interesting brain sources typically interact so ICA will fail to characterise them properly (Nolte *et al*., 2005). In keeping with this view, Li *et al*. (2006) suggest a sparse factorisation approach based on the wavelet packets transform to estimate $\boldsymbol{A}$ from the observed EEG data matrix $\boldsymbol{x}$, and present a linear programming method for evaluation of the EEG source components $\boldsymbol{s}$. The authors claim that, compared to ICA, the sparse factorisation approach has two important advantages, namely: (i) the sources do not necessarily have to be mutually independent, and (ii) the number of sources can be greater than the number of sensors (i.e. an over-complete case with $b>n$), and it can even be unknown.

In addition, Nolte *et al*. (2005) present a BSS technique called interacting source analysis, which uses anti-symmetrised cross-correlation matrices and subsequent diagonalisation for the suppression of spurious interactions stemming from volume conduction. This technique is based on second order statistics but is only sensitive to interacting sources and thus can be applied to systems with an arbitrary noise structure. Another powerful BSS strategy is the temporal decorrelation source separation (TDSEP) algorithm developed by Ziehe and Müller (1998). Here the mixing matrix is determined by means of an approximate joint diagonalisation of several time-lagged covariance matrices in order to minimise the temporal cross correlations between the output signals. This method is suitable for signals with a strong and distinct temporal structure.

3.4. Extracting Spatial, Temporal and Spectral Information from Brain Signal Recordings

Numerous signal processing methods exist to enable maximal extraction of spatial, temporal and spectral information from EM brain signals, an area of constant research and development. Spectral analyses involving the fast Fourier transform (FFT) have been widely used for the analysis of neurophysiological signals (Bruns, 2004). However the FFT, which is a frequency transformation of the measured signal, does not cater for variations in the statistical properties of the data with time, making it unsuitable for non-stationary signals. For this reason, this analysis is often carried out repeatedly with a sliding time window to provide a continuous evaluation of spectral parameters over time. This method, known as the Short Time Fourier Transform (STFT), is very useful in the study of brain dynamics (Bruns, 2004). An alternative to the STFT is the Wavelet Transform (WT), which can represent finite, non-periodic and/or non-stationary signals. The idea of the WT is to convolve the measured signal with a number of oscillatory filter kernels, each representing different frequency bands. In this way, the temporal characteristics of a signal are represented by its spectral components in the frequency domain. In STFT, a square-wave window is used for all frequencies, such that the resolution of the analysis is the same at all locations in the time-frequency plane. Wavelet theory furthers this idea by introducing variable-sized windowing, where, in contrast to the STFT, short windows are used at high frequencies and long windows at low frequencies. However, WTs take much longer to compute (Gramatikov and Georgiev, 1995). These analyses provide spectral parameters such as amplitude and phase, from which a variety of important coupling measures, such as coherence and phase synchrony, can be derived.

As explained in Chapter 2, neurons and neuronal populations interact with each other in an orchestral manner to enable the execution of different sensorimotor and cognitive tasks

(Horowitz, 2003). Coherence (Shen *et al*., 2002), phase synchrony (Lachaux *et al*., 1999) and Granger causality (Hess *et al*., 2003) have been studied extensively in the literature with the aim of quantifying such neuronal interactions between widely distributed brain regions during various cognitive processes (Quian Quiroga *et al*., 2002; Pereda *et al*., 2005).

3.4.1. Coherence

Coherence is a traditional linear method for calculating the degree of linear association between two signals, i.e. the degree of correlation between two random processes as a function of frequency (Shen *et al*., 2002). Phase coherence then represents the amount of phase lead/lag of one process with respect to the other (Whiting *et al*., 1989). Hence coherence can be interpreted as phase shifts and amplitude changes between two correlated sequences at one particular frequency. The estimation of coherence is based on the Fourier Transform (FT) and is defined as the average FT of the normalised cross-correlation of two simultaneously measured, discrete univariate time series (Quian Quiroga *et al*., 2002). Some researchers have extended this concept to the time-frequency domain in order to obtain information about the temporal structure of coherence which is useful for the study of brain dynamics, leading to the concept of wavelet coherence (Klein *et al*., 2006; Liu *et al*., 2006; Zhan *et al*., 2006).

However, this measure does not separate out the effects of amplitude and phase in the interrelation between two signals. Lachaux *et al*. (1999) discuss the limitations of coherence as a tool to indicate brain interactions, namely that coherence can be applied only to stationary signals and that it does not specifically quantify phase relationships. Coherence increases with amplitude covariance, although the relative contribution of amplitude and phase correlations in the coherence value is not clear. As coherence mixes the amplitude information with that of phase, it is not considered suitable for the detection of phase locking of brain oscillators. For these reasons, phase synchrony – a measure that indicates whether the phase shift between two signals is close to a constant over the specified time interval – is used as a separate measure. Here, the phase component is obtained separately from the amplitude component for a given frequency (Tcheslavski and Beex, 2006). Phase locking is in fact sufficient to conclude that two brain signals interact. Moreover, phase synchrony can be properly detected in short data segments although the detection of coupling is clearly improved as the length of the time series increases.

3.4.2. Phase Synchrony

Buzsáki and Draguhn (2004) suggest that band-limited oscillators in distinct brain areas can be phase coupled and that such phase interactions may result in precise neuronal discharges without direct anatomical connections. Phase synchrony (PS) is a viable indicator of this coupling (Quian Quiroga *et al*., 2002; Pereda *et al*., 2005) and can be seen as a mechanism for dynamic integration of distributed neuronal networks. On the other hand, decreased synchrony is associated with active unbinding of the neural assemblies and preparation of the brain for the next mental state (Song *et al*., 2005). PS is useful because it is independent of the signals amplitude; Pereda *et al*. (2005) explain how the phases of two coupled nonlinear (noisy/chaotic) oscillators may synchronize even if their amplitude remains uncorrelated. Thus, PS can indicate instances where two signals are phase locked whilst their amplitudes vary independently (Hurtado *et al*., 2004). In the study of human brain synchrony, two scales of PS can be distinguished: (i) short range (local scale) synchrony between adjacent areas within the same hemisphere, and (ii) long range (large scale) synchrony between widely separated brain regions, i.e. between opposite hemispheres or not immediate special neighbours (Wang *et al*., 2006). PS can be evaluated according to the following procedure:

(i) *Estimation of the instantaneous phase of each signal*

This can be achieved by using the Hilbert Transform as a means of estimating the instantaneous phase, hence finding the phase difference between any two signals (Taner *et al*., 1979; Rosenblum *et al*., 1996). Quyen *et al*. (2001) obtained the phases by convolving each signal with a complex wavelet function and then compared the results with those derived using the Hilbert Transform. This study demonstrates that the differences between the two methods are minimal and they are fundamentally equivalent for the study of neuroelectrical signals.

(ii) *Evaluating the degree of phase locking*

This entails the formulation of a phase locking value as an index that gauges the phase difference between two signals over a specified time window (Lachaux *et al*., 1999, Hurtado *et al*., 2004).

(iii) *Establishing a statistical criterion to quantify the degree of phase locking*

Phase locking statistics determine the degree of statistical significance of each phase locking value, hence distinguishing significant interactions from background fluctuations (Lachaux *et al*., 1999). This is required since detecting phase locking between recordings from two distant scalp sensors is largely hampered by background noise and volume conduction.

In scalp EEG, the signal to noise ratio is low and true synchrony is always buried in a considerable amount of background noise (Wang *et al*., 2006), whereas the main limitation in the understanding of short range synchrony is the distinction between volume conduction and true synchrony (Lachaux *et al*., 1999). Human studies use surface electrodes that integrate neural activity over large volumes; when the volumes recorded by two sensors overlap, the shared neuronal population creates spurious connectivity between the signals. Thus distinction of this type of conduction synchrony and actual neuronal coupling is required to assess significant brain areas interactions. This separation is made even more difficult by the fact that in band-limited EEG these two types of synchrony occur at the same latencies and in the same frequency band. This goes against the general assumption that conduction synchrony is broadband and roughly constant in time whereas true synchrony is more specific (Lachaux *et al*., 1999). To reduce volume conduction one should rely on recordings with high spatial resolution in which the overlap between the brain volumes recorded by different probes is minimal. The spatial precision of EEG may be improved by using techniques such as inverse deblurring or surface Laplacian (Srinivasan, 1999; Sweeney-Reed, 2007). Alternatively, MEG recordings may be used since MEG has a higher spatial resolution as the brain's magnetic field does not get diffused by its tissue.

3.4.3. Applications of Coherence and Phase Synchrony Measures

Coherence and PS have been applied for a vast body of biomedical applications. They have been used to investigate the interactions of the supplementary motor area and the primary motor area during left and right hand movements; this is vital for assessing the recognition of motor imagery in brain computer interfacing (BCI) (Song *et al*., 2005; Wang *et al*., 2006). Epilepsy is another major area of application, particularly for predicting the onset of epileptic seizures (Mormann *et al*., 2000). Pereda *et al*. (2005) reported that a decrease in PS was normally detected prior to the onset of a seizure. Meanwhile, the work by Netoff and Schiff (2002) showed that synchronisation increased as seizures decayed, which suggests that asynchrony is necessary to maintain a high level of activity in neuronal networks for sustained periods of time. Wang *et al*. (2006) then suggest that phase coupling between distant brain areas, (which was here manifested as synchronisation in the alpha *f*-band), is critically important for maintaining spontaneous functioning of the healthy brain.

Furthermore, it is suggested that subjects with pathologies usually have a decrease in long-range synchrony (Pereda *et al*., 2005). The work by Barry *et al*. (2002) investigated the difference in intra-hemispheric and inter-hemispheric EEG coherences between ADHD and control children

and between children with combined and inattentive type of ADHD, and reported specific differences in coherence in cortico-cortical circuits involving theta activity. Tcheslavski and Beex (2006) employed PS and coherence, and claimed that by using the proper selection of electrode pairs, EEG rhythm and task they could discriminate between the EEG of ADHD and non-ADHD children by 63.2 % correct classification.

Other coherence applications include speech (Petsche *et al*., 1996) and language processing (Weiss and Mueller, 2003) and the distinction between different modalities of the human thinking processes (Schack and Krause, 1996). Schizophrenia studies (Spenser *et al*., 2003) and studies on the mechanisms of memory maintenance (Tallon-Baudry *et al*, 2001) have made use of PS measures. Tass *et al*. (1998) employed PS to study MEG recordings of Parkinsonian patients. Note that PS amongst multi-channel MEG recordings is the result of a group of synchronously firing neurons within a single area generating a magnetic field, which is then captured by the MEG system. Any synchronous neural activity between remote brain areas is then reflected as phase locking between the distinct MEG channels.

3.4.4. Granger Causality

In neuroscience the brain is seen as a dynamic system in which causal influences between different components may have significant implications. These are often examined by means of time series analysis techniques such as Granger causality (Hesse *et al*., 2003), which quantify interdependencies between brain signals/processes. For a dynamic system, a process X is said to Granger-cause another process Y if knowledge of the past of X improves the prediction of Y, compared to when the past of process Y alone is used. This relation between time series is not commutative; this means that X may cause Y without Y necessarily causing X. Granger causality, unlike coherence and PS, provides insight into the directionality of information flow (X→Y) or (Y→X) (Astolfi *et al*., 2006). This measure is usually estimated by means of vector autoregressive models (AR), where univariate and bivariate AR models are fitted to the signals of interest (Hesse *et al*., 2003). Therefore, (following the above definition), in univariate AR modelling the prediction error (i.e. the uncertainty in the prediction of the next signal value) depends on the past of the signal itself. In the bivariate model, the prediction error depends on the past of the signal itself together with the past of the second signal. Then, if the signal X causes the signal Y, the variance of the prediction error decreases for the bivariate model when the past of X is taken into account for the prediction of Y.

This procedure can be extended to multivariate systems by fitting an *n*-dimensional multivariate vector AR model to the *n*-channel data (Winterhalder *et al*., 2005). Amongst others, Neumaier and Schneider (2001) developed an algorithm (ARfit) for the estimation of the parameters of these models. To substantiate the causality between two signals, statistical evaluation by means of surrogate data is often performed (Hesse *et al*., 2003; Gautama and Van Hulle, 2003; Elsner, 2007). The surrogate time series retain the autocorrelation structure of the original series but remove the specific temporal ordering. Surrogates may be created by randomisation of the phases from the series' Fourier spectrum (Kaplan, 1995). The inference of the Granger causality in the frequency domain led to the development of techniques such as partial directed coherence (Baccala and Sameshima, 2001; Schelter *et al*., 2006) and directed transfer function (Franaszczuk and Bergey, 1998).

Finally, it is argued that the application of coherence, PS and Granger causality on scalp recordings, which are only a diffused representation of the actual brain sources, may lead to spurious results (Delorme *et al*., 2002). Moreover, (as explained earlier), volume conduction effects make large parts of the cortex seemingly interact, although in reality such couplings are purely artifactual. This can be avoided by applying these measures to the brain sources derived from BSS methods, such as ICA. ICA removes the background coherence by eliminating the "crosstalk" caused by volume conduction and by separating unrelated noise sources, while maintaining the same time resolution as the recorded EEG/MEG. For instance, Londei *et al*. (2007) combined ICA with Granger causality for the analysis of fMRI data involving the listening of high frequency words, non-words and reversed words. The causality between ICs was estimated in order to establish the functional relation between the sources, hence detecting possible cognitive causal relationships in neuroimaging data.

3.4.5. ICA and the Notion of Independence

Once ICA demixes the sensor observations into a number of independent sources, coherence, synchronisation and causality measures can be applied on the ICs. However, one may argue that if two time series are completely independent their mutual synchronisation vanishes. Moreover, theoretically, if the original source signals are synchronised, ICA cannot recover them since the independence condition of ICA would be violated (as coupled sources are not independent). Yet, Meinecke *et al*. (2005) show that synchronised signals remain synchronised even if they are linearly transformed in the measurement space. Therefore, in such a case, ICA would not succeed in extracting the original sources; nonetheless, the ICA *estimates* would still be synchronous. If on the other hand, the brain sources are independent (not synchronised) ICA

would be able to separate them, consequently removing any spurious synchronisation. Some examples of this methodology can be found in the works by Hong *et al*. (2005:2006), where an ICA-PS analysis was performed to investigate the dynamics of neural synchrony between different cortical regions by measuring PS between ICs characterised by distinct spatial patterns.

Delorme and Makeig (2004) demonstrate that even though ICs are maximally independent over the whole time range, they may exhibit partial but statistically significant synchronisation within specific ER time-frequency windows. This is explained by the fact that ICs returned by ICA are *maximally* (not completely) independent. Moreover, Delorme *et al*. (2002) suggest that the interpretation of electrode coherence patterns can be ambiguous since these may arise from various amplitude changes in several processes at different brain locations. For instance, coherence increase between two electrodes may be accounted for by an increase in the power of a single major EEG source projecting to both electrodes and thus synchronizing the recorded activity. On the other hand, cross-coherences between different ICs can directly assess the relationship between different brain areas. Furthermore, in practical applications of ICA, one can often observe violations of the independence assumption and it is possible to find couples of estimated ICs such that they are clearly dependent on each other. To this end, Hyvärinen *et al*. (2001) proposed a new methodology whereby the residual dependency structure of the components could be estimated and used to define a topographic order for the components based on the distance between them. In this way, a linear decomposition into a set of approximately independent components is obtained and the dependency of any two ICs is approximated by the proximity of the ICs in the topographic representation.

3.5. Summary

In this chapter the key analytical challenges in analysing VLF brain activity in EM brain signal recordings, including the intrinsic $1/f$ nature of electrophysiological data, have been identified. Several BSS techniques, including ICA, have been introduced as a means of achieving denoising and dimensionality reduction of multichannel EM recordings. These methods demix the sensor measurements, which represent a summation of electrical activity from several brain sources mixed with artifactual noise sources, in order to extract components of interest from the data. Coherence and phase synchronisation can be used to quantify the brain networks activation patterns during, for example, resting states and during task-related active processing, whereas Granger causality provides a measure of linear feedback (noting the directionality of information flow) between channels and/or brain sources. Their applications in the field of biomedical signal processing have been discussed. These tools could be used (with caution) on the brain sources extracted by the BSS algorithms in order to eliminate the effects of volume conduction, hence

establishing a faithful representation of the true connectivity and/or causality of disparate brain regions. It is important to note that although the focus of this work lies in the region below 0.5 Hz, these techniques are obviously not restricted to the analysis of such low frequencies.

The next chapter provides a brief description of several neuroimaging and EM recording systems, which act as windows into the human brain, with special emphasis on the mechanisms of EEG and MEG.

Chapter 4

IMAGING AND ELECTROMAGNETIC SENSOR SYSTEMS IN NEUROSCIENCE

Being able to understand brain function and localising functional areas in the brain are major milestones in neuroscience. This chapter describes some neuroimaging, and electro- and magneto-physiological recording systems as valuable, non-invasive tools for gaining insight into the integrated processing that takes place in the human brain. Whilst fMRI pinpoints functional foci during vision, motor, language and memory tasks, EEG and MEG act as direct neuronal probes that can be used to characterise the electrical activity of the central nervous system and the associated magnetic fields. This is vital for exploring how the brain orchestrates the vast array of dynamic processes contributing to all aspects of cognition, perception and action.

4.1. Neuroimaging Techniques

Different types of functional and structural neuroimaging methods, each exploiting different physical principles and reflecting various neurophysiological processes, are available to explore the human brain in a non-invasive, safe and well-tolerated manner (Buxton, 2009; Ulmer and Jansen, 2010; Mulert and Lemieux, 2010). Computerized X-ray tomography (CT) scanners and magnetic resonance imaging (MRI) are two such methods that render information on brain structure and anatomy. CT scanners use digital geometry processing to generate a 3-dimensional (3-D) image of the inside of the brain by means of a large array of 2-D X-ray images taken around a single axis of rotation. This technique is limited by the skull but can pick up large abnormalities of the brain tissue (such as tumours) and is often used to detect blood in or around the brain soon after a haemorrhage. MRI, invented around the 1970s, provided a real revolutionary methodology for neuroimaging, through its ability to represent the distribution of

transverse magnetization in the brain with a spatial resolution of better than 1 mm (Al-Chalabi *et al*., 2006). The basic concepts of this technology are briefly described below.

4.1.1. Magnetic Resonance Imaging (MRI)

In MRI, the signal that is measured arises from the nuclei of the tissue's hydrogen atoms; nuclei containing an odd number of protons and/or neutrons have a characteristic motion or *precession*. Because nuclei are charged particles, this precession produces a small magnetic moment. When placed inside a magnetic field, many of the free hydrogen nuclei align themselves with and precess about the magnetic field direction – a movement termed as *Larmor precession*, (Figure 4-1). The frequency of Larmor precession is proportional to the applied magnetic field strength as defined by the Larmor frequency:

$$\omega_0 = \kappa B_0 \tag{4.1}$$

where κ is the gyromagnetic ratio, which is a nuclei specific constant (42.6 MHz/T for hydrogen), and B_0 is the strength of the applied magnetic field (Mulert and Lemieux, 2010).

In brain imaging studies, the participant is placed in a cylindrical coil that surrounds the head. The coil is exposed to a strong static magnetic field, B_0, which causes a macroscopic magnetisation to build up parallel to this field. As a result, the brain's hydrogen nuclei align with the magnetic field and create a net magnetic moment, M, parallel to B_0, as illustrated in Figure 4-1 (b). A radio-frequency (RF) pulse, B_{rf}, with the Larmor frequency and duration of a few milliseconds is then applied perpendicular to B_0, which gives rise to a tilt and a subsequent precession of the magnetisation vector, (Figure 4-1 (c)). This only works if the RF signal is at exactly the protons' Larmor frequency, hence exhibiting a resonance effect. Once the RF pulse stops, the nuclei realign themselves such that their net magnetic moment, M, is again parallel to B_0 – a return to equilibrium termed as *relaxation*. During relaxation, the nuclei lose energy by emitting their own RF signal, as shown in Figure 4-1 (d). A detector (a conductive field coil placed around the object being imaged) tuned to the Larmor frequency is switched on to detect the transmitted signal. Next, the spatial resolution of the protons – i.e. their x (left/right), y (anterior/posterior) and z (superior/inferior) coordinates – is derived in order to obtain 3D grey-scale MR spatial images.

Resolving along the three axes involves the concept of frequency encoding, phase encoding and slice selection respectively (Buxton, 2009; Mulert and Lemieux, 2010):

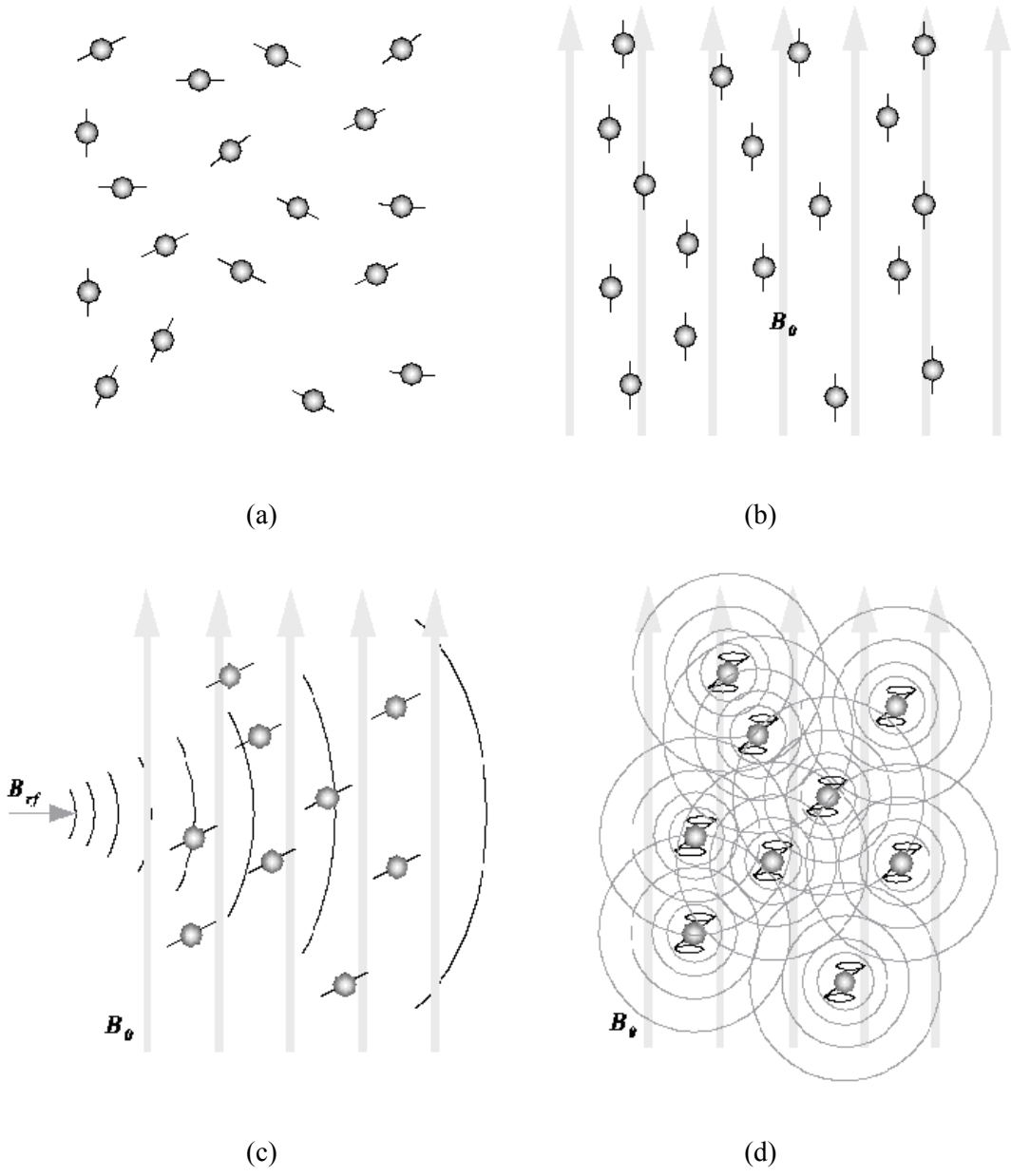

Figure 4-1. Magnetic Resonance Imaging (MRI): (a) In the absence of a strong magnetic field, hydrogen nuclei are randomly aligned; (b) A strong magnetic field, B_0, causes the hydrogen nuclei to precess about the direction of the field. (c) An RF pulse, B_{rf}, causes the net magnetic moment of the nuclei, M, to tilt away from B_0. (b) When the RF pulse stops, the nuclei return to equilibrium such that M is again parallel to B_0. During realignment, the nuclei lose energy, emitting a measurable RF signal. Adapted from (Buxton, 2009).

- *Frequency encoding* (*x-direction*) – the magnetic field is known to increase linearly in the *x*-direction. Therefore, during acquisition, the protons' Larmor frequencies depend on their positions inside the brain and their *x*-coordinates can be deduced from the frequency spectrum (through the Fourier transform) of the signal they send out.

- *Phase encoding* (*y-direction*) – protons with different *y*-coordinates precess with different frequencies, leading to different starting points (phases) when the acquisition begins. This implies that the *y*-coordinates can be deduced from their phases.
- *Slice selection* (*z-direction*) – protons with different *z*-coordinates have different Larmor frequencies. This means that an RF pulse with a specific frequency (f_0) can only excite protons within a certain axial slice and cannot influence those in other parts of the brain because their Larmor frequencies are higher or lower than f_0 such that no resonance is possible.

Further details regarding these concepts go beyond the scope of this work but can be found in the works by Buxton (2009), and Mulert and Lemieux (2010).

4.1.2. Functional MRI (fMRI)

fMRI in a broad sense refers to any MRI technique that goes beyond anatomical imaging and provides information on physiological function. Functional brain imaging was first performed using positron emission tomography (PET) in 1973. This technology makes use of a short-lived radioactive tracer isotope (introduced in the body on a biologically active molecule such as fludeoxyglucose, an analogue of glucose) which is usually injected into the patient's (or participant's) blood circulation (Young *et al*., 1999). The system detects pairs of annihilation gamma photons emitted indirectly by the tracer during positron emission decay. Computer analysis is then employed to reconstruct images of the tracer concentration in 3-D space within the brain. This technique is heavily used in oncology, for clinical diagnosis of dementia, and has led to a greater understanding of Parkinson's disease (Young *et al*., 1999; Al-Chalabi *et al*., 2006). Single photon emission computed tomography (SPECT), provides similar information to PET. However, in contrast with PET, the tracer used in these scans emits gamma radiation that is measured directly, the scans provide a lower spatial resolution (around 1 cm) and are significantly less expensive. SPECT has been used for mapping hemodynamic changes during sleep and in epilepsy, amongst others (Baumgartner *et al*., 1998).

More recently, fMRI methods have dominated the field of functional neuroimaging primarily based on a phenomenon known as the blood oxygenation level dependent (BOLD) effect. With brain activation, glucose and oxygen metabolism, cerebral blood flow and blood volume all increase in the active area. However, the fraction of the delivered oxygen that leaves the blood and is metabolized in the cells decreases with activation, and this phenomenon is exploited in fMRI in order to infer the underlying local changes in neuronal activity. In essence, this method is founded on the hemodynamic response – blood releases oxygen to firing neurons more quickly

than to inactive neurons. Haemoglobin is diamagnetic when oxygenated but paramagnetic when deoxygenated. This implies that the MR signal of the blood will differ according to the level of oxygenation – whenever the increases in cerebral blood flow exceed changes in oxygen consumption the BOLD signal intensity is increased (and vice-versa). This is captured by the MRI scanner and can indicate which areas of the brain are active during a particular thought, action or experience (Buxton, 2009). Consequently, fMRI BOLD imaging has been extensively used for providing a representation of the spatial organization of the healthy and the pathological human brain (Ulmer and Jansen, 2010).

In a prototypical fMRI experiment, blocks of stimulus presentation ("on" periods of activation) are altered with equally long ("off") control periods while a series of dynamic images is collected with an echo planar imaging pulse sequence (Buxton, 2009). The signal time course for each voxel of the image is analyzed to test for significant correlations of the signal with the stimulus (i.e. to test whether the signal increased during the "on" blocks). Alternatively, an fMRI experimental protocol, analogous to an ERP experiment, is set up where single trials of a particular stimulus are presented and the responses are averaged time-locked to the stimulus onset; Figure 4-2 illustrates the characteristics of such an averaged BOLD response. This method provides a direct measure of the hemodynamic response on a voxel-by-voxel basis. Since the aim of these experiments is to detect a weak signal change (for example on the order of 1% for a 50% change in cerebral blood flow at 1.5 T), many repetitions of one action or thought are required to allow sufficient averaging for detecting such minute signal changes. Statistical analysis of BOLD measurements is then carried out for reliable identification of these changes in the MR signal (Buxton, 2009; Baudelet and Gallez, 2005).

Despite the vast use of the fMRI-BOLD method in neuroscience, it is as yet unclear how the changes in the BOLD signal relate to concurrent spatial and magnitude variations of neuronal events (Debener *et al*., 2006). The aspect of neuronal activity which best predicts changes in BOLD contrasts (i.e. combined neuronal spiking, local field potentials, changes in spontaneous rhythms, etc.) has not been established definitely (Huettel *et al*., 2004). Hence, there may be a degree of incongruence between hemodynamic signals and electrical brain activity. Moreover, despite the excellent spatial resolution of neuroimaging techniques, the temporal resolution is poor; for example, whereas fMRI clinical scanners can have an in-plane resolution exceeding 1 mm, their temporal resolution is in the range of few hundred milliseconds or even 1 second, depending on the technique and the paradigm used (Ulmer and Jansen, 2010). This means that information of particularly fine temporal structure, which may be embedded in the time domain, is not accessible to these techniques because they are limited by scan times and physiology, as

well as by the sluggishness of the hemodynamic signal. For these reasons, EEG and MEG are often employed to monitor the information processing in the brain; these high temporal resolution modalities can also supplement the spatial information from fMRI (Mulert and Lemieux, 2010).

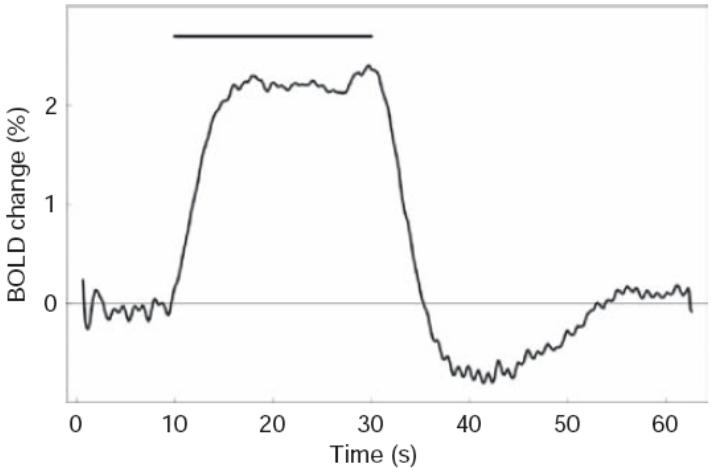

Figure 4-2. A typical BOLD response (averaged over a number of stimuli) measured in the visual cortex at 3 T. Note the initial delay of 1–3 s after the initiation of the stimulus (marked by a horizontal bar), a 5-8 s ramp-up towards a plateau, a post-stimulus ramp-down of several seconds and an undershoot (w.r.t. the original baseline) which takes about 20 s to resolve (Buxton, 2009).

4.2. Electro- and Magneto- Neurophysiology

"With present methods the skull and the scalp are too much in the way, and we need some new physical method to read through them. In these days we may look with some confidence to the physicists to produce such an instrument, for it is just the sort of thing they can do."

E.D. Adrian: Brain Rhythms, Nature (1944).

This forward-looking, challenging statement has been taken to heart by scientists, and today EEG and MEG systems provide excellent tools by which electrophysiological correlates of neuronal activity can be examined (Fisch, 1999; Bear *et al*., 2001; Khader *et al*., 2008). As illustrated in Figure 4-3, cellular currents in an active neuron population give rise to extracranial electric potentials and magnetic fields; EEG measures the potential differences on the scalp whereas MEG captures the resultant magnetic fields. Hence both methodologies detect neural currents directly rather than the associated hemodynamic changes, providing direct information on the brain's spatio-temporal activation during sensory, cognitive, attentional and motor information processing. Moreover, EEG and MEG are the only two methods that offer sub-millisecond time resolution and can thus record brain activity in real-time (Figure 4-4).

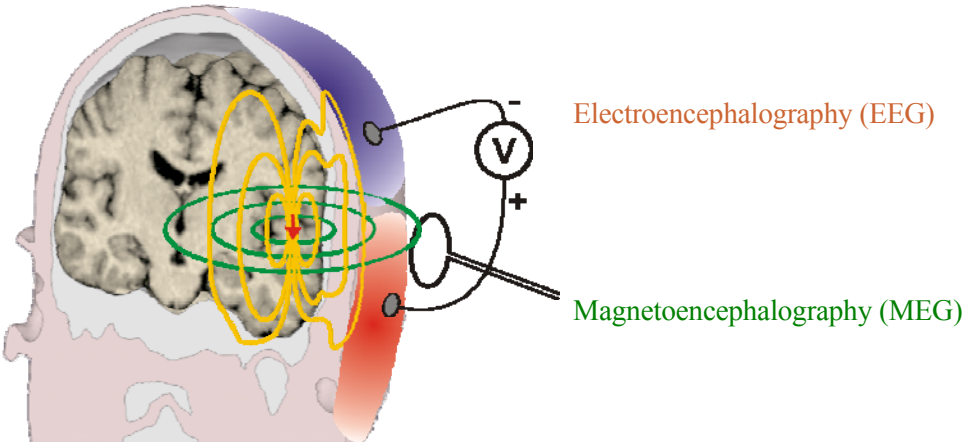

Figure 4-3. Electro- and Magneto- Neurophysiology: EEG measures the potential differences on the scalp which reflect the summation of synchronous activity of many neurons. This net effect of ionic currents forms current dipoles; MEG records the extracranial magnetic fields surrounding the dipoles' axis. Adapted from (Elekta Neuromag® MEG System Description, 2006).

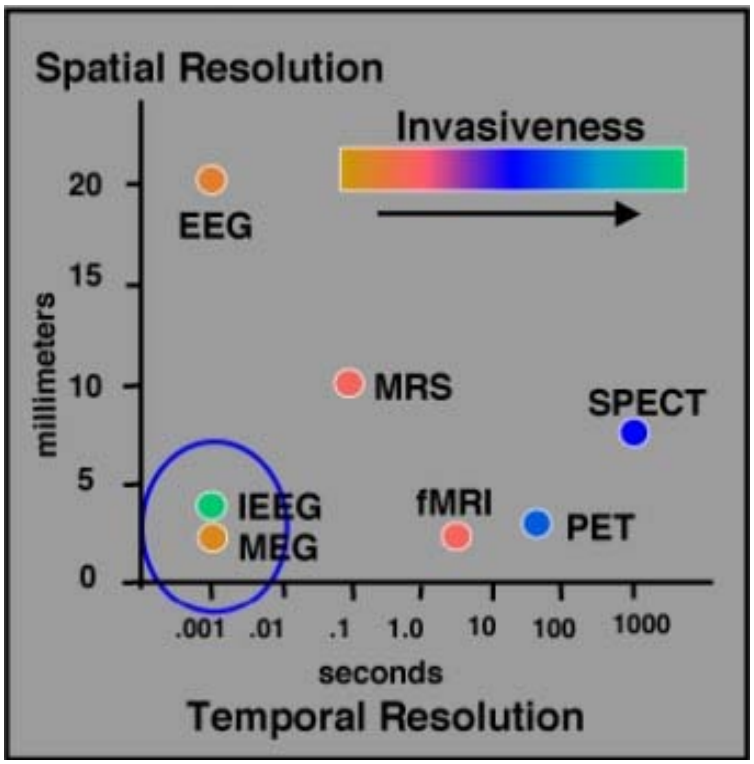

Figure 4-4. Temporal and spatial resolution, and the level of invasiveness of electromagnetic and neuroimaging techniques. (IEEG – Intracranial EEG, MRS - Magnetic resonance spectroscopy); (Elekta Neuromag® MEG System Description, 2006).

4.2.1. Electroencephalography (EEG)

EEG was first introduced to the study of the human brain by Hans Berger in 1929, (Berger, 1929). The recorded signals are small voltage fluctuations, in the order of tens of micro-Volts, generated by synaptic excitation and inhibition of dendrites of the pyramidal neurons in the cerebral cortex, which constitute 80% of the brain's mass (Bear *et al*., 2001). The recording is done by means of sensors (electrodes) attached to the scalp (generally according to the International 10-20 System: Jasper, 1958), which reflect the net average of the electrical potentials in the corresponding areas of the cortex. It is believed that the EEG signal originates from correlated post-synaptic potentials of cortical neurons with probable contribution from intrinsic cell currents, rather than from individual action potentials, since the action potentials field distribution is too small to be captured at scalp level (Fisch, 1999). The post-synaptic potentials result from synaptic transmission caused by the release of chemical neurotransmitters at the synapse (an area of near contact between two neurons) from the pre-synaptic neuron (Figure 4-5). The signal is then modulated (attenuated) as it propagates through brain parenchyma, dura, cerebrospinal fluid, bone, and scalp (Fisch, 1999).

Synchronous firing of millions of neurons enhances the amplitude of the EEG as the small signals all sum up to create one large surface signal. EEG has limited anatomical specificity when compared with neuroimaging techniques (Figure 4-4). Furthermore, since voltage fields decay with the fourth power of the radius, the deeper the sources, the more difficult it becomes to detect their activations at the scalp. EEG signals have the statistical properties of random variables or band-limited white noise (Freeman, 1988), and so, as described in earlier chapters, numerous signal processing methodologies can be employed to assist their interpretation.

Figure 4-6 shows the EEG electrode set-up for one participant who took part in the experiments reported in Chapters 7 and 8 of this work, using a Neuroscan SynAmps2 70-channel EEG System[1] located in the Institute of Disorders of Impulse and Attention (IDIA) lab of the School of Psychology at the University of Southampton. The electroculogram (EOG), which measures the resting potential of the retina (Levin and Lüders, 2000), was recorded using two electrodes attached below the eyes to monitor eye blinks and eye movement.

[1] http://www.compumedics.com/ and http://www.neuroscan.com/

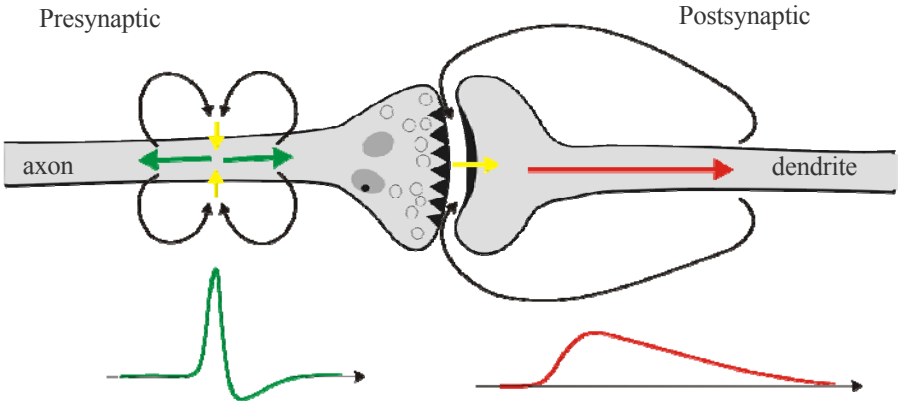

Figure 4-5. Electric Currents in Axons and Dendrites: Neurons create action potentials, which are discrete electrical signals that travel down axons and cause the release of chemical neurotransmitters at the synapse. This neurotransmitter then fits into a receptor in the dendrite of the post-synaptic neuron. When combined with the receptor, the neurotransmitter causes an electrical current within the dendrite of the post-synaptic neuron. Action potentials (green curve) are short lived with rapidly diminishing fields, whereas postsynaptic potentials (red curve) act like "small batteries" that contribute to the scalp EEG. Adapted from (Elekta Neuromag® MEG System Description, 2006).

Figure 4-6. Recording of the EEG: A 66-channel EEG cap with Ag/AgCl electrodes; a high chloride, abrasive electrolyte gel is inserted in each electrode location to achieve a DC-stable skin-gel contact for stable operation of the electrodes. Electrodes attached below the eyes for recording of the EOG.

4.2.2. Magnetoencephalography (MEG)

MEG reflects the neurophysiological measurements of the minute magnetic field generated by the electrical activity of neurons, as illustrated in Figure 4-3. The signals from a MEG system derive from the net effect of ionic currents flowing in the dendrites of neurons during synaptic transmission. These net currents (generated by more than 50,000 neurons for detectable signals) form current dipoles, each having an associated position, orientation and magnitude but no spatial extent, which in turn produce an orthogonally oriented magnetic field (in accordance with Maxwell's equations) that flows around the axis of its vector component (by Fleming's right hand rule), as illustrated in (Figure 4-7). As with EEG, MEG has a real-time resolution (in the order of ms) but can provide a higher spatial resolution (in the order of mm) especially when coupled with structural models for accurate source analysis (Malmivuo and Plonsey, 1995). This is because the homogenous conductivity of MEG is not distorted by the scalp, skull, brain and cerebrospinal fluid.

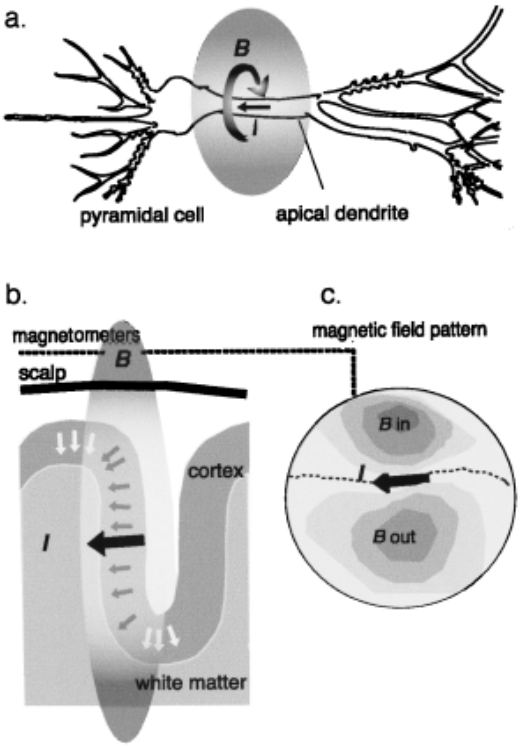

Figure 4-7. EM activity of the central nervous system captured by MEG: (a) The intracellular current in the apical dendrite of a pyramidal cell is associated with a surrounding magnetic field B. (b) The tangential currents contribute to the magnetic field detected by the SQUIDs. (c) Top view of a dipolar magnetic field pattern (Malmivuo and R. Plonsey, 1995).

MEG uses extremely sensitive magnetometers known as superconducting quantum interference devices (SQUIDS) that measure the strength of the magnetic field at a number of points around

the head. These devices have noise levels as low as 3 $fT \cdot Hz^{-½}$ and act as low-noise, high-gain, current-to-voltage converters that give the MEG system the ability to detect neuromagnetic signals of only a few (10-100) femtoTesla (fT). They are immersed in liquid helium to superconducting temperatures (-269 ºC) and lie at a distance of 3-4 cm from the cortex (Paetau, 2002). Field distribution is sampled by pick-up loops at distinct locations which are configured into a large number of channels (≈300) using, for instance, triple sensor elements comprising two planar gradiometers and one magnetometer (Figure 4-8). Such high density systems can provide whole-head coverage that enables the mapping of activity throughout the cerebral cortex, or beyond – this is critical for detecting propagating or widespread epileptic activity for example (Ulmer and Jansen, 2010).

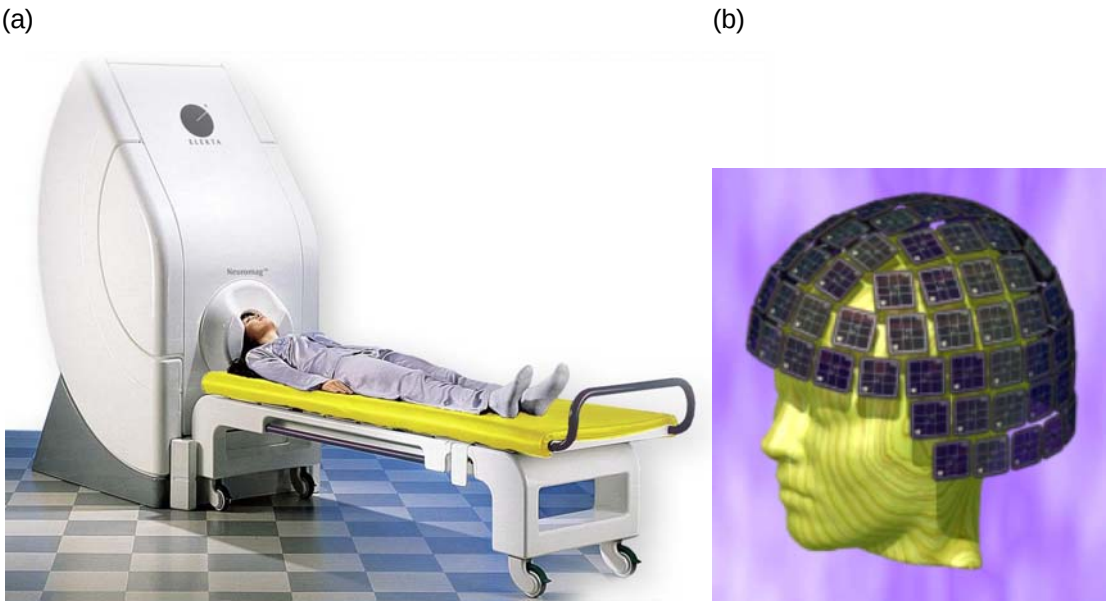

Figure 4-8. Magnetoencephalography, Elekta Neuromag®: (a) The MEG system; (b) 306-sensor SQUID sensor array, each sensor consists of two planar gradiometers and one magnetometer (Elekta Neuromag® MEG System Description, 2006).

In order to reduce the magnetic noise reaching the bio-magnetometer from various sources such as the earth's steady magnetic field (≈ 10^{-5} T) and environmental noise fields (≈ 10^{-7} T), the MEG system is operated in a magnetic and radio-frequency shielded room made of mu-metal and aluminium. State of the art MEG systems passively dampen the interference by excellent wall structures and feedback coils located inside and outside the room; any remnant interfering field is measured and actively cancelled by noise cancellation algorithms (Ulmer and Jansen, 2010). Head motion can severely compromise the quality of the MEG signals especially in recordings of infants and patients suffering from pathologies such as Parkinson's disease and epilepsy. New MEG models comprise continuous head position monitoring, whereby four or five head position

indicator coils are attached to the subject's head and digitized. During the recording each coil is energized continuously with sinusoidal signals that have different frequencies outside the frequency range of the signals of interest such that the measured magnetic field is the sum of the brain activity and the signals from the coils. The head positions with respect to the sensor array are computed offline at selected intervals and the data is then transformed to a static reference head position (Elekta Neuromag® MEG System Description, 2006).

The major limitation of MEG is that the localisation of the underlying brain sources of electrical activity from the scalp magnetic measurement is complicated and does not have a unique solution – the so-called *ill-posed inverse problem*. *A priori* constraints imposing assumptions on the solution (based on its mathematical nature, and according to anatomical and physiological knowledge) are commonly employed to evaluate a stable inverse solution (Ye and Hu, 2005). Standardized and exact low resolution brain electromagnetic tomography (sLORETA and eLORETA), equivalent current dipoles and synthetic aperture magnetometry are a few of the solutions proposed in the literature (Darvas *et al*., 2004).

4.3. EEG and MEG Systems

Cheap instrumentation coupled with modest site requirements, make mobile, long-term recordings easier to achieve through an EEG system. Moreover, EEG can extract both radial and tangential sources (while MEG has only a tangential field pattern) and deep sources have a stronger contribution than in MEG. On the other hand, MEG requires a much quicker setup since no electrodes need to be fitted. DC and VLF signals are easier to measure with MEG and the recordings are less susceptible to muscle artifacts. Due to its higher spatial resolution, brain sources are easier to estimate because details of the conductivity geometry and actual conductivity values have a small effect on the recordings. Moreover, in contrast to scalp EEG, MEG is reference-free – this is a remarkable advantage because an active reference can lead to serious difficulties in the interpretation of EEG data.

Both systems have been extensively used to study cognition and for condition monitoring to aid the prognosis and diagnosis of neuronal pathologies. Epilepsy is a major area of application for EEG – long recordings are often collected in Epilepsy Monitoring Units in order to asses the patient's condition, localise seizure foci prior to surgery, characterise seizures for purposes of treatment, and for predicting seizure onsets (Jerger *et al*., 2001; Gupta *et al*., 2008). Deep brain stimulation for Parkinson's disease**,** localisation of brain tumours and monitoring of the depth of

anaesthesia in surgical wards, are amongst the vast range of applications of EEG. Particular features within the EEG are also being exploited to control BCI (Wang and James, 2007). In addition, EEG and MEG studies assist in the investigation of how normal processes are affected in neuronal and biobehavioural disorders, such as schizophrenia, Alzheimer's disease, autism and ADHD, to distinguish clinical from control groups (Georgopoulos *et al*., 2007).

Finally, it is worth mentioning that the understanding of how the signals obtained from neuorimaging and electrophysiology relate to each other, is a fundamental problem. For instance, one might assume that increased signal in EEG or MEG would be positively correlated with an increase in fMRI BOLD, but this is not always the case. This is partly due to the fact that the EM response is a weighted sum of the postsynaptic potentials in the brain occurring on a millisecond scale, whereas the BOLD signal is a hemodynamic response resulting from a convolution over several seconds of the temporal mean of cortical activity (Ulmer and Jansen, 2010). Furthermore, it is conceivable that some activity patterns picked up by the EEG are not visible in the BOLD signal, and vice versa (Nunez and Silberstein, 2000). The same can be said for EEG and MEG – both methodologies reflect synchronous activity of pyramidal neurons, but both measures are differently sensitive to the orientation and distance of neural sources. Moreover, about 20% of all grey matter neurons are of non-pyramidal type and express metabolic activity that may be well reflected in the BOLD signal, but not in EEG or MEG. MEG and EEG signal amplitudes depend on (amongst other biophysical properties) the number, orientation, and on the synchronisation of pyramidal neurons, but the latter effect may not be well represented in the BOLD signal. More multimodal research is definitely required; current progress in the field of simultaneous EEG-fMRI research shows promising results which may aid in establishing a more complete understanding of the precise relationship between the evoked neuro-electric and magnetic response and the BOLD signal (Debener *et al*., 2006; for review see Herrmann and Debener (2008); Mulert and Lemieux, 2010).

4.4. Summary

In this chapter the different neuroimaging methods available to neuroscience have been briefly introduced as vital windows into the human brain. Functional neuroimaging techniques, in particular fMRI-BOLD imaging, enable the precise localisation of the metabolic activity and blood flow changes that follow neural activity. The identification of functional foci within the brain could greatly improve surgical planning for epilepsy and tumor dissection, and potentially for deep brain stimulation. Meanwhile, electro- and magneto- physiological systems (EEG and MEG) capture the fluctuating electric and magnetic fields (measured at the scalp or near the

head), and provide 'direct' information on electrical events within the brain in a non-invasive manner. For these reasons, they could shed light on how neuronal populations interact and undergo self-organising processes to form dynamical assemblies for the execution of higher-order functions such as thought, perception, memory and action. Lastly, multimodal research comprising fMRI and EEG/MEG can play a significant role in improving our understanding of brain activity by exploiting the advantages of both modalities, namely the high temporal resolution of EEG/MEG and the better spatial coverage available from fMRI.

Further chapters in this work focus on the signal processing methodologies carried out on EEG and MEG data to examine VLF neuronal activity. In particular, the next chapter gives a detailed description of the ICA algorithms for the analysis of EM recordings.

Chapter 5

ICA FOR NEUROPHYSIOLOGICAL SIGNAL ANALYSIS

This chapter describes the ICA techniques, particularly single-channel and space-time ICA, for the analysis of neurophysiological signal recordings. These are used for the first time in this work to investigate the slow waves in EM data; hence a thorough grasp of the decomposition process underlying each method is fundamental to this work. For this reason, these algorithms were first applied to readily available and well-labelled epileptic seizure EEG data for better understanding of this recently-introduced framework whereby source analysis is undertaken through the use of temporal or spatio-temporal information.

5.1. Background

The EEG and MEG systems described in Chapter 4 are valuable tools that allow insight into the human brain; in essence they provide recordings of sets of signals which are the result of brain function added to other physiological (ocular, muscular and cardiac) and ambient (environmental electric and magnetic disturbances) artifacts (Vigario *et al*., 2000; James and Hesse, 2005; James and Gibson, 2005). These artifacts may have higher amplitudes than those of active brain sources of interest, and their resemblance to neural responses may also lead to misinterpretation of the data. Hence, it is required to efficiently isolate meaningful neurophysiological sources from the recorded (mixed) signals. As explained in Chapter 3, ICA – a BSS technique for the extraction of statistically independent components from a set of sensor measurements – has been extensively used for the analysis of EM brain signals (Makeig *et al*., 1997; Vigario *et al*., 1998; Kobayashi *et al*., 1999; Jung *et al*., 2001b; Muller *et al*., 2004), as well as other biomedical signals (McKeown *et al*., 1998; Comani *et al*., 2004; Mantini *et al*., 2006), and other signal types altogether (Back and Weigend, 1997; Torkkola, 1999).

ICA on multiple-recording channels, in its basic form, achieves the separation of *spatially* distinct sources due to the fact that multiple-recording channels usually have a distinct spatial organisation. It does this through the assumption of statistical independence of the underlying sources and is therefore more powerful in the separation process than classical methods such as principal component analysis (PCA) which is based on decorrelation (second order statistics) of the sources (Shlens, 2003). Multi-channel ICA is usually applied to ensemble time series measurements – here this is called *ensemble ICA* (E-ICA) – and in practice, the observed time series are generally a band-limited mixture of the signals of interest corrupted by noise. However, in recent years, a new technique – single channel ICA (SC-ICA) – has been introduced, which can be applied to extract underlying sources from a single recording channel by using only the *temporal* information inherent in the signal dynamics (Hyvärinen *et al*., 2001 pp. 355–370; James and Lowe, 2003; Davies and James, 2007). This algorithm has been employed to extract epileptic seizure components from noisy EEG data (James and Lowe, 2000; James and Hesse, 2005; James *et al*., 2006), as well as foetal heart sounds from noisy abdominal phonograms (Jiménez-González and James, 2009). Both E-ICA and SC-ICA make different underlying assumptions for the separation process and result in differing capabilities for both algorithms.

The natural extension of the SC-ICA algorithm comes in the form of Space-time ICA (ST-ICA) whereby SC-ICA is in effect applied to a number of recording channels, hence providing both temporal *and* spatial information to inform the ICA process (James *et al*., 2007; James, 2008). This is a specific form of BSS that exploits the rich, dynamical time structure of electrophysiological data as well as the multi-channel nature of the recordings. Consequently, it is able to extract underlying temporal generators within the data by analyzing fewer channels distributed across the scalp (James, 2008). ST-ICA has been successfully applied to ictal (seizure) EEG data (James *et al*., 2008), and BCI data (Davies *et al*., 2007). The cost of adding more channels, (hence providing more information to the ST-ICA algorithm), is a greater processing load, as well as issues related to the assumed number of underlying sources being far less than the number of measurement channels – this problem is compounded in ST-ICA.

In this chapter the theory behind E-ICA and SC-ICA is outlined, followed by an explanation of the augmented ST-ICA algorithm. The SC- and ST-ICA methods are illustrated on a segment of epileptic seizure data since the morphology of ictal sources is well recognised and explained in the literature (Kobayashi *et al*., 1999; James and Lowe, 2000; James, 2008). In the EEG, seizures (sudden disturbances in brain activity) are manifest predominantly as rhythmic activity which can be distributed as focal, multi-focal or generalised across the recording channels. Seizure

activity is an appropriate candidate for ICA techniques because this activity is superimposed onto the background EEG and its separation from ongoing activity and artifacts is generally beneficial for the diagnosis and prognosis of the patient's condition. Particularly, spatio-temporal techniques such as ST-ICA are of great clinical relevance for this pathology since the multi-dimensional nature of the recordings, in addition to the rich dynamical time structure of EEG data, can be used to track changes in the spatial distribution and morphology of the epileptic sources over time – two very useful pieces of information for epileptologists (James *et al*., 2007; James, 2008).

5.2. Ensemble ICA (E-ICA)

E-ICA (which can also be referred to as spatial ICA) represents the 'standard' ICA procedure which is often employed in the literature for physiological data analysis (James and Hesse, 2005), feature extraction, audio signal processing (Torkkola, 1999), and for decomposing ER brain signals (Makeig *et al*., 1997; Muller *et al*., 2004). In this model, the sensor measurements $\boldsymbol{x}(t) = [x_1(t), ..., x_n(t)]^T$, obtained, say, from an EEG or MEG system, are assumed to be made up of a linear instantaneous mixture of independent sources, $\boldsymbol{s}(t) = [s_1(t), ..., s_b(t)]^T$, such that

$$\boldsymbol{x}(t) = \boldsymbol{A}\boldsymbol{s}(t) + \boldsymbol{n}(t), \tag{5.1}$$

where $\boldsymbol{A}$ denotes the $[n \times b]$ mixing matrix and $\boldsymbol{n}(t)$ is additive sensor noise (generally assumed to be spatially or temporally white noise, or temporally coloured noise) corrupting the measurements $\boldsymbol{x}(t)$. In this general case a linear solution is possible if the mixing matrix is full column rank and the number of observations is greater than the number of source signals ($n>b$) (Hyvärinen, 2001). A schematic representation of the ICA method is given in Figure 5-1.

To simplify the extraction process it is further assumed that the mixing is square, linear and noiseless ($\boldsymbol{n}(t)=0$), and that both the source signals and the mixing process are stationary. Most importantly, the input data are assumed to be a linear and instantaneous mixture of mutually independent source signals. This means that each source is generated by a random process which is independent of the random processes generating other sources. Provided that these conditions are fulfilled, ICA produces an unmixing matrix $\boldsymbol{W}$ in order to demix the measurements and provide an *estimate*, $\hat{\boldsymbol{s}}(t)$, of the independent sources, $\boldsymbol{s}(t)$. This can be expressed by

$$\boldsymbol{y}(t) = \hat{\boldsymbol{s}}(t) = \boldsymbol{W}\boldsymbol{x}(t), \tag{5.2}$$

such that $\boldsymbol{y}(t)$ contains the independent components (Comon, 1994; Hyvärinen and Oja, 2000; Stone, 2004:2005). Note that ICA arrives at an intermediate level (a thinner sphere of influence)

between the brain sources and the measured signals such that the recovered components are as independent as possible, and are not *necessarily* actual brain sources.

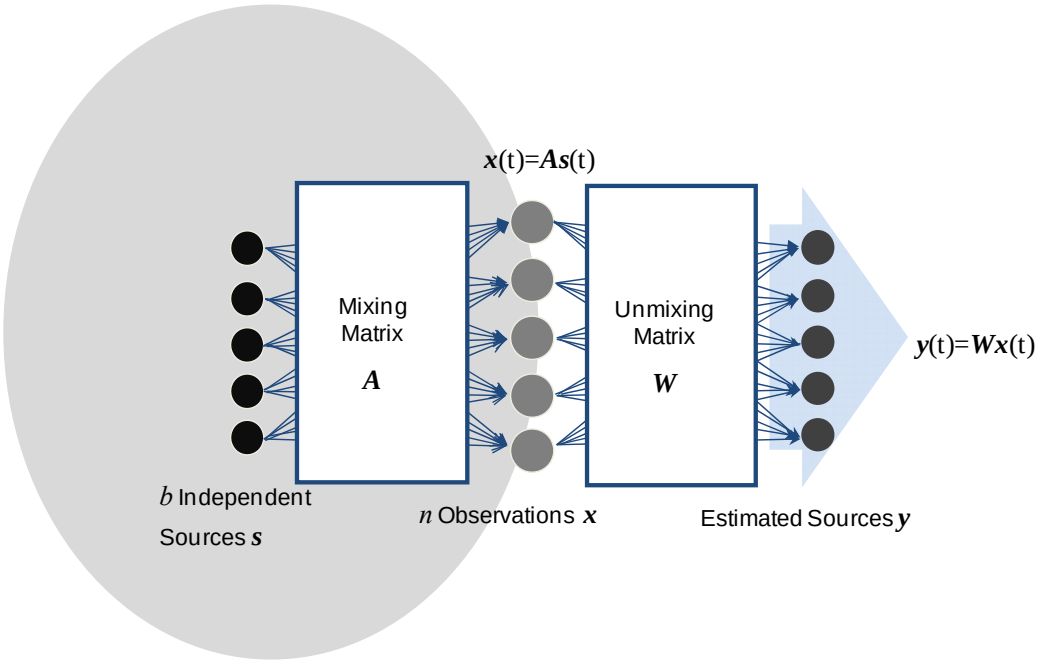

Figure 5-1. Schematic representation of the general ICA process: The sensor observations $\boldsymbol{x}(t)$ are assumed to be linear mixtures of the independent sources $\boldsymbol{s}(t)$. ICA learns an unmixing matrix $\boldsymbol{W}$ ($\boldsymbol{W} = \boldsymbol{A}^{-1}$) to demix the measurements, hence providing an estimate of the independent sources $\boldsymbol{y}(t)$.

Centering and whitening are usually performed prior to ICA in order to make the ICA estimation problem simpler and better conditioned (Hyvärinen and Oja, 2000; Vigario *et al.*, 2000). Centering changes the observed vector x_i into a zero-mean variable by subtracting its mean, $v_i = E\{x_i\}$, from x_i. After estimating $\boldsymbol{A}$ with centered data, the mean of $\boldsymbol{s}$, given by $\boldsymbol{A}^{-1}\boldsymbol{v}$, can then be added to the centered estimates of the sources. The centered signals are then linearly transformed to obtain $\tilde{\boldsymbol{x}}$, a set of measurements which are uncorrelated and their variances equal to one. This procedure is referred to as whitening or sphering, and implies that the covariance matrix of $\tilde{\boldsymbol{x}}$ becomes equal to the identity matrix

$$E\left\{\tilde{\boldsymbol{x}}\tilde{\boldsymbol{x}}^T\right\} = \mathbf{I}\,. \tag{5.3}$$

Whitening is often achieved by means of an eigen decomposition of the covariance matrix

$$E\left\{\boldsymbol{x}\boldsymbol{x}^T\right\} = \mathbf{E}\mathbf{D}\mathbf{E}^T\,, \tag{5.4}$$

where $\mathbf{E}$ is the orthogonal matrix of eigenvectors of $E\left\{\boldsymbol{x}\boldsymbol{x}^T\right\}$ and $\mathbf{D}$ is the diagonal matrix of its eigenvalues, $\mathbf{D} = \mathrm{diag}(\lambda_1,...,\lambda_n)$. The whitening vector is then given by

$$\tilde{\boldsymbol{x}} = \mathbf{E}\mathbf{D}^{-1/2}\mathbf{E}^{\mathrm{T}}\boldsymbol{x}\,, \tag{5.5}$$

where $\mathbf{D}^{-1/2} = \mathrm{diag}\left(\lambda_1^{-1/2},...,\lambda_n^{-1/2}\right)$.

This whitening transformation is generally possible (given that $\boldsymbol{x}$ is full rank, i.e. none of its eigenvalues are zero), and is useful since it transforms the original mixing matrix into a new orthogonal mixing matrix

$$\tilde{\boldsymbol{x}} = \mathbf{E}\mathbf{D}^{-1/2}\mathbf{E}^{\mathrm{T}}\boldsymbol{A}\boldsymbol{s} = \tilde{\boldsymbol{A}}\boldsymbol{s}\,. \tag{5.6}$$

Since $\tilde{\boldsymbol{A}}$ is orthogonal, whitening reduces considerably the number of parameters to be estimated, (say for an $n \times n$ mixing matrix one only needs to estimate $n(n-1)/2$ parameters). Further simplification following the whitening procedure can be made by discarding the eigenvalues of $E\left\{\tilde{\boldsymbol{x}}\tilde{\boldsymbol{x}}^T\right\}$ which are too small – this has the effect of reducing noise and preventing overlearning (Hyvärinen and Oja, 2000). Note that for the rest of this chapter it is assumed that $\boldsymbol{A}$ and $\boldsymbol{x}$ are pre-processed, hence the tildes are omitted.

In most popular implementations of ICA one restriction is that in order for $\boldsymbol{A}$ to be identifiable, the statistical distributions of each source must be non-Gaussian; in practice exactly one IC is allowed to be Gaussian (Hyvärinen *et al*., 2001). Consequently, the search for independent sources is replaced by a search for non-Gaussian sources and the ICs are extracted by maximizing the non-Gaussianity of $\boldsymbol{W}\boldsymbol{x}(t)$. Higher order statistics (HOS) techniques which implement ICA in this way use measures such as kurtosis, negentropy, mutual information and maximum likelihood to quantify the non-Gaussianity and hence find linear projections within the data that maximise the independence of the sources (Hyvärinen, 1999a,b; Hyvärinen *et al*., 2001). Infomax (Bell and Sejnowski, 1995), JADE (Muller *et al*., 2004) and FastICA (Hyvärinen, 1999b) are amongst the most popular ICA algorithms developed over the years and all are HOS-based. FastICA, which achieves the identification of non-Gaussian sources by maximizing the norm of the kurtosis (the fourth order cumulant) is used extensively due to its ease of implementation, and its speed and stability of convergence. This has been recently refined as Robust ICA (Baloch *et al*., 2005; Zarzoso and Comon, 2007).

5.2.1. Time Structure Based Methods

An alternative approach to ICA considers the time structure of the input data. This has several advantages when compared to HOS-based methods; here the ICs need not be Gaussian and

shorter sensor observations with fewer samples than that required for HOS techniques can be successfully decomposed (Hyvärinen *et al*., 2001; James and Hesse, 2005).

The basic aim of this approach is to capture the dependency structure of the observed sources using a stack of matrices. The de-mixing matrix would then be the joint diagonaliser of the stack

$$\mathbf{C}_s^k = \boldsymbol{W}\mathbf{C}_x^k\boldsymbol{W}^T, \tag{5.7}$$

where $\mathbf{C}_x^k$ is the k^{th} covariance matrix of the data $\boldsymbol{x}$, $\mathbf{C}_s^k$ is the corresponding covariance matrix of the sources $\boldsymbol{s}$ and $\boldsymbol{W}$ is the de-mixing matrix (Figure 5-2). The assumption here is that independent sources underlying the measurements do not have any spatial-temporal or spatial time-frequency correlations. This implies that $\mathbf{C}_s^k$ should be diagonal and therefore, the coefficients of $\boldsymbol{W}$ can be optimised in such a way as to make this matrix as diagonal as possible. The sum of the squared off-diagonal elements is used as a diagonality measure. Note that the index k is a pointer into the matrix stack and can have different interpretations depending on the quantities being measured (James and Hesse, 2005).

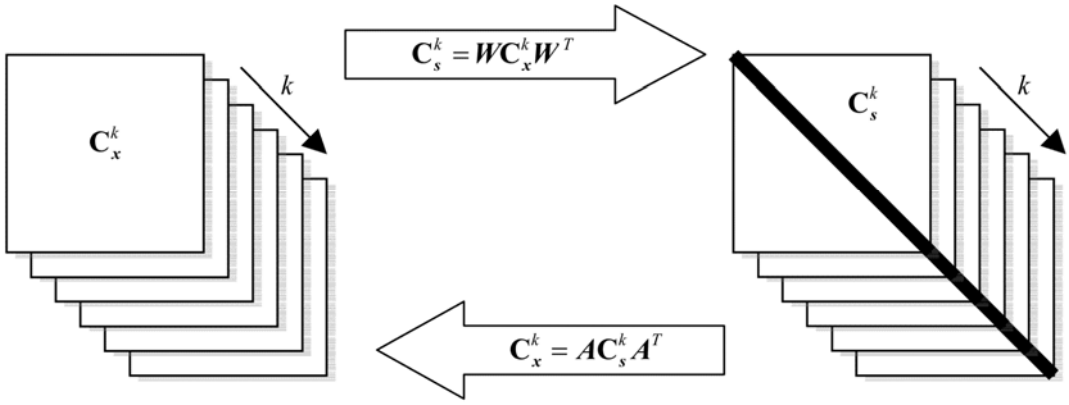

Figure 5-2. The relationship between the two covariance matrix stacks $\mathbf{C}_x^k$ and $\mathbf{C}_s^k$. The mixing matrix $\boldsymbol{A}$ links the covariance stack of matrices of the sources to the measurements stack, while $\boldsymbol{W}$ links the two stacks in the opposite direction. Adapted from (James and Hesse, 2005).

The simplest form of time structure is given by the covariance of the signal at different time points – this forms the basis of *ICA by temporal decomposition*. Temporal decorrelation source separation (TDSEP) algorithm developed by Ziehe and Müller (1998) is another popular ICA technique based on this principle.

A. TDSEP ICA

This is a specific time structure based ICA method which assumes a well-defined autocorrelation of the underlying sources ***s***. Here, a cost function *l* is defined as

$$l\left(\mathbf{C}_{ij}\right)=\sum_{i\neq j}\left\langle y_i(t)\,y_j(t)\right\rangle^2+\sum_{k=1}^{\hat{N}}\sum_{i\neq j}\left\langle y_i(t)\,y_j(t+\tau_k)\right\rangle^2, \tag{5.8}$$

where τ is a time lag, the choice of which is crucial since it needs to ensure that the $\hat{N}$ delayed correlation matrices carry maximally different information, and $\langle\ \rangle$ denotes a time average.

The cost function is then minimized with respect to **C**, using for example, the method of gradient descent, $\Delta\mathbf{C}\propto-\eta\,\partial l/\partial\mathbf{C}$ (where η is the learning rate), in order for the cross-correlations between the output signals to vanish. However, this is computationally expensive especially when the number of sources is large (Ziehe and Müller, 1998).

Therefore, the following procedure involving whitening and joint diagonalisation of the covariance matrices is implemented instead:

(i) A sample estimate of the correlation matrix for the observed signals is defined as $\mathbf{C}_{\tau(x)}=\left\langle \boldsymbol{x}(t)\boldsymbol{x}(t-\tau)^T\right\rangle$.

(ii) Whitening is performed such that the first term of the cost function in equation (5.8) is set to zero.

The whitening transform **T** is determined by PCA or by taking the inverse square root of the covariance matrix by means of an eigenvalue decomposition (previously explained),

$$\mathbf{T}=\mathbf{C}_{(\boldsymbol{x})}^{-1/2}=\left(\mathbf{V}\Lambda\mathbf{V}^T\right)^{-1/2}=\mathbf{V}\Lambda^{-1/2}\mathbf{V}^T. \tag{5.9}$$

This transforms the sensor observations ***x*** to a transformed signal ***z*** in a new basis.

(iii) The transformation matrix is then estimated by several Jacobi rotations.

Following whitening, any time delayed correlation matrices for ***z*** should be approximately diagonal up to a transformation **R**. This rotation matrix is orthogonal $\left(\mathbf{I}=\mathbf{R}\mathbf{R}^T\right)$ and, for the case of τ = 2, it can be obtained by eigenvalue decomposition of the time-delayed correlation matrix such that

$$\mathbf{C}_{\tau(\boldsymbol{z})}=\left\langle \boldsymbol{z}(t)\boldsymbol{z}(t-\tau)^T\right\rangle=\mathbf{R}^T\mathbf{C}_{\tau(\boldsymbol{s})}\mathbf{R}=\mathbf{R}^T\Lambda_\tau\mathbf{R}. \tag{5.10}$$

For τ>2, **R** can be approximated by a sequence of elementary rotations (a.k.a. Jacobi rotations), $J_k\left(\phi_k\right)$, each aiming to minimise the off-diagonal elements of the respective correlation matrices. The final rotation is then obtained by $\mathbf{R}=\prod_k J_k\left(\phi_k\right)$.

This procedure results in an estimate of the mixing matrix as follows

$$\hat{\mathbf{A}} = \mathbf{T}^{-1}\mathbf{R} . \tag{5.11}$$

A further simplification of step (iii) is possible by taking the average over the set of delay matrices, $\tau_k \left(k = 1,...,\hat{N}\right)$, $\mathbf{C}_{avg} = \frac{1}{\hat{N}} \sum_{k=1}^{\hat{N}} \mathbf{C}_{\tau_k(z)}$. This averaged correlation matrix is then used to compute one rotation **R** instead of taking several rotations $J_k\left(\phi_k\right)$ for every lagged correlation matrix. This gives a crude approximation to the actual minimization of the cost function *l* but it proves to be very efficient especially in high dimensional problems (Ziehe and Müller, 1998).

One issue with this algorithm is the appropriate choice of the number of time lags to use in order to capture the spatio-temporal covariance of the data; this is usually set through empirical observation (James and Hesse, 2005). Other time structure based methods include *ICA by sub-band decorrelation* – where the time structure in different frequency bands is exploited (Cichocki and Belouchrani, 2001), and *ICA by time-frequency decorrelation* – representing the signals dependency structure in terms of their spatial time-frequency distributions (Amin and Belouchrani, 1998).

Finally, note that all these ensemble-ICA techniques make use of spatial information from the physical arrangement of the recording sensors in the separation process. Therefore, the columns of the mixing matrix ***A*** represent a set of spatial filters derived from multi-channel observations, and hence the extracted sources must have different spatial profiles for them to occupy distinct columns of ***A***. This implies that sources with non-distinct or completely overlapping spatial distributions cannot be resolved by E-ICA.

5.3. Single Channel ICA (SC-ICA)

The possibility of extracting multiple underlying sources from single channel recordings starts with the assumption that the brain can be modelled as a dynamical system, its dynamics residing on some unobservable manifold embedded in the phase space. A relatively small number of underlying generators contribute to this unobservable manifold, such that measured brain signals are the result of nonlinear interactions of just a few degrees of freedom with additive noise (James and Lowe, 2000:2001 and 2003; Woon and Lowe, 2004). Takens' theorem allows for the reconstruction of the unknown dynamical system that generated the measured time series through the formation of a new state space based on successive observations of the time series (Takens, 1981).

This can be achieved by constructing a matrix $\boldsymbol{Q}$ of delay vectors V_k, for consecutive values of k, from the scalar time series $x(t)$

$$V_k = \left[x_k, x_{k+\tau}, \ldots, x_{k+(m-1)\tau} \right]^T,$$

$$\boldsymbol{Q} = \begin{bmatrix} x_k & x_{k+\tau} & \cdots & x_{k+N\tau} \\ x_{k+\tau} & x_{k+2\tau} & \cdots & x_{k+(N+1)\tau} \\ \vdots & \vdots & \ddots & \vdots \\ x_{k+(m-1)\tau} & x_{k+m\tau} & \cdots & x_{k+(m+N-1)\tau} \end{bmatrix}, \tag{5.12}$$

where τ is a lag term (usually set to 1 for simplicity), N is the vector length which must be set such that $\boldsymbol{Q}(t)$ covers a quasi-stationary signal, and m is the number of delay vectors (a.k.a. the embedding dimension). This has to be large enough to capture the signal dynamics and if the time series data is heavily correlated, then more time series samples are needed to make up the required information content of the delay vector (James and Lowe, 2003). If the acquired data has a sampling rate, f_s, that is set according to the Nyquist criterion, the practical minimum size for m can be approximated based on the lowest frequency of interest in the measured signal, f_L, such that (James and Lowe, 2001)

$$m \geq f_s / f_L . \tag{5.13}$$

This method is generally known as the *method of delays* (Broomhead and King, 1986) as illustrated in Figure 5-3.

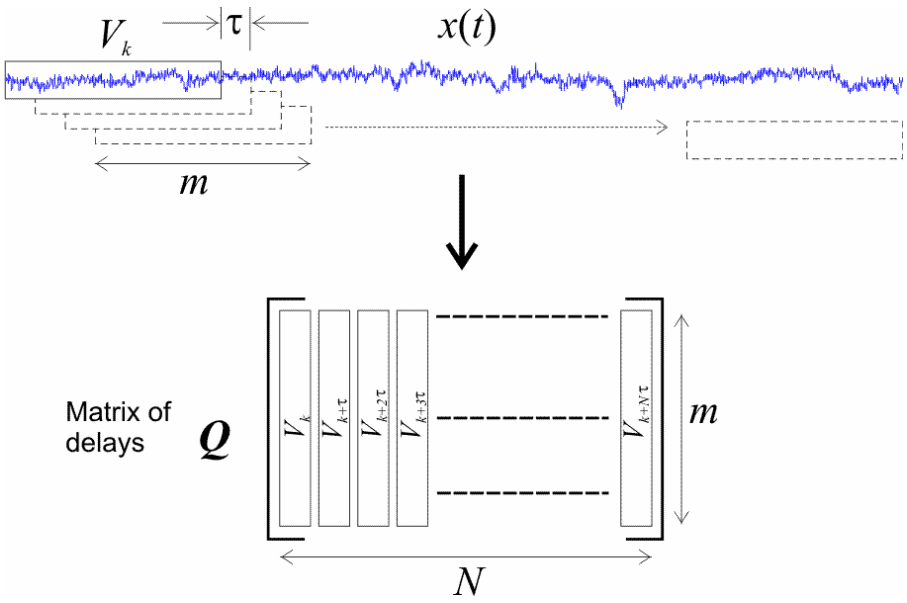

Figure 5-3. Method of Delays: A multidimensional representation of the measured signal $x(t)$ is achieved by constructing a matrix $\boldsymbol{Q}$ of delay vectors V_k, for consecutive values of k, from $x(t)$. N is the number of samples per channel, τ is the lag term and m is the number of delay vectors.

Each delay vector V_k represents a point on the system manifold and together all the columns of the delay matrix $\boldsymbol{Q}(t)$ trace a trajectory on this manifold generated by the Euclidean embedding (James and Lowe, 2003). This trajectory can be spanned with an appropriate basis (such as ICA) in an attempt to extract and interpret the underlying sources in the delay matrix. Note that the mapping of a scalar time series onto a multidimensional model implies that the sources can only be successfully identified provided that they have disjoint spectral support, i.e. non-identical magnitude frequency responses. This is equivalent to learning a set of filters to discriminate between data components with distinct frequency responses. Consequently, when ICA is applied to $\boldsymbol{Q}(t)$ it learns a mixing matrix $\boldsymbol{A}$, the columns of which contain sets of finite impulse response (FIR) filters and shifted versions of the same filters.

We recall that in 'standard' ICA, $\boldsymbol{x} = \boldsymbol{A}\boldsymbol{s}$ where $\boldsymbol{A} = \left[A_1, ..., A_n \right]$, and the vectors A_i form a basis in the signal space in such a way that an inverse equation can be uniquely defined as $\boldsymbol{s} = \boldsymbol{W}\boldsymbol{x}$, where $\boldsymbol{W} = \boldsymbol{A}^{-1}$ and $\boldsymbol{s}$ is the matrix of underlying independent sources s_i. Thus, source separation *and* reconstruction in the observation domain can be achieved by the application of an unmixing and mixing pair

$$\boldsymbol{x}_s^i = \boldsymbol{A}_{(:,i)}\boldsymbol{W}_{(i,:)}\boldsymbol{x}\,, \tag{5.14}$$

where $\boldsymbol{x}_s^i$ is the i^{th} source projected back onto the measurement space.

It can be shown that for the temporal model represented by $\boldsymbol{Q}(t)$, this procedure actually translates to

$$x_s^i(t) = \frac{1}{m} a_i(-t) * w_i(t) * x(t)\,, \tag{5.15}$$

which is equivalent to passing $x(t)$ through a set of separating filters f_p, ($*$ denotes convolution). For each source p, the corresponding filter is then given by

$$f_p(t) = \frac{1}{m} a_i(-t) \;*\; w_i(t)\,, \tag{5.16}$$

where $a_i(t)$ is the FIR filter associated with the column of $\boldsymbol{A}(:,i)$ and $w_i(t)$ is the FIR filter associated with the row of $\boldsymbol{W}(i,:)$. If we assume that the signal has been pre-whitened, then $a_i(t)=w_i(t)$ since $\boldsymbol{W}$ is orthogonal, and the filters become symmetric around $t=0$ and have zero phase. Note that spatial pre-whitening in standard ICA translates to temporal pre-whitening in SC-ICA (Davies and James, 2007).

5.3.1. Independent Mixtures of Processes in SC-ICA

The main question that arises from the above explanation is whether or not the extracted sources $x_s^i(t)$ would be independent. Cardoso (1998) has shown that a random *n*-dimensional vector $\boldsymbol{x}$ admits a multi-dimensional ICA (MICA) decomposition into *C* components if there exist *C* linearly independent component subspaces, $\{E_1,...,E_C\}$ of $\Re^n$, on which the linear components of $\boldsymbol{x}$ are statistically independent. This decomposition can be obtained by 'standard' ICA, by first estimating one-dimensional components and then grouping them based on dependency. Thus, the mixing matrix $\boldsymbol{A}$ can be organised into a set of *C* submatrices, $\boldsymbol{A} = [A_1,...,A_C]$, where A_p spans subspace E_p. Consequently, MICA presents an appropriate model for SC-ICA.

Here it is assumed that the scalar time series $x(t)$ can be decomposed into the sum of mutually independent random processes, $x_p(t)$, such that

$$x(t) = \sum_p x_p(t), \tag{5.17}$$

where each $x_p \in \Re^m$ is the p^{th} multi-dimensional component spanned by an n_p-dimensional subspace E_p and the set $\{E_1,...,E_C\}$ are assumed to be linearly independent of each other.

It is further supposed that each stochastic process $x_p(t)$ is a filtered independent identically distributed random process

$$x_p(t) = h_p(t) * s_p(t), \tag{5.18}$$

where $h_p(t)$ is an FIR filter of length *M*.

If the time series is represented as an *m*-dimensional delay matrix $\boldsymbol{Q}(t)$, as in equation (5.12), then equation (5.17) can be written as $\boldsymbol{Q}(t) = \sum_p \boldsymbol{H}_p \boldsymbol{s}_p(t)$ where $\boldsymbol{H}_p$ is the Toeplitz matrix associated with filter $h_p = \left[h_p(0),...,h_p(M-1)\right]^T$ and

$\boldsymbol{s}_p(t) = \left[s_p(t), s_p(t-1)..., s_p(t-m-M+2)\right]^T$, (Davies and James, 2007).

Now, for a single source, solving for $s_1(t)$ (i.e. C =1) is the blind deconvolution problem. When full ICA is applied to $\boldsymbol{Q}(t)$, it provides a full unmixing matrix $\boldsymbol{W}$, the rows of which consist of *m* approximate shifted versions of the deconvolution filter. If one assumes that there are multiple

components, each h_p is non-invertible and each corresponding matrix $\boldsymbol{H}_p$ is rank deficient, i.e. its columns only span a subspace E_p in $\Re^m$, then the vectors $\boldsymbol{Q}_p(t) = \boldsymbol{H}_p \boldsymbol{s}_p(t)$ lie in this subspace. Moreover, if all the subspaces, $\{E_p\}$, are linearly independent then this becomes a valid MICA model.

Therefore, ICA can decompose any such SC-ICA process into basis vectors a_i which can be grouped into C subsets δ_p that span the independent subspaces E_p, (i.e. if $i \in \delta_p$, then $a_i \subset E_p$). Now these basis vectors spanning E_p are shifted approximations of the generating filter h_p, implying that all the basis vectors associated with the subset δ_p will have very similar spectral support. On the other hand, the other basis vectors (filters) will have a disjoint spectral support, and so components can be grouped based on the transfer function of their corresponding generating filter. This implies that individual independent processes can be identified and obtained by computing the summation of the contributions from the separate ICA components. Each component contribution can be estimated using the filter defined in equation (5.16). This renders the following estimate for $x_p(t)$,

$$x_p(t) = \sum_{i \in \delta_p} f_i(t) * x(t) . \tag{5.19}$$

5.3.2. Using ICA to solve the SC-ICA Problem

SC-ICA can be implemented according to the following procedure:

(i) The matrix of delays $\boldsymbol{Q}(t)$ is constructed out of the signal (as shown in Figure 5-3), which is then temporally whitened and dimension reduction methods such as PCA are applied. This is required since electrophysiological time series may contain short-term temporal correlations, which may lead to correlations of the rows of the embedding matrix. This step also provides the possibility of noise reduction (by, for example, truncation of the PCA transformation after a certain number of eigenvectors: Shlens, 2003).

(ii) An ICA algorithm (such as FastICA) is applied to establish the mixing matrix $\boldsymbol{A}$ (and the unmixing matrix $\boldsymbol{W}$) and the corresponding set of ICs.

(iii) The magnitude transfer functions of the columns of $\boldsymbol{A}$, $\left|A_i(\omega)\right|^2$, are calculated. Filters with similar magnitude frequency response $\left|f_i(\omega)\right|$ (but different phase responses) are grouped into C subsets δ_p spanning linearly independent subspaces E_p. This can be done by using a standard clustering algorithm such as K-means (Jiménez-González and James, 2009), or by manual selection.

(iv) The separating/reconstructing filter, f_p, for each source p is then formed by

$$f_p = \sum_{i \in \delta_p} f_i \qquad \text{where } f_i = \boldsymbol{A}_{(:,i)} \boldsymbol{W}_{(i,:)}. \quad (5.20)$$

(v) $\boldsymbol{Q}(t)$ is passed through these filters (i.e. projected back onto the measurement space), $\hat{\boldsymbol{Q}}_p(t) = f_p.\boldsymbol{Q}$, to form the independent processes $\{P_1, \ldots, P_C\}$ spanned by $\{E_1, \ldots, E_C\}$. Therefore, each process P_i spanned by subspace E_i is manifested in the measurement space by a matrix of delays $\hat{\boldsymbol{Q}}_i$. Moreover, since this is a lossless procedure, summing $\{\hat{\boldsymbol{Q}}_1, \ldots, \hat{\boldsymbol{Q}}_C\}$ returns the original time delay matrix $\boldsymbol{Q}$.

(vi) These delay matrices are then unembedded to form the one-dimensional, independent process time-series, $x_p(t)$, by performing an average of the rows of $\hat{\boldsymbol{Q}}_p$,

$$x_p(t) = \frac{1}{m} \sum_{k=1}^{m} \hat{Q}^p_{k,(t+k-1)}, \quad (5.21)$$

for t = 1,2,…N, where $\hat{Q}^p_{k,(t+k-1)}$ refers to the element of $\hat{\boldsymbol{Q}}_p$ indexed by row k and column (t+k-1).

The clustering of multiple ICs underlying each process (step (iii) above) can be avoided by using a quicker approach introduced by Davies and James (2007) and updated into a completely automated algorithm – fast independent process analysis (FastIPA) – by James and Davies (2008). In FastIPA one component is extracted by ICA in a deflationary manner and a separation filter $g_p(t)$ is formed. The signal $x(t) = r_0(t)$ is filtered and the residual $r_p(t)$ is calculated. The next source is then extracted from this residual

$$r_p(t) = r_{p-1}(t) - g_p(t) * r_{p-1}(t). \quad (5.22)$$

The process is terminated when no more sources can be found in the residual. This eliminates the clustering procedure and is more computationally efficient. However, the filters are only an approximation of the actual generating filter, making this technique an approximate solution.

5.3.3. SC-ICA vs Empirical Mode Decomposition

A signal processing method that shares some similarities with SC-ICA is empirical mode decomposition (EMD) first presented in geophysics by Huang *et al.* (1998). EMD is a data-driven, time-frequency decomposition of a scalar signal into frequency modulated components known as intrinsic mode functions (IMFs). EMD works as an iterative sifting process which

progressively isolates high frequency oscillations from broadband signals. A residual containing lower frequency information remains after every iteration and the process is repeated until the mean-square error between consecutive IMFs becomes negligible. The overall sum of the IMFs must be quasi-identical to the original signal

$$x(t) = \sum_{i=1}^{n} IMF_i(t) + R_n(t), \tag{5.23}$$

where n is the total number of IMFs and R is the residue at the end of the sifting process at time t (Huang *et al*., 1998).

The IMFs must satisfy two conditions: (i) the number of extrema and zero crossings must differ by a maximum of one and, (ii) the mean value of the upper and lower envelopes, defined by spline interpolation of local extrema, must be zero at all points. The use of splines implies that information is extracted from the signal (or the residual) at local time points *not* globally, thus allowing a physical interpretation by ensuring that the IMF properties are well localised in time (with reference to the original time series).

Figure 5-4 shows an example of this technique when applied to synthetic data comprising two pure sine waves (at 5 Hz and 25 Hz) and additional background EEG (acting as a known noise source) at an SNR of 16 dB. The EMD algorithm used here is based on the MALTAB code adapted from the work by Rilling *et al*. (2003). Twelve IMFs were extracted from the single channel signal; only the time series and the PSDs (estimated using the Welch method: Welch, 1967) of the first six are shown here, the first two belonging to the two sine waves with the highest frequency content. The other IMFs are related to the background EEG at lower frequencies. This shows that potentially EMD acts as a time-variant, adaptive, signal-dependent filter bank (Flandrin, 2004).

Therefore, as with SC-ICA, this technique provides a phase-preserving, time-frequency decomposition of scalar time series and avoids the use of arbitrary bandpass filtering, since it yields a signal decomposition that is adaptive to the frequency content of the data. However, the main drawback of EMD is that it is by definition an empirical process and to date it does not possess a theoretical basis. Moreover, it fails to decompose properly certain signals like chirps (Sweeney-Reed, 2007) and transients such a spikes, and the decomposed IMFs cannot be defined as statistically independent brain or artifactual processes.

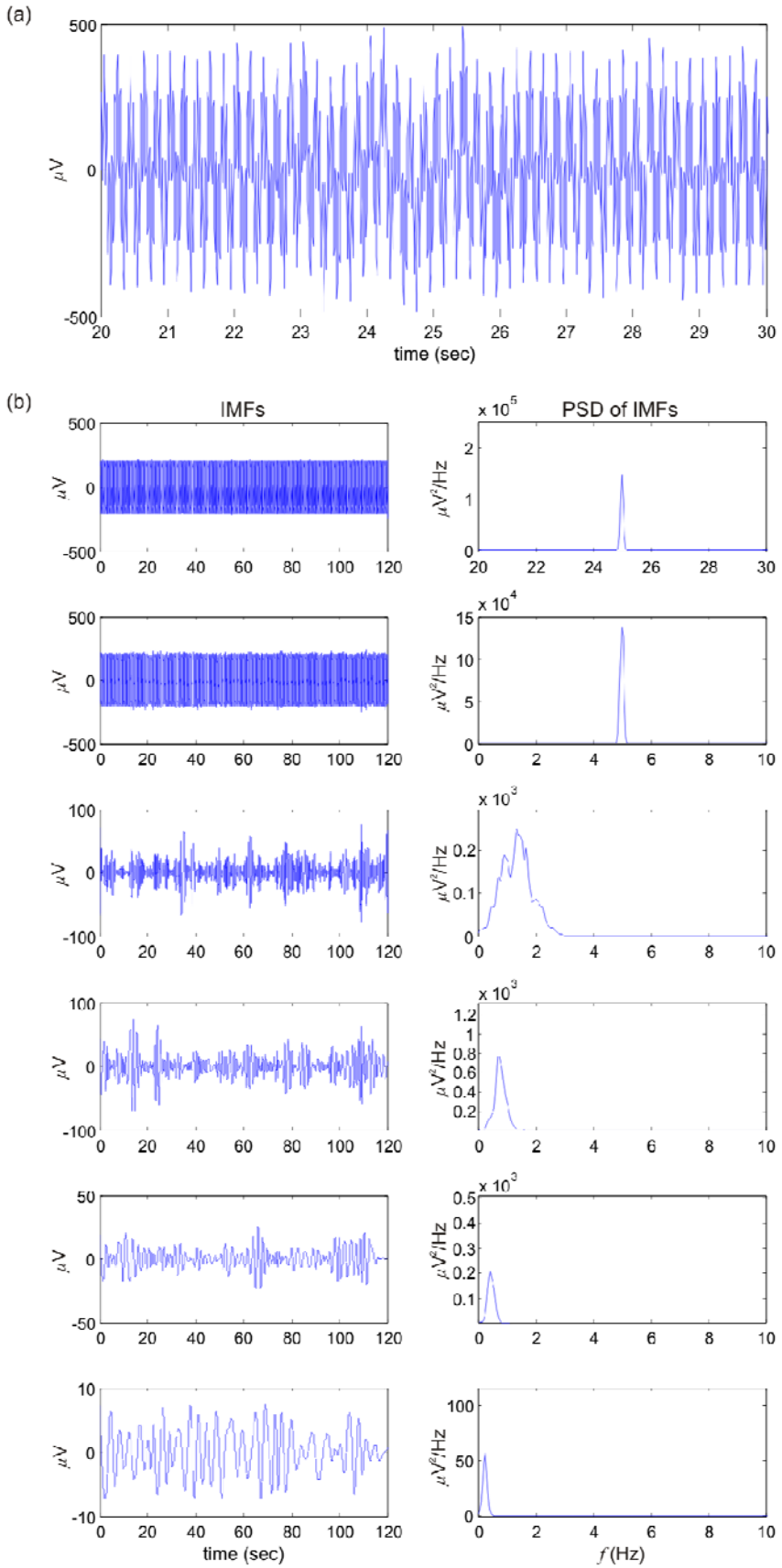

Figure 5-4. EMD single-channel decomposition: (a) 10 sec segment from the 2-minute signal composed of 2 sine waves at 5 Hz and 25 Hz with additional background EEG at an SNR of 16 dB; (b) The first 6 IMFs and their corresponding PSDs (showing power per unit frequency).

5.4. Space-time ICA (ST-ICA)

This is a simple augmentation of the SC-ICA method seen in the previous section, whereby the matrix of delays is constructed from n channels of interest such that the new overall delay matrix $\boldsymbol{Q}^{tot}$ becomes

$$\boldsymbol{Q}^{tot} = \left[\left(\boldsymbol{Q}^1\right)^T \ldots \left(\boldsymbol{Q}^n\right)^T \right]^T . \tag{5.24}$$

Thus, for an n-channel system of N samples per channel, $\boldsymbol{Q}^{tot}$ has dimension (nm x (N-m+1)), where m is the number of delay vectors (as in equation (5.12)). FastICA is then applied to $\boldsymbol{Q}^{tot}$ to obtain the mixing matrix $\boldsymbol{A}$ and the ICs. Every column of $\boldsymbol{A}$ (corresponding to one IC) contains n superimposed filters, which have similar *but not identical* frequency responses due to possible subtle variations of the underlying sources in different spatial locations. In this way, there is an FIR filter for every selected scalp location representing full spatial-temporal filtering (Figure 5-5). As for SC-ICA, some of the columns of $\boldsymbol{A}$ and corresponding rows of $\boldsymbol{W}$ represent repeated FIR filters pertaining to the same independent process (and hence spanning the same subspace), which can be grouped together to form C sets of n generating filters. The multichannel projections of the underlying independent processes $\{P_1, \ldots, P_C\}$ are then obtained by filtering and unembedding, as for the single-channel case.

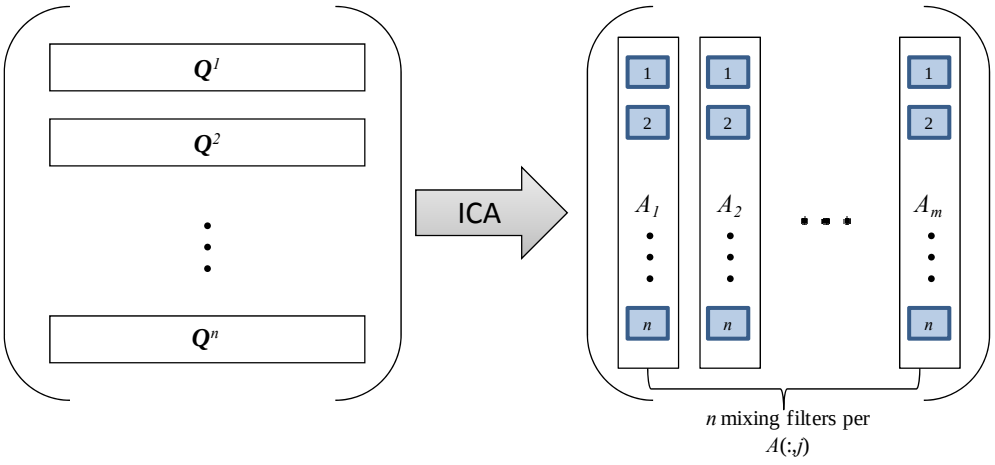

Figure 5-5. ST-ICA Procedure: A matrix of delays $\boldsymbol{Q}$ is created for each channel of interest to form the overall delay matrix $\boldsymbol{Q}^{tot}$, which is then decomposed into its constituent underlying independent processes through an ICA algorithm. ICA learns a mixing matrix $\boldsymbol{A}$, the columns of which contain sets of spatio-temporal filters (i.e. an FIR mixing filter per measurement channel).

To date, the clustering (grouping) procedure is being based on the similarity of the magnitude frequency response of these filters, although ST-ICA presents the opportunity to cluster based on both the filters' frequency responses and/or their spatial patterns. Furthermore, it is important to

note that, as for SC-ICA, multiple mixing filters can span separate underlying subspaces, although in this case the mixing filters are also distributed across *n* spatial locations. This means that in ST-ICA a number of independent processes are extracted (as for the single channel case), but spatial information is incorporated into the separation process. Consequently, ST-ICA also yields information on the spatial distribution of the underlying independent processes.

5.4.1. Applying SC-ICA and ST-ICA to Seizure EEG Data – An Example

In this section the application of SC-ICA and ST-ICA is illustrated on multi-channel ictal scalp EEG data recorded from patients who were undergoing continuous scalp EEG monitoring for possible epileptic surgery. Five minute seizure segments, including a pre-ictal (pre-seizure) period of 3 minutes were studied. The data were recorded using 19 electrodes placed on the scalp according to the International 10-20 electrode placement system, using reference FCz. The data were sampled at 200 Hz at 12 bit resolution and digitally stored. Figure 5-6 depicts one such example of an ictal EEG segment with a rhythmic seizure component of a left fronto-temporal origin occurring about 3 minutes into the segment. Note that the segment is severely contaminated with ocular artifact throughout.

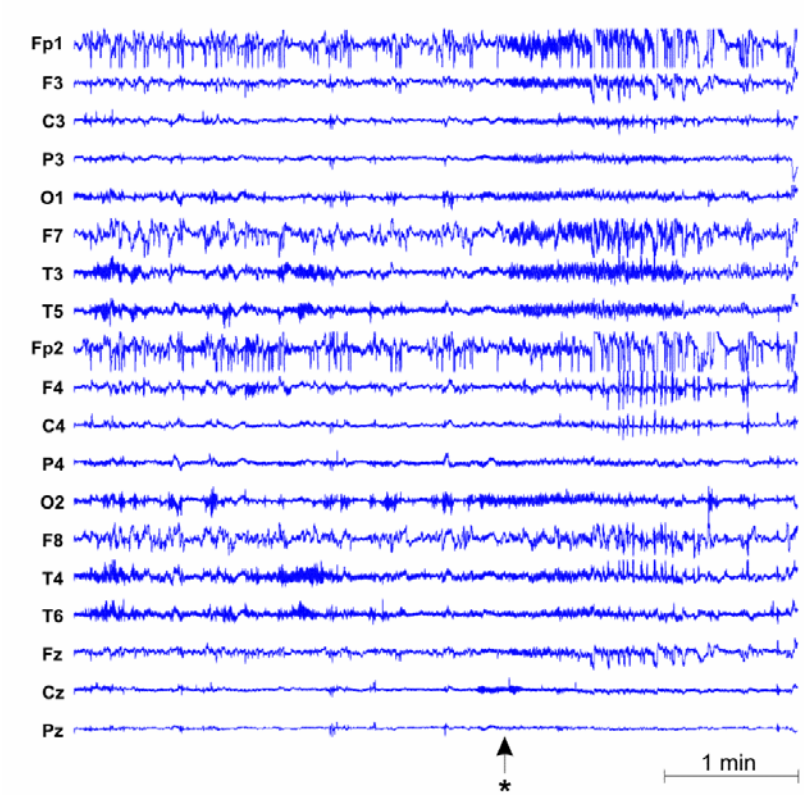

Figure 5-6. A 5-minute segment of multi-channel ictal EEG is depicted; a seizure with a sudden left fronto-temporal onset occurs at the point indicated by the marker (*). The recording is severely contaminated with ocular artifact throughout.

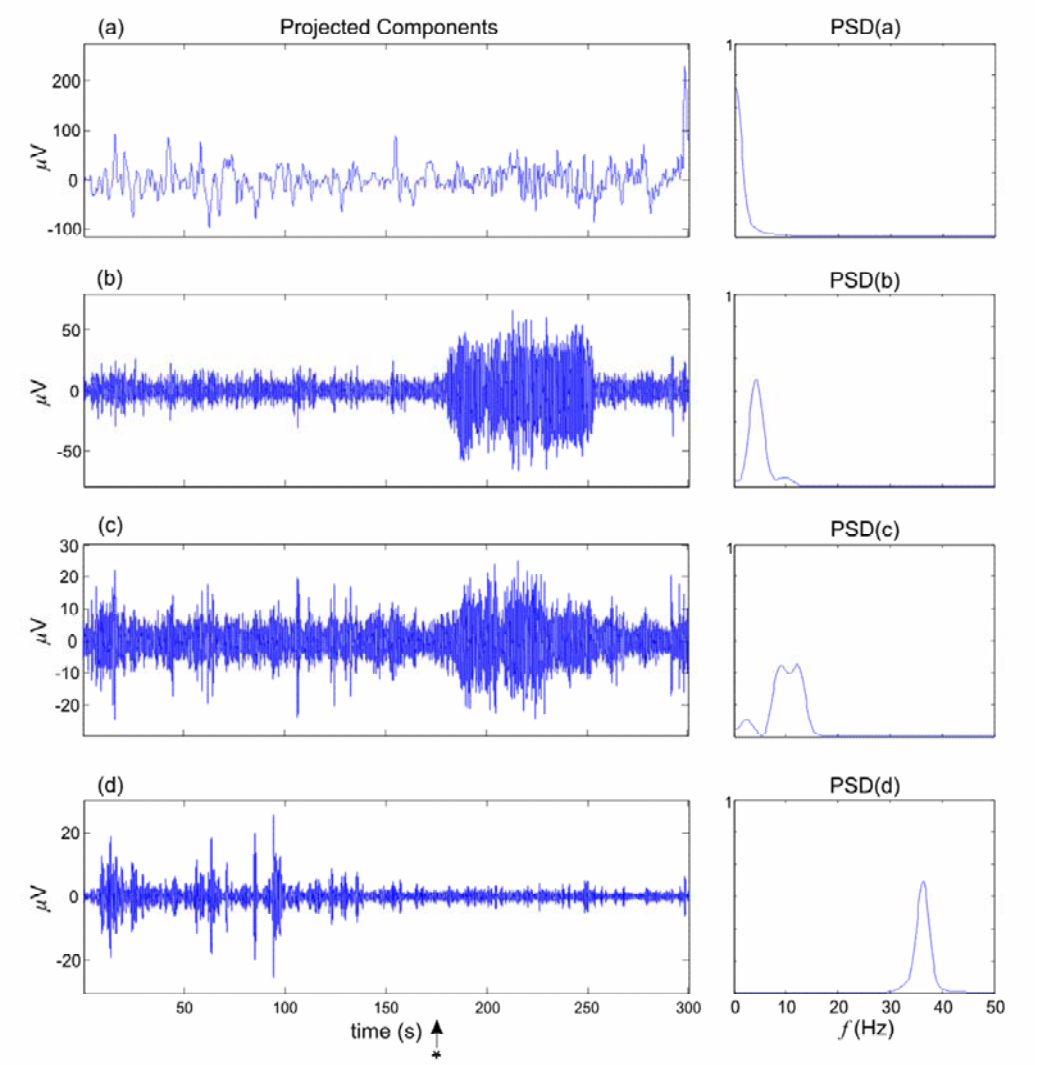

Figure 5-7. Decomposition of one channel of seizure EEG data T5, (as shown in Figure 5-6), by SC-ICA. Processes (b) and (c) are ictal processes centered around 4 Hz and 10 Hz respectively, whereas processes (a) and (d) are low and high frequency artifacts. Note the clear disjoint PSDs for each source (plotted on a linear scale).

SC-ICA (m=95) was first applied to channel T5 (which is the recording channel sited over the seizure focus) after first subtracting the mean value of the signal, constructing $\boldsymbol{Q}$ and reducing its dimensionality by PCA to a dimension of 30, (obtained by observing the structure of the singular-spectrum and choosing a value which depicts the start of the noise floor). Note that the choice of m was based on earlier empirical work on determining the optimal embedding dimension for this type of data (James et al., 2007). After ICA, the filters (columns of $\boldsymbol{A}$) with the same magnitude frequency response were manually grouped together to form a set of generating filters with disjoint power spectra. The corresponding band-limited sources (after projection onto the measurement space and unembedding) are illustrated in Figure 5-7. Groups (a) and (d) depict

low and high frequency artifacts respectively, whilst groups (b) and (c) represent the seizure sources, their onsets corresponding to the seizure onset times in the raw recordings.

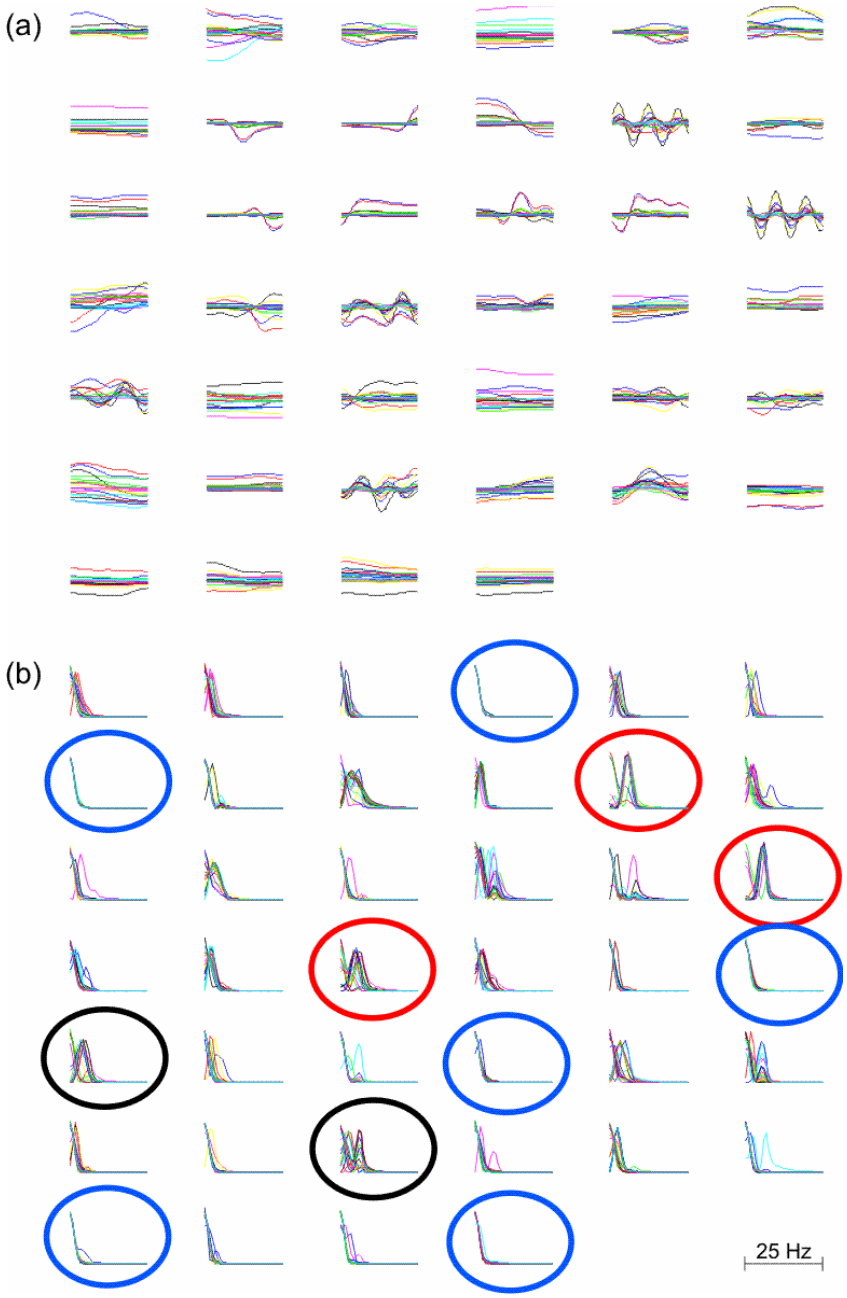

Figure 5-8. The characteristics of spatio-temporal filters obtained from ST-ICA for the seizure dataset shown in Figure 5-6. Plots of the (a) impulse response and (b) frequency response of the 19 filters (of order m=95) for each of the 40 columns of the mixing matrix, obtained by applying FastICA on the overall delay matrix $\boldsymbol{Q}^{tot}$. Note that: (i) Each column has 19 superimposed filters which have similar *but not identical* coefficients and frequency responses, due to subtle variations of the underlying source in different spatial locations; (ii) Some of the 40 columns contain repeated FIR filters pertaining to the same independent process (for example, red circles represent Process 1, and black circles represent Process 2 (which are both seizure processes) whereas the blue circles represent a slow process related to ocular artifacts).

Next, ST-ICA was applied to all the 19 channels (m=95). Again, the mean value of each recording was first subtracted and the dimensionality of $\boldsymbol{Q}^{tot}$ was reduced to 40 by SVD. The columns of the mixing matrix $\boldsymbol{A}$ learnt by FastICA were manually grouped according to the spectral information they contained. An example of the impulse and frequency response of the filters and their grouping is given in Figure 5-8. Projection of the corresponding groups of components and unembedding of the resultant matrices yielded a number of multi-dimensional identified processes underlying the measured EEG, three of which are illustrated in Figure 5-9. Groups 1 and 2 depict ictal processes – note the onset times which are co-incident with the onset times in the raw recordings and the left fronto-temporal focus of the seizure. Process 3 represents an ocular artifact, the amplitude and intensity of this artifact increases about 30 seconds into the seizure onset; this is evident in the raw recordings too.

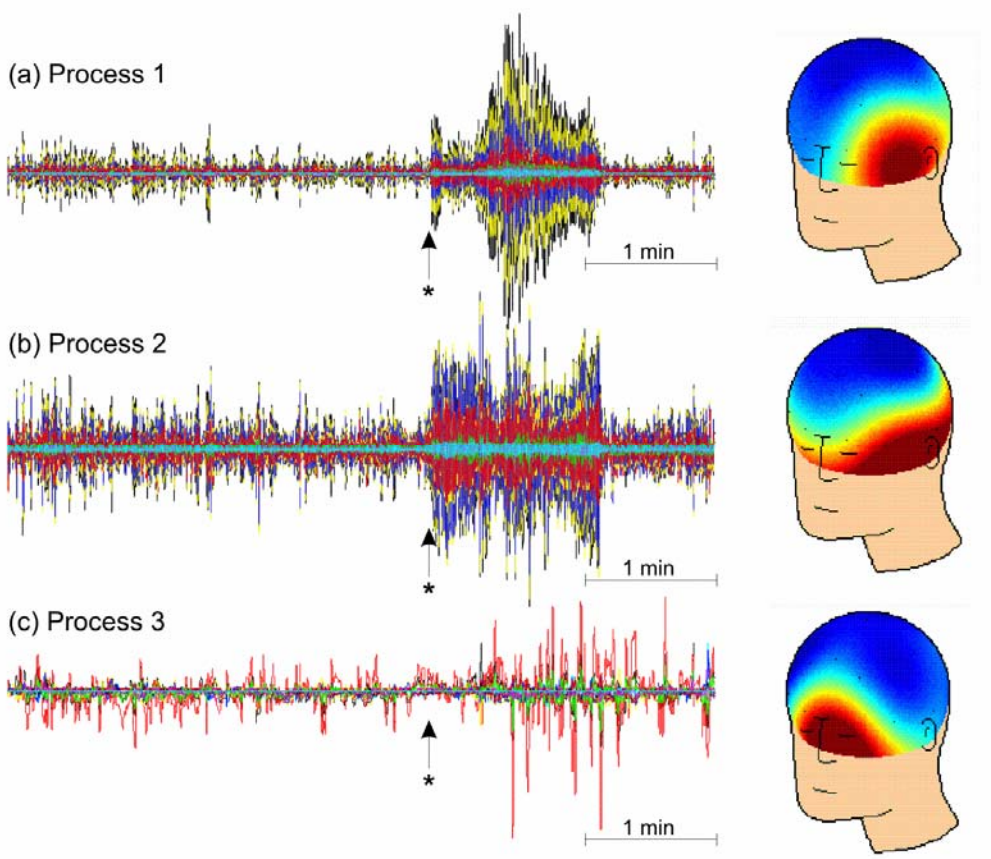

Figure 5-9. Butterfly plots of three of the identified processes (projected to the measurement space) underlying the measured data and their topographic distribution. (a) Process 1 and (b) Process 2 represent ictal sources – note the onset times which are co-incident with the onset times in the raw recordings, and their left fronto-temporal foci. (c) Process 3: ocular artifact with a frontal distribution, the amplitude and intensity of this artifact increases about 30 s into the seizure onset (as in the raw recordings).

As explained earlier, in this example and in all the other implementations of ST-ICA on EM data in relation to the slow waves in this work, the selection of underlying independent processes is solely based upon the similarity of the frequency responses of the FIR filters that ICA learns in the ST-ICA model. This means that although spatial and temporal information is used in the ST-ICA decomposition, the clustering part of the procedure could be neglecting useful information, which may in turn lead to ill-defined processes. Further research is required in order to establish an automated clustering method that uses both the spatial *and* spectral content of the filter such that the underlying processes could be defined based on the similarity of both quantities, as explained in James and Demanuele, (2009).

5.5. Summary

This chapter considered three types of BSS algorithms, namely E-ICA, SC-ICA and ST-ICA. The popularity of standard 'spatial' ICA as a neurophysiological signal analysis tool evolved over the years because of its potential not only to denoise the data by distinguishing artifacts from the actual brain sources, but also to *identify* other independent sources within the data. Crucially, the notion of statistical independence translates well to neurophysiological independence, implying that the independent sources extracted by ICA are generally quite neurophysiologically meaningful (James and Hesse, 2005). However, this form of ICA is limited in that it can only extract sources which are spatially distinct and it does not fully exploit the information embedded in the temporal dynamics of electrophysiological data. Consequently, SC-ICA was developed as a temporal decomposition method, which is able to isolate sources from single channel measurements (Davies and James, 2007).

SC-ICA is a much more powerful method than the traditional application of filters to a single channel recording, which uses "general" filters that have been designed according to the frequency bands of interest in the data and have fixed time-invariant coefficients. When an ordinary filter is employed, even if its exact coefficients are known, these would have to be adapted to cater for the changes in physiological signals for each participant and for every set of recordings. On the other hand, SC-ICA is an exercise of feature discovery that explores the input data to establish a set of band-limited filters from the data itself, which in turn results in the extraction of the underlying independent sources. Moreover, unlike other single-channel and adaptive methods such as EMD, SC-ICA has a strong mathematical derivation which facilitates the interpretation of results. However, since the sources are extracted from a scalar time series, SC-ICA does not provide any information about their spatial distribution. Another downside of SC-ICA is spectral overlapping of the sources – the greater the overlap between the sources in

the frequency domain, the more difficult it becomes for SC-ICA to learn a filter bank that separates out the sources distinctly.

It was shown that the natural extension of the above two methods yields the newly-developed ST-ICA algorithm, which learns a set of spatio-temporal filters from the data based on the independence criterion of the underlying brain processes. ST-ICA allows for the extraction of brain sources that overlap spatially *or* spectrally, and that hence cannot be extracted by either ICA or SC-ICA separately. Moreover, ST-ICA facilitates the analysis of high density systems (such as MEG systems), by allowing the extraction of brain sources from a few selected channels of interest, hence reducing the system's dimension. The data matrix ($\boldsymbol{Q}^{tot}$) contains both spatial information (through n selected channels) *and* temporal information (through the method of delays applied on each channel), which makes it possible to analyse fewer channels whilst still retaining an information-rich dataset to inform and update the standard ICA algorithm. In contrast, reducing dimensions in this manner is not advisable for 'standard' spatial ICA, because this algorithm can only make use of spatial information (from the physical arrangement of the recording sensors) in the separation process. ST-ICA also provides a wealth of information about the spectral characteristics, the temporal dynamics and the spatial distribution of the extracted sources, which facilitates the interpretation of these sources as well as any further analysis that needs to be carried out on them. The downside of this algorithm is that it can lead to large data matrices (due to the stacking of the delay matrices constructed for each channel of interest), thus making it computationally expensive.

As can be seen, each of these algorithms has specific merits as well as shortcomings and it ultimately depends on the researcher to select the technique that best suits the problem at hand. The following chapters will show the application of these techniques for the analysis of MEG data recorded from a high-density 148-channel system, and for exploring an EEG dataset specifically recorded for the investigation of the slow waves during various experimental conditions.

Chapter 6

INVESTIGATING SLOW WAVES IN BRAIN SIGNAL RECORDINGS: INITIAL FINDINGS

This chapter gives an account of the analyses carried out on EM brain signal recordings in order to establish ways for investigating VLF (<0.5 Hz) activity, and to gain insight into the effect the slow waves have on brain function. Primarily, a procedure for removal of the $1/f$ *trend in EM data is presented. Then, the methodologies and results obtained from two separate studies on MEG recordings of children with ADHD and controls are described. These studies employ the single channel and space-time ICA algorithms explained in the previous chapter.*

6.1. $1/f$ Spectral Compensation

In this section two methods that can be used to achieve spectral normalisation, i.e. the removal of the intrinsic $1/f$ in EM brain signal recordings to provide a flat spectral base onto which task- or condition-related brain activity is superimposed, are described. The first method is based in the frequency domain, its main aim being to investigate the spectral characteristics of EM signals and to provide a basis for normalisation. The second method is a time domain approach whereby the spectral trend is removed by filtering the raw signals prior to further data analysis. This is a simple but effective method which conserves the phase information of the input signal. For these reasons, it is applied to a variety of EM brain signal recordings namely: epileptic seizures, VLF EEG recordings, MEG recordings and ERP data to illustrate its function.

6.1.1. Normalisation in the Frequency Domain

Normalisation of the spectrum can be achieved in the frequency domain by dividing any EEG spectrum by an established background $1/f^{\gamma}$ spectrum. This concept was tested on the multi-

channel EEG datasets of two participants recorded by the School of Psychology at the University of Southampton as part of a larger unrelated study. 32 EEG channels were used and electrode placement was set in accordance to the International 10-20 system. Impedance levels were set at less than 5 kΩ. No filters were switched on during the recordings such that DC activity could be captured, and DC-stable sintered electrodes were used. The data was sampled at 250 Hz with a 12 bit ADC and was digitally stored. Before analysis the data was low-pass filtered to 5 Hz and then downsampled to 10 Hz – this was done to ensure an adequate number of samples to represent the very low frequencies, which were at the focus of the experiment. Detrending was then carried out for removal of the mean shift (over 5 or 10 minutes) in each dataset.

In these recordings, every participant followed a 10-minute driving task, where the participant was meant to trail a plain winding track on screen by pressing the arrow buttons on the keyboard. This was followed by a 5-minute eyes-closed resting condition during which the participant was seated on a reclining chair. A 10-minute arrows task followed, during which the participant was asked to press a button whenever the arrow appearing on screen pointed left or right (according to the instructions given). The participant's recording was concluded by a 5-minute eyes-open resting period again seated on a reclining chair. For every participant these segments of data were analysed separately. The expectation was that these task conditions, which require the participants' attention, yield a predominant low frequency activity around 0.1 Hz.

For a particular participant, the spectrogram of one EEG channel was calculated. The median across all time windows was found for every frequency point. Thus, a graph of the median PSD value for every frequency was obtained. The same procedure was repeated for all the EEG channels. Then, the overall median of the median PSD curves of all the channels was calculated. The same was done for each of the task and rest conditions. The average was then calculated across all conditions and this was used as the normalisation curve (black dashed curves in Figure 6-1 (a) and (b)). The reason for considering all channels and all conditions to obtain this curve was to be able to establish a general base picture of the underlying brain activity that gives rise to this $1/f^{\gamma}$ distribution. The spectrogram of the EEG data to be analysed, (e.g., Participant 1, driving task), was then calculated and each time window of the spectrogram was divided by this normalisation curve, in the frequency domain.

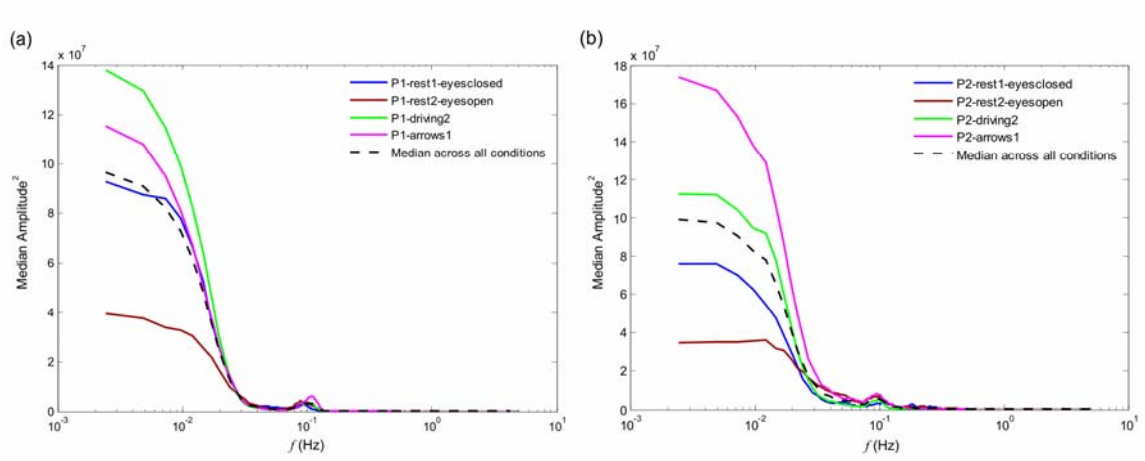

Figure 6-1. Median PSD curves for participants 1-(a) and 2-(b), showing the relation of the EEG in all conditions. For each participant, the median across the 4 conditions forms the normalisation curve (--).

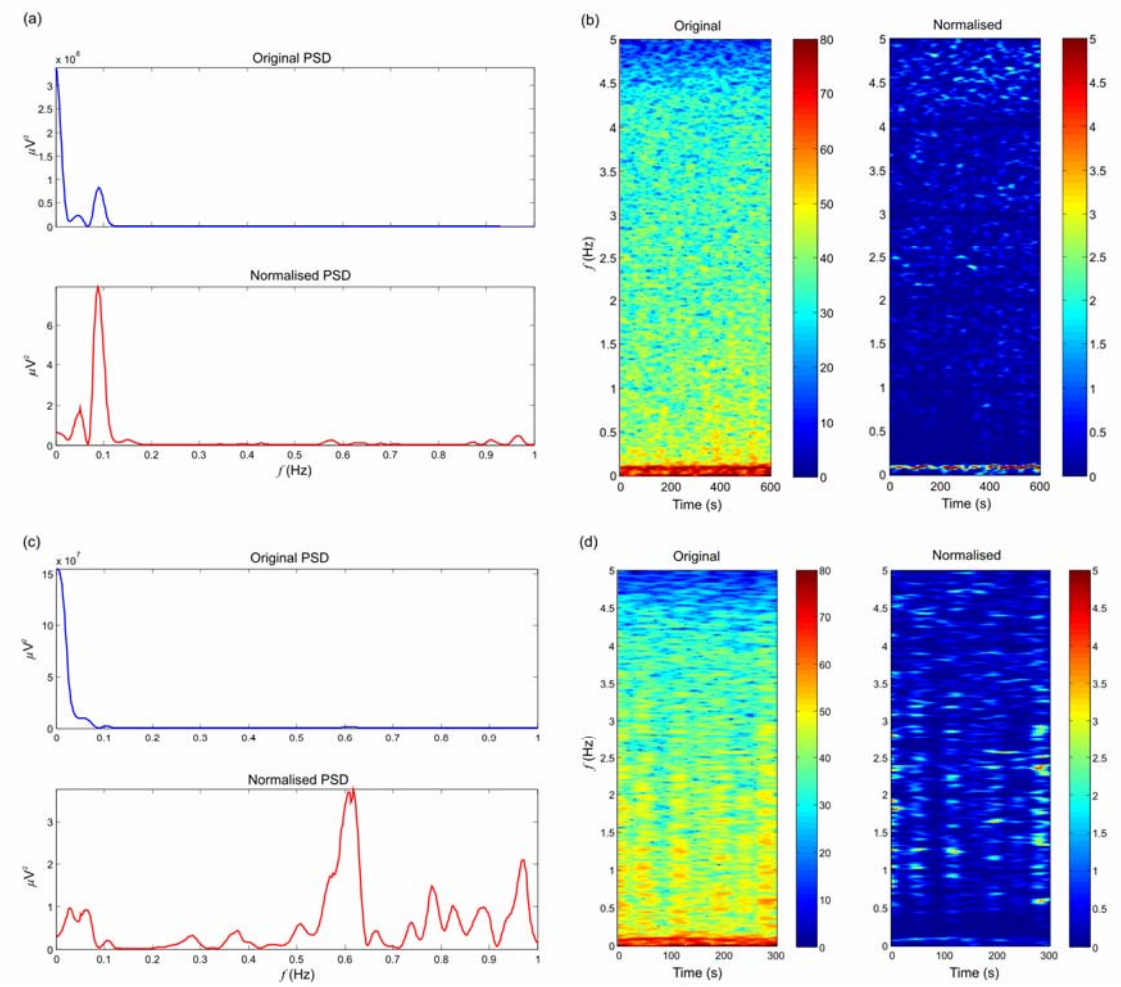

Figure 6-2. Normalisation in the frequency domain: (a) The PSD for one channel for Participant 1 during the driving task, (b) Corresponding spectrograms, (c) The PSD for one channel for Participant 1 Eyes-open condition, (d) Corresponding spectrograms.

From the plots in Figure 6-1 the $1/f^{\gamma}$ nature of the EEG can be observed in all median curves; this gives confidence in the current method of estimation of the normalisation curve. The plots in Figure 6-2 show the normalised spectrum – the $1/f^{\gamma}$ trend is removed and task-related peaks can be easily distinguished from ongoing brain activity. A peak at 0.1 Hz can be clearly seen in (a), and this is manifested in the normalised spectrogram of (b). In (c) no appreciable VLF peaks can be seen and (d) shows the normalised spectrogram with no prominent VLF activity. Note that Figure 6-2 (a) and (c) show the PSDs of the original and normalised signal at one electrode for one time window in the spectrogram.

6.1.2. A Time Domain Spectral Normalisation Approach

This type of normalisation can be achieved by passing the EEG input signal through a filter that cancels the $1/f^{\gamma}$ spectral behaviour prior to any signal analysis. This inverse filter can be established by modelling the normalisation curve shown in Figure 6-1 by an autoregressive (AR) or a moving average (MA) model and then reversing the coefficients to obtain its inverse. Hence

$$\frac{A}{f^{\gamma}} \times Bf^{\gamma} \approx AB \,, \tag{6.1}$$

where A/f^{γ} is the EEG power spectrum with the intrinsic $1/f^{\gamma}$ characteristics, Bf^{γ} is the inverse filter spectral contribution (which is square of the filter transfer function) and AB is the result of their interaction, implying that the output is a whitened spectrum. The $1/f^{\gamma}$ curve can be modelled as an FIR model such that its inverse will be an infinite impulse response (IIR) model. However the problem is the lack of control on the FIR coefficients since these are already predetermined by the shape of the normalisation curve. Thus, if the resultant FIR model is not minimum phase, the inverse IIR model will not have all its poles inside the unit circle and system stability becomes a major issue. Moreover the filter needs to have a linear phase response to avoid distorting the phase of the input signal – and an IIR filter will not meet this requirement.

Another possible approach is that of modelling the normalisation curve as an AR model such that its inverse is an MA model and stability is guaranteed. The time domain representation of the normalisation curve obtained in the frequency domain is found by computing its inverse FT. The AR coefficients of an IIR filter are then obtained using the Yule-Walker equations (Hayes, 1996) on the absolute value of this time domain signal. The AR frequency response obtained with filter transfer function [1.0000, 1.0000 -0.9772 -0.0066 -0.0010 -0.0033 0.0013 -0.0070] ([*b*, *a*] where *b* and *a* refer to the parameters used in extracting the system's zeros and poles respectively) provides an estimate of the normalisation curve as shown in Figure 6-3 (a). Reversing the

coefficients of this model provides an MA (FIR) filter [1.0000 -0.9772 -0.0066 -0.0010 -0.0033 0.0013 -0.0070, 1.0000], which has a frequency response that is the inverse of the estimate of the normalisation curve, Figure 6-3 (b).

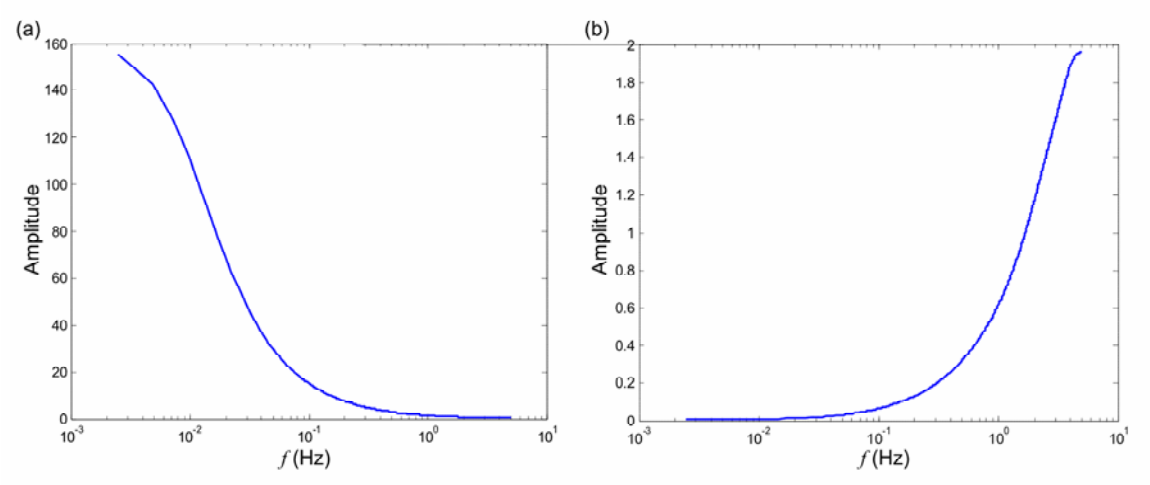

Figure 6-3. Modelling the inverse filter: (a) An estimate of the normalisation curve showing a $1/f^{\gamma}$ frequency response obtained by a 6th order AR model, (b) The inverse filter frequency response obtained from the corresponding 6th order MA model.

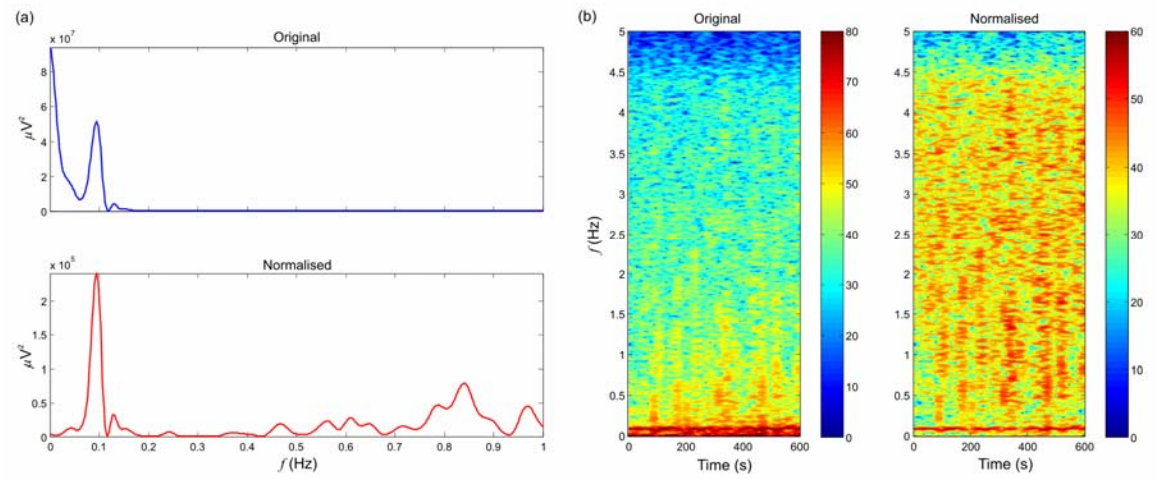

Figure 6-4. Time domain spectral normalisation by ARMA modelling: (a) The PSDs (for one time window in the spectrograms) showing normalisation achieved by the inverse (MA) filter, (b) The corresponding spectrograms of the original EEG signal and of the filtered signal showing a dominant peak around 0.1 Hz.

Although this approach gives the expected results (as can be seen in Figure 6-4), it is quite an involved method since it uses the normalisation curve in the frequency domain in order to derive the appropriate inverse filter.

A. Approximating the Inverse Filter by a Differentiator

Figure 3-1 shows $1/f^{\gamma}$ curves superimposed on the power spectral density of a typical EEG channel, with γ varying from 1 to 3. Generally, the $1/f$ and the $1/f^2$ curves follow closely the EEG spectral trend across the entire frequency band; the better fit of the two for the lower or higher frequencies varies across recordings. Setting γ to 1, i.e. assuming a 1/*f* spectral trend, requires a filter with a $\sqrt{f}$ frequency response (i.e. an *f* squared magnitude response). This can be designed through the MATLAB function *fir2*, which provides the transfer function *h*[*n*] of an FIR filter, that approximate a given desired magnitude frequency response and exhibit a linear phase response. In practice, some of the filter coefficients (representing *h*[*n*]) can then be tweaked to provide a response as close as possible to $\sqrt{f}$ at all frequencies, as shown in Figure 6-5 (a) (a 16th order filter, h[0] adjusted). Figure 6-5 (b) illustrates the PSD of one signal before and after filtering, estimated using the Welch method (Welch, 1967; with a frequency resolution of 0.02 Hz). The normalised PSD exhibits partial removal of the 1/*f* spectral trend shown as a reduction in amplitude for frequencies below 0.05 Hz and an enhancement of the peak around 0.1 Hz, similar to that obtained in Figure 6-4 for the same dataset.

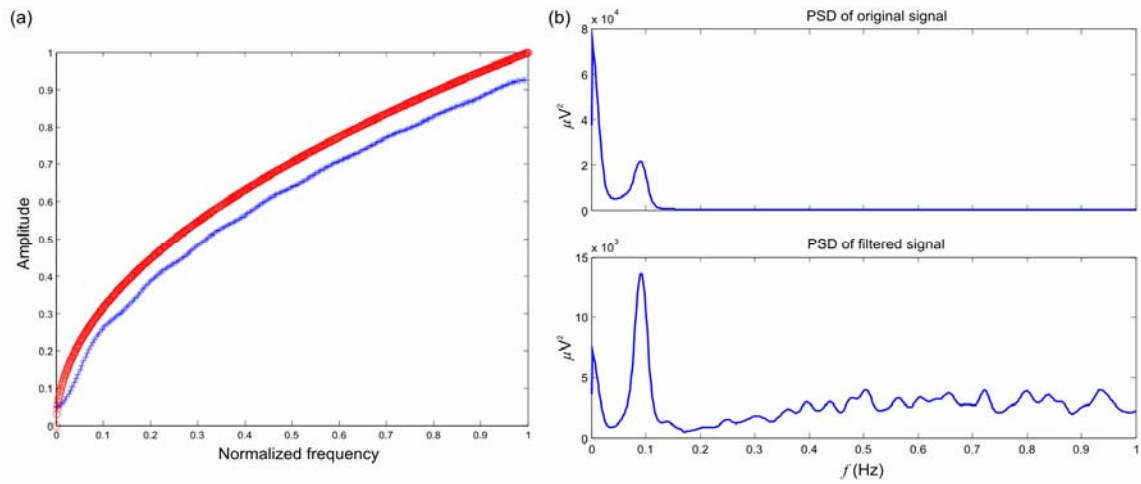

Figure 6-5. Spectral normalisation by a $\sqrt{f}$ filter for removal of the 1/*f* EEG spectral trend: (a) The desired $\sqrt{f}$ frequency response (red), the actual frequency response achieved by a 16th order FIR filter (blue); (b) The original and filtered PSDs of the signal, showing partial removal of the trend for frequencies below 0.05 Hz, and revealing the prominent peak around 0.1 Hz.

If the normalisation curve is approximated by a $1/f^2$ curve, i.e. setting γ to 2, the inverse filter can be obtained by applying a differentiator with an *f* transfer function. This could be done using the *cfirpm* function in MATLAB, which provides a set of filter coefficients that simulate a linear

phase differentiator. Alternatively, the differentiator can also be modelled as a 2nd order MA filter, given by

$$y(t) = \frac{x(t) - x(t-1)}{\Delta t}, \tag{6.2}$$

where $x(t)$ is the input signal, $y(t)$ is the filtered output and $\Delta t = T_s = 1/f_s$, f_s being the sampling frequency. Thus the MA filter coefficients can be set as $1/T_s$ and $-1/T_s$. This is more straightforward method to implement than the $\sqrt{f}$ filter: it requires fewer coefficients to model its transfer function, and it does not need any tweaking of $h[n]$ to achieve the desired frequency response. Moreover, it provides a better suppression of the spectral trend at very low frequencies as demonstrated in the following sections.

B. Differentiator Characteristics

The differentiator, with its f frequency response cancels out a $1/f^2$ trend in the EEG spectrum as illustrated in Figure 6-6. Figure 6-7 then shows the magnitude and phase response of the differentiator. The filter exhibits a linear phase response and a constant group delay. The linear phase response makes it easier to compensate for the phase delay at one particular time instant by sample-shifting the pre-recorded data accordingly.

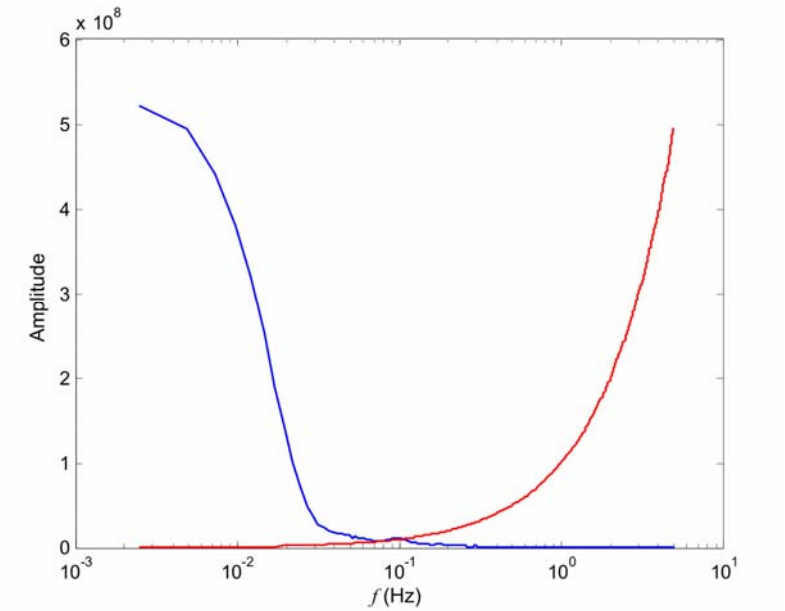

Figure 6-6. The function of the differentiator in spectral normalisation: f frequency response of the differentiator (red), EEG PSD (blue).

The effect of the differentiator on the phase of the input EEG signal can be seen in Figure 6-8. Although the phase difference between the input and the output of the filter is not constant across time, due to variation in the signal frequency content, the general shape of the phase is preserved. Moreover since the phase response of the filter is known and fixed, any input signal will experience the same phase delay at one particular frequency. Consequently if one is interested in establishing the phase synchronisation between two channels (which is computed at one specific narrow frequency band), the phase relationship of the two signals will not be distorted by the filter since both signals will be delayed by the same amount at that frequency.

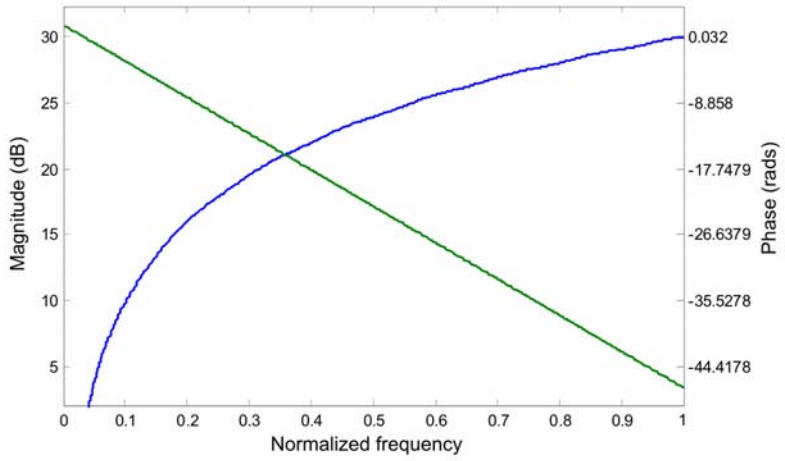

Figure 6-7. Magnitude (blue) and phase (green) frequency response of the differentiator.

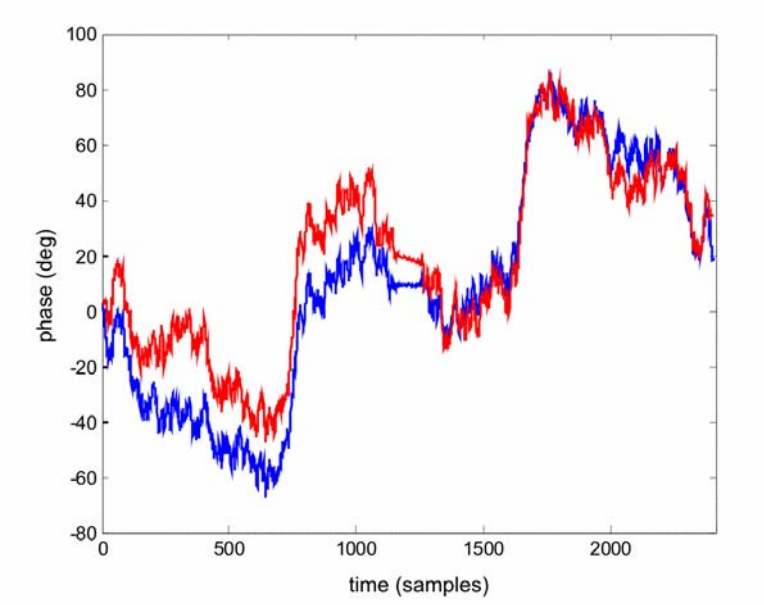

Figure 6-8. The phase effect of the differentiator on the input EEG signal; the phase of the EEG signal before (blue) and after (red) filtering.

This analysis shows that performing normalisation in the time domain by using a differentiator is an attractive approach. This is because, although the frequency domain method produces a

normalised spectrum without assuming that the underlying bias is a strict $1/f$ or $1/f^2$ (since the normalisation curve is modelled directly from the dataset), the phase information of the EEG signal is lost. Consequently, it is not possible to fully reconstruct the time series from the normalised spectra. Moreover, the differentiator is the simplest filter for normalisation in the time domain in comparison to those achieved through ARMA models or the $\sqrt{f}$ filter. For these reasons, it is used here to filter different datasets in order to demonstrate its function as a tool for spectral normalisation. The results are illustrated next.

6.1.3. Applying the Differentiator to Various Datasets

A. Synthetic Data

The differentiator was applied to two sinusoidal signals of frequencies 0.1 Hz and 0.5 Hz respectively, superimposed on normal background EEG. The SNR of the higher frequency signal (SNR2) was kept fixed at 15 dB whereas that of the lower frequency signal (SNR1) was varied from 0 to 47 dB. Each SNR was measured by calculating the ratio of power of the sine wave to that of the background EEG.

When SNR1 is less than SNR2 (Figure 6-9 (a) and (b)) the filter attenuates the low frequency component significantly by removing the $1/f^2$ trend. In the second case (Figure 6-9 (c) and (d)) the magnitude of the 0.1 Hz filtered component becomes equal to that of the 0.5 Hz component since SNR1 is high enough to compensate for the $1/f^2$ intrinsic spectral behaviour. This means that the SNR of the lower frequency component needs to be twice that of the higher frequency component to place it above the $1/f^2$ curve and let it be apparent at the output. Any SNR1 value exceeding this threshold results in the low frequency component being larger than the high frequency component after filtering (Figure 6-9 (e) and (f)).

Figure 6-10 shows the SNR for an input sine wave as its frequency is varied from 0.1 Hz to 12 Hz. It is clear that for every input frequency the SNR before filtering varies linearly with that after filtering. Moreover, lower frequencies have a lower SNR after filtering due to the $1/f^2$ base spectrum. This is shown in Figure 6-11 where for a particular SNR before filtering, the SNR after filtering increases as the frequency of the input signal becomes higher. The curves in this figure can be approximated by an inverse $1/f^2$, which implies that the differentiator is attenuating lower frequencies more than higher frequencies hence compensating for the $1/f^2$ bias.

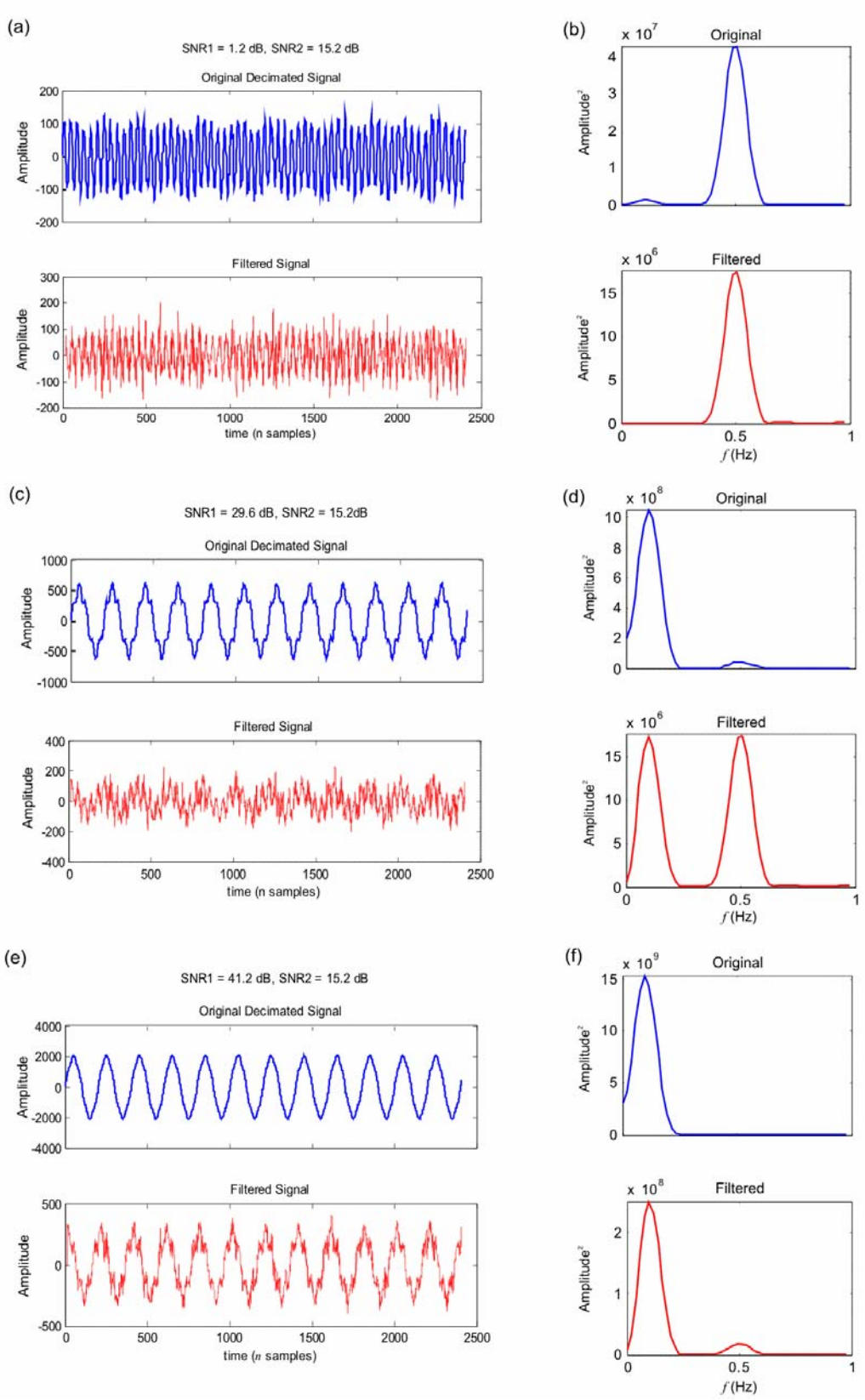

Figure 6-9. Time domain signal consisting of 2 sine waves at 0.1 Hz and 0.5 Hz of varying SNR (SNR1 and SNR2 respectively) filtered through the differentiator and their corresponding spectra before and after filtering: (a) SNR1 is less than SNR2, (c) SNR1 is approximately twice SNR2, (e) SNR1 is much higher than SNR2; (b), (d) and (f) show the corresponding PSDs.

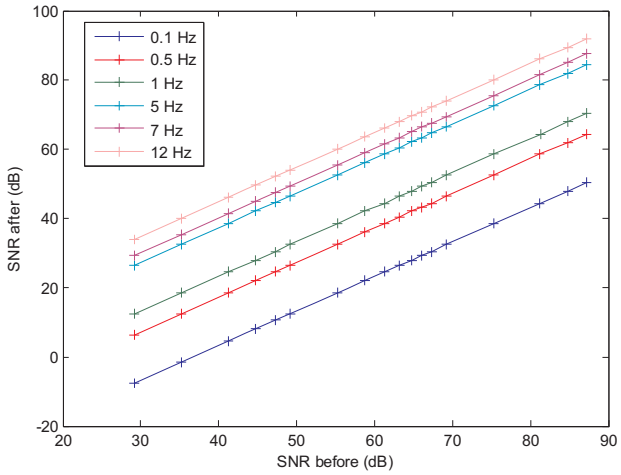

Figure 6-10. SNR before and after filtering for various input frequencies of a sine wave used as the input signal to the differentiator.

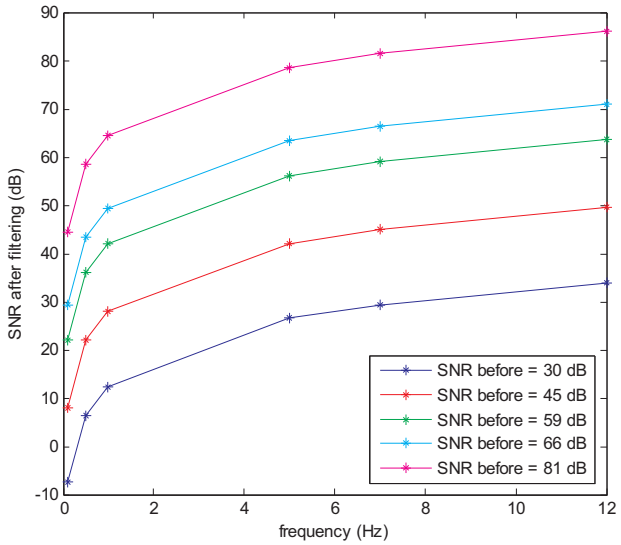

Figure 6-11. Variation across frequencies of the output SNR for fixed SNRs of the input signal.

B. Epileptic Seizure Data

Focal epileptic seizure data recorded using 25 electrodes placed on the scalp according to the International 10-20 system with reference at FCz, was used as input to the differentiator. The 3-minute long data recording was sampled at 200 Hz and digitally stored at 12 bit resolution. The recording included pre-ictal, ictal and post-ictal activity, and the seizure was focused on the left-temporal lobe (around T3). For this data, the relationship between SNR before and after filtering showed the same linear trend as that obtained for synthetic data. Here, the SNR was computed by finding the ratio of power of the 3-minute EEG incorporating seizure activity to the power of

ongoing background EEG activity of the same duration recorded for the same subject. This procedure was carried out on the data before and after passing it through the differentiator.

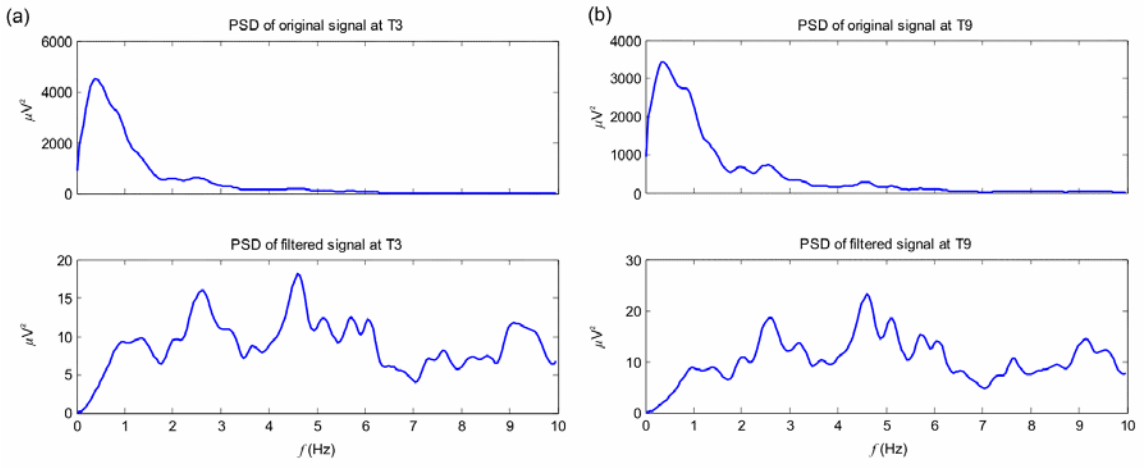

Figure 6-12. The effect of the filter on the spectrum of the signals recorded around the seizure focus: (a) T3 signal spectrum, (b) T9 signal spectrum; Note the removal of the 1/*f* trend and the clear peak around 4.5 Hz indicative of the rhythmic seizure activity.

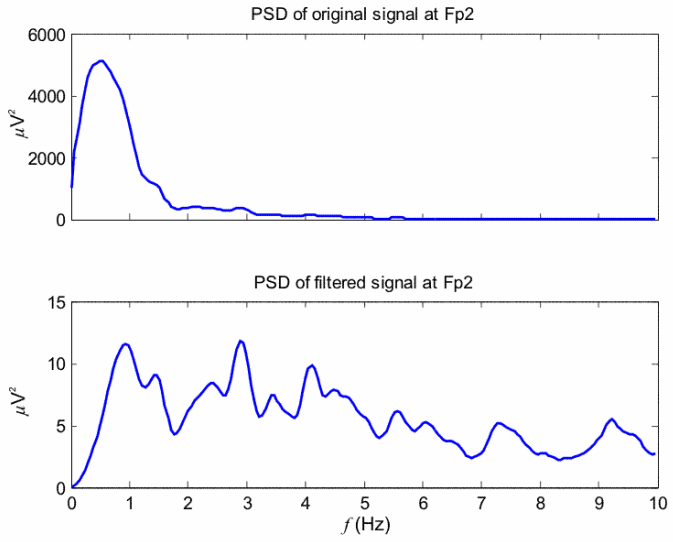

Figure 6-13. The spectra of Fp2 (channel with ocular activity): Eye movement activity has lower frequency peaks which are more pronounced in the normalised spectrogram.

Figure 6-12 and Figure 6-13 show the effect of filtering on the spectrum of selected EEG channels; the spectra were computed using the Welch method with a frequency resolution of 0.2 Hz. After filtering the original spectra in Figure 6-12 (a) and (b) are flattened and the $1/f^2$ trend is clearly removed. Moreover, the peak around 4.5 Hz, which is related to the rhythmic seizure activity, becomes much more pronounced in the filtered spectra. The spectrum of the

frontopolar channel (Fp2) in is also whitened by the differentiator and low frequency peaks due to eye-related activity become visible.

C. EEG Data with Low Frequency Activity

When the same EEG data used in Section 6.1.1 was applied to this filter the spectra were normalised as expected, as shown in Figure 6-14. The 0.1 Hz activity visible in the original signal spectra in (a) and (b) become more prominent after filtering; both spectra have been computed using the Welch method with a frequency resolution of 0.02 Hz, and selected channels for Participant 1 during the driving task are shown as an example (since the results for the other datasets were very similar). No significant low frequency activity can be seen in the normalised spectrum of (c), during the eyes-open condition for the same participant. Thus the resultant spectra obtained by normalising in the frequency domain and those obtained by normalising in the time domain are very similar, in that they both show a peak around 0.1 Hz during the driving task and a flat spectrum when no extra low frequency activity was expected: compare Figure 6-2 (a) (normalisation in the frequency domain) and Figure 6-14 (a) & (b) (normalisation in the time domain) for the same dataset. Moreover, the result of Figure 6-14 (a) is also comparable to that obtained by the $\sqrt{f}$ filter in Figure 6-5 (b), implying that our approximation of the spectral trend with γ is 1 or 2 renders similar outputs and it indeed practical to use the simpler method.

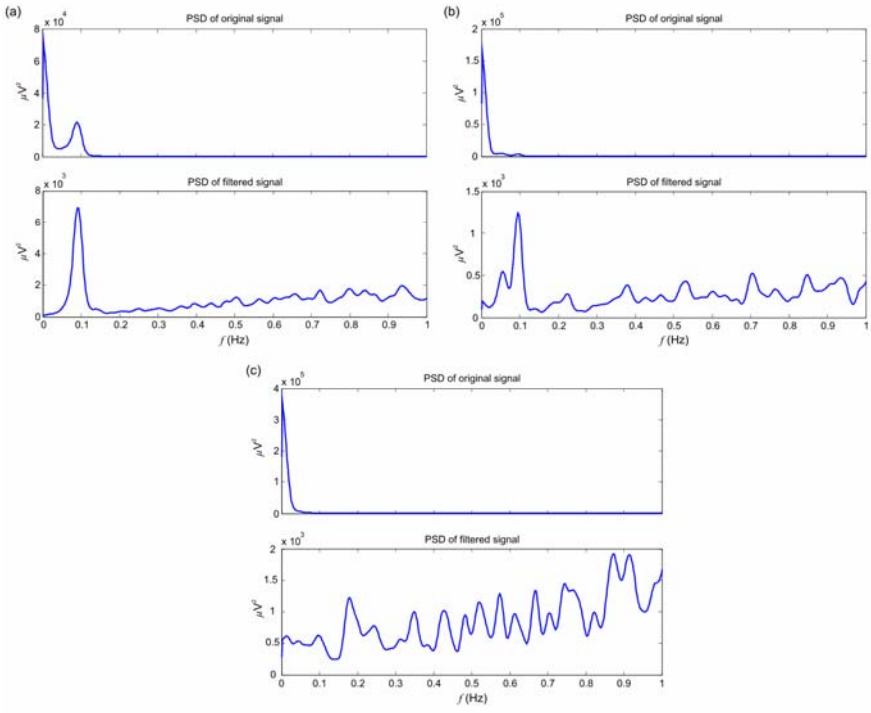

Figure 6-14. The normalised spectra (a), (c) and (e), and the corresponding spectrograms (b), (d) and (f) of the EEG data with low frequency activity.

D. MEG Data

Another useful application of the differentiator lies in the analysis of MEG data. A CTF Systems 151 channel MEG was used to record over 20 minutes of ongoing activity in a normal, healthy volunteer. The data was downsampled to a sampling rate of 100 Hz, and was used as the input of the differentiator. The original and the normalised spectra computed by the Welch method (with a frequency resolution of 0.1 Hz) for some of these channels are shown in Figure 6-15. The examples given here demonstrate that passing MEG data through the differentiator achieves normalisation of its spectra.

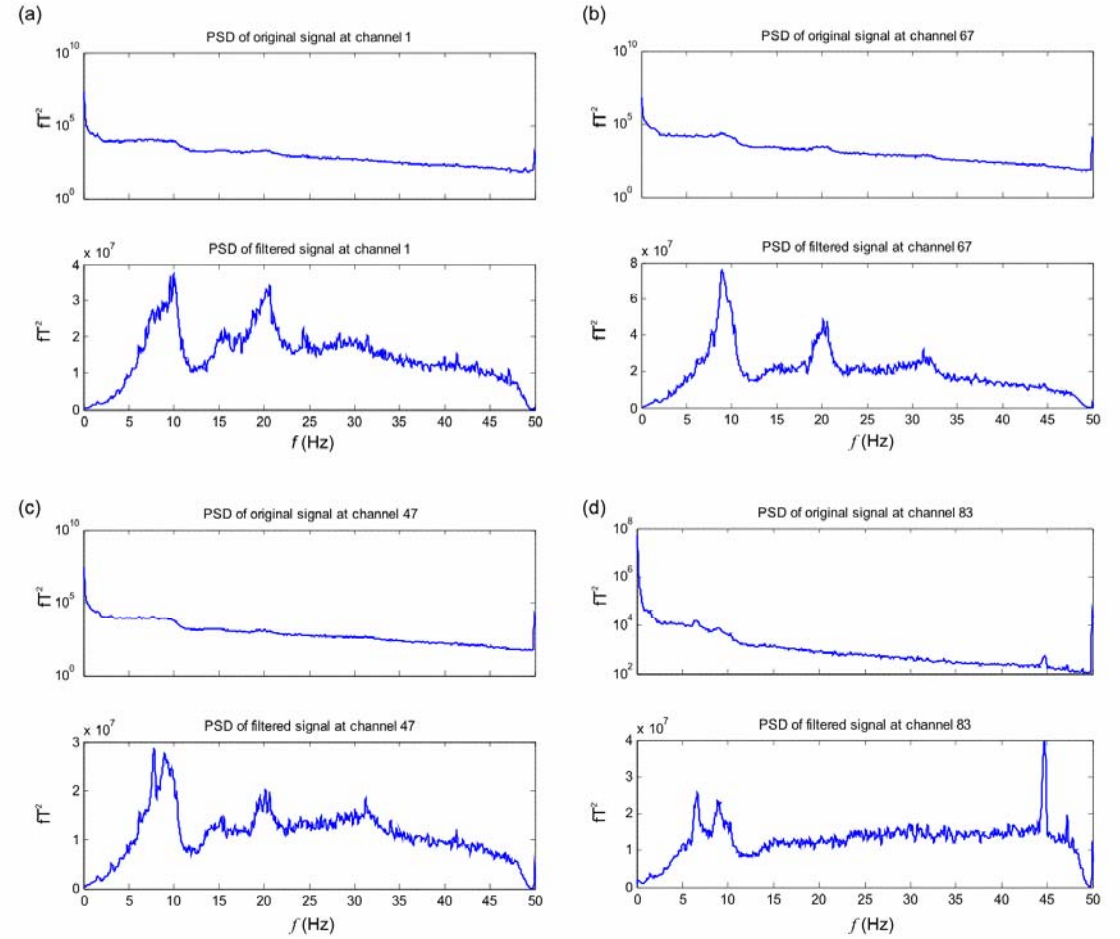

Figure 6-15. Normalised spectra of selected MEG channels: Note the prominent peaks in the PSDs of the filtered signals (y-axis in linear scale), which were previously obscured by the $1/f^2$ trend in the original PSDs of the raw unfiltered signal (y-axis in logarithmic scale).

The peaks around 10 Hz and 20 Hz in Figure 6-15 (a) and (b) are barely visible in the original PSD due to the $1/f^2$ trend but become very evident after filtering. In (c) and (d), the distinct theta frequency components around 7 Hz and 9 Hz are much more pronounced in the normalised spectrum. Moreover, the filtered spectrum in (d) shows an artifactual peak at 44 Hz of a much higher amplitude (relative to the lower frequency components) once the $1/f^2$ trend is

compensated for. This shows the importance of this technique for clearly distinguishing prominent frequency components as well as for comparing signal power in different frequency bands. Note that the original spectra are shown on a logarithmic *y*-axis scale to allow the higher frequency peaks to be at least slightly visible prior to filtering, (if these are shown on a linear scale any activity above 2 Hz will be completely masked because of the high amplitude difference introduced by the intrinsic $1/f^2$ trend).

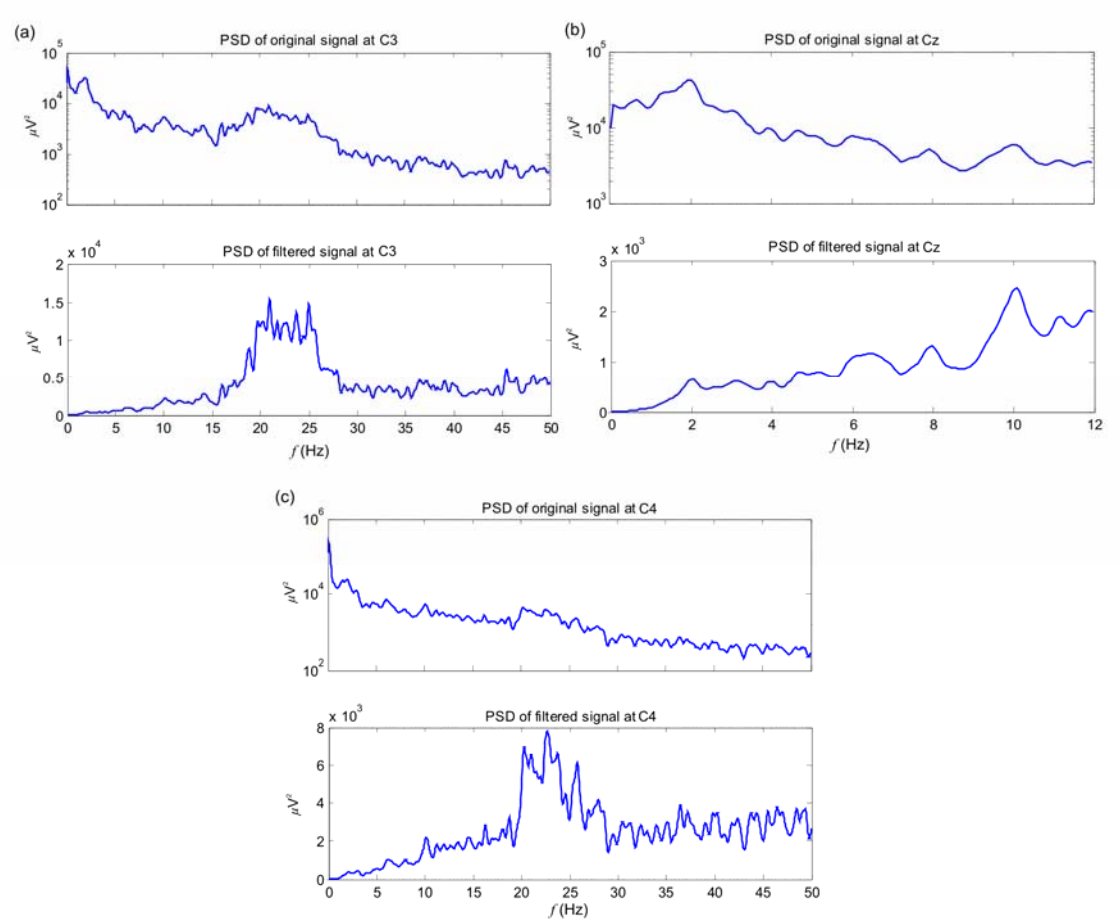

Figure 6-16. ERP data normalised by the differentiator: PSDs of original and filtered signals at Channel C3 (a), Cz (b) and C4 (c). Original spectra shown on a logarithmic *y*-axis scale for better visualisation. Note the low frequency peak apparent at 10 Hz corresponding to a weak P300 response in (b), and the clear prominent activity in the gamma band around 20-30 Hz in (a) and (c).

E. Evoked Response Potential Data

Another important set of EEG signals are those involving ERPs such as the P300 responses. One minute worth of EEG data sampled at 240 Hz for electrodes C3, Cz and C4 (where the P300 response was expected to be most prominent) was used here. The participant was presented with a 6 by 6 matrix of characters. The task was to focus attention on characters in a word prescribed by the investigator, one character at a time. The data contained 35 epochs of 1.5 second duration

each, (stimulus onset at 0.5 seconds). On computing the PSD of the three EEG signals using the Welch method (with frequency resolution of 0.2 Hz), it became evident that these also exhibit $1/f^2$ spectral behaviour. This was expected because evoked responses share the same physical model as the EEG, the only difference being that evoked potentials are time-locked to a stimulus and generally have lower amplitudes than ongoing EEG. Filtering can thus be used to normalise their spectra for clearer data analysis, as shown in Figure 6-16.

6.1.4. Discussion

In this section, several procedures for achieving spectral normalisation have been explored as a way of revealing relevant task- or condition-related peaks, which may otherwise be obscured by the $1/f^{\gamma}$ spectral trend inherent in EM brain signals. The most straightforward and simplest method for normalisation was achieved in the time domain by assuming $\gamma=2$, hence implementing a 2nd order differentiator with an f^2 power spectrum and a linear phase response. Suppression of the inherent trend was achieved for all types of EM recordings; this demonstrates that the spectral trend for the underlying background EM brain activity can be considered as $1/f^2$, and the approximation to model its inverse by a differentiator is suitable.

The following section describes two separate studies carried out on MEG recordings of children with ADHD and controls. Details of the MEG dataset and the experimental protocols used are first given, followed by a description of the motivation behind the two studies and the methodologies employed in each. The first study tackles phase synchronisation in the slow wave band between the processes extracted by SC-ICA. The second study explores a novel way of investigating the effect of the slow waves on brain function by considering the nature of the trial-to-trial variability in evoked neural responses, mainly the M100, which have been extracted through ST-ICA. The results obtained from each study are presented and discussed.

6.2. MEG dataset

The MEG dataset comprising recordings of ADHD and control children was supplied by the MEG centre, Complutense, University of Madrid (UCM) in Spain. The data was collected by means of a whole-head magnetometer (Magnes 2500®, 4D NeuroImaging Technologies Inc., San Diego CA, USA) consisting of 148 sensors (Figure 6-17) as part of an unrelated study. The recordings were digitized at a rate of 678 Hz and subsequently downsampled offline to a rate of 100 Hz. Participants' information and the experimental protocols are given below.

A. Participants

18 children with ADHD (11 boys) and 11 healthy controls (6 boys) took part in the study. Children's ages ranged from 7 to 11 years (mean age 8.7±1.1 years). All participants were right-handed, had normal vision, and had an IQ higher than 85 (WISC-IV, Wechsler, 2005). ADHD children who were treated with stimulant medication (Concerta®) (3 ten-year-old children – 1 boy and 2 girls) were asked to discontinue the treatment for 72 hours prior to the MEG recordings. The rest of the sample was not taking any medication. Children with ADHD were recruited from different schools from the urban and suburban district in Madrid.

ADHD diagnosis was based on the Behaviour Assessment Scale for Children (BASC, Reynolds and Kamphaus, 1992). The BASC is a multimethod and multidimensional approach that measures adaptive as well as clinical dimensions of behaviour and personality based on the Diagnostic and Statistical Manual of Mental Disorders (DSM-III R, American Psychiatric Disorder, 1987). Due to its excellent psychometric properties, the BASC is a frequently used measure in the clinical domain (Ellison and Semrud-Clikeman, 2007; Semrud-Clikeman *et al*., 2008). Furthermore, the BASC has been adapted and standardized for the Spanish population (Reynolds and Kamphaus, 2004). The main constituents of the BASC are the Teacher Rating Scales (TRS), the Parent Rating Scales (PRS) and the Self-Report of Personality (SRP). In addition to these scales, a supplementary component of the BASC, the Structured Developmental History (SDH), was used.

The first stage in the recruitment of the ADHD sample involved an interview to parents of sixty-three potential participants. After signing the consent form, parents filled in the SDH and PRS. This information was used to exclude potential participants who met criteria for either psychiatric, neurological or behavioural disorders, or learning disabilities. In addition, children who scored higher than 60 in the PRS Hyperactivity and/or Attention scales were selected for the

next recruitment stage. Subsequently, teachers of the selected subsample filled in the TRS. Eighteen children also showed a score above 60 in the TRS Hyperactivity and/or Attention scales and therefore they were included in the study. After selecting the ADHD sample, control participants from the same classroom were recruited and the same screening procedure was repeated for them. Exclusion criteria for control children were the same as noted above. In addition, the inclusion criteria were a score below 60 in both the PRS and the TRS Hyperactivity and Attention scales of the BASC.

The ADHD and control groups were also matched by psychosocial adversity measure and socioeconomic status. For the former measure two indices were used. The first one assessed six areas (Brown *et al*., 1981; Max *et al*., 2005), namely: (1) child not living with biological or adoptive parents; (2) sibship of at least four children or a person-to-room ratio exceeding one; (3) admission of the child into the care of the local authority because of family difficulties; (4) maternal "malaise inventory" score of 7 or more; (5) paternal criminality; and (6) father or mother with an unskilled or semiskilled job. The second one provided a measure for parental problems of adjustment (White, 1982; Fergusson *et al*., 1994), and included: (1) whether the child's parents had ever used cannabis or other illicit drugs; (2) whether there was a parental history of problems with alcohol or other substance abuse; (3) whether there was a parental history of offending; all assessing the time before the children reached the age of 7. For each item with no suggested adversity a score of 0 was given, whereas a score of 1 was assigned to areas where there was adversity. The ADHD and control groups both had a psychosocial index of (0.46±0.52) whilst their index for parental problems of adjustment was (0.27±0.47) and (0.19±0.41) respectively, hence showing group matching for both aspects.

Socioeconomic status (SES) assessment was accomplished through the Barratt Simplified Measure of Social Status (BSMSS) (Barratt, 2006), which considers parents' education levels and job categories as measures for a socioeconomic status index. The BSMSS is built on the work of the Hollingshead Four Factor Measure (Hollingshead, 1975) and provides an updated list of occupations to better address current occupations as they relate to social status. Stay-at-home mothers are not included in the BSMSS calculation. The Four Factor Index of Social Status scores range from 8 to 66, with higher scores indicating higher educational and occupational levels and higher SES. The SES media from the control group mean was 45.50 and the ADHD group mean was 44.50 (cf. Table 6-1).

		Education level			Score occupation			Barrat Simplified Measure of Social Status
GROUP	**AGE**	**Mother**	**Father**	**(Mother + Father) /2**	**Mother**	**Father**	**(Mother + Father) /2**	
CTRL	7	12	9	10.5	25	30	27.5	38
CTRL	8	21	21	21	40	40	40	61
CTRL	8	9	6	7.5	25	15	20	27.5
CTRL	8	15	9	12	10	20	15	27
CTRL	8	12	15	13.5	25	30	27.5	41
CTRL	8	12	6	9	15	10	12.5	21.5
CTRL	8	21	21	21	45	45	45	66
CTRL	9	12	12	12	30	30	30	42
CTRL	9	18	21	19.5	35	40	37.5	57
CTRL	10	21	21	21	40	45	42.5	63.5
CTRL	10	21	21	21	35	35	35	56
ADHD	7	12	21	16.5	25	30	27.5	44
ADHD	8	21	21	21	35	35	35	56
ADHD	9	6	6	6	15	20	17.5	23.5
ADHD	9	15	15	15	35	35	35	50
ADHD	9	12	9	10.5	25	25	25	35.5
ADHD	10	12	21	16.5	.	35	17.5	34
ADHD	10	9	9	9	25	30	27.5	36.5
ADHD	10	21	21	21	45	35	40	61
ADHD	10	12	21	16.5	25	30	27.5	44
ADHD	10	12	21	16.5	25	30	27.5	44
ADHD	11	21	21	21	40	40	40	61

Table 6-1. Socioeconomic status assessment through the Barratt Simplified Measure of Social Status (BSMSS) (Barratt, 2006), for ADHD and control groups.

Before the MEG recordings, written informed consent detailing the procedures of the study and approved by the Ethics Committee of the Complutense University of Madrid in accordance with the ethical standards laid down in the 1964 Declaration of Helsinki, was provided by a parent. In addition, all children provided oral assent to participate in this study. Due to excessive head-movement artifacts in the MEG signal, 7 ADHD children were excluded from the MEG analysis since their recordings were unusable. This was decided upon calculation of the variance of the signal as a test for non-biological noise in the recordings – a high variance is an indicator of noisy recordings. The remaining ADHD subsample consisted of 11 children (8 boys).

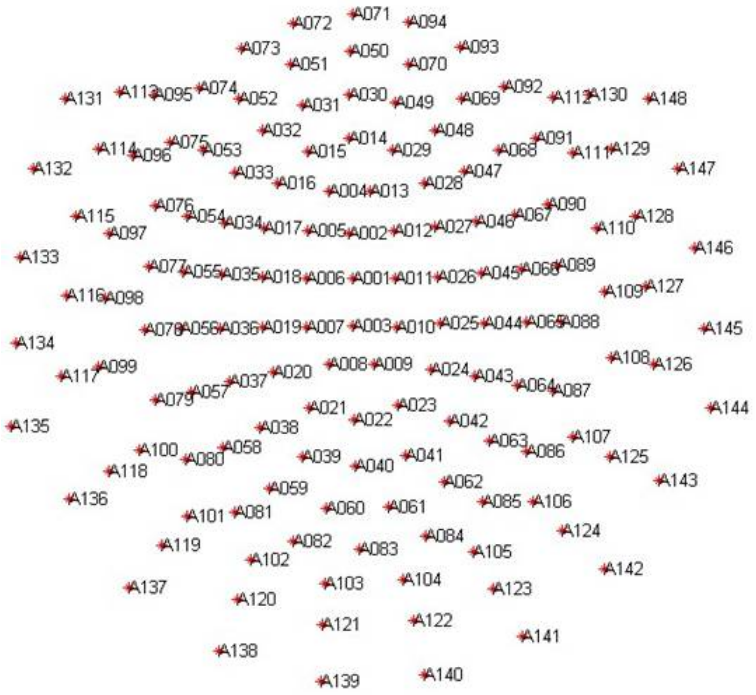

Figure 6-17. Location of the 148 channels in the Magnes 2500® Whole-Head MEG system (4D NeuroImaging Technologies Inc., San Diego CA, USA).

B. Experimental Protocol

Two types of experiments were carried out for every participant, namely the perceptual (passive) and the attention (active) tasks. In the perception task two stimuli (circles and lines) appeared on the screen and the participants were advised to look at the centre of the screen without attending to the stimuli. This task consisted of 3 blocks of 3 minutes each and lasted for around 11-12 minutes, Figure 6-18 (a). The variability was due to the variable interstimulus interval and the variable resting time for every participant (since the participants were allowed to decide when they were ready to start the following block), Figure 6-18 (b). In the attention task, the same stimuli appeared on the screen but the participants had to focus on the right, left, or on both sides of the screen (depending on the instruction given, Figure 6-19 (a)) and press a button whenever a line appeared on that side. Here the lines were the targets and the circles were the distractors, each with a probability of occurrence of 50%. The participants were always instructed to look at the centre of the screen, independently of the side where they were supposed to focus their attention on. The attention task recording consisted of 5 blocks of 3 minutes each and lasted for around 19-21 minutes, Figure 6-19 (b).

(a)

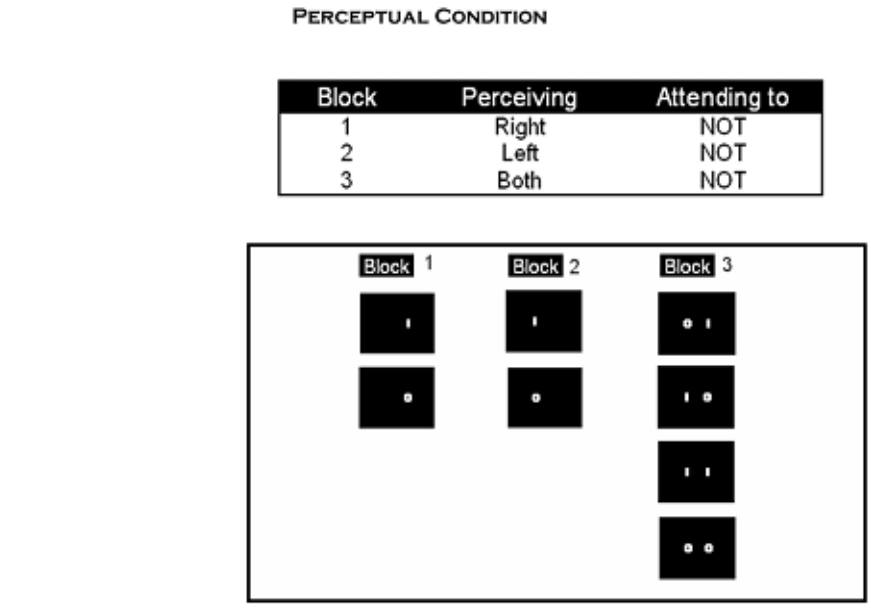

(b)

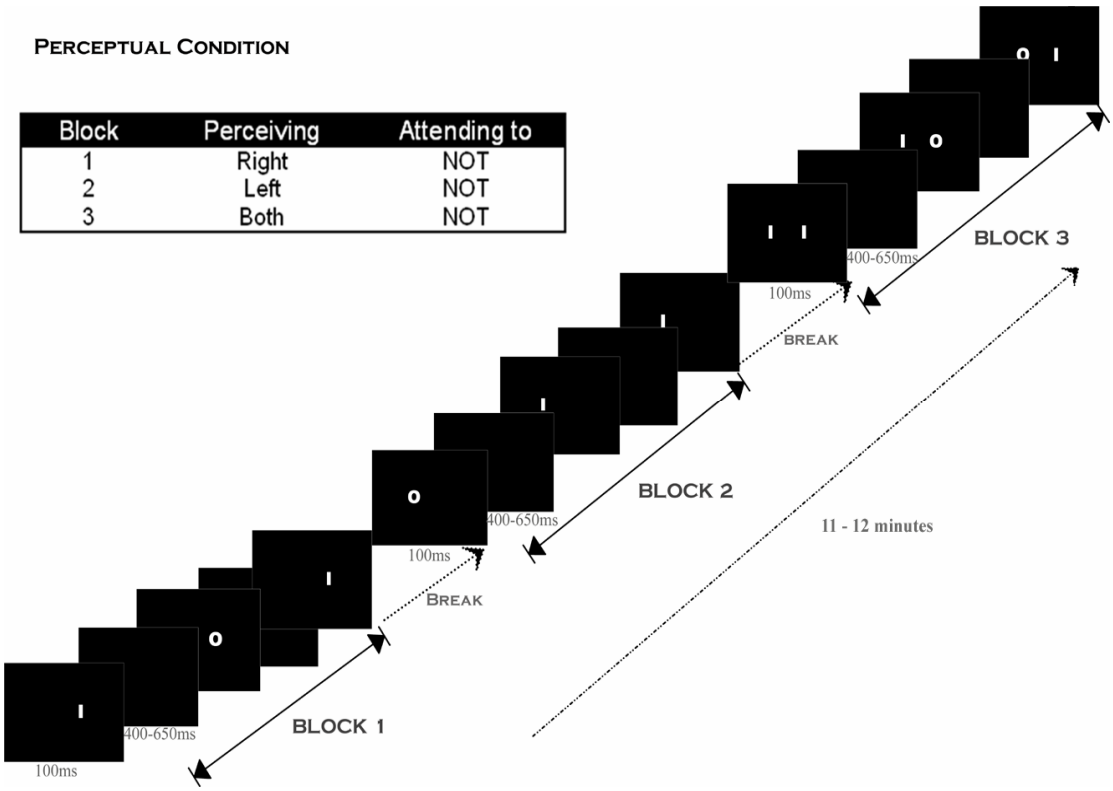

Figure 6-18. Schematic representation of Perception task: (a) Stimuli appearing on the screen (on the right/left/both sides) but no action required; (b) Three 3-minute task blocks separated by a variable resting time (marked as 'BREAK' here).

(a)

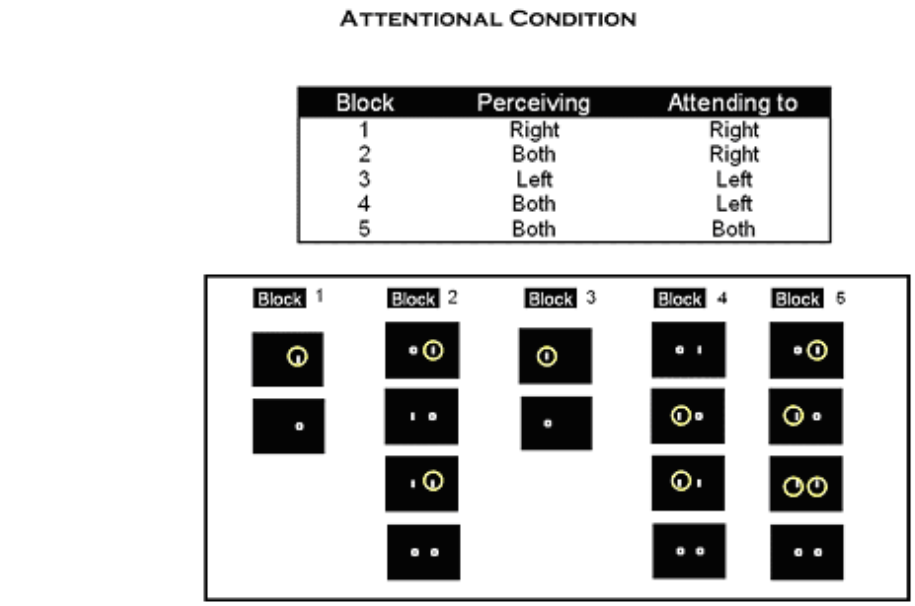

Block	Perceiving	Attending to
1	Right	Right
2	Both	Right
3	Left	Left
4	Both	Left
5	Both	Both

(b)

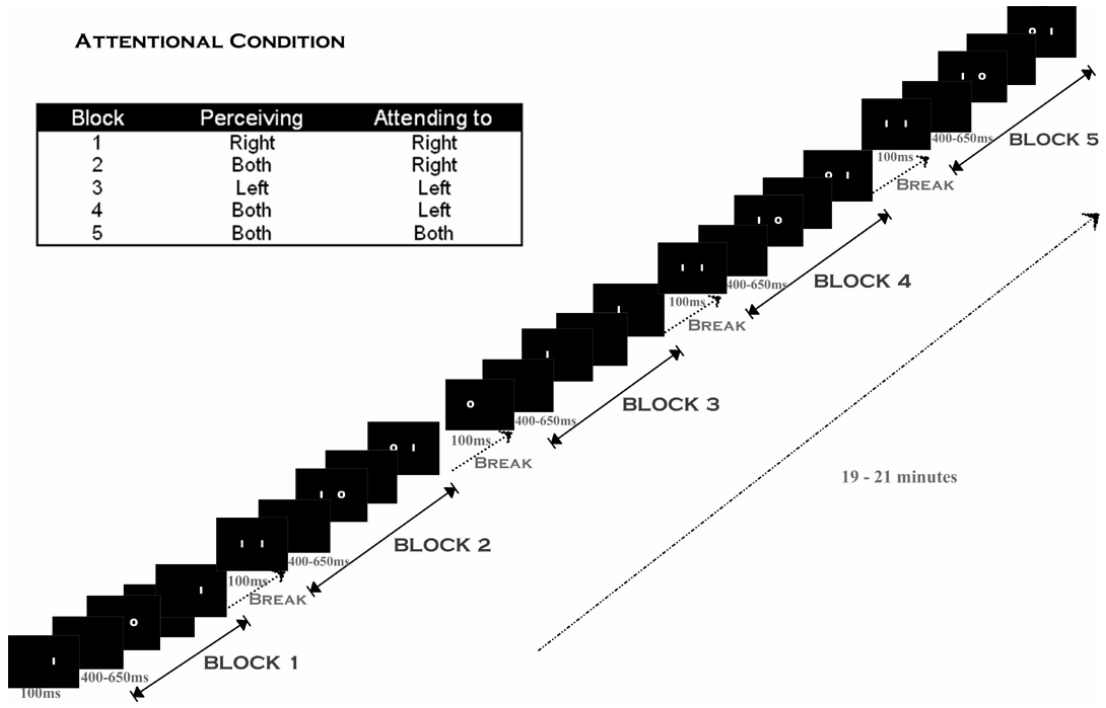

Block	Perceiving	Attending to
1	Right	Right
2	Both	Right
3	Left	Left
4	Both	Left
5	Both	Both

Figure 6-19. Schematic representation of Attention task: (a) Stimuli appearing on the right/left/both sides of screen, button pressed whenever a target (line) appeared on that side, (b) Five 3-minute task blocks separated by a variable resting time (marked as 'BREAK' here).

Stimuli were 100 ms long, each followed by a variable interstimulus interval of 400-650 ms. This duration was chosen to focus on aspects of selective rather than sustained attention. The order of the two tasks was counterbalanced across participants. During the recordings participants were lying in supine position and instructed to avoid head movements and eye blinking as much as possible. The stimuli were presented by an LCD video projector (SONY VPL-X600E) outside of the magnetically shielded room onto a series of in-room mirrors, the last of which was suspended 1 m above the participant's face.

6.2.1. Low Frequency Phase Synchronisation Analysis using SC-ICA

As explained in the first chapters of this work, fMRI studies have shown that the brains of individuals undertaking no externally imposed cognitive tasks display patterns of spontaneous intrinsic activity synchronised across widely distributed brain regions; one of such networks is the default mode network (Fransson, 2005). Spontaneous VLFOs associated with the DMN are commonly attenuated during task. However, they sometimes re-emerge during periods of active processing, competing and interfering with goal-directed attention. This results in low frequency toggling between the task-independent (-negative) and task-positive components and presents a potential source of attention deficit during active task performance. This forms the basis of the DMI hypothesis described in Chapter 2. Furthermore, Sonuga-Barke and Castellanos (2007) consider the possibility of ADHD being a default-mode deficit disorder in relation to the impairments in sustained attention experienced by individuals with this disorder. Application of the DMI hypothesis to ADHD then suggests that such sustained attention lapses would be *slow and periodic*, resulting from the intrusion of the task-negative component. In addition, most ADHD studies postulate the involvement of multiple brain areas and are backed up by the notion that ADHD is a highly heterogeneous disorder (Johnson *et al*., 2007).

The first study involved a preliminary investigation of these findings conducted on the MEG recordings. The aim was to address the following issues:

(i) Can these VLFOs associated with the DMN be identified within MEG recordings?
(ii) Which distinct brain areas are interacting during different rest and task conditions (forming network(s) of brain activity)?
(iii) Is there a change in this interaction with a switch from rest to task?
(iv) What are the differences (if any) between ADHD and controls?

The interaction between pairs of distant MEG channels can be quantified by phase synchronisation. As explained in Chapter 3, this is widely used in the literature as a vital mechanism for dynamic integration of distributed oscillators within the brain (Lachaux *et al*.,

1999; Quian Quiroga *et al*., 2002). It is a measure that shows whether the phase shift between two signals is close to a constant over the specified time interval. Phase synchrony proves to be very useful because it is independent of the signals' amplitudes and can thus indicate instances where two signals are phase locked whilst their amplitudes vary independently (Lachaux *et al*., 1999).

Classical methods for establishing phase synchrony, however, require the signals to be narrowband (Quian Quiroga *et al*., 2002). This implies that phase locking results would depend greatly on the chosen frequency band. It also requires filters with good resolution in both time and frequency and which do not cause any phase distortion. The 148 channels of MEG data may be phase locked in various frequency bands thus making the analysis quite cumbersome. Furthermore, MEG data is obtained from an inherently noisy recording process, which implies that denoising techniques involving BSS would be best employed for proper analysis of any true underlying networks.

SC-ICA provides an optimal analysis method for this problem due to its ability to isolate underlying components using only temporal information inherent in single channel recordings (Davies and James, 2007). The 148 channel MEG system is highly dense and channels that are close to each other tend to be influenced by activity from similar brain areas. By analysing fewer channels in specific brain regions one would still be able to extract underlying temporal generators contributing to the measured signals. Moreover, as explained in Chapter 5, the separated independent sources identified by SC-ICA have disjoint spectra. This is very powerful since it automatically locates the frequency bands of interest and allows for the extraction of sources with some overlapping frequency content. Meanwhile, it simultaneously performs denoising, extracting artifactual as well as neurophysiologically meaningful sources.

Consequently, this BSS technique has been used here to isolate the VLFOs associated with the default network within the MEG recordings. Phase synchronisation analysis was then carried out on the extracted band-limited sources to establish which brain areas were interacting throughout the course of the task. Before moving on to the methodology applied for this analysis, the procedure for measuring phase synchronisation is described next.

A. Phase Synchronisation

This is defined as the locking of the phases of two oscillators for a specified time duration

$$\Delta\varphi(\mathrm{t}) = |n\varphi_1(t) - m\varphi_2(t)| \approx \text{constant}, \tag{6.3}$$

where $\varphi_1(t)$ and $\varphi_2(t)$ denote the instantaneous phase sequences of the 2 channels, and n and m are integers which indicate the ratios of possible frequency locking. Since the multivariate signals come from the same physiological system (the brain) we can consider $n = m = 1$ (Le van Quyen *et al*., 2001).

As briefly introduced in Chapter 3, a measure for phase synchronisation between signal pairs can be derived following a three step procedure:

(i) Estimation of the instantaneous phase of each signal

This can be achieved using the Hilbert transform as a means for estimating the instantaneous phase and hence finding the phase difference between two given signals. The Hilbert transform (Rosenblum *et al*., 1996) gives the instantaneous amplitude and phase of a signal $x(t)$ via the construction of an analytic signal, $\zeta(t)$, which is a complex function of time defined as

$$\zeta(t) = x(t) + i\tilde{x}(t) = A(t)e^{i\varphi(t)}. \tag{6.4}$$

The function $\tilde{x}(t)$ is the Hilbert transform of $x(t)$ and is given by the convolution of the signal with the function $1/\pi t$

$$\tilde{x}(t) = \frac{1}{\pi} P.V. \int_{-\infty}^{\infty} \frac{x(\tau)}{(t-\tau)} d\tau . \tag{6.5}$$

where *P.V.* is the Cauchy principal value.

The instantaneous amplitude $A(t)$ and phase of the signal $\varphi(t)$ are uniquely defined from equation (6.4), where the phase is given by

$$\varphi(t) = \arctan \frac{\tilde{x}(t)}{x(t)}. \tag{6.6}$$

Application of the convolution theorem turns equation (6.5) into

$$\tilde{x}(t) = -i\mathrm{FT}^{-1}\left[\mathrm{FT}\left[x(t)\right] sign(\omega)\right], \tag{6.7}$$

where FT denotes the Fourier transform and FT^{-1} denotes its inverse.

Hence, this transform performs a phase shift of the original signal by $\pi/2$ in the frequency domain while the power spectrum remains unchanged. In addition, the instantaneous phase as

defined in equation (6.6) is restricted to the interval [0, 2π] (Aihua and Yuhan, 2005). This implies that the Hilbert transform is actually a filter with unit gain at every frequency so that the whole range of frequencies is taken into account in defining the phase of the analytic signal. If the signal is broadband, as usually happens with EEG/MEG, the Hilbert transform fails to give a proper estimation of the phase (Pikovsky *et al*., 2002). Chavez *et al*. (2006) show that for a broadband signal, this transform actually yields a representation which exhibits multiple centres of rotations in the complex plane such that the instantaneous phase cannot be well defined.

Moreover, EEG and MEG signals are not periodic, and hence this notion of *instantaneous* frequency and phase becomes important. The concept of PS is based on the assumption that there is a dominant frequency in the signal that leads to a well defined and unique value of the phase for each interacting channel. If the signals to be analysed have a broadband or a multimodal spectrum, then the definition of the phase can be troublesome since instantaneous amplitude and phase have a clear meaning *only* if the signal is narrowband. This is another reason why all analyses are done around a specific frequency band and pre-filtering of the signals (with a filter that does not introduce phase distortions) is necessary (Pereda *et al*., 2005).

Phase Wrapping

Hurtado *et al*. (2007) also demonstrate that for the phase construction to be meaningful it is important that the time series is oscillatory – i.e. there are significant peaks in the power spectrum. However, when dealing with noisy or chaotic systems such as EEG and MEG, it turns out that the signal's phase can exhibit rapid phase jumps (discontinuities) of 2π. Due to these phase jumps, the instantaneous frequency is strongly affected by noise which makes it an inadequate measure for synchronisation in noisy time series (Pikovsky *et al*., 2002). Consequently, the signal's phase is normally unwrapped by adding multiples of $\pm 2\pi$ when the absolute jumps between consecutive points in the phase time series are greater than or equal to the default jump tolerance of π radians. The unwrapped phases are then used to compute the phase difference between the two signals (as in equation (6.3)). This observation is also made by other researchers in the field (Tass *et al*., 1998; Hurtado *et al*., 2007).

(ii) Establishing an index to quantify phase synchrony

A popular coefficient is the phase locking value, (PLV), defined as

$$PLV = \left| \frac{1}{N_{trial}} \sum_{n=1}^{N_{trial}} e^{j(\Delta\varphi(t,n))} \right|, \tag{6.8}$$

where N_{trial} is the length of the window in samples and $\Delta\varphi(t,n)$ is the phase difference between the two channels, n representing the time instant at which the analysis ends.

Hence, this index defines a measure of the inter-trial variability of the phase difference within a given time window (Lachaux *et al*., 1999). The chosen length of the time window is very important since if this is too long stationarity will be compromised whereas if it is too short important interactions can be mimed especially if these are weak or masked by noise. A 1.5- to 20-second time window is usually considered (Hurtado *et al*., 2007). The PLV is independent of the signals' amplitude, makes no assumptions about the nature of the signals and provides a non-parametric measure that quantifies the interaction of two signals over time.

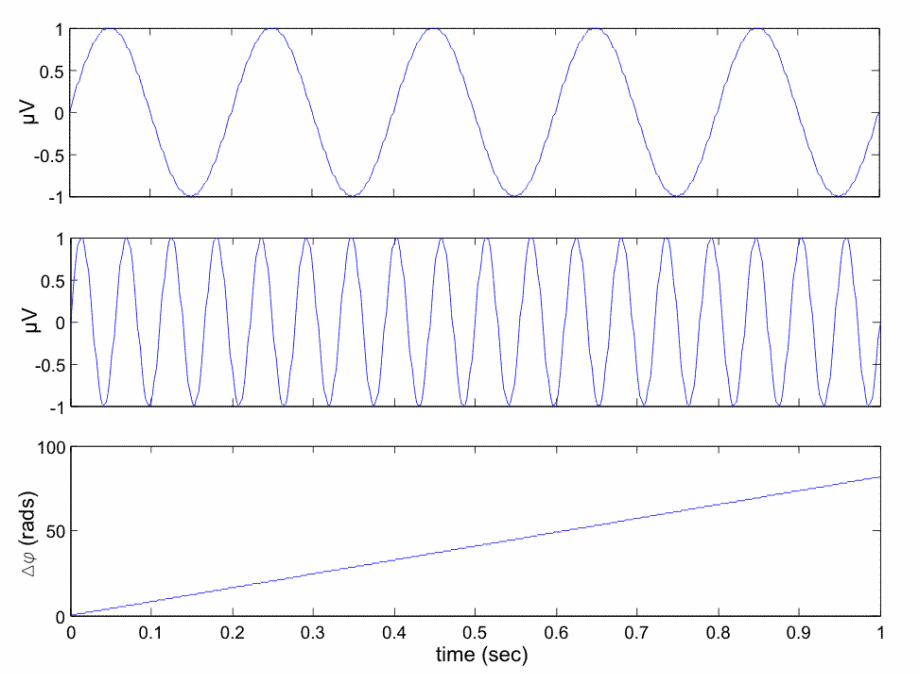

Figure 6-20. The phase difference between two sine waves of different frequencies (5 Hz and 18 Hz) accumulates over time.

From equation (6.8) it is evident that if the phase difference for a given time period varies very little across trials then the PLV would be close to 1, otherwise it is close to zero. Moreover, for periodic signals with a dominant frequency component, the PLV is expected to be high if both signals are in the same frequency band since the phase difference between them, $\Delta\varphi(t,n)$ remains constant. On the other hand, the phase difference between two signals at different frequencies accumulates over time. This is shown in Figure 6-20 – here the phase difference of the two sine waves of frequencies 5 Hz and 18 Hz starts at zero but increases monotonically over the duration of time considered. Evaluation of the expected value of the PLV for two signals at different frequencies can be found in the work by Tcheslavski (2005).

Figure 6-21 shows an example of the phase locking between pairs of ictal EEG signals containing an epileptic seizure with a left temporal focus. The signals were band-pass filtered between 4 and 8 Hz. The signals' instantaneous phases have been unwrapped (and also detrended for illustration purposes only). It is clear that the phase difference between T3 and Fz varied throughout the 2.6-minute recording (Figure 6-21 (a)) whereas that between T3 and T9 (around the seizure focus) remained relatively low (Figure 6-21 (b)). Therefore, when the PLV was evaluated for 3-second time windows with 50 % overlap, T3-Fz had low PLVs whereas the PLVs for T3-T9 were close to one for nearly all time windows, since the phase difference between these two channels stayed relatively constant during the 3-second segments.

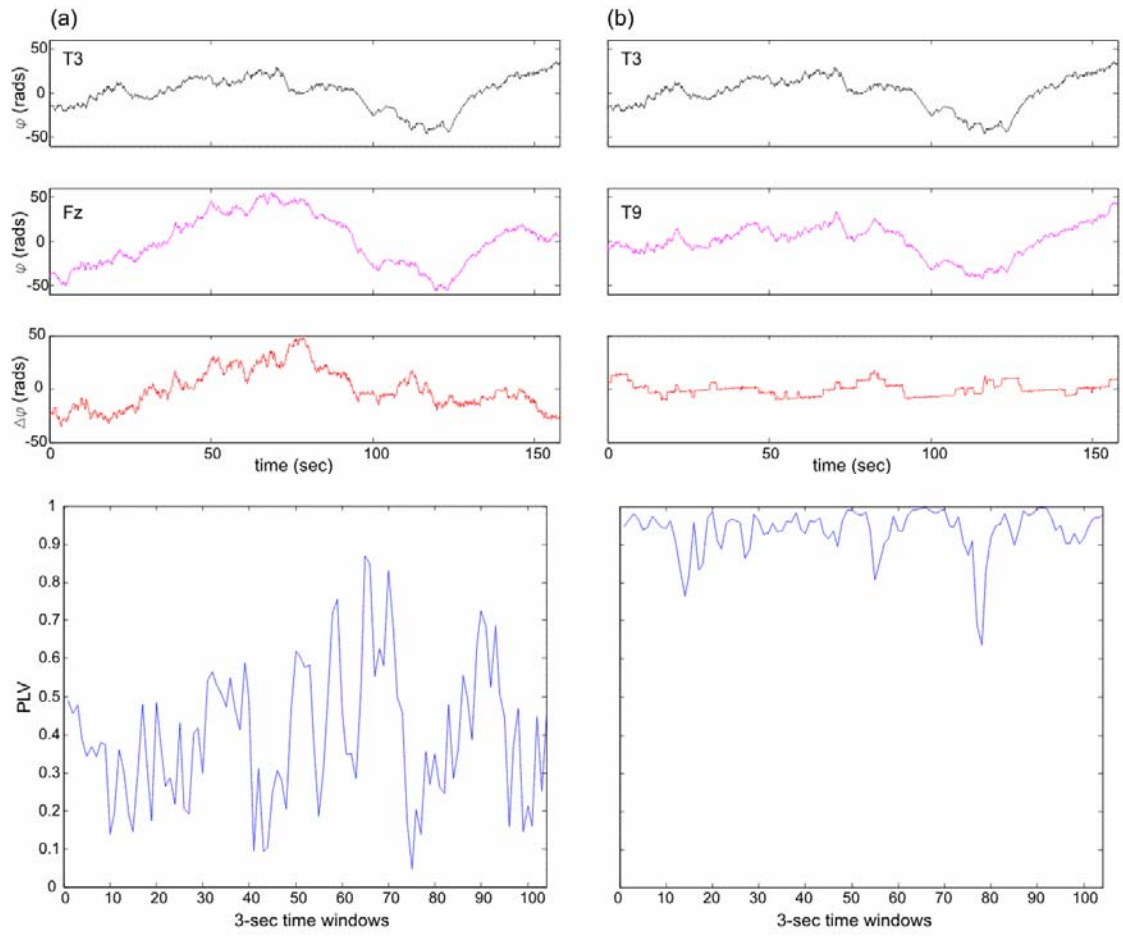

Figure 6-21. PLV as an indicator of the phase difference $\Delta\varphi$ between two signals: (a) A varying phase difference between T3 and Fz during the 3-second time windows results in a low PLV; (b) A more constant phase difference between channels T3 and T9 during the 3-second segments results in a PLV which is close to 1 for nearly all time windows.

(iii) Establishing a statistical criterion to quantify the degree of phase locking

Phase locking statistics (PLS) are used to determine the degree of statistical significance of each PLV in order to distinguish significant PLVs from background fluctuations. This is done by comparing the original PLV between two channels to surrogate PLVs. There are several ways to construct these surrogates such as, assembling surrogate time series by drawing samples from a Gaussian distribution that preserves the mean and variance of the original series, or by generating surrogate phase series directly (Hurtado *et al*., 2007). More commonly, surrogate values are obtained from the original signals (say x and y) but after permuting the order of all the trials of y. This can be achieved by shuffling the y time series as done by Lachaux *et al.* (1999). However, it is argued that shuffling the data changes its autocorrelation structure, which may in turn affect the values of the synchronisation indices. This is because shuffling provides a white noise-like version of the data such that prominent autocorrelations inherent to neurophysiological signals are destroyed. This turns the surrogates into very unlikely realisations of any neurophysiological process (Pereda *et al*., 2005).

Therefore, it is essential to construct surrogates that preserve the individual structure of the data while destroying all interdependencies between the signals. This can be achieved by comparing the original version of one of the signals with a temporally shifted version of the other. Such randomized time shifts destroy any temporal structure if present in the original time series (Pereda *et al*., 2005). A significance threshold for the original PLV is then established by comparing this value to a number of surrogates (typically 200) (Lachaux *et al*., 1999; Theoden *et al*., 2002). This threshold is usually set by constructing a distribution for the surrogate PLVs and then taking its 95% quantile. This is equivalent to taking the mean ± twice the standard deviation if the surrogates distribution is normal (Figure 6-22), (Theoden *et al*., 2002). This procedure is carried out for each time window such that the PLS threshold also varies with time. With reference to Figure 6-23, the original PLV between two channels is considered significant whenever it lies outside the low (5%) and high (95%) percentiles. Due to the nature of the PLV index, (i.e. high PLV implies synchronisation), the PLV is said to be significant whenever it exceeds the 95% PLS threshold; otherwise it is considered spurious and is set to zero. It is important to note that with such method the conclusions will depend strongly on the assumptions that are made in generating the surrogate time series.

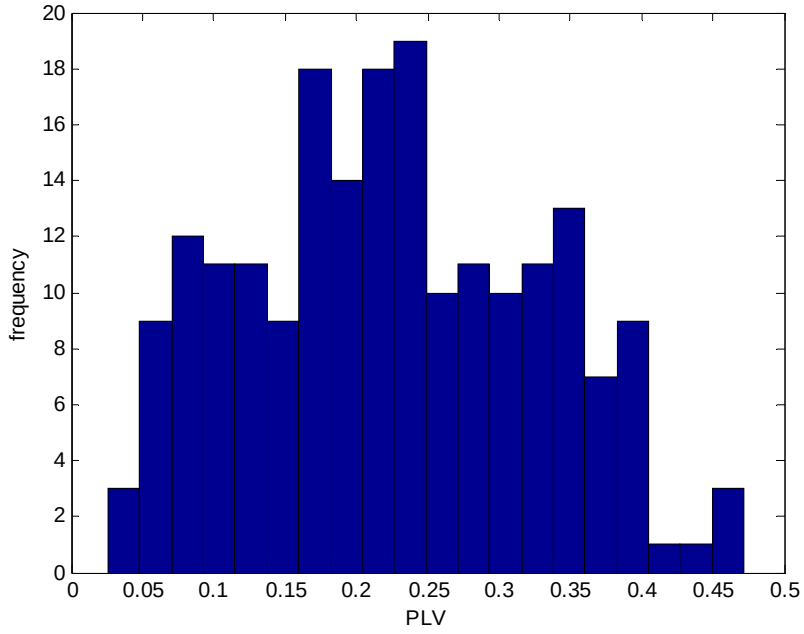

Figure 6-22. Distribution of the surrogate PLVs for one particular time window.

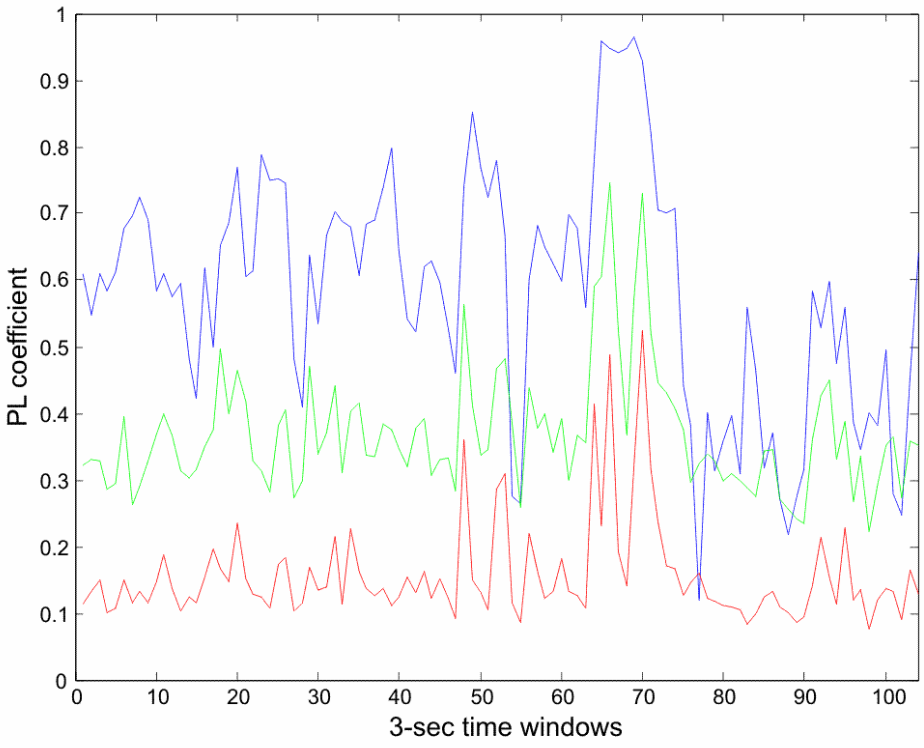

Figure 6-23. The original PLV between 2 channels (blue) is compared to the low (red) and high (green) PLS percentiles derived from the 5% and 95% limits of the surrogates' distribution for each time window. When the original PLV lies outside these percentiles it implies significant phase synchrony.

B. MEG Data Analysis

The SC-ICA and phase synchronisation methodology (based on the preceding theory), and the results obtained from the MEG dataset are described below.

Pre-processing: The multichannel raw data was first analysed using FastICA (Hyvärinen, 1999b) and ICs related to eye blinks, eye movement and ECG were subtracted from the data. This was done to ensure that any low frequency peaks inherent in the data were not due to known artifacts having low frequency characteristics. This data was low pass filtered to 2 Hz by a 64th order FIR filter, and down-sampled to a sampling rate of 10 Hz.

Channel Selection and SCICA: Since various brain regions may be involved in the underlying networks, five channels were selected from distinct areas, namely the frontal, central, occipital, and left and right parietal regions (Figure 6-24). The whole recording for both tasks (20 or 12 minutes) was used in the analysis to include enough cycles to accommodate the slow waves. The delay dimension m for SC-ICA was chosen to be 200, providing a frequency resolution of 0.05 Hz (according to equation (5.13)). The selected channels were temporally whitened and dimensional reduction was achieved by the discrete cosine transform (DCT); this transform expresses the signal into a sum of cosine functions oscillating at different frequencies. The DCT is widely used in signal and image processing because of its strong energy compaction property: most of the signal information tends to be concentrated in a few low frequency coefficients, and small high-frequency ones can be easily discarded (Feig and Winograd, 1992). The FastICA algorithm was then employed in deflationary mode following the quicker approach, a.k.a. FastIPA, explained in Chapter 5.3.2. For each channel, the underlying processes were extracted and their magnitude frequency response was found, as shown in Figure 6-25.

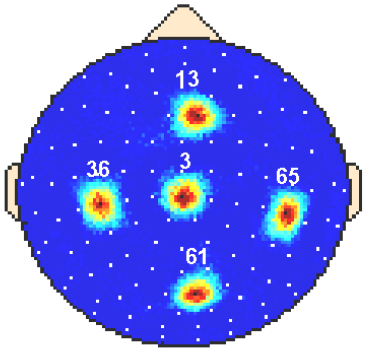

Figure 6-24. Location of the MEG Channels chosen for SC-ICA analysis.

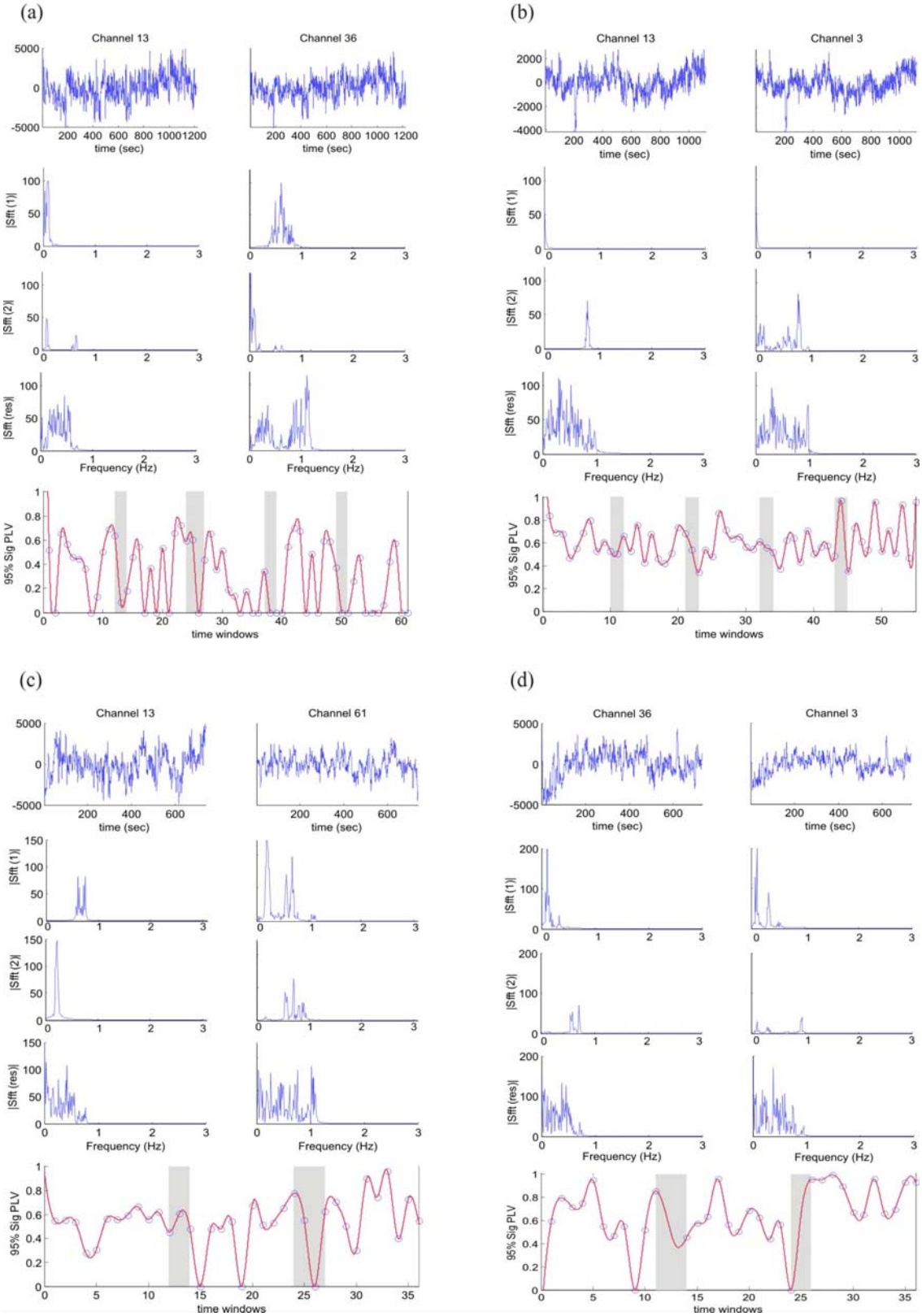

Figure 6-25. Each quadrant shows two channels (ECG and eye artifacts removed), and the frequency response graphs of their independent processes extracted by SC-ICA; |Sfft(*i*)| denotes the magnitude of the single-sided amplitude spectrum for process (*i*). The 95% significant PLV plot for the two channels shows the overall phase synchrony obtained by considering the maximum significant PLV between all pairs of processes with overlapping frequency content. The resting periods are shaded in grey, following the task periods. Quadrant (a) shows ADHD attention, (b) Controls attention, (c) ADHD perception and (d) Controls perception task.

Phase Synchrony: For each participant only the phase locking between processes having overlapping frequency bands was considered, since those with non-overlapping frequencies could not be phase locked (as explained in Figure 6-20). The processes time series were divided into time windows of 20 second duration, and the PLV and the corresponding 95% PLS were calculated for each window. The PLS was found by considering 200 randomly cycle-shifted surrogates. Once all the relevant phase locking between the processes belonging to a particular pair of channels had been established, a graph of the maximum 95% significant PLV was plotted (Figure 6-25). This showed the overall significant phase locking between the two channels. The timing of the rest and task block periods recorded during the experiment were then superimposed on the phase locking graph to give an indication of the fluctuations in phase synchrony of these channels when switching from task to rest. This was done for all combinations of pairs of channels considered and for every set of recordings (one participant - one task). This procedure was repeated on the 8 datasets considered. Selected results for ADHD and control children whilst performing the different tasks are shown in Figure 6-25 to highlight the typical responses obtained.

C. Discussion

This preliminary investigation showed that SC-ICA decomposition was able to single out processes of a low frequency time signature (below 1 Hz and as low as 0.05 Hz) from the MEG data. Results show phase synchronisation between fronto-central, central and parietal areas thus providing evidence of the underlying networks of activity across diverse brain areas. A drop in phase locking can be noted in all the significant PLV plots in the four quadrants following a switch from task to rest. There are more fluctuations in synchronisation during attention task blocks for ADHD than for control participants, (Figure 6-25 (a) and (b)). In general, synchronisation was higher for controls during the attention task. These results can be viewed in relation to the DMI hypothesis; the drop in synchronisation during resting periods may be due to suppression of the task-positive component in the resting brain, and may represent desynchronisation in preparation for the next cognitive act. Meanwhile, task-negative components may re-emerge in a more persistent manner during task blocks for ADHD participants causing synchronisation levels to drop more often. These drops in synchronisation may be linked to lapses in attention during the course of the task (which are more frequent in ADHD).

Although these results are promising, the procedure is quite involved for repetition on a large number of participants, mainly because of the separate channel decomposition achieved by SC-ICA. Moreover, the experimental protocol used for the MEG recordings led to relatively short

(< 1 minute) and variable resting periods in comparison to task blocks. This limited the choice of analysis for comparison between these two conditions. Consequently, the MEG dataset was further exploited by examining the responses to stimuli *within* task blocks, particularly the M100 responses, in order to (i) shed light on how the brain of ADHD and control participants distinguishes and filters relevant and irrelevant information, and (ii) investigate whether these early sensory components, elicited during task, were in any way being affected by the slow waves in the brain. In the following study, the ST-ICA algorithm was used because of its capability to simultaneously extract spatially *or* temporally distinct brain sources from multi-channel recordings.

6.2.2. Trial-to-trial Variability in Evoked Neural Responses

As explained in earlier chapters, fMRI studies have shown that when the intrinsic spontaneous and task-independent VLF oscillations evident in the BOLD signal during rest persist into task sessions, they can predict trial-to-trial variability in both evoked behavior and brain responses. The general notion is that they provide a baseline onto which deterministic responses elicited by the task are superimposed (Fox *et al*., 2006; Fox and Raichle, 2007). Moreover, recent works in the literature indicate that this VLF activity may not be visible in the data as specific brain source(s), but rather, as a mechanism(s) that modulates or even stimulates and/or controls underlying brain processes – analogous to the function of a heart's pacemaker (Monto *et al*., 2008). To this end, an alternative approach for investigating the contribution of VLFOs in brain function in MEG recordings is considered here, based on the assumption that brain sources are superimposed on this intrinsic slow wave activity. This is tested by investigating the inter-trial variability in the amplitude and latency of the evoked brain responses associated with stimulus processing, and examining whether this variability demonstrates a very low frequency nature, which could then infer information about the underlying slow waves. Therefore, the question raised is: does the trial-to-trial variability in MEG ERF components exhibit a VLF temporal signature, in the same frequency range as the previously observed spontaneous fluctuations in the BOLD responses?

The focus is on the visual M100 component which is known to be regulated by attention. This is a marker, localized in the vicinity of the primary visual areas, the amplitude of which is higher when stimuli are attended, as opposed to irrelevant unattended stimuli – the so-called *attentional effect* (Jonkman *et al*., 2004; Mulas *et al*., 2006). This attenuation is due to an inhibitory mechanism for invalid stimuli. Recent studies demonstrate that ADHD children have specific early selective-attention deficits, which may be due to an early filtering deficit, in both the

auditory (Jonkman *et al*., 1997; Ozdag *et al*., 2004; Mulas *et al*., 2006) and visual modalities (Karayanidis *et al*., 2000; Jonkman *et al*., 2004). Particularly, in a visual ERP study, Perchet *et al*. (2001) show that control children exhibit the attentional effect, whereas ADHD children have equal M100 amplitudes in response to relevant and irrelevant stimuli.

This work first investigates the attentional effect. Then it assesses the extent to which the M100 component is modulated by VLFOs and explores variations in these effects as a function of the presence of ADHD by comparing 11 cases against 11 controls. The aims of this pilot study have been to:

(i) Extract M100 components by the newly-developed ST-ICA algorithm employed to perform denoising and dimensionality reduction of the 148-channel MEG data.

(ii) Investigate the attentional effect in ADHD and controls by comparing the amplitude of the M100 components during attention and perception tasks.

(iii) Investigate the trial-to-trial variability of individual M100 components during the attention task by analysing the 'clean' M100 processes extracted by ST-ICA, thus making sure that the inter-trial variability does not arise from internal and/or external noise sources.

(iv) Examine whether this variability exhibits a VLF time signature.

(v) Explore whether these VLF patterns of modulation are different for ADHD and control children.

The methodology used in this work is illustrated in Figure 6-26.

It is important to mention here that generally ER data is analysed by evaluation of the coherent average of the evoked responses. Although this is good for noise reduction, it neglects the fact that the response to individual stimuli may vary widely across trials in amplitude, time course and scalp distribution. Hence, such averaging presents only a first approximation of the brain response to the stimuli and conceals any temporal and spatial variability (Kolev and Yordanova, 1997). On the other hand, the analysis of single trial event-related epochs can potentially reveal more information about the brain dynamics but suffers from poor SNR and masking by artifacts (Jung *et al*., 2001a). These effects can be eliminated by applying the trial-by-trial analysis on the processes extracted by ST-ICA rather than on the raw MEG data itself.

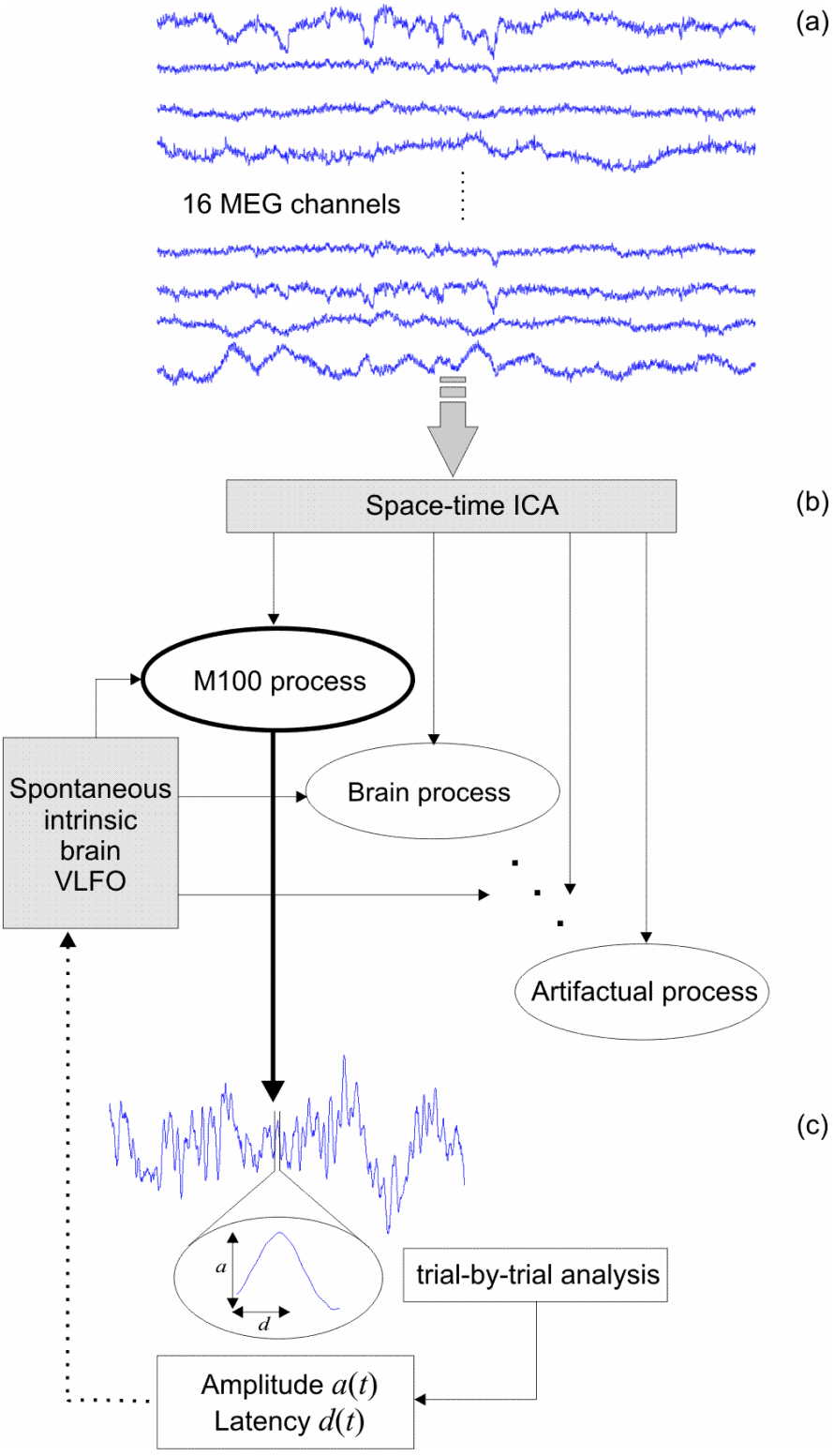

Figure 6-26. Testing the VLF modulation of the M100: (a) The MEG data comprises a mixture of artifacts and brain activity, which are thought to be superimposed on spontaneous VLFO intrinsically generated by the brain. (b) ST-ICA is employed to learn a set of spatio-temporal filters that demix the data into its constituent independent processes, which are affected by these VLFO. (c) Trial-by-trial analysis is then carried out on *the extracted M100 process* in order to obtain the amplitude, a, and latency, d, of each individual M100 response. This generates two time series, $a(t)$ and $d(t)$. The frequency characteristics of $a(t)$ and $d(t)$ are then investigated to infer information about the underlying VLFO, which may be modulating the M100 process, hence accounting for the inter-trial variations of the sensory responses.

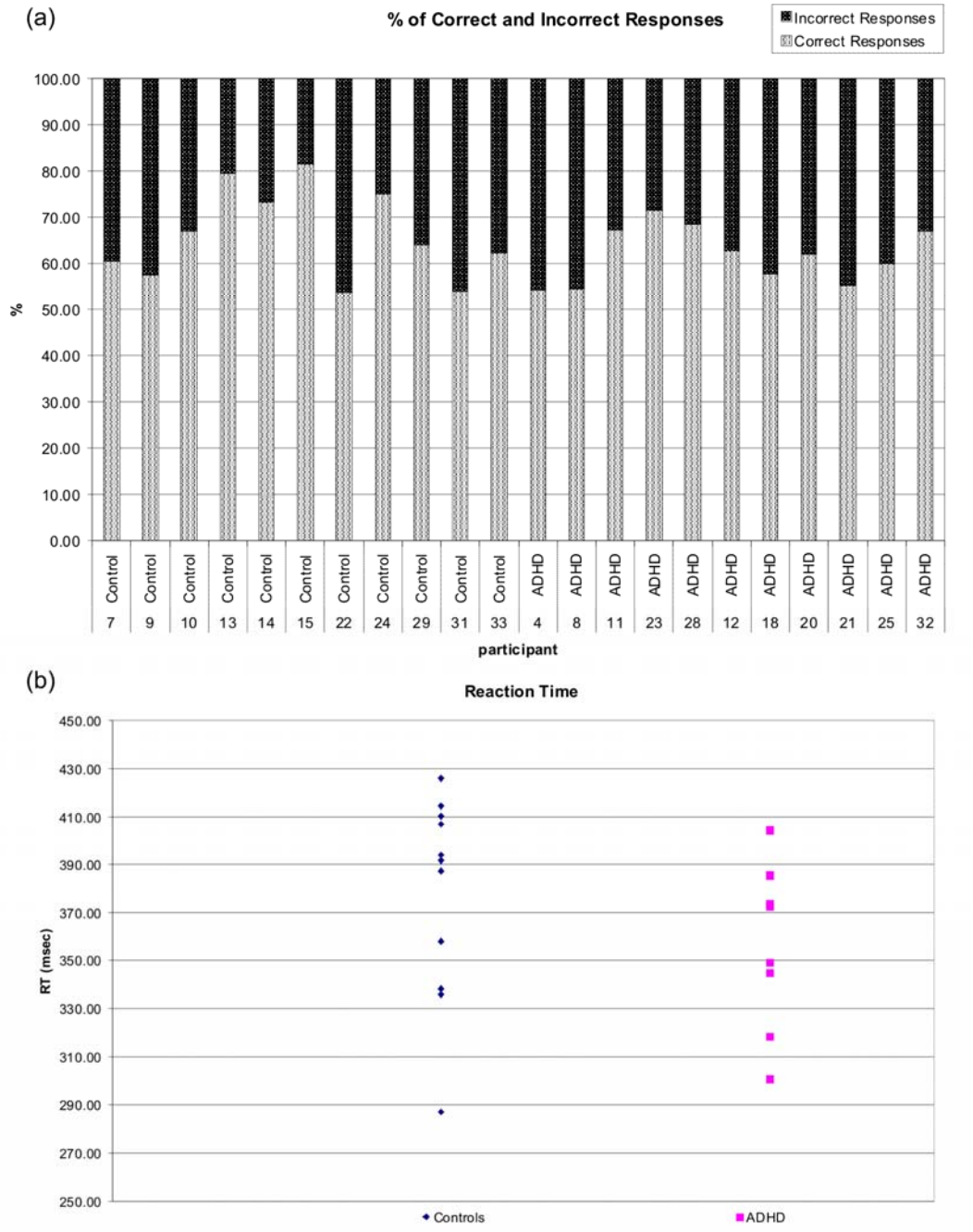

Figure 6-27. Behavioral data: (a) Percentage of correct responses (including % of hits and % of correct rejections) and percentage of incorrect responses (including % of misses to target presentations and % of false alarms), (b) Mean reaction time to button presses during the attention task for all participants in the two groups.

A. Behavioural data

Preliminary analyses were performed on the behavioural data. The following measures were recorded for the attention task: reaction time to button presses, percentage of hits and percentage of correct rejections (together forming the correct responses), as well as percentage of misses to target presentations and percentage of false alarms (comprising the incorrect responses). There

was no significant difference between the two groups for the mean reaction time during task performance and for the percentage of correct responses (cf. Table 6-2). Figure 6-27 shows (a) the percentage of correct and incorrect responses, and (b) the mean RT during task for all participants in the two groups.

	Mean Reaction Time	**Correct Responses**
Mean Controls:	377.21 ms	66.17 %
Mean ADHD:	364.77 ms	61.84 %
T (statistic):	0.764	1.242
Degrees of freedom	20	20
95 % Confidence Interval for the difference between groups	[-21.51 46.38] ms	[-2.94 11.59] %
***p*-value**	0.454 (>0.05)	0.229 (>0.05)

Table 6-2. Performance data for ADHD and control groups during the attention task. Note that there is no significant difference between the two groups for the mean reaction time during task and for the percentage of correct responses, both having a *p*-value greater than 0.05.

B. Extraction of M100 process by ST-ICA

As previously explained, the MEG data is obtained from an inherently noisy recording process; the recordings are the result of brain function added to other physiological and ambient artifacts, which may be many orders of magnitude larger than the signals of interest. Moreover, the large 148-array of sensors creates a data deluge problem resulting in long computational times and large memory requirements for any subsequent data analysis. For these reasons, the ST-ICA algorithm was employed here and the analysis was carried out on 16 channels (out of the 148-MEG channels) chosen such that their position coincided with the channel location of the International 10-20 System, as shown in Figure 6-28. This considerably reduced the number of spatial channels in the analysis thus achieving dimensionality reduction, whilst still rendering an overall representation of the spatial distribution of activation of the brain sources around the head. The delay matrix $\boldsymbol{Q}^n$ corresponding to the n^{th} channel was constructed with an embedding dimension m of 200 in order to provide a frequency resolution of 0.5 Hz (James and Lowe, 2001). Thus the overall delay matrix $\boldsymbol{Q}^{tot}$ had a length of 3200 (i.e. 200×16), which had its dimensionality reduced in the usual manner by SVD (from 3200 to 100 or 40 depending on the structure of its eigenvalues) in order to reduce excessive redundancy.

FastICA (Hyvärinen, 1999b) was then applied on the resultant $\boldsymbol{Q}^{tot}$ to learn a set of space-time filters (residing in the columns of the mixing matrix) for the extraction of the underlying

independent processes. The columns of ***A*** were manually grouped according to the overall shape of their frequency response and the corresponding ICs were then projected back onto the measurement space to form the independent processes. Once the processes underlying that dataset were established, the coherent average of the 16 projected ICs forming each process was found. The M100 process was chosen according to two criteria: (i) the coherent average of the ICs forming that process had a peak around 100 ms following stimulus onset, and (ii) the process topography had most power in the occipital region – typical of the M100 response, in accord with previous research (Jonkman *et al*., 2004). Other brain or artifactual processes would have a different coherent average, different scalp topography and/or time-frequency characteristics.

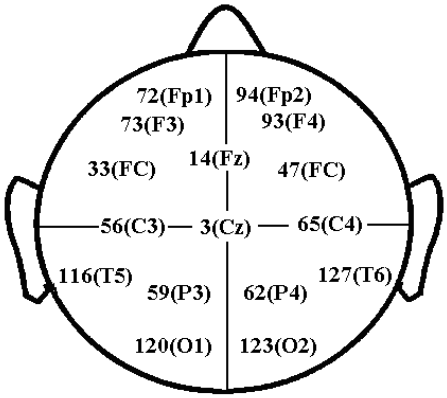

Figure 6-28. Selected MEG channels for ST-ICA analysis. 16 out of the 148 MEG channels, their position chosen to correspond to the channel location of the International 10-20 system. The channels from 1 to 16 are in the following order: [Fp1, Fp2, F3, F4, Fz, FC(left), FC(right), C3, C4, Cz, P3, P4, O1, O2, T5, T6].

The time and frequency characteristics of a typical M100 process are shown in Figure 6-29 (a)-(f). It is important to note the very clear dipolar structure of the MEG responses in separate brain locations as illustrated by the positive and negative peaks in (e). In contrast, (g)–(j) show the characteristics of an artifactual process. The topographies in this figure illustrate the spatial distribution of the root mean square (RMS) power of the 16 projected ICs forming one process. Note that the power of the M100 process is concentrated in the occipital region (as shown in (f)). This procedure was repeated on all the datasets considered (namely two 3-minute task blocks which involved attending or perceiving to the right, for each participant) in order to extract the process corresponding to the M100 response. As can be seen from Figure 6-29 (d) and (j), ST-ICA provides 16 projected ICs which together constitute one process. In order to facilitate further analysis of the M100 process, the cross-correlation between its 16 ICs was calculated, these bipolar components were separated accordingly, and the sign of the negative waveforms was altered in order to establish an overall positive M100 time series for each dataset.

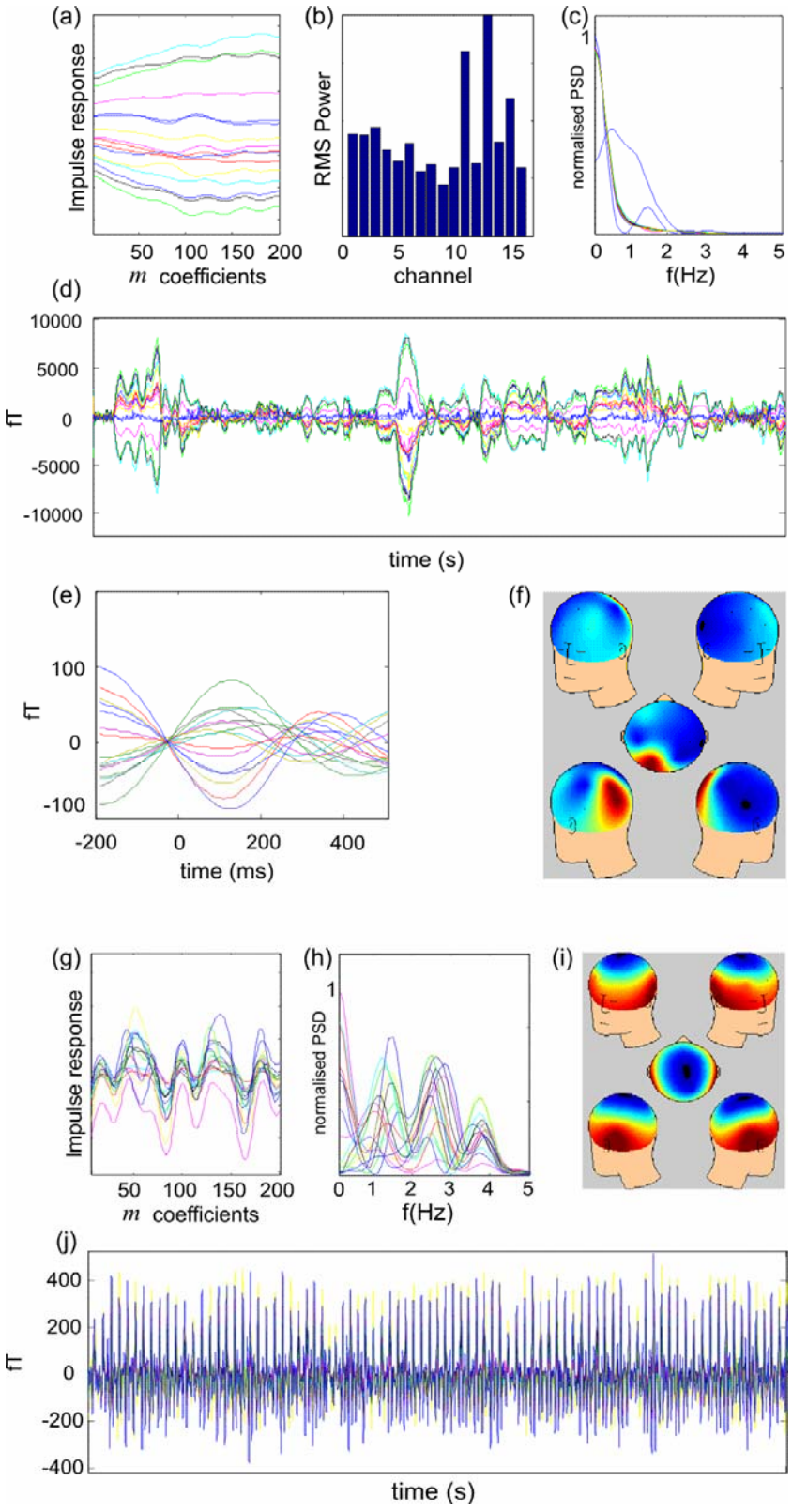

Figure 6-29. Processes extracted by ST-ICA. *The M100 process:* (a)-(c) The impulse response, RMS power distribution and frequency response of the filters for this process, learnt by the algorithm. (d) Waveforms of the 3-minute long ICs when passed through these filters, i.e. when projected back onto the measurement space. (e) The coherent average of the projected ICs showing a positive/negative peak around 100 ms. (f) Topography of the RMS power distribution of these projected components forming the M100 process. *An artifactual process:* (g)-(i) The time and frequency responses of the filters for this process, and the topography of the RMS power distribution of the projected ICs respectively; (j) The projected (3-minute long) ICs.

C. Testing the attentional effect

The individual (per patient) and the grand coherent averages across patients (per group, per task) for the M100s are illustrated in Figure 6-30. The amplitude of the grand average M100 responses (represented as dotted curves in this figure) was noted to investigate the attentional effect of the two groups during the attention and perception tasks. A 2-way analysis of variance (ANOVA) test was performed on these results to test for significance of this interaction (group × task). Although the interaction was not significant, a Tukey post-hoc test showed that in the perception condition the ADHD group has a tendency to have a higher amplitude than the control group (*p*-value = 0.072).

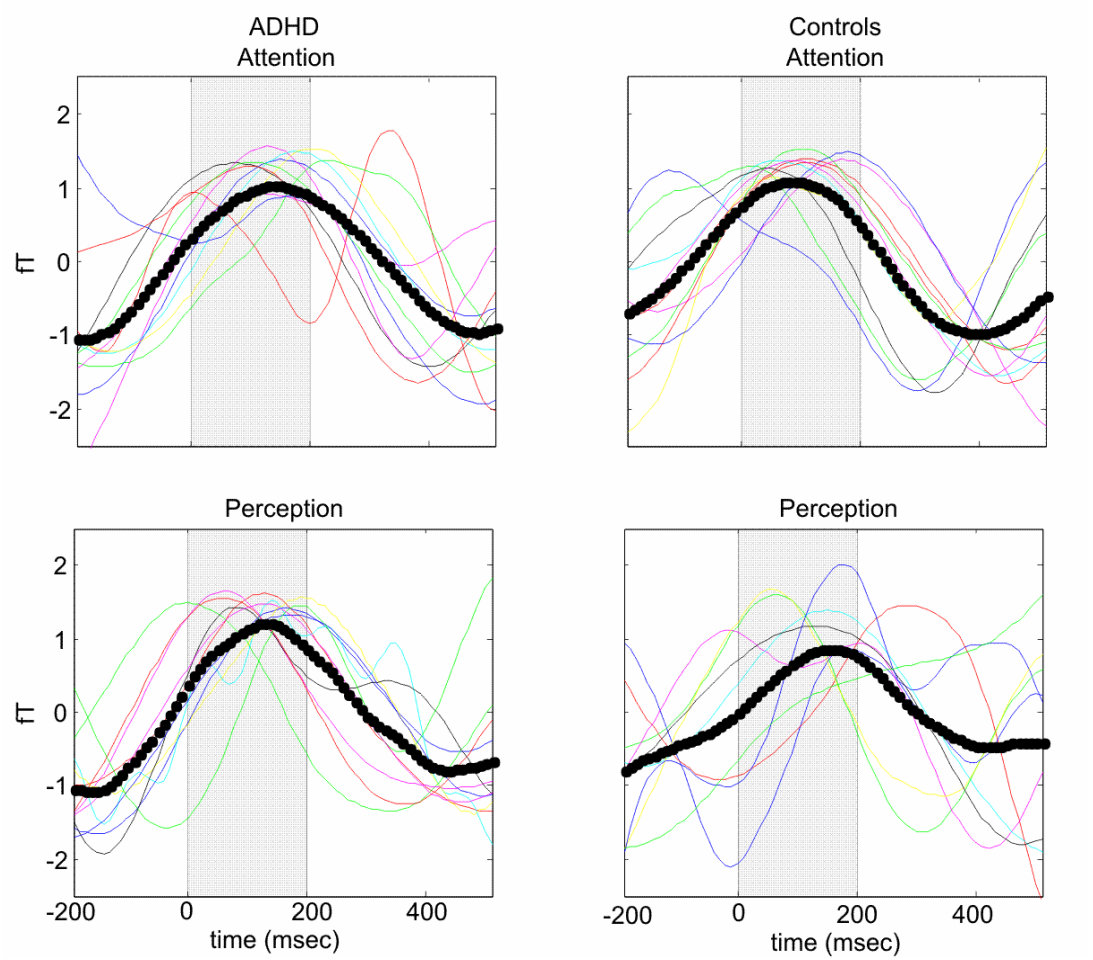

Figure 6-30. Investigating the attentional effect. Individual (colored curves) and grand (dotted curves) coherent averages of the M100 responses for the ADHD and control groups during the attention (active) and the perception (passive) tasks. Control children show an attenuation of the M100 response during the perception task (mean group amplitude = 0.87) in comparison to the attention task (mean group amplitude = 1.1), hence exhibiting the attentional effect and showing proper distinction between relevant and irrelevant stimuli. The amplitude of the M100 grand average remains nearly intact during the two tasks for ADHD children due to deficits in early (0-250 ms post-stimulus onset) selective attention.

D. Trial-to-trial variability

Next, the variability in the amplitude a and latency d of the sensory ERF component was investigated by considering individual responses to stimuli within a post-stimulus interval of 0-250 ms. For this part of the study, a single 3-minute attention task block was considered for every participant. The M100 process time-series extracted for the attention task block by ST-ICA was subdivided into 300 segments, time-locked to the stimuli. For each segment, the amplitude and latency of the M100 response were recorded to form two sets of points, a and d (see Figure 6-26 and Figure 6-31(a)). The null values (where no clear M100 peak was detected in that segment) were disregarded. Cubic, shape-preserving interpolations were constructed for these points in order to form time series $a(t)$ and $d(t)$ with an equal sampling period. This was done in order to compensate for the variable inter-stimulus delays, as shown in Figure 6-31 (b).

The PSDs of $a(t)$ and $d(t)$ were found using the Welch method. Two power ratios were then computed on these PSDs: (i) the ratio of power in the infraslow ($0.01<f<0.1$ Hz) band to the total power in the series (0-50 Hz), and (ii) the ratio of power in the ($0.1<f<0.5$ Hz) band to the total power in the series (0-50 Hz). These were found to examine the VLF modulatory effect on the trial-to-trial variability of the M100 process. Independent t-tests were computed to test for any significant differences between the ADHD and control groups power ratios. These gave p-values greater than 0.05 for the power ratios in both frequency bands (Table 6-3).

	***t*-value**	**Degrees of freedom**	***p*-value**
(i) Band $0.01<f<0.1$ Hz PSD($a(t)$)	0.133	20	0.895
Band $0.01<f<0.1$ Hz PSD($d(t)$)	-0.703	20	0.490
(ii) Band $0.1<f<0.5$ Hz PSD($a(t)$)	1.061	20	0.301
Band $0.1<f<0.5$ Hz PSD($d(t)$)	1.434	20	0.167

Table 6-3. t-tests on (i) the ratio of power in the infraslow-f band ($0.01<f<0.1$ Hz) to the total power (0-50 Hz), and (ii) the ratio of power in the frequency band ($0.1<f<0.5$ Hz) to the total power (0-50 Hz), in the spectra of the inter-trial amplitude and latency variations for M100 processes, [i.e. PSD($a(t)$) and PSD($d(t)$)], to test for any significant differences between ADHD and control groups.

This indicates that the inter-trial amplitude and latency VLF variations were no different for the two groups. In order to obtain a representation of the overall frequency characteristics of the inter-trial variability for the two groups, the *group average M100 process* was calculated. The PSD of the $a(t)$ and $d(t)$ for the groups' M100s are illustrated in Figure 6-32. Spectrograms showing the time-frequency characteristics of this variability were also obtained in order to show

that the VLF fluctuations of the M100 are deterministic because the power in these frequency bands is evenly distributed across the entire task block. Figure 6-33 shows the spectrogram for the control group as an example (since the spectrograms for the ADHD group showed similar characteristics).

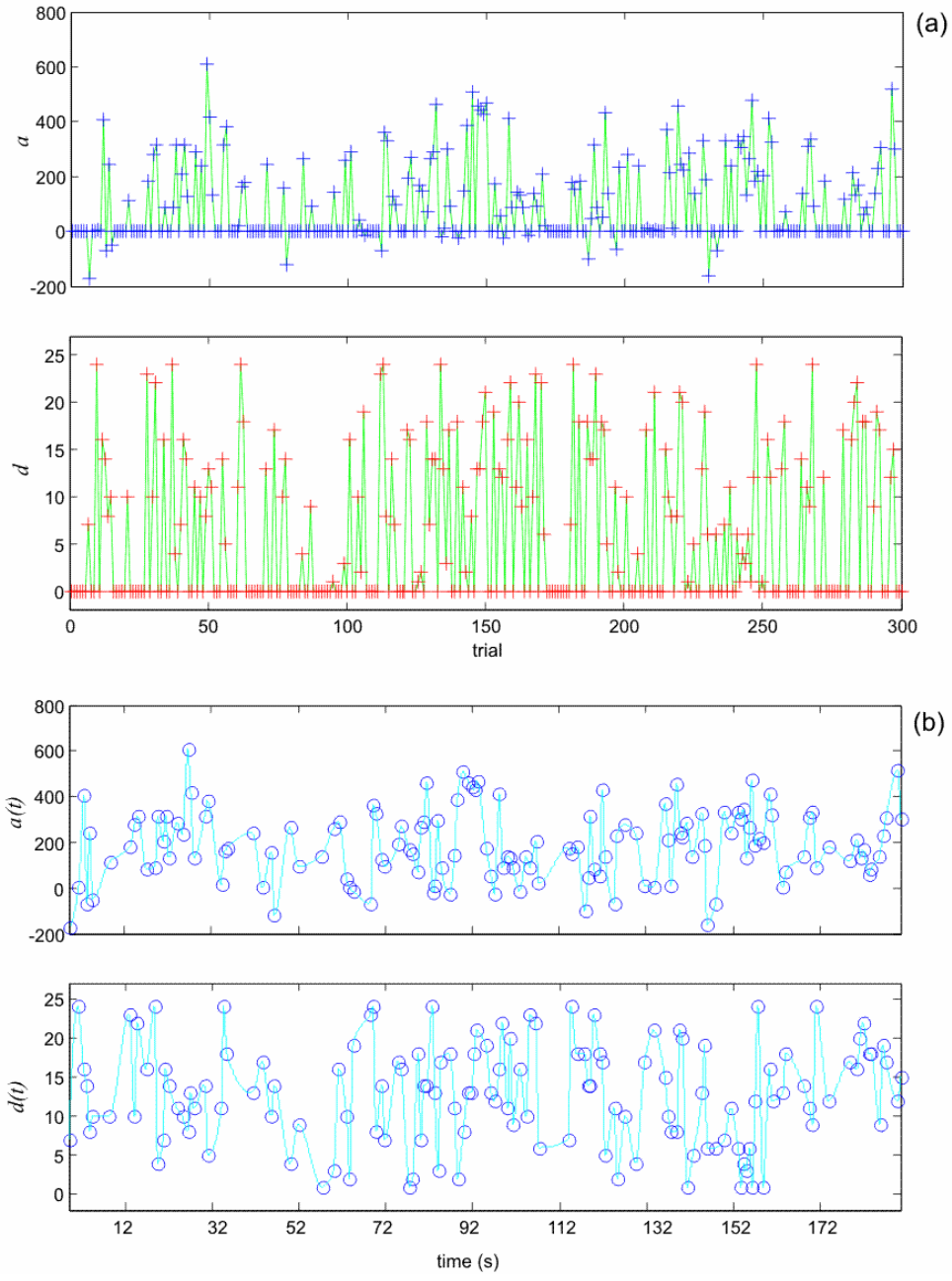

Figure 6-31. An example of the trial-to-trial variability in the amplitude and latency of the M100 responses (showing results for the grand M100 process of the control group): (a) 300 *a* and *d* values of the M100 time-series (one for each trial/stimulus); (b) Cubic, shape-preserving interpolations constructed through these points (o) to attain time series $a(t)$ and $d(t)$, with an equal sampling period. Note the cyclical behavior in the time series indicating VLF modulation of these sensory responses.

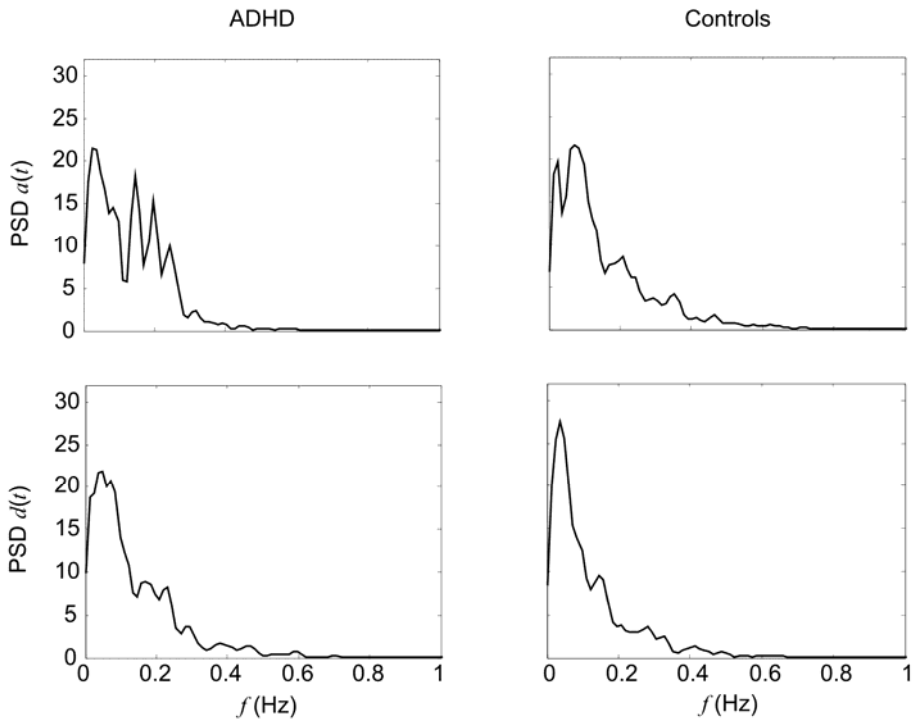

Figure 6-32. Spectra of the inter-trial amplitude and latency variations for the *groups' overall M100 processes*. Note the very low frequency peaks (<0.1Hz) indicating that the trial-to-trial variations in the amplitude and latency of the M100 responses follow a slow wave pattern, which is in keeping with the notion of VLF modulation.

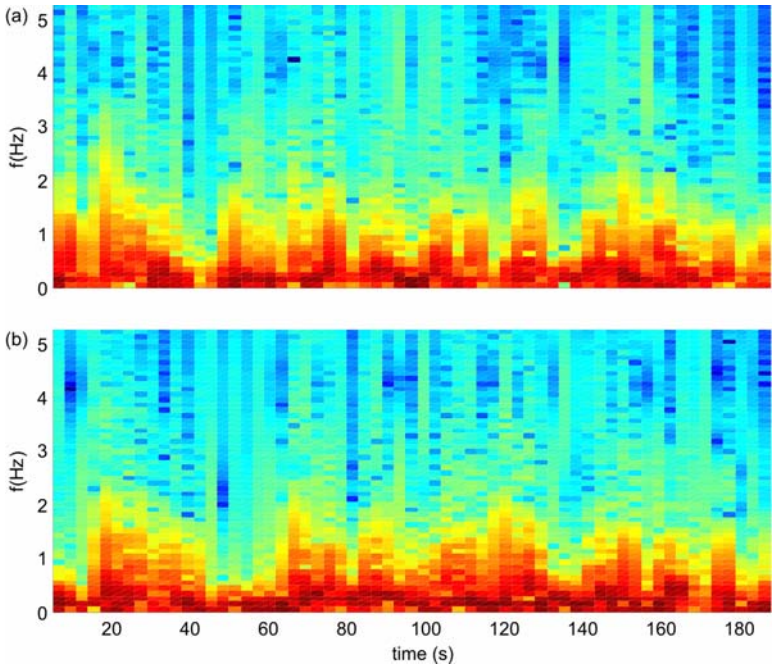

Figure 6-33. Spectrogram showing the time-frequency characteristics of the inter-trial variability of the M100 process. Variability in the: (a) amplitude and (b) latency of the M100 responses; the spectrograms for the control group are shown as an example. Note the variation in the frequency content and the persistent presence of low frequency activity indicating a deterministic effect of the VLFOs.

E. Discussion

This study primarily investigates the attentional effect, i.e. the attenuation of the M100 response in the presence of irrelevant stimuli. The results presented show that, for the analysed datasets, the amplitude of the average M100 response stays relatively the same during attention and perceptual tasks for the ADHD group, whereas the control group experiences a tendency of decrease in the M100 amplitude during the perception task, appropriately exhibiting the attentional effect. Despite this tendency in the ERF analysis, the performance data recorded for this study showed no significant difference between ADHD and control groups. This concurs with the findings reported in several ADHD-ERP studies which show differences in ER components in the absence of significant performance disparities in their datasets (Barry *et al*., 2003; Andreou *et al*., 2007). This may be due to a processing deficit that behavioural measures are not sensitive enough to detect, or because of compensatory strategies during task performance.

The second part of the analysis assesses whether the trial-to-trial variability in the amplitude and latency of the visual M100 response follows a VLF pattern. In line with our hypothesis (Figure 6-26), children showed clear evidence of the VLF modulation of the M100 component (Figure 6-32). The VLF nature of this variability may arise due to the spontaneous intrinsic fluctuations in brain activity. Consequently, these results can be interpreted in view of previous findings in BOLD imaging studies, which show that the evoked responses and the intrinsic VLF brain activity are superimposed, the latter accounting for trial-to-trial variations in evoked responses (Fox *et al*., 2006; Fox and Raichle, 2007). The difference between the ADHD and control groups in the infraslow (<0.1 Hz) band of the inter-trial variability spectra was minimal and was not statistically significant (cf. Table 6-3). Meanwhile, group differences were more pronounced in the ($0.1<f<0.5$ Hz) band; here the ADHD group exhibits more power than controls in the spectra of the M100 trial-to-trial variations, and shows other high-energy peaks in the $a(t)$ PSD, which are not apparent in the $a(t)$ PSD of the control group (Figure 6-32).

Although these results do not significantly distinguish between the clinical and control groups, closer inspection suggests that there may be potential differences in the effect that the VLFOs have on the two groups. They tentatively suggest that the ADHD group is spreading the VLF power during task performance. This could be indicative of effortful attention - ADHD children have to stretch the VLF power and may increase the overall power in order to compensate for and disrupt the dominant intrinsic VLF activity in their brains. This is in keeping with the premise that ADHD children fail to appropriately modulate slow wave activity during neuronal

events (Castellanos *et al*., 2005). Controls, on the other hand, exhibit a more narrowband spectrum for the amplitude and latency variability of the M100 responses, which could indicate that the VLF modulation of the responses is more specific, and that this group could attend to the task at hand irrespective of the presence of intrinsic slow waves. The lack of statistical significance may be attributed to the simplicity of the experimental task and to the small sample size, which is a major limitation of this study.

6.3. Summary

The first part of this chapter has shown that the $1/f^{\gamma}$ trend inherent in EM brain signals results in spectra with high power at low frequencies. Spectral normalisation renders a flat base spectrum when no extra low frequency activity is present in the data and reveals distinct peaks related to specific cognitive tasks or mental conditions (such as resting states). This is particularly important for the analysis of very low frequency oscillations (<0.5 Hz) apparent in EEG and MEG signals. In this work a time domain normalisation approach, which employs a differentiator to cancel the $1/f^2$ trend, was proposed. This is a simple, non-parametric solution, which leaves the signal phase intact due to its linear phase characteristics. Its application on a broad range of physiological signals, including epileptic seizure data, EEG data with very low frequency characteristics, MEG data and ERP recordings, was demonstrated. In each case, spectral normalisation helped to highlight peaks of interest across the spectra.

The second part of the chapter dealt with two studies carried out on the MEG data which was supplied from the University of Madrid. This data was *not* recorded with the specific aim of analysing low frequency brain activity or the distinction between rest and task conditions, which are both central to this work. Nonetheless, it was successfully exploited and new ways have been proposed for the investigation of the presence and effect of the slow waves in the MEG recordings with the use of newly-developed BSS algorithms. First, a SC-ICA and phase synchronisation methodology was employed to isolate low frequency brain processes within the data in the presence of higher frequency brain activity and artifacts, and to investigate brain areas interactions during rest as opposed to attentional and perceptual tasks. Preliminary results indicate potential phase locking between fronto-central, central and parietal areas, as well as variations in the phase locking of ADHD and controls following a switch from rest to task.

The second study on the MEG recordings examined the responses to stimuli *within* task blocks. The focus was on the M100 component known to be regulated by attention, in order to provide

information about the early stages of stimulus processing (i.e. 0-250 ms post stimulus onset) for ADHD and controls. The VLF modulation of evoked responses was then investigated from a magnetophysiological perspective. It was posited that this modulation would manifest itself in the trial-to-trial variations of attentional processes, indexed by the M100 component. Space-time ICA, which uses both temporal and spatial information of selected MEG channels to inform a standard ICA algorithm such as FastICA, was used for the extraction of the M100 process.

The results demonstrate, for the first time, the potential of this BSS algorithm for the analysis of systems with high spatio-temporal complexity. ST-ICA was able to extract the M100 process in the presence of artifactual components and allowed for dimensionality reduction of the high density MEG system by just considering 16 out of the available 148 channels, whilst still achieving a reliable decomposition of the underlying processes. Moreover, a trial-by-trial analysis on the 'clean' M100 processes could be conducted – an analysis which would have been much harder to perform reliably on raw data given the poor SNR of individual ERF responses. Results show that children with ADHD tend to fail to exhibit the attentional effect when subject to irrelevant stimuli (i.e. during the perception task), this being indicative of early selective filtering deficits in comparison to controls. More central to the aim of the work however, are the results which demonstrate that the trial-to-trial variability in the amplitude and latency of the M100 responses exhibits a very low frequency time signature (<0.1 Hz). This may arise due to spontaneous VLFOs intrinsically generated by the brain which were observed in BOLD imaging studies.

The next chapter describes a complete set of EEG experiments that were specifically designed for direct investigation of the slow waves within electrophysiological data of normals, during periods of quiet wakefulness and whilst performing tasks of various difficulty levels.

Chapter 7

THE DESIGN OF EEG STUDIES TO TEST THE BRAIN UNDER LOAD

This chapter describes the EEG experiments designed with the aim of investigating the functional role of slow waves in brain signal recordings and the changes that they undergo during various task and rest conditions. The rationale behind the experiments, the experimental protocol and participants' information are presented, followed by a brief description of the analysis to be carried out on the data. The analysis methodology and results are described in the next chapter.

7.1. Motivation

The human scalp EEG displays oscillations of varying frequencies, ranging from 0.5 Hz up to several hundreds of hertz, which arise from the coordinated excitation of many neurons within cortical networks (Buszáki and Draguhn, 2004). A large body of literature has attempted to characterise the functional and clinical correlates of these relatively fast oscillations. In addition, in recent years some studies have also demonstrated VLF fluctuations during, for instance, deep sleep and epileptic events (Vanhatalo *et al*., 2003). The mechanism of these slow rhythms is as yet unclear, however evidence suggests that they have a neurological origin and are not simply physiological noise. These oscillations consume approximately two-thirds of the brain's energy resources and are thought to be present in order to maintain a stable 'ready' state, which allows the cortex to execute different cognitive functions depending on the presence or absence of stimulation (Balduzzi *et al*., 2008). It is proposed that they represent an intrinsic continuous process which is required to maintain awareness of ourselves, of our surroundings and of the passage of time (Fransson, 2006). As seen in Chapter 6, these slow waves may cause inter-trial variability in evoked responses and may be promoting synchronisation between diverse neuronal networks. Moreover, BOLD studies in fMRI have shown that infraslow fluctuations observed during the course of a task are smaller than those during rest (Fox and Raichle, 2007). This

suggests that they are, to some extent, being attenuated during task in order to allow goal-directed active processing to dominate. However, the DMI hypothesis posits that this is not always the case – sometimes these oscillations re-emerge, they compete and interfere with task-oriented processing, hence presenting a potential source of attention deficit during task performance.

The study presented in this chapter has been specifically designed to investigate the functional role of these slow waves in the EEG during rest sessions (when participants are relaxed), and whilst performing stimulus-based tasks. In these experiments, the brain is viewed as a system consisting of a number of band-limited sources, or oscillators (Karakas *et al*., 2000; Buzsáki and Draguhn, 2004), which are interacting together in an unknown (linear – additive, or non-linear) manner, as illustrated in Figure 7-1. During rest, the system is in its most basic, spontaneous (background) state. Stimulus-based tasks load the brain and tax the underlying oscillators eliciting a definitive standard evoked response in the EEG, namely the P300. In fact, one of the models for ERP generation (termed as the phase reset model) suggests that stimulus processing causes the oscillators to undergo a change in phase such that activity at particular frequencies becomes phase locked, resulting in a non-zero average evoked response (Sauseng *et al*., 2007). The parameters of this response (such as its amplitude and latency) would then somehow reflect the loading levels on the brain.

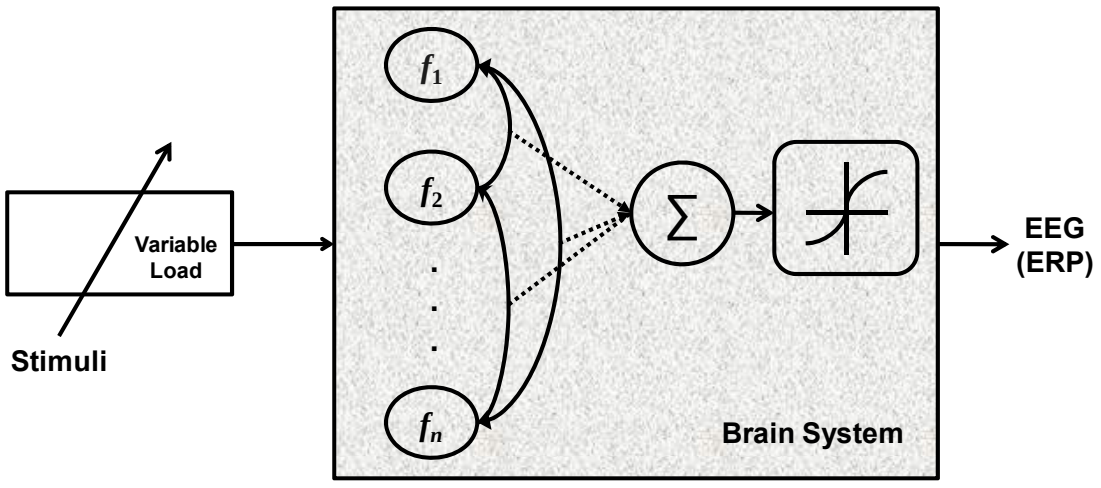

Figure 7-1. The brain is modelled as a system comprising a number of oscillators which interact in a linear/nonlinear manner. Stimulus-based tasks impose a variable load on the brain, taxing these oscillators. This impact can be assessed by the parameters of the ERP response.

It is important to note here that the slow waves can be viewed as a distinct oscillator that is affected by the input stimuli and interacts with higher frequency oscillators in order to generate

the output response. Alternatively, they could be providing the background activity of the cortex, this being like a "*sea undulating gently*" and the evoked task-related responses are like "*small ripples on its surface*" (Balduzzi *et al*., 2008). In this case, the slow wave mechanism affects, drives or perhaps even governs the other underlying brain processes, as suggested by the M100 study reported in Chapter 6.

Throughout the course of this experiment, three task conditions have been implemented such that the load was varied in a graduated manner (higher loading implies greater task difficulty) in order to further assess the impact on the underlying oscillators, particularly the slow waves. This also allows for a more thorough comparison between rest and task activity. For example, the amount (if any) of attenuation of the slow waves during task as opposed to the default mode (rest), as indicated by the DMI hypothesis, can be investigated. One can also test whether this attenuation varies with the level of task difficulty.

7.2. P300 Responses

The P300 is the most studied late ERP component which is evoked using a stimulus delivered by one of the sensory (visual, auditory or somatosensory) modalities. It is thought to be produced by a distributed network of brain processes associated with attention and memory operations (Polich, 2007). There is a vast amount of literature devoted to the understanding of this ERP, its subcomponents and its biological correlates, mainly because of its sensitivity to cognitive processing (Karakas *et al*., 2000; Herrmann and Knight, 2001; Datta *et al*., 2007; Polich, 2007; Smallwood *et al*., 2007). Its amplitude reflects the probability and task-relevance of a stimulus while its latency indicates the duration of stimulus evaluation. This component is also strongly affected by genetic factors (Polich, 2007).

The context-updating theory of the P300 provides a theoretical framework for stimulus processing underlying the generation of this ERP component. When stimuli enter the processing system, a memory comparison between the current and the previous stimulus is performed. If the incoming stimulus has not changed, the neural model of the stimulus environment is also unchanged and only the sensory evoked potentials (N100, P200, N200) are prominent in the coherent average. When the individual is exposed to a different, infrequent stimulus (dubbed the "target"), more attentional resources are allocated to the stimulus, which causes the neural representation to be updated and a P300 potential generated in addition to the sensory evoked

potentials (Polich, 2007). Consequently, discriminating the target from a majority of standard stimuli produces a robust P300.

This P300 response is then affected by the probability of occurrence of the stimuli. For example, Katayama and Polich (1996) have shown that component amplitude is inversely proportional to the probability, whereas no reliable latency effects were reported. Moreover, it is proposed that the size of this ERP component is proportional to the amount of change required to update the memory representation of the task environment during stimulus processing. This may be the reason for a lower P300 amplitude and higher component habituation during passive tasks (where the intentional discrimination between stimuli is not required) as opposed to active tasks, this being more emphasised in visual than in auditory modalities. In addition, the amplitude of the response is further reduced for passive tasks due to more attentional resources being appointed to task-unrelated events (Bennington and Polich, 1999; Jeon and Polich, 2001). Target-to-target interval is another attribute affecting the P300 amplitude since it determines how quickly resources can be redirected to process target stimuli (Polich, 2007).

The P300 amplitude is also influenced by the intensity, energy required and level of arousal tied to a specific task – easy tasks generally result in relatively large amplitude and short peak latency, whereas tasks that recruit more attentional resources generate responses of smaller amplitudes and longer latencies, since more processing resources are allocated for task performance (Comerchero and Polich, 1998; Hagen *et al*., 2006). Furthermore, neurological disorders typically show a reduction in amplitude, schizophrenia being a case in point suggesting impairment of controlled information processing (Jeon and Polich, 2003).

The latency of the P300 varies across the scalp, with a shorter latency over frontal than parietal regions. Across individual participants, it is found that this is correlated with cognitive performance – a shorter latency being indicative of superior cognitive capabilities. P300 latency decreases as children develop and increases with normal aging, dementia, brain injury and schizophrenia (Polich, 2007; Jeon and Polich, 2003).

7.2.1. The P300 Complex

The P300 response is composed of two subcomponents namely, the P3a and P3b, and the resultant P300 scalp topographies vary with the stimuli and task conditions eliciting them. The P3a component (also termed as the 'novelty' P300) is large over frontal/central areas and has

been reported for all sensory modalities. It is thought to mark initial signal evaluation since it seems to originate from the frontal lobe and readily habituates (Comerchero and Polich, 1998; Hagen *et al*., 2006). Meanwhile, the centro-parietal P3b is elicited by the infrequency target stimuli. This subcomponent is generated when subsequent memory processes are engaged to store stimulus information and represents the executive control of focussed attention (Bledowski *et al*., 2004; Polich, 2007).

Various ERP and fMRI studies suggest that the P300 responses, arising from different stimulus contexts, reflect brain areas that are related to specific stimulus evaluation processes. Correlations between volume measurements obtained from MRI gray matter and P300 amplitudes indicate that frontal areas produce stronger associations with non-targets, whereas parietal areas are more linked to target stimuli. Moreover, such studies indicate frontal lobe activity for the detection of rare but alerting stimuli (Comerchero and Polich, 1998). Specifically, in a combined event related and fMRI study, Bledowski *et al*. (2004) found that frontal areas and the insula contributed mainly to the P3a, whereas the P3b was mainly produced by parietal and inferior temporal areas. This is the first indication that higher visual areas in the inferior temporal cortex contribute to the P3b scalp potential. Although these two ERP subcomponents have distinct topographic amplitude distributions, they exhibit a spatiotemporal overlap; however, they can still be successfully separated into independent processes via spatial ICA decomposition (Makeig *et al*., 1999b; Debener *et al*., 2005).

Therefore, the formation of cognitive P300 activity can be described as follows: when sensory input is processed, activation of the frontal lobe from the attention-driven working memory changes generates the P3a, while the activation of temporal/parietal lobe from memory updating operations produces the P3b. Together these two subcomponents indicate a circuit pathway for transmission of task/stimulus information between frontal (P3a) and temporal/parietal (P3b) brain regions. Various neurotransmitter mechanisms underlying P300 generation are implicated, with P3a more commonly associated with frontal/dopaminergic and P3b with parietal/norepinephrine pathways (Polich, 2007).

7.2.2. Time-frequency Analysis of the P300

The findings discussed above suggest that the P300 is not a unitary phenomenon but is composed of a number of overlapping functional processes. For this reason, wavelet transforms have been extensively used to construct a time-frequency decomposition of this heterogeneous ERP (Kolev *et al*., 1997). The study by Yordanova *et al*. (2000) suggests that ER oscillations, particularly

delta (0.1-4 Hz), theta (4-7 Hz) and alpha (7-14 Hz), are sensitive to the processing conditions eliciting the P300, and that P300 variations are directly influenced by these oscillations. For example, in the late P300 time period, there is a parietal delta component reflecting a mechanism for processing resources, in parallel with a frontal theta component that may be related to working memory. Moreover, Karakas *et al*. (2000) show (by means of a band pass filtering method) that the interplay between delta and theta oscillations is responsible for the morphology and amplitude of the P300 component during two different (mismatch negativity and oddball) experimental paradigms.

It is worth mentioning here that there is a broad range of applications for the P300 in scientific research, ranging from investigating attention disorders (ADHD), anxiety disorders such as obsessive compulsive disorder and post-traumatic stress disorder, to depression and alcoholism (Hansenne, 2000). Moreover, the consistent nature of the P300 waveform, the fact that it is elicited under specific conditions in nearly all individuals and is easily detectable with standard measurement techniques, makes it an ideal candidate for applications in BCI (Piccione *et al*., 2006). Advances in this field aim to provide a means for decision making and communication mechanism for patients suffering from severe motor impairments. Audiology is another field of interfacing where the P300 could be used as a measure of quality for cochlear implants – if the target is poorly transferred or distorted by the hearing apparatus it will not elicit a substantial P300 (Beynon and Snik, 2004).

7.2.3. Experimental Paradigms for the P300

Oddball and Go No-go paradigms are two ER task-types particularly aimed at eliciting the P300 response, which have been well tested and documented in the literature (Katayama and Polich, 1996; Comerchero and Polich, 1998; Hagen *et al*., 2006; Datta *et al*., 2007; Smallwood *et al*., 2007).

A. Oddball Paradigm

The traditional form of the oddball paradigm involves the recognition of an infrequent target stimulus, from a sequence of more frequently occurring standard stimuli. This task is very popular amongst researchers since it engages a number of important resources, including attention allocation, short term memory, memory updating for stimulus recognition and decision making for a response (Karakas *et al*., 2000). A variation of this task involves the addition of a non-target stimulus, termed as the 'distractor', that does not require a response (Katayama and Polich, 1996; Comerchero and Polich, 1998; Hagen *et al*., 2006). In this scenario, while the

attentional system is captured by the physical difference between the target and the standard stimuli, it is repeatedly disrupted by the forceful distractor. Hence, the P300s from this infrequent but typical stimulus renders useful information about the neural operations which is not readily available from the traditional task.

In such experiments, the perceptual discrimination difficulty between the target and standard stimuli can be varied to provide an easy or difficult task environment. When the target/standard discrimination task is relatively easy, a central/parietal P300 is elicited. A high discrimination difficulty (i.e. smaller physical differences between the target and the standard stimuli) recruits more sensory and working memory functions. This appears to engage frontal attentional mechanisms more strongly, producing large frontal/central P300 components when a distracting stimulus interrupts attentional control (Comerchero and Polich, 1998; Hagen *et al*., 2006). Moreover, high difficulty levels are thought to increase the attentional resources consumed for the task, resulting in P3b amplitude reduction and a longer peak latency. Such effects are more likely to be seen if the difficulty levels induce more than 10-15% error rates (Hagen *et al*., 2006).

B. Go No-go Task

The Go No-go sustained attention to response task (SART) requires the participant to respond to one stimulus type (Go) and withhold a response to an infrequent stimulus (No-go) appearing in an unpredictable manner. As the name indicates, the SART assesses self-maintained attention to current action. The rhythmic nature of the task, together with the lack of selection, is designed to establish a relatively automatic, task-driven response (Datta *et al*., 2007). This has proven to be sensitive to the frequency of everyday action lapses in both traumatically brain injured patients and in healthy controls, and can thus be used to establish a measure for sustained attention (Smallwood *et al*., 2007). For example, Datta *et al*. (2007) found that when the P300 amplitude was relatively low, errors were more likely. This implies that an increased P300 amplitude across a task may be indicative of an individual's capacity to achieve a higher resistance to inhibition errors, hence maintaining an overall attentive state. Moreover, a lower error rate with respect to No-go trails is related to how well individuals are able to maintain active control over their responses, rather than allowing themselves to be "driven along" by the rhythmic tempo of the task, entering into a state of "mind wandering" (Smallwood *et al*., 2007).

In this respect, Smallwood *et al*. (2007) suggest that mind wandering competes with task-relevant information, thus diminishing the cognitive analysis of external events. Here, the P300 ERP component for non-targets was found to decrease prior to both behavioural and subjective reports of mind wandering. This study revealed that the mind naturally flows into off-task thinking whenever it tries to engage attention in a sustained manner, and the extent to which this

happens can be indexed by the P300. Interestingly, fMRI studies have linked such behavioural lapses to increased BOLD activity in the default network; when the mind wanders it is no longer being externally stimulated, so the default mode network is recruited. Otherwise, stimulus processing may be partially inhibited by the default network activity such that the attentional resources are split between external stimuli processing and the default mode – as indicated by the DMI hypothesis (Sonuga-Barke and Castellanos, 2007). ADHD is a group shown to experience recurrent phases of mind wandering coupled with poor response inhibition due to dysfunction in premotor and prefrontal systems (Wodka *et al*., 2007).

The study carried out here involved two sets of recordings, one based on the three stimulus oddball paradigm with Easy and Hard task conditions, and another one based on the Go No-go task. In each recording, task blocks were separated by a resting block for testing of the hypothesis presented.

7.3. Experiments

The study was approved by the ethics committees of the School of Psychology and of the ISVR at the University of Southampton in compliance with the University policy. Twenty-three healthy adult controls aged between 24 and 40 were recruited and written informed consent was obtained. Before the EEG recording, the Barkley Adult ADHD rating scales and demographics data (re: epileptic seizures incidents, head injuries, vision or hearing problems and the participants' use of medication or psychoactive substances) were collected for every participant. The former is an ADHD self-report scale which contains 18 questions derived from the 18 ADHD symptom criteria for both inattention and hyperactivity/impulsivity factors reported in the DSM-IV. For clinical diagnosis of ADHD a participant must show 12 out of the 18 symptoms. None of the participants recruited for this study reached this limit, as can be seen from the participants' information in Table 7-1. Moreover, none of the participants were taking any medication, none suffered from any head injuries or pathologies and all had normal or corrected-to-normal vision. All the relevant forms related to this experiment can be found in Appendix I.

7.3.1. EEG Recording

The scalp DC-EEG was recorded using a Neuroscan SynAmps2 70-channel EEG system[1] at 250 Hz, with a low-pass filter at 70 Hz (Figure 7-2). Participants were fitted with an electrode

[1] http://www.compumedics.com/ and http://www.neuroscan.com/

cap (Easycap; Hersching, Germany) and EEG was recorded from 66 equidistant Ag/AgCl electrodes, with the reference electrode attached to the nose as shown in Figure 7-3. The EOG was recorded using electrodes below the left and right eye. Impedance for all electrodes was kept below 5 kΩ. A high chloride, abrasive electrolyte gel was used to achieve a DC-stable skin-gel contact in order to ensure stable operation of the Ag/AgCl electrodes (Vanhatalo *et al*., 2005).

Participant ID	Sex	Age (years)	Handedness	ADHD score	Cap Diameter (cm)
cd01	Male	33	Left	0	58
cd02	Female	40	Right	0	56
cd03	Female	28	Right	0	56
cd04	Male	29	Right	10	58
cd05	Female	29	Right	2	58
cd06	Female	36	Right	2	56
cd07	Male	25	Right	0	58
cd08	Female	25	Right	0	54
cd09	Male	36	Right	7	58
cd10	Female	24	Right	3	58
cd11	Male	24	Right	0	58
cd12	Male	29	Right	7	56
cd13	Male	26	Right	1	58
cd14	Female	29	Right	0	56
cd15	Male	24	Right	2	56
cd16	Female	27	Left	0	56
cd17	Male	26	Right	4	58
cd18	Female	26	Left	1	56
cd19	Female	30	Right	0	56
cd20	Female	38	Right	0	58
cd21	Male	29	Right	0	56
cd22	Female	25	Right	3	58
cd23	Male	26	Left	3	58

Table 7-1. Participants' Information.

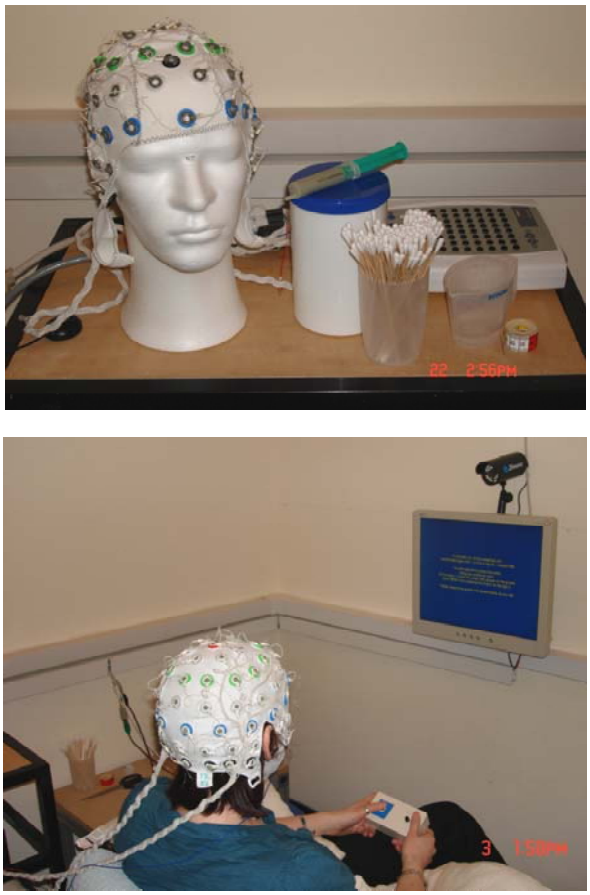

Figure 7-2. Experimental set-up and recording using Neuroscan Synamps^2 70-channel EEG System, in IDIA Lab, School of Psychology, University of Southampton.

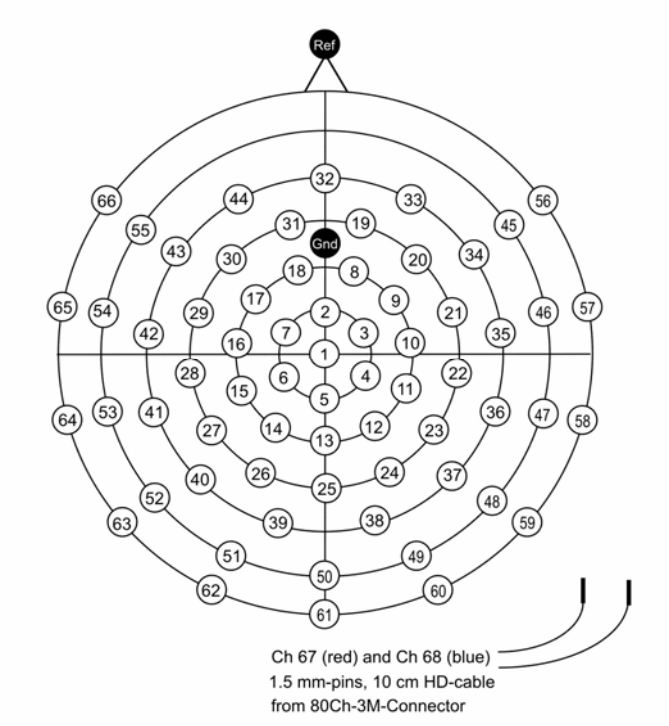

Figure 7-3. 66 Channel Infracerebral EEG Recording Cap. The positions on the central anterior-posterior line are equivalent to 10%-positions (e.g. 1 = Cz, 32 = Fpz, 50 = Iz, etc).

A. Protocol for the Three-Stimulus Oddball Task

Participants were asked to complete a 22-minute three-stimulus oddball visual task, consisting of two 8-minute task blocks separated by a 6-minute rest block. In this task, the target stimulus (probability of occurrence of 0.12) was a blue circle 4 cm in diameter, and the distracter stimulus (probability of occurrence of 0.12) was a 16 cm^2 square with a black and white checkerboard pattern (1 cm checks). As for the target, the standard stimulus was a blue circle (probability of occurrence of 0.76), the diameter of which was systematically altered from 2.8 cm for the Easy to 3.6 cm for the Hard task conditions. This was done in order to grade the perceptual discrimination difficulty, and increase error rates and response time across task conditions, as in the work by Comerchero and Polich (1999). The stimuli were presented once every 1.2 seconds for a 250 ms duration, (i.e. 400 stimuli per task block). Stimuli presentations were randomised and condition order counterbalanced across participants. Participants were given a practice block consisting of 15 stimulus trails before each condition. During the rest block participants were asked to look at the computer screen in a relaxed manner while focussing on a fixation cross at the centre of the screen in order to avoid extraneous movement.

B. Protocol for the Go No-go (SART) Task

The Go No-go SART task consisted of two 10-minute task blocks separated by a 6-minute rest block. During this task single, randomised digits from 1 to 9 were presented on the computer screen at a regular, invariant rate. Participants were asked to use the index finger of their preferred hand to press a single button for each digit as it appears with the exception of the digit 3, as in the work by Datta *et al*. (2007). Stimuli were presented every 1.2 seconds for a 250 ms duration (Datta *et al*., 2007), implying a total of 500 stimuli per task block, amongst which 60 were No-go stimuli (i.e. 12% No-go stimuli). As for the oddball task, during the rest block participants were asked to focus at the fixation cross at the centre of the screen.

The order of the two tasks was counterbalanced across participants. Throughout the recordings participants were seated on a comfortable chair in a quiet room free from distractions and with the LCD screen standing around 60 cm away. They were asked to avoid unnecessary head movements and to respond to the task at hand '*as quickly and as accurately as possible*'. After the first task participants were allowed to take a break until they felt ready to continue with the experiment. The length of the experiment recordings was specifically chosen to accommodate the long-period slow waves.

7.4. Avenues for Data Analysis

The data analysis proposed has two main approaches:

(a) Preliminary analysis of the evoked potentials within the task blocks, and

(b) Analysis and comparison of EEG activity during task and rest blocks in order to differentiate between brain activity in the presence and absence of stimulation (i.e. under load/ no load).

As explained in the previous sections, the nature of the task protocols selected for this study allows for the use of ERP component measures (such as the P300 amplitude and latency) to gauge the amount of loading on the brain as well as to monitor the participants' performance during tasks (Herrmann and Knight, 2001). For example, the level of sustained attention could be established by considering the mean value of the P300 across the whole SART block (Katayama and Polich, 1999). Behavioural data, such as reaction times, error rates and percentage of false alarms could also be used for this purpose. Therefore, the first part of the investigation deals with the analysis of ERPs and performance measures for the three experimental conditions (SART, Oddball Easy and Oddball Hard).

Secondly, a BSS-ICA methodology is employed in order to isolate neurophysiologically meaningful brain sources, such as the P300 complex, from the rest and task blocks separately. As seen in the MEG data analysis, ICA is compatible with the assumption that an ERP is the sum of coherent activations in a number of brain regions, their spatial projections being fixed across time and task conditions (Makeig *et al.*, 1999b). In keeping with that held in the literature, the view adopted here is that slow waves act as a driver which affects the overall brain activity in both conditions. Therefore, these slow oscillations may not be apparent in the data as independent sources *per se* but rather as a mechanism that affects underlying brain processes. For this reason, the slow waves are objectively investigated by considering all the independent components comprising each task block when filtered in the $(0<f<0.5)$ Hz band, rather than choosing and analysing only those brain sources (i.e. ICs) with a low-frequency time signature.

Furthermore, as explained above, the DMI hypothesis proposes an attenuation of slow wave power with a switch from rest to task. To this end, a new approach based on neural networks is implemented in order to provide an objective comparison between the brain sources in the slow wave band during rest and task conditions. The notion of whether different tasks and difficulty levels (i.e. different loading) are an attribute of this variation is investigated. The results for the slow waves are also contrasted with those of the delta, theta and alpha oscillators.

7.5. Summary

This chapter presented the motivation and design of an experimental framework to test the functional significance of the slow waves (in contrast to other brain oscillators) during resting states (spontaneous brain activity) and task-related (triggered) active processing. Details about the experiments carried out on 23 healthy adult controls were presented. The brain has been envisaged as an oscillatory system, which reacts (and may be reorganised) by the presence of external stimulation. This view is supported, amongst others (Karakas *et al*., 2000; Buzsáki and Draguhn, 2004), by a very recent publication entitled "*Brain oscillations forever*" by Rothenberger (2009) which, based on current research, suggests that several child psychiatric problems such as Tourette's syndrome, ADHD and autism may be related to dysfunctional brain oscillations that could be disturbing certain vulnerable neural circuits. Rothenberger goes on to propose that:

" … *for forward-thinking future research in child psychiatric neurophysiology, the brain should be considered primarily as an oscillatory system and investigating stability and/or variation of certain brain oscillation frequencies under different conditions should play the major role*."

This ties very strongly with the work conducted in this study, whereby two main paradigms, the Go No-go (SART) and a three-stimulus oddball task with two difficulty levels (Easy and Hard), have been employed to tax the brain oscillators, and in turn elicit a P300 response – a well-studied ER component associated with attention and memory operations. The tasks have been specifically chosen to grade the imposed load from the simple repetitive SART to the more attention-demanding oddball task. Features of the brain oscillators in different frequency bands during these tasks would then be contrasted with those during set periods of rest, when the oscillators generate spontaneous brain activity.

In the next chapter, each step of the methodology developed for the data analysis briefly introduced here will be explained in detail, and the group results obtained will be presented and discussed.

Chapter 8

ON THE ANALYSIS OF BRAIN OSCILLATIONS IN REST AND TASK EEG

This chapter deals with the methodology and the results obtained from the EEG experiments carried out for comparison of brain activity during rest and task conditions, as explained in the previous chapter. The first section provides a description of each module in the multistage system developed for this analysis, namely: (i) the application of blind source separation for denoising the data and extracting the underlying brain sources, (ii) subspace analysis of the task ICs based on hierarchical clustering, (iii) the extraction of features from the amplitude and phase of the ICs in different frequency bands, and (iv) classification of these features based on a neural network approach for pattern recognition using the Neuroscale algorithm and Gaussian Mixture Models. This procedure was then applied to the EEGs of 20 participants collected during the Go No-go (SART) and Oddball (OB) tasks. The second section of this chapter presents specific and combined results and describes further analysis carried out on the output of this multistage system.

Section 1 – The Multistage System

8.1. Preliminary Data Analysis

EEG data recorded at 250 Hz was low pass filtered at 16 Hz, and downsampled offline to a sampling frequency, f_s, of 100 Hz. Gross artifact laden channels, arising mainly from faulty electrodes in the electrode-cap, were replaced by the average of their neighbouring channels and the overall dataset was re-referenced to the average of all the channels. Twenty-five out of the 66 channels were then selected, their position corresponding to the electrode location of the International 10-20 System as shown in Figure 8-1 (a). Since the experiment was based on visual

stimuli the data was heavily contaminated by ocular artifacts (Figure 8-1 (b)). Consequently, each recording was divided into 4-5 minute segments, and decomposed by TDSEP-ICA (Ziehe and Müller, 1998) in order to identify the underlying brain sources and artifacts. The length of each segment was determined to ensure that an adequate number of low frequency cycles (including infraslow (<0.1 Hz) oscillations) could fit into each segment.

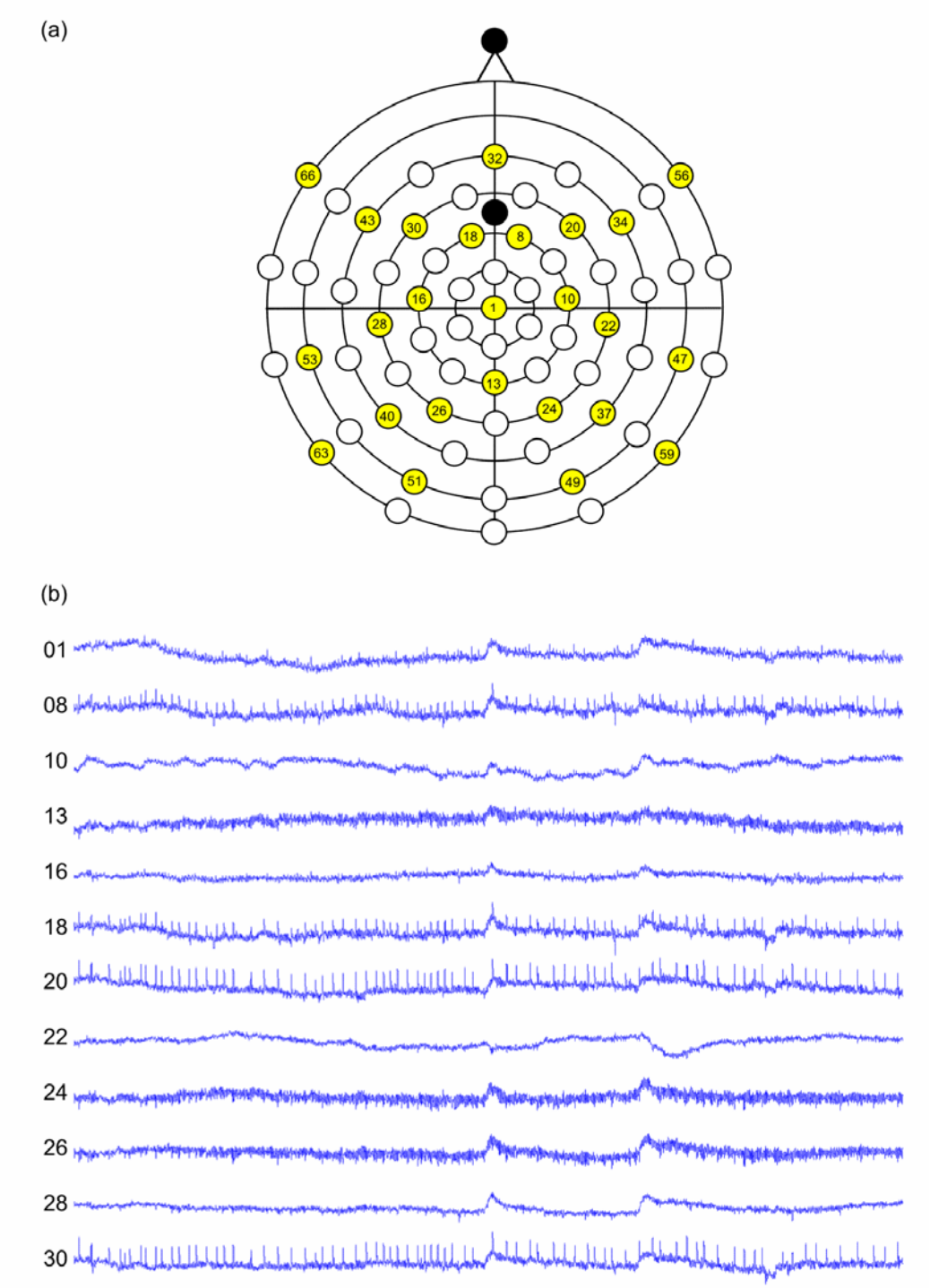

Figure 8-1. (a) 25 out of the 66 recording channels selected for analysis (marked in yellow), their position corresponding to the electrode-location of the International 10-20 System. (b) A sample of 5 minutes of raw data from 12 electrodes prior to denoising by ICA.

8.2. Extracting Brain Sources by TDSEP-ICA

As explained in Chapter 5.2.1, TDSEP is a specific ICA algorithm that achieves source separation by minimising temporal cross-correlations between the output signals. In essence, this algorithm determines the demixing matrix $\boldsymbol{W}$ for a set of sensor observations $\boldsymbol{x}$, by performing joint diagonalisation of several time-lagged covariance matrices, $\mathbf{C}_\tau = \left\langle \boldsymbol{x}(t)\boldsymbol{x}(t-\tau)^T \right\rangle$, such that the source covariance matrix $\mathbf{C}_s^\tau$ is diagonal for all time lags τ, $\mathbf{C}_s^\tau = \boldsymbol{W}\mathbf{C}_x^\tau\boldsymbol{W}^T$ where $\mathbf{C}_x^\tau$ is the signal covariance matrix (Ziehe and Müller, 1998). TDSEP was chosen since, unlike HOS-based methods such as FastICA (Hyvärinen, 1999b), it exploits the strong temporal structure inherent in ERP signals.

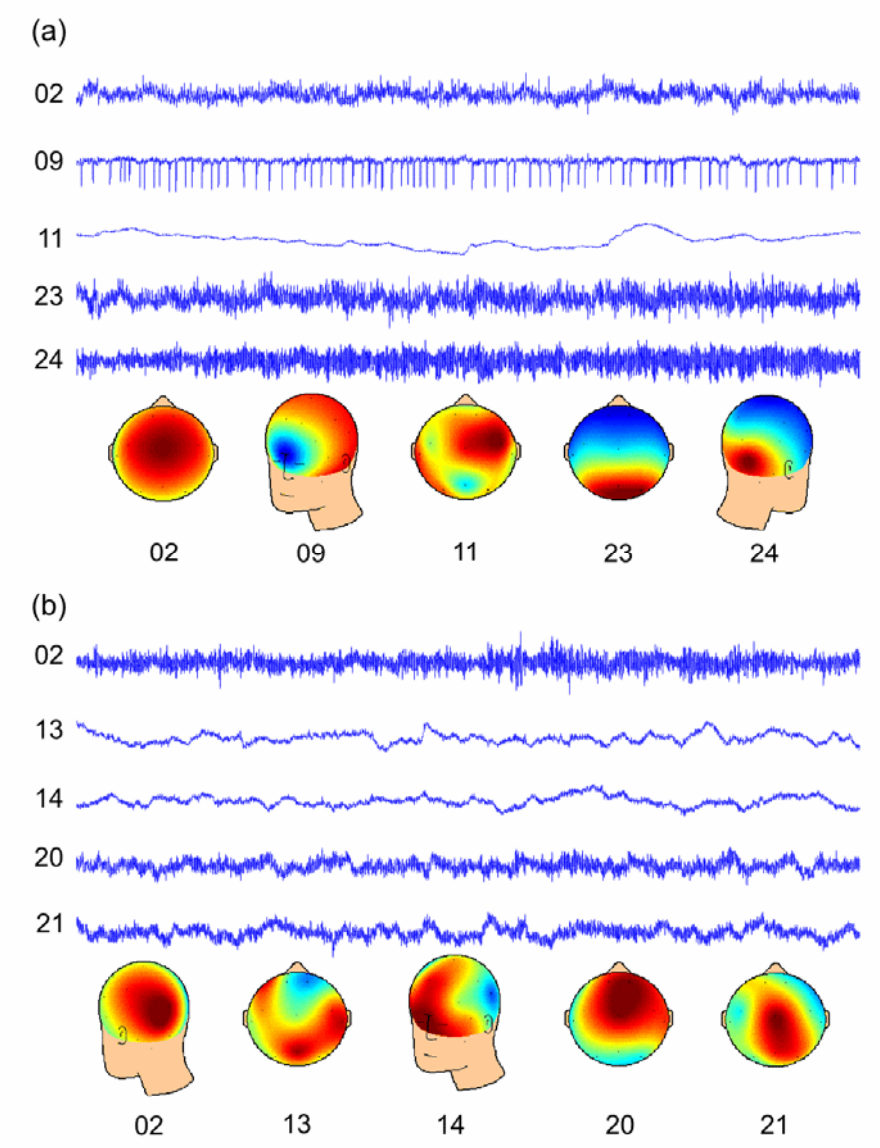

Figure 8-2. TDSEP-ICA decomposition (results of 1 participant shown as an example): (a) Five of the 25 ICs and their spatial distribution extracted by TDSEP-ICA during SART, and (b) Rest.

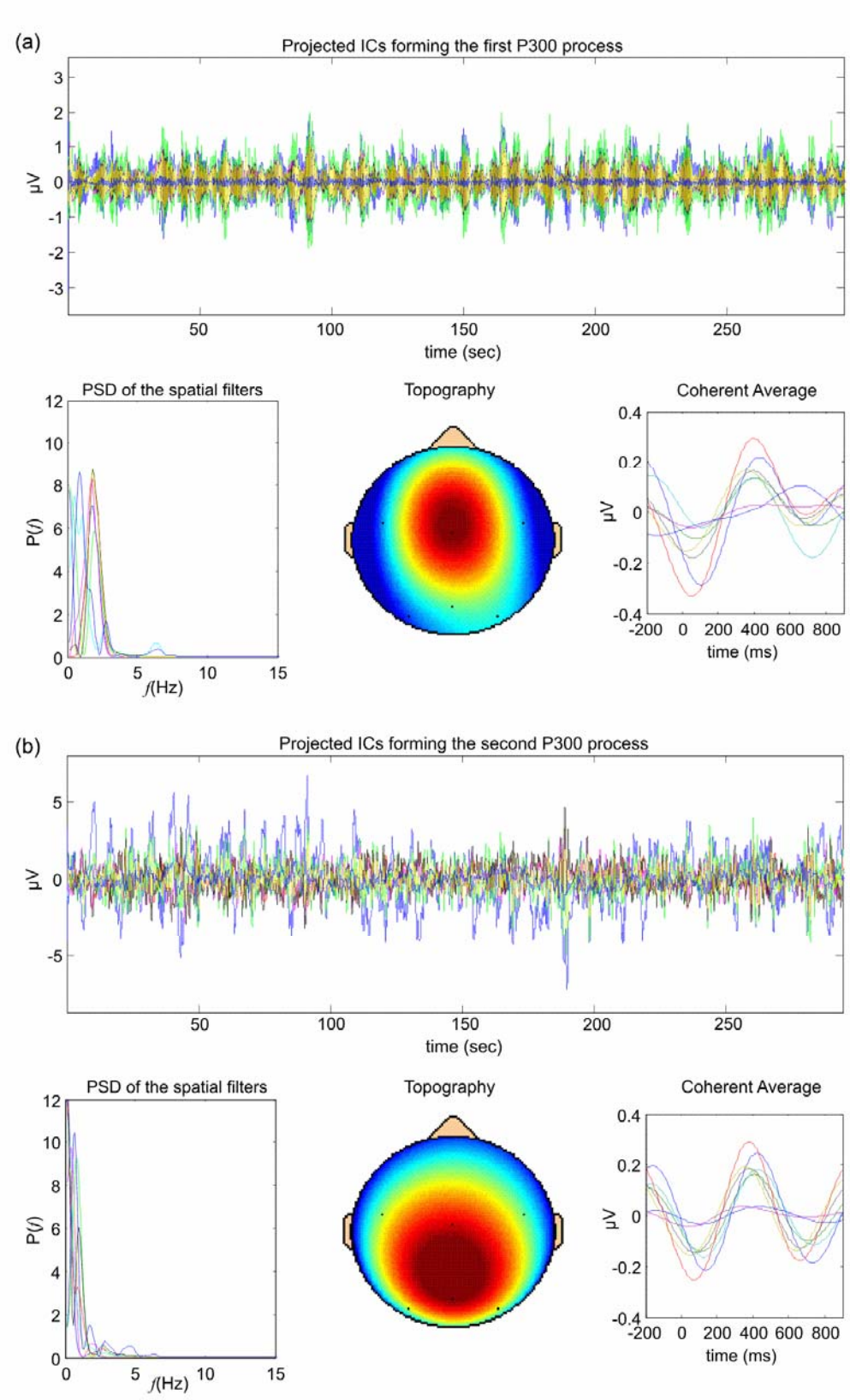

Figure 8-3. An example of two P300 processes (a) and (b) extracted by employing 8-channel ST-ICA (m=200) on one dataset. For each process is shown: the frequency response of the spatial filters (columns of the mixing matrix), the waveforms of the ICs projected back onto the measurement space, the topography of the RMS power distribution of these projected components forming the P300 process, and the coherent average of the projected ICs showing a peak around 400 ms.

Figure 8-2 (a) shows 5 of the 25 Task ICs of one participant during the Go No-go task; note the clear eye blink component (IC9), a low frequency component (IC11) and the strongest ER ICs (IC 2, 23 and 24) with central and parietal spatial distributions typical of the P300 complex. Meanwhile, Rest ICs show most power in the frontal regions (due to visual fixation) and occipital regions (alpha power associated with relaxation and absence of task-engagement), Figure 8-2 (b).

Note that ST-ICA could also be applied here as a BSS tool to extract the P300 processes, as shown in Figure 8-3. However, as explained in Chapter 5, in ST-ICA the number of delay vectors m needs to be approximately greater than f_s / f_l, f_l being the lowest frequency of interest in the signal. Therefore, in our case we would need around 1000 delay vectors (f_s=100 Hz and f_l<0.1 Hz ideally) in order to be able to directly investigate the slow waves *within* the recordings, in addition to long signal durations. This leads to very large delay matrices (≈1000 by 30,0000 samples for each channel of interest) which would drastically increase computational time and memory requirements. Moreover, further research is required on ST-ICA to interpret and analyse the extracted processes, and to manipulate the wealth of spatial and temporal information inherent in each. Since the problem at hand is novel it is best tackled with well-established algorithms that render a manageable output. This is another reason for choosing TDSEP-ICA for decomposing the data in these EEG experiments.

8.3. Hierarchical Clustering of Task ICs

Implementation of ICA on data recorded during task sessions renders three types of ICs: ER (task-related) ICs such as those forming the P300-complex, ICs constituting the background brain activity and artifacts, as illustrated in Figure 8-2. This grouping is commonly done by visual inspection of the topographies and time series of the estimated sources. Here, a more objective method based on hierarchical clustering (HC) is proposed in order to group together ICs with similar morphology, thus forming a hierarchy of nested partitions (Everitt, 1993). The procedure is as follows:

(i) Compute the coherent average of the ICs forming an r-by-s matrix E where r is the number of ICs and s is the number of samples comprising each coherent average (in this case, 111 samples covering from -200 ms before to 900 ms after stimulus onset).

(ii) Find the Euclidean distance between the coherent averages as a measure of similarity.

For every pair of averages in the dataset, i.e. for vectors E_{r_1} and E_{r_2}, this is defined as

$$d^2_{r_1 r_2} = \left(E_{r_1} - E_{r_2}\right)\left(E_{r_1} - E_{r_2}\right)^T. \tag{8.1}$$

(iii) Link pairs of averages which are in close proximity to generate a hierarchical tree, i.e. a dendrogram, using a distance measure between the binary clusters.

This step uses the distance information generated in (ii) to pair objects into binary clusters. Then, the newly formed clusters are grouped into larger ones until a dendrogram is formed. Here, several distance measures can be used as a proximity measure including weighted or unweighted average distances, Centroid distance or the Ward distance (a.k.a. the inner squared distance). The latter is often used because it tends to produce homogenous compact groups (Milanesi *et al*., 2008). The Ward metric uses the incremental sum of squares, i.e. the increase in the total *within-cluster sum of squares* as a result of joining clusters *a* and *b*. Specifically, the within-cluster sum of squares is defined as the sum of the squares of the distances between all objects in the cluster and the centroid of the cluster. The equivalent distance is given by

$$W^2_{dist}\left(a,b\right) = n_a n_b \frac{\left\|\bar{x}_a - \bar{x}_b\right\|_2^2}{\left(n_a + n_b\right)}, \tag{8.2}$$

where n_a and n_b are the number of objects in clusters *a* and *b* respectively, and $\|\ \|_2$ denotes the Euclidean distance between the centroids of clusters $\bar{x}_a$ and $\bar{x}_b$. These are defined as $\bar{x}_a = \frac{1}{n_a}\sum_{i=1}^{n_a} x_{ai}$, where x_{ai} is the i^{th} object in cluster *a*, i.e. the Euclidean distances from step (ii), (MathWorks Documentation, 2007).

(iv) Determine the number of natural clusters in the data by selecting an appropriate level on the dendrogram.

This is done by comparing the height of the links in the cluster tree with the heights of neighbouring links below it in the tree. Links where the distance between the objects joined is approximately the same as the distances between the objects they contain, exhibit a high level of consistency and shows natural cluster divisions in the data (e.g. the blue cluster in Figure 8-4).

Note that the cluster tree can be verified by calculating the cophenetic correlation coefficient. This compares the height of the links (a.k.a. the cophenetic distances) with the Euclidean distances generated in step (ii). If the clustering is accurate, the linking of objects in the dendrogram would

be strongly correlated with the distances between objects in the Euclidean distance vector, and the coefficient would have a value close to one (MathWorks Documentation, 2007).

Figure 8-4 shows an example of this HC procedure applied to the 25 SART ICs of which 5 are shown in Figure 8-2. The blue cluster in the dendrogram corresponds to the background ICs (including IC11), the red and green clusters and the individual branches correspond to the ER components, with the exception of IC9 (eye blinks are often time-locked to the visual stimuli thus having a high coherent average). The cluster tree has a cophenetic correlation coefficient of 0.89 implying a good representation of the natural grouping in the input data (i.e. the coherent averages of the ICs).

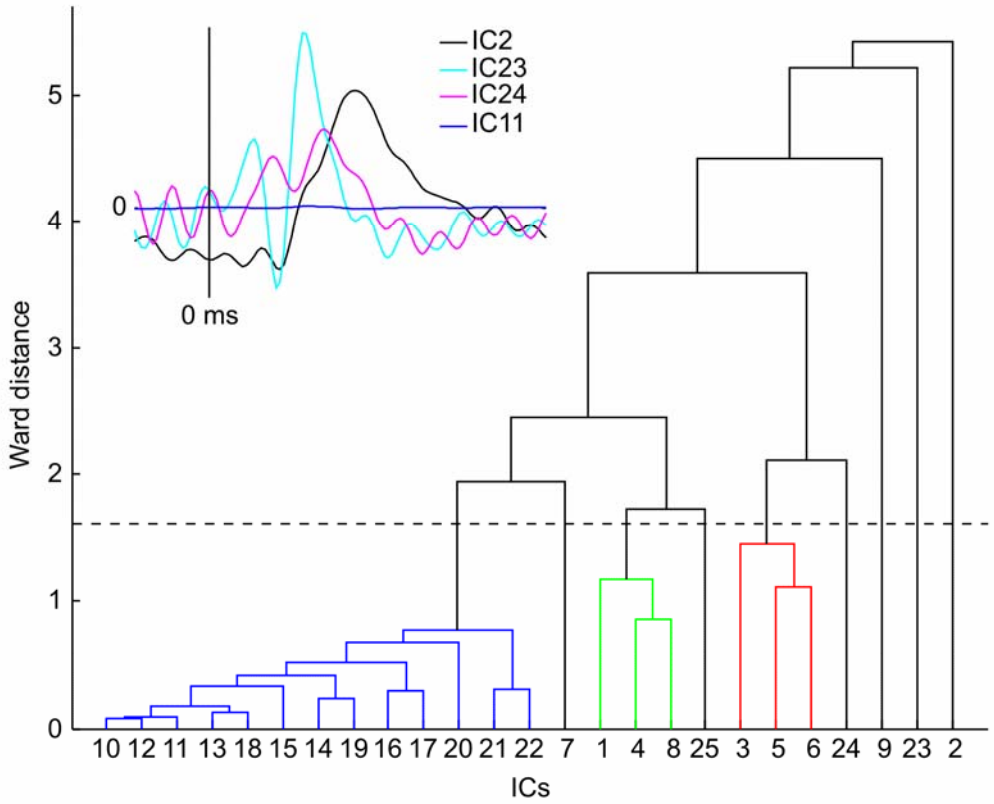

Figure 8-4. Hierarchical Clustering. Dendrogram built on the coherent averages of the ICs (selected traces shown): blue cluster corresponds to the background ICs, the red and green clusters and the individual branches correspond to the large ER-ICs, with the exception of IC9 (eye blinks).

To verify this result, an ERP-image as proposed by Delorme and Makeig (2004) was constructed for selected ICs (Figure 8-5). This is a two-dimensional representation of the event-related data sorted in order of some relevant measure (in this case, the participant's reaction time (RT) to button presses). Every horizontal line in the ERP image represents a potential time series during a single epoch, with changing colour values indicating the potential at each time point in the trial. A

moving average across adjacent single trials is being used as a way of smoothing in order to highlight trial-to-trial consistency. The ERP images for ICs 2, 23 and 24 show consistent evoked responses for every trial whereas IC11 (which forms part of the blue cluster in the dendrogram) is clearly not event related. This conforms to the results from the HC procedure, which illustrates that this method is successfully separating the two types of task ICs.

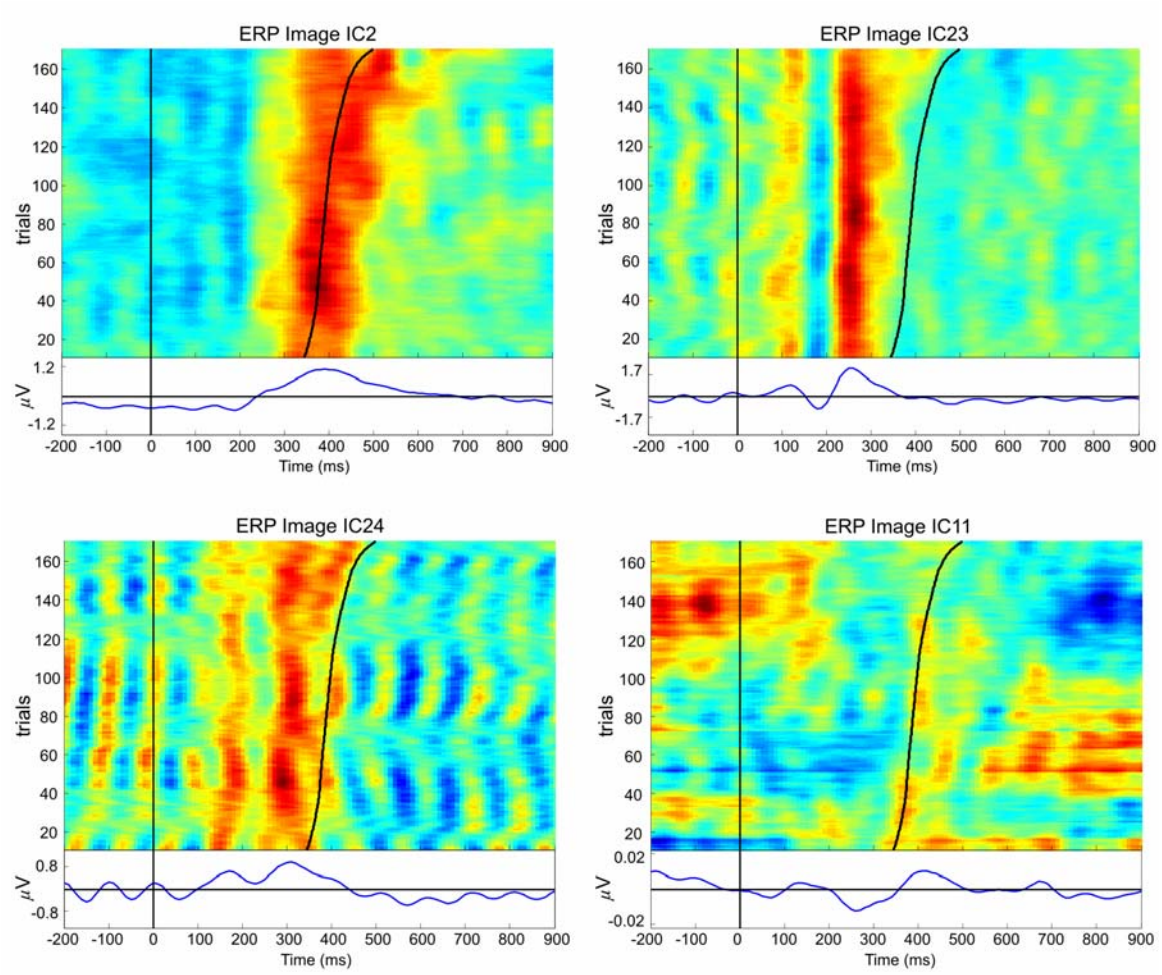

Figure 8-5. ERP images of selected ICs evoked responses (trials ordered according to their corresponding reaction time). The blue curve underneath each image represents the coherent average across trials. The black curve superimposed on the images shows the participant's RT for each trial (used to sort the individual trails comprising the image in ascending order)

The above BSS and HC procedure was employed on 4-5 minutes data segments from the EEG recordings during task in order to form a databank of ER and Background task ICs. Artifactual ICs, such as eye-blinks and eye movements, were immediately eliminated based on their morphology and topography. The remaining steps of the multistage system are demonstrated in the next sections on a subset of EEG recordings of ten participants during the Oddball Hard task environment (i.e. Oddball Hard – Rest). Here, TDSEP and HC were applied to three 4-minute

task segments (1st 4 minutes, 2nd 4 minutes and an overlap - i.e. 2 to 6 minutes) consecutively, and for every participant. Across participants this gave a databank of 371 ER and 316 Background ICs after HC. The Rest ICs were then extracted from a 4-minute segment (1-5 minutes into the rest block), with a total of 230 Rest ICs across the 10 participants.

8.4. Rest ICs

Typically the Rest ICs do not exhibit a specific response and should represent the activity of the brain in default mode – i.e. in the absence of stimulation. However, visual inspection of the Rest ICs after the removal of obvious artifactual sources showed that three types of components were manifested in each recording, mainly: the ICs with a slow and low-delta time-signature, those with an intermediate (high-delta and theta) frequency content, and those with a dominant alpha frequency content. Therefore, for better understanding of brain activity during the resting state, the Rest ICs were ordered based on their frequency content. For each IC, the ratio of power in the slow and low-delta frequency band ($0<f<1$ Hz) to the total power in ($0<f<f_s/2$ Hz) was found and the ICs were grouped accordingly, as shown in Figure 8-6. Note that this grouping procedure is suboptimal and is simply done to aid in the interpretation of results in later stages.

8.5. Extracting IC Features

The previous steps resulted in a databank comprising three main classes of ICs, namely: Task-ER, Task-Background and Rest. Next, ways of assessing the differences between the classes as a function of frequency had to be established in order to understand how the presence or absence of stimulation (i.e. external loading) was affecting the brain's oscillators, with particular attention to the slow waves. Therefore, it was required to describe the ICs by a set of features which could then be classified based on their level of similarity. Consequently, the ICs were filtered in four frequency bands: slow ($0<f<0.5$ Hz), delta ($0.5<f<4$ Hz), theta ($4<f<8$ Hz) and alpha ($8<f<12$ Hz) band, and for each band-limited IC the instantaneous amplitude and phase were obtained using the Hilbert transform (explained in Chapter 6.2.1; Le Van Quyen *et al*., 2001).

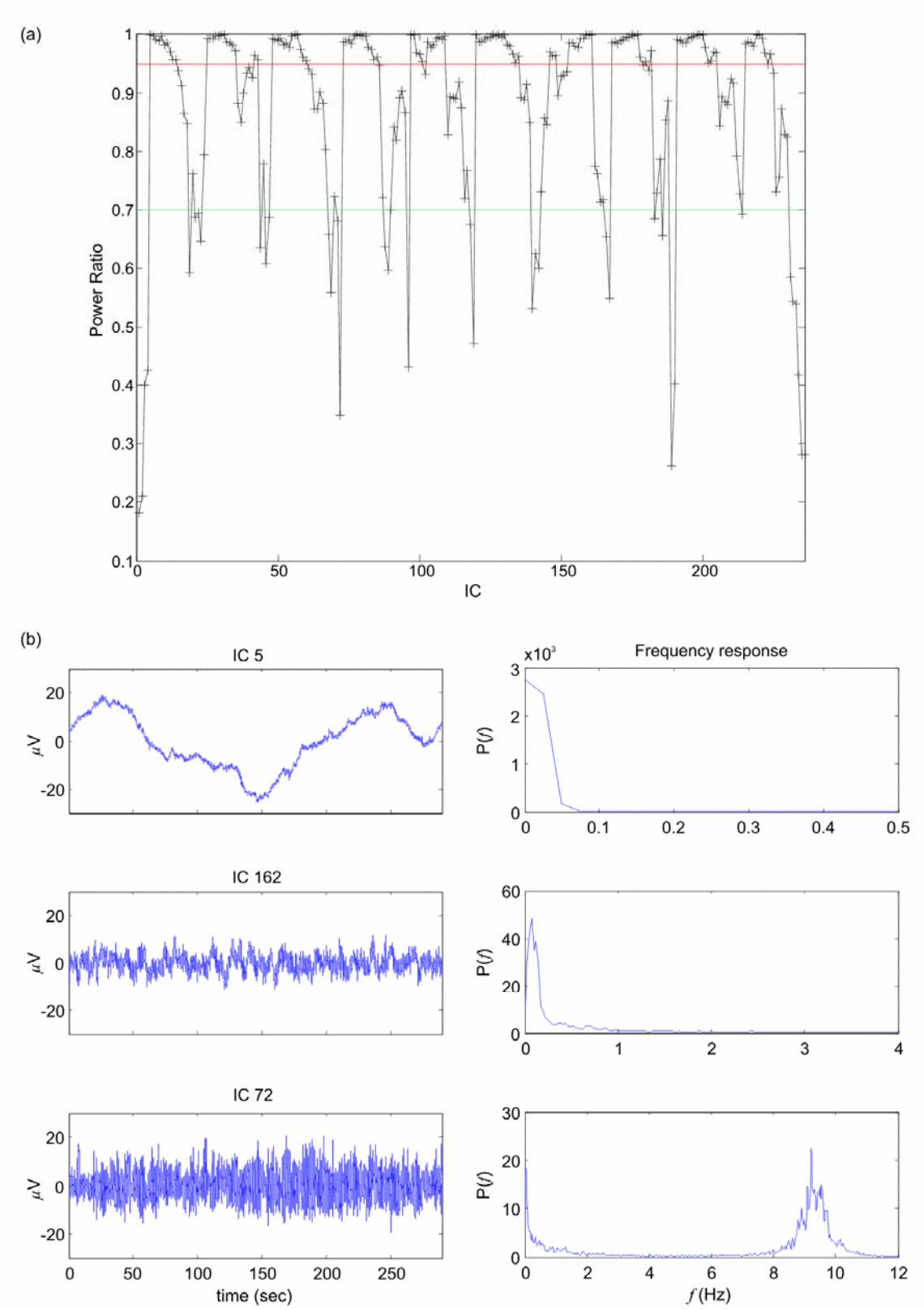

Figure 8-6. Ordering of Rest ICs based on their frequency content: (a) When the ratio of power in the ($0<f<1$ Hz) band to the power from 0-$f_s/2$ was greater than 0.95, the ICs were marked as slow ICs. For power ratios between 0.7 and 0.95 the ICs had an intermediate frequency content. When the power ratio was less than 0.7 the ICs had a predominantly high (alpha) frequency content; (b) An example of each type of IC and their PSDs.

8.5.1. First Set of Features

Each IC was represented by 16 features: the power in the instantaneous amplitude envelope and the second to forth order moments of the instantaneous phase (i.e. the variance, skewness and kurtosis) for each frequency band (i.e. 4 features per frequency band). Figure 8-7 illustrates the method of feature extraction for the slow wave band. Figure 8-8 then shows the power in the slow wave envelope and the moments of the slow wave phase for each IC in the three classes; the Oddball Hard task environment features are shown as an example. At first glance, these features already indicate that both the amplitude and phase of the ICs in the slow wave band undergo a change in the three classes. However, these features may not be capturing the whole morphology and structure over the 4 minute time-series for each IC. Therefore, a second set of features was derived by fitting 12th order AR models to the instantaneous amplitude and phase time series of each IC separately and for each frequency band.

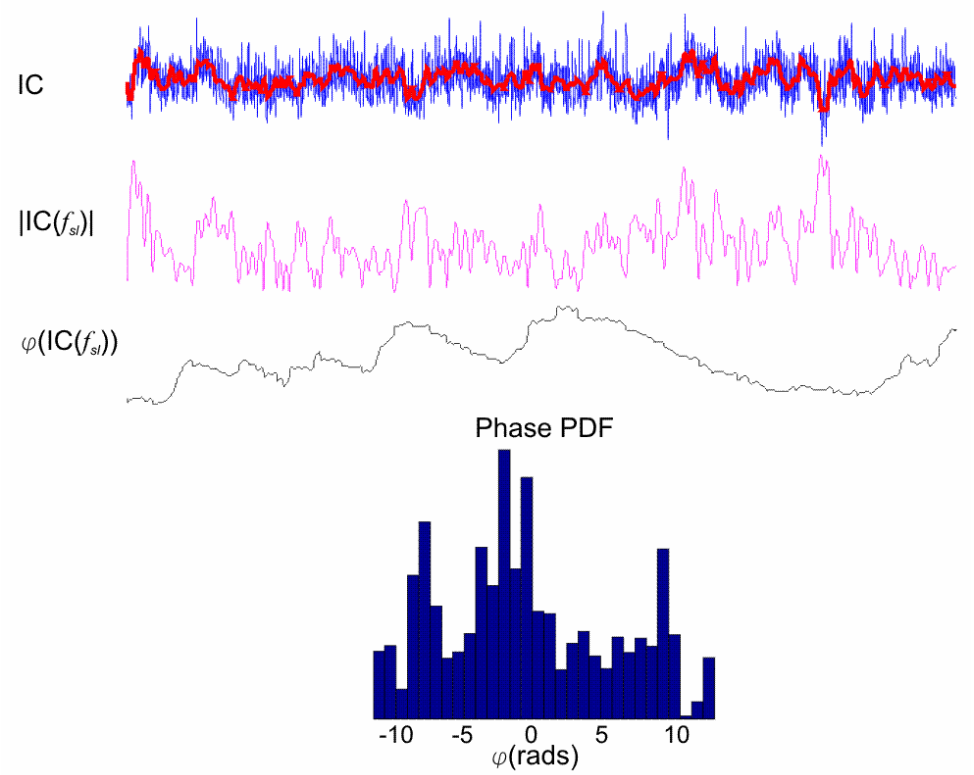

Figure 8-7. Extracting IC features: One IC (blue trace), 0<f<0.5 Hz filtered IC (superimposed red trace), the instantaneous amplitude |IC(f_{sl})| and phase φ(IC(f_{sl})) of the filtered IC; the instantaneous slow wave phase PDF.

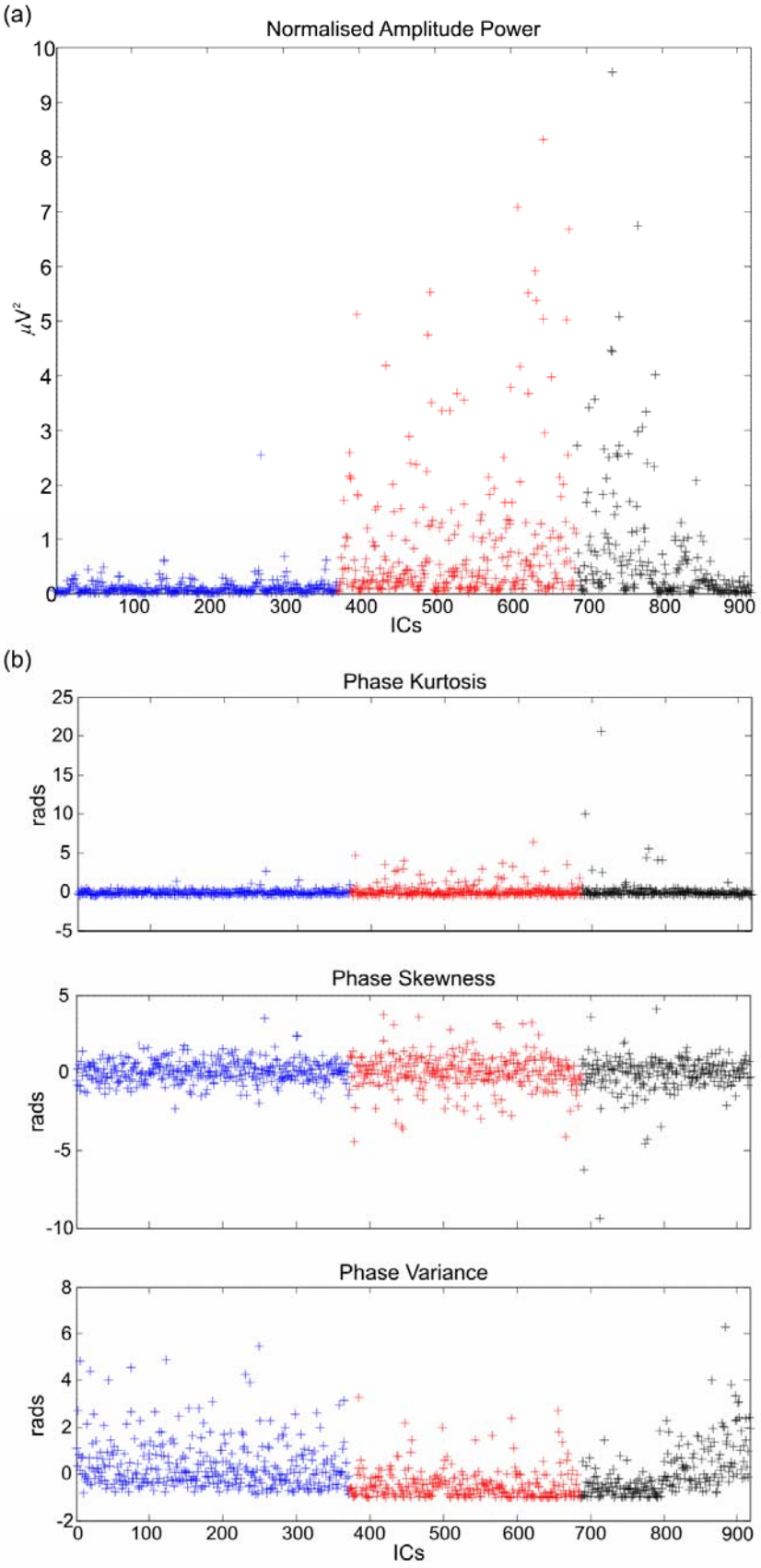

Figure 8-8. (a) The power in the slow wave envelope; (b) The phase kurtosis, skewness and variance for the slow wave phase for each IC in the Oddball Hard task environment. Blue (+) represent the ER, red (+) the Background and black (+) the Rest ICs features.

8.5.2. AR Models

Autoregressive (AR) models are used to model a signal at the output of an all-pole filter driven by a spectral white input. One of the most commonly employed methods is linear prediction, which involves defining the signal x as a p^{th} order AR process such that the current value, $x(n)$, can be predicted from p past samples

$$\hat{x}(n) = -\sum_{k=1}^{p} a_k x(n-k). \tag{8.3}$$

The coefficients a_i are chosen to minimise the prediction error $e(n)$, (i.e. the uncertainty in the prediction of the next signal value), such that $e(n) = x(n) - \hat{x}(n)$.

The Yule Walker (a.k.a. the autocorrelation) method is often employed to estimate the AR parameters by minimising $e(n)$ in the least-squares sense. Essentially, the Yule Walker equations describe the relationship between the AR parameters and the autocorrelation function of $x(n)$, and are solved using the Levinson-Durbin recursion algorithm (Hayes, 1996). Since the method characterises the data using an all-pole model, model order selection is of fundamental importance. If the model order is too low the ability of the linear system for modelling the data will be limited, whereas if it is too high there will be over-fitting of the data with spurious information present in the output.

In order to characterise the changes in the instantaneous amplitude or phase of the ICs at one particular frequency band, these time series were individually parameterised with an AR model. Here, the AR model was intended to capture the structure of the time series across the 4 or 5 minute segment considered. Then, the distance between ICs (i.e. the degree of similarity between the ICs belonging to one class and dissimilarity between ICs of different classes) needed to be estimated by calculating the distance between the two sets of AR parameters for each pair of ICs instantaneous amplitude or phase time series. Note that the Euclidean distance between the AR models is not an appropriate measure because the AR parameters of two separate time series may be heavily correlated. For example, two sets of parameters for two different time series may exhibit strong correlations between some of their parameters (say for the first three parameters, since the difference between them might reside in the detail, i.e. in the remaining parameters). This could potentially lead to artificial similarity, as in the Euclidean distance measure the parameters are all equally weighted. A measure is needed that quantifies the similarity between the signals being modelled, rather than the similarities between the pairs of model parameters alone; for this reason the Itakura-Saito Distance (Itakura, 1975) was employed here, as explained next.

8.5.3. Itakura-Saito Distance

The Itakura-Saito Distance (ID) is widely used in speech processing applications (Itakura, 1975) but has also been applied for quantifying changes in the EEG due to brain damage in neonates (Kong *et al*., 1995), during epileptic seizure, as well as to investigate the connection between EEG and EOG signals during different sleep stages (Estrada *et al*., 2005). The ID is computed as follows. Suppose the band-limited (filtered) IC_1, $x(n)$ time series, is modelled by an AR process $a_x = [1 \ -a_{11} \ -a_{12} \ \ldots \ -a_{1p}]$ and IC_2, $y(n)$, is modelled by $a_y = [1 \ -a_{21} \ -a_{22} \ \ldots \ -a_{2p}]$. The mean square error (MSE) for $x(n)$ is defined as

$$MSE_{x,x} = a_x^T R_x(p) a_x, \tag{8.4}$$

where $R_x(p)$ is the p+1 autocorrelation matrix for $x(n)$, given by $R_x(p) = E\left\{x(n)x(n)^T\right\}$.

Meanwhile, the MSE of $y(n)$ passing through the model for $x(n)$ is $MSE_{x,y} = a_y^T R_x(p) a_y$. Therefore, the ID for IC_2 with respect to IC_1 can be defined as

$$id_{x,y} = log\left(\frac{MSE_{x,y}}{MSE_{x,x}}\right) = log\left(\frac{a_y^T R_x(p) a_y}{a_x^T R_x(p) a_x}\right). \tag{8.5}$$

The MSE of $x(n)$ passing through the $y(n)$ model, $MSE_{y,x}$, can also be found in order to establish the ID in the other direction (i.e. IC_1 with respect to IC_2),

$$id_{y,x} = log\left(\frac{MSE_{y,x}}{MSE_{y,y}}\right) = log\left(\frac{a_x^T R_y(p) a_x}{a_y^T R_y(p) a_y}\right). \tag{8.6}$$

The symmetric ID for ICs 1 and 2 can then be obtained by combining equations (8.5) and (8.6) such that (Estrada *et al*., 2005)

$$ID_{x,y} = \frac{1}{2}\left(id_{x,y} + id_{y,x}\right). \tag{8.7}$$

An example of the symmetric ID matrix between the parameters of the AR models for the instantaneous amplitude of the ICs in the slow wave band during the Oddball Hard task environment is illustrated in Figure 8-9. The ID between the ICs features pertaining to the same class should be close to zero (blue); whilst that between different classes should be higher (tending towards red). Here, note the difference in the ID of the three classes, where ER class contains parameters corresponding to ICs 1:371, the Background (Bgd) contains parameters of ICs 372:687 whereas the parameters of ICs 688:917 form the Rest Class. It is already evident that

there is overlap between the Rest class with both the Background and ER classes: the features of the Rest ICs with a slow morphology overlap with the Background class (hence the continuation from the Background into the Rest for 687:805), whilst the features of the Rest ICs with a higher frequency morphology (806:971) overlap with the ER class.

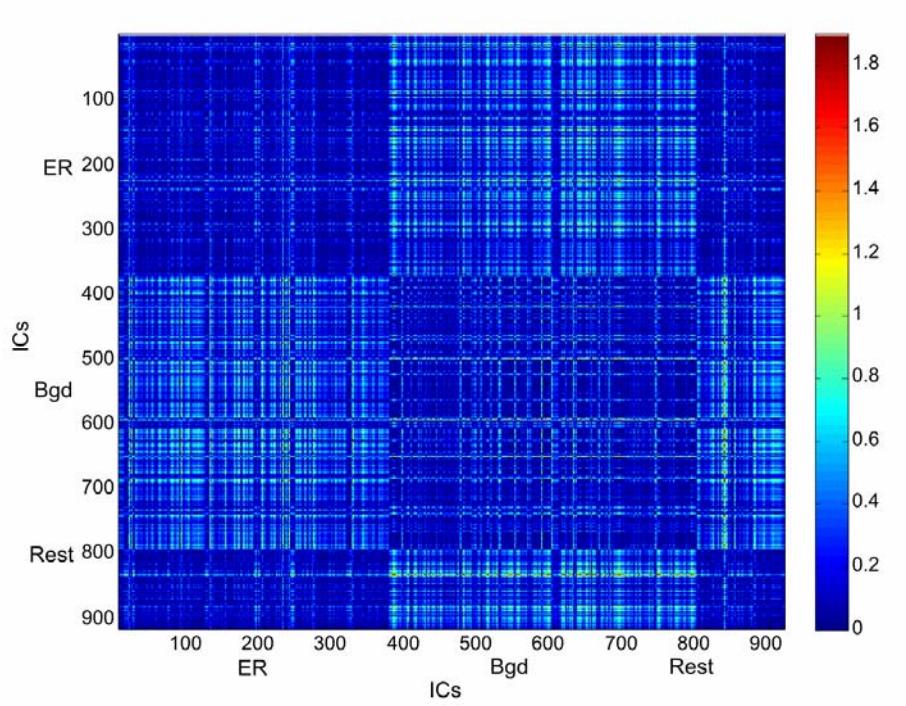

Figure 8-9. Scaled image of the ID between the AR models of the ICs slow wave instantaneous amplitude for the Oddball Hard task environment. Note that points 1:371 represent the ER class, 372:687 the Background class and 688:917 the Rest class.

8.6. Classification of ICs Parameters: A Neural Network Approach

At this stage there was a *P*-dimensional space representing the ICs in the three classes; *P* varied from 16 (for the 1st set of features based on amplitude power and phase moments) to 13 (for the 2nd set based on 12th order AR models and ID method). The next step was to perform a nonlinear transformation of this *P*-dimensional space into a 2-D space for better visualisation of the natural divisions already apparent in the data. This was implemented through a neural network approach, known as the Neuroscale algorithm.

8.6.1 Neuroscale

Neuroscale is a clustering process (Lowe, 1993; Lowe and Tipping, 1996:1997; Nabney, 2004) which performs a dimension-reducing, nonlinear transformation of the original input data. This 'topographic' transformation optimally preserves the geometric structure of the data by ensuring

that the inter-point distances in the feature space correspond as closely as possible to the distances in the data space. This is implemented by means of a radial basis function (RBF) neural network (Bishop, 1995) which is used to predict the co-ordinates of the data in the transformed feature space. The weights of the network are adjusted in order to indirectly determine the locations of the feature points. The transformation is then achieved by optimising the network parameters such that a suitable error measure is minimised. This procedure is described below.

Consider a *P*-dimensional input space of *N* data points $\mathbf{x}_i$; the RBF generates a *Q*-dimensional feature space of points $\mathbf{y}_i$ on condition that the relative positions of $\mathbf{y}_i$ minimise the *stress* term

$$E_{stress} = \sum_j \sum_{i>j}^{N} \left(d_{ij}^* - d_{ij} \right)^2, \tag{8.8}$$

where the d_{ij}^* are the inter-point Euclidean distances in the data space $d_{ij}^* = \sqrt{\left(\mathbf{x}_i - \mathbf{x}_j\right)^T \left(\mathbf{x}_i - \mathbf{x}_j\right)}$, and the d_{ij} are the corresponding distances in the feature space $d_{ij} = \sqrt{\left(\mathbf{y}_i - \mathbf{y}_j\right)^T \left(\mathbf{y}_i - \mathbf{y}_j\right)}$. Therefore, minimising E_{stress} ensures that the inter-point distances in the feature space are matched with those in the data space.

Specifically, $\mathbf{y}_i = \mathbf{f}(\mathbf{x}_i;\mathbf{W})$, where $\mathbf{f}$ is the nonlinear transformation obtained by the RBF with weights $\mathbf{W}$. Therefore, the distances in the feature space can be expressed as $d_{ij} = \left\| \mathbf{f}(\mathbf{y}_i) - \mathbf{f}(\mathbf{y}_j) \right\|$, such that

$$d_{ij}^2 = \sum_{l=1}^{Q} \left(\sum_k \mathbf{W}_{lk} \left[\phi_k \left(\left\| \mathbf{x}_i - \mathbf{c}_k \right\| \right) - \phi_k \left(\left\| \mathbf{x}_j - \mathbf{c}_k \right\| \right) \right] \right)^2, \tag{8.9}$$

where $\phi_k()$ are the basis functions, $\mathbf{c}_k$ are the 'fixed' centres of the functions and $\mathbf{W}_{lk}$ are the weights from the basis functions to the output (Lowe and Tipping, 1996).

The disadvantage of this method is that, being a nonlinear optimisation process, it can be computationally expensive to train and the dimensions of the desired feature space needs to be specified *a priori*. On the other hand, neuroscale results in a generative solution and provides a transformation rather than a mapping of the 'training' (input) data points. Consequently, new test data can be projected onto the feature space using the fixed RBF structure learnt in the training stage by simply modifying the parameters of the network (Lowe, 1993). Note, however, that the output of this algorithm is strictly determined by the spatial distribution of the data points and does

not take into consideration additional information, such as class labels, linked to the input data. To overcome this limitation supervised neuroscale was developed in Low and Tipping (1996:1997).

Supervised Neuroscale

This is a modification of the above method which allows for the inclusion of subjective knowledge in the training process. This additional information could, at varying degrees, affect the objective topology generated by the spatial input data. The distance being used for training d_{ij}^{*} is replaced by δ_{ij}

$$\delta_{ij} = (1-\alpha) d_{ij}^{*} + \alpha s_{ij} , \tag{8.10}$$

where d_{ij}^{*} is the Euclidean distance between input data points (for the first set of features), or the ID matrix (for the second set). s is another distance metric, where the distance between points in the same class is set to zero, while that between points in different classes is non-zero (Nabney, 2004). For example, this study entails three main classes. Based on prior knowledge regarding the ICs morphology and type of brain activity in the three conditions, the distance between ER and Background was assigned to one (since these two classes, though different, both represent task activity), distance between Background and Rest was 2 whereas that between ER and Rest was set to 3 (since brain activity during rest was expected to differ more from event-related than from background activity during task), as shown in Figure 8-10. Note that these numbers for ***s*** have been chosen to indicate expected relative differences between the three classes.

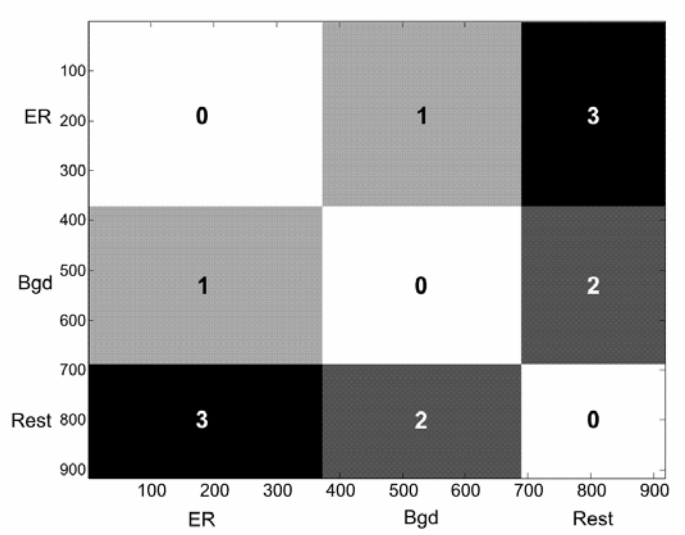

Figure 8-10. Scaled image of the distance matrix ***s*** (i.e. the distance metric s defined for each pair of points in the whole dataset) used in supervised neuroscale as a means of introducing subjective information in the training process.

The parameter α varies from 0 – the original, objective, unsupervised method based solely on the distribution of the original data, to 1 – the completely supervised method that is no longer explicitly dependent on the data distribution. A value of $\alpha = 0.5$ strikes a balance between objective and subjective approaches, hence maintaining the spatial topology of the original data whilst improving the visualisation of the feature points by achieving a more distinct separation between the classes (Lowe and Tipping, 1996).

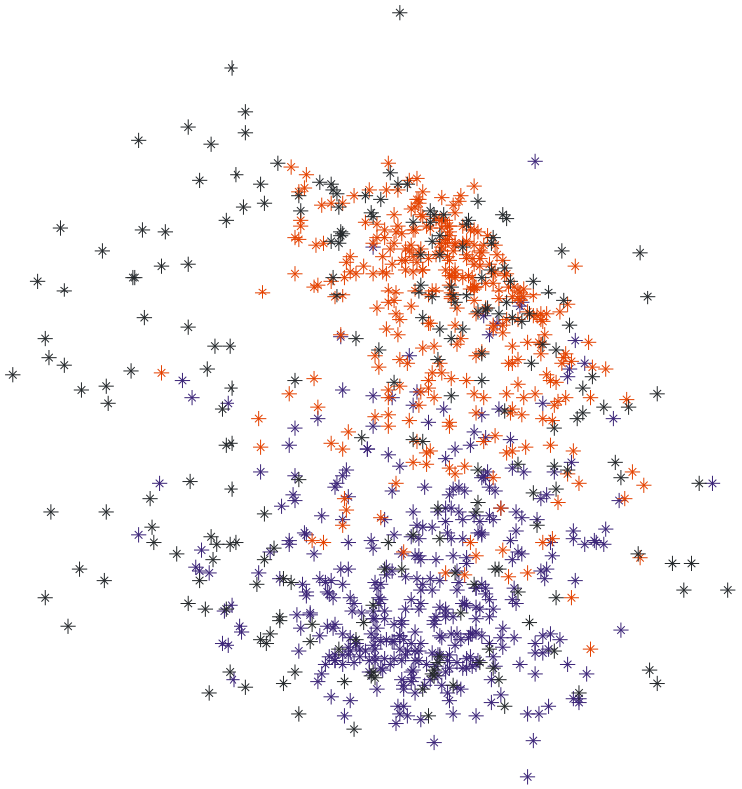

Figure 8-11. The 2-D output from supervised neuroscale ($\alpha = 0.5$, number of basis functions centres = 80) for the 13-D input space based on the slow wave amplitude features derived using AR models and ID method for Oddball Hard task environment. Blue represent ER ICs features, red the Background features and black the Rest features. (Note that the axis scales are arbitrary).

Figure 8-11 shows an example of the supervised neuroscale algorithm 2-D output (trained using number of basis functions centres $k = 80$ (chosen by trial and error) and $\alpha = 0.5$), for the ICs slow wave features derived by the AR ID method, and using the ID matrix of Figure 8-9 (for d_{ij}^{*}) and the $\boldsymbol{s}$ matrix in Figure 8-10. The three classes occupy specific locations in the 2-D space, with the ER and Background features being well separated, whilst the Rest class overlaps with the two task classes. This is in keeping with existing theoretical models and fMRI BOLD imaging studies on the slow waves (Fox *et al*. 2006; Fransson, 2006; Fox and Raichle, 2007), which suggest that despite experiencing changes during different brain states, the slow wave mechanism is always actively affecting underlying brain processes.

This example demonstrates that although the neuroscale clustering process can separate the three classes, both the features and the classifier itself are not perfect. This leads to misclassification of a number of input data points. Moreover, as in the example given, the classes themselves may naturally possess overlapping traits. For this reason, the PDF space formed by the three classes must be characterised in order to be able track the probability of classification per class, i.e. the probability of each data point (in this 2-D space) belonging to each of the three classes. This was done via Gaussian Mixture Models (GMMs).

8.6.2 Mixture Models

Mixture models belong to the class of pattern recognition systems and are extensively used as a classification tool in a wide variety of applications, when the data of interest comprises a number of populations mixed together in varying proportions (Bishop, 1995; Nabney, 2004). Each population or cluster is mathematically represented by a parametric component distribution such as Gaussian (continuous) or Poisson (discrete). Mixture models with high likelihood tend to have component distributions with high peaks such that the data points in one cluster are tight. Moreover, the data is well-covered in order to capture all its dominant patterns. These models are a semi-parametric alternative to non-parametric histograms and provide greater flexibility and precision in modelling the underlying statistics of sample data. Once a model is generated, conditional probabilities can be computed for each input data point. Mixture models can also be viewed as a form of generalised RBF network in which each component is a basis function or 'hidden' unit. The component probabilities can then be viewed as weights in an output layer (Bishop, 1995; Nabney, 2004). Mixture models that use a multivariate Gaussian mixture density to define the probability density function of the observed variables are commonly known as GMMs. Given a series of inputs, the weights of each distribution are computed by means of expectation-maximization algorithms (Martinez and Martinez, 2002).

A. Gaussian Mixture Models

In GMMs, the probability density function is expressed as a linear combination of Gaussian basis functions. Let the conditional density of a data point (for example, one data point in the 2-D output feature space generated by neuroscale) be a mixture with M component densities (Bishop, 1995; Martinez and Martinez, 2002)

$$p(y) = \sum_{j=1}^{M} P(j)\, p(y|j), \tag{8.11}$$

where a mixing parameter $P(j)$ corresponds to the prior probability that data point y was generated by component j, and where $\sum_{j=1}^{M} P(j) = 1$.

The latter requisite arises because for a function to be a valid PDF it must be non-negative everywhere and integrate to 1 over the entire space. This mixture model is *generative* since it involves the process of generating samples from the density it represents (Franc and Hlaváč, 2004; Nabney, 2004). Primarily, one of the components j is chosen at random with *prior* probability $P(j)$. A data point is then generated from the corresponding density $p(y|j)$. The corresponding posterior probabilities can then be written, using Bayes' theorem, in the form

$$P(j|y) = \frac{p(y|j)P(j)}{p(y)}, \tag{8.12}$$

where $p(y)$ is given by equation (8.11). These posterior probabilities satisfy the constraints

$$\sum_{j=1}^{M} P(j|y) = 1, \quad 0 \le P(j|y) \le 1. \tag{8.13}$$

Since each mixture component is a Gaussian with mean vector μ of dimension d and covariance matrix Σ_j, (which, for a spherical covariance mixture model, this is some scalar multiple of the identity matrix I, such that $\Sigma_j = \sigma_j^2 \mathrm{I}$, (Nabney, 2004)), its density function can be defined as (Franc and Hlaváč, 2004)

$$p(x|j) = \frac{1}{(2\pi)^{d/2}|\Sigma_j|^{1/2}} exp\left\{-\frac{1}{2}(y-\mu_j)^T \Sigma^{-1}(y-\mu_j)\right\}. \tag{8.14}$$

B. Expectation-Maximisation Algorithm

The GMM parameters for a set of training data are estimated by the maximum likelihood criterion using the well-established expectation-maximization algorithm (Nabney, 2004; Martinez and Martinez, 2002). This algorithm iteratively modifies the GMM parameters in order to minimise the negative log likelihood E (i.e. maximize the likelihood) of the data

$$E = -ln\, L = -\sum_{n=1}^{N} ln\, p(y^n) = -\sum_{n=1}^{N} ln\left\{\sum_{j=1}^{M} p(y^n|j)P(j)\right\}, \tag{8.15}$$

at each step until a local minimum is found (Bishop, 1995). It calls for *a priori* model order selection in the form of the number of M components which are to be incorporated into the model. Often a suitable number may be selected by the user roughly corresponding to the number of distinct classes forming the dataset to be modelled (in this case, the feature space) or by using

exploratory data analysis to look for clusters or other group structures. This algorithm also requires an initial estimate for the value of the component parameters. This can be achieved by performing a rough clustering of the data using, for example, the *K*-means algorithm as explained in the work by Nabney (2004).

The posterior probabilities, which show the likelihood that a point belongs to each of the separate component densities, are determined according to equation (8.12). This estimated posterior probability is then used to obtain a weighted update of the parameters (i.e. prior probabilities, means and variances) for each component (Bishop, 1995; Martinez and Martinez, 2002).

The mixing coefficients update equation is defined as

$$\hat{P}(j) = \frac{1}{N}\sum_{n=1}^{N} \hat{P}\left(j \middle| y^n\right), \tag{8.16}$$

where $j = 1,\ldots,M$, which implies that the prior probability for the j^{th} component is given by the posterior probabilities for that component, averaged over the dataset.

Moreover, the mean of the j^{th} component is the mean of the data vectors, weighted by the posterior probabilities that the corresponding data points were generated from that component

$$\hat{\mu}_j = \frac{\sum_n \hat{P}\left(j \middle| y^n\right) y^n}{\sum_n \hat{P}\left(j \middle| y^n\right)}. \tag{8.17}$$

The variance of the j^{th} component is then given by the variance of the data with respect to the mean of that component, again weighted by the posterior probabilities

$$\hat{\sigma}_j^2 = \frac{1}{d}\frac{\sum_n \hat{P}\left(j \middle| y^n\right) \left\| y^n - \hat{\mu}_j \right\|^2}{\sum_n \hat{P}\left(j \middle| y^n\right)}. \tag{8.18}$$

In summary, the procedure of the expectation-maximization algorithm can be described as follows (Martinez and Martinez, 2002):

1. Determine the number of component densities *M* in the mixture (i.e. the dataset).
2. Initialise the component parameters, i.e. the mixing coefficients, means and variance matrices for each normal density.
3. Calculate the posterior probabilities using equation (8.12) for each data point.
4. Update the parameters of the individual components following equations (8.16) to (8.18).
5. Repeat steps 3. and 4. until the estimates converge (i.e. until changes in the estimates at each iteration are less than some pre-set tolerance).

C. GMMs on the Neurosale Output

In this step, a set of GMMs were obtained in order to define the distributions of the neuroscale output. Figure 8-11 indicates that the task ER and Background classes were separable, whereas the Rest had some overlap with both other classes. Therefore, the assumption used here was that the task ER and Background data could be confidently labelled as process A and B respectively, whereas from the Rest data there could be unlabelled points that belonged to either labelled sets. Therefore, the structure was first set up and the two GMMs of the labelled data were trained. Then these GMMs, derived from the two definite (strong) processes, were used to train a new GMM for the unlabelled data, (which is here being called process C for convenience but it was not defined as a distinct process *per se* because of the overlap with the first two). Figure 8-12 shows the contour plots for these GMMs; note the distinct ER and Background contour plots (each derived with $M = 2$) whilst the Rest GMM ($M = 5$) overlaps with both. The posterior probabilities obtained by each GMM, namely P_A, P_B and P_{mix}, were normalised such that together they added up to one, as illustrated in Figure 8-13.

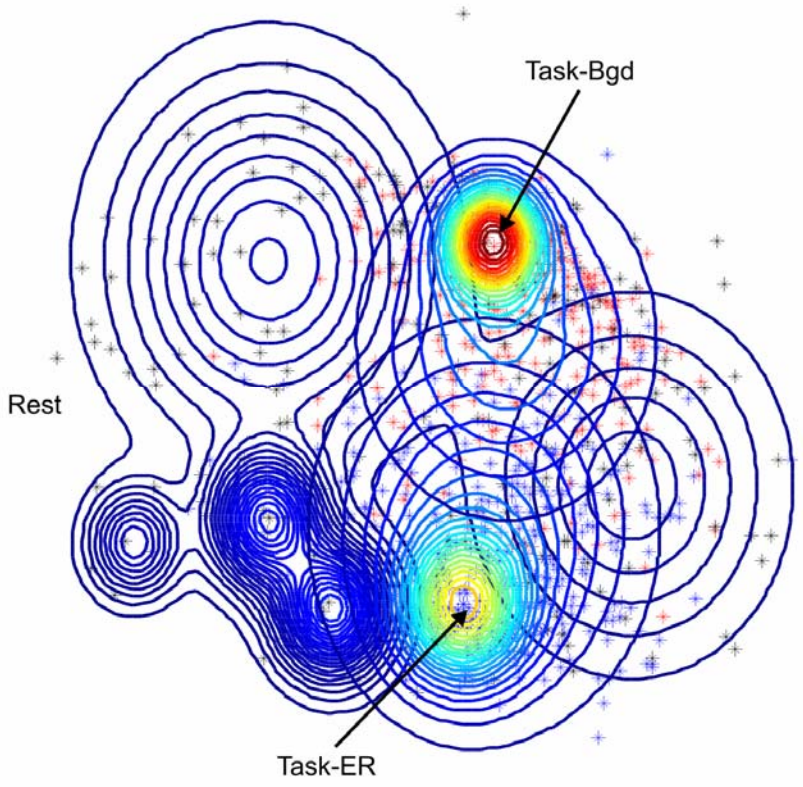

Figure 8-12. The three GMMs derived for the neuroscale output for the Oddball Hard task environment based on the slow wave amplitude features. Note the distinct ER (modelling the blue points in Figure 8-11) and Background (modelling the red points) GMMs; the Rest GMM (modelling the black points) overlaps with both, but still occupies a partially-distinct space.

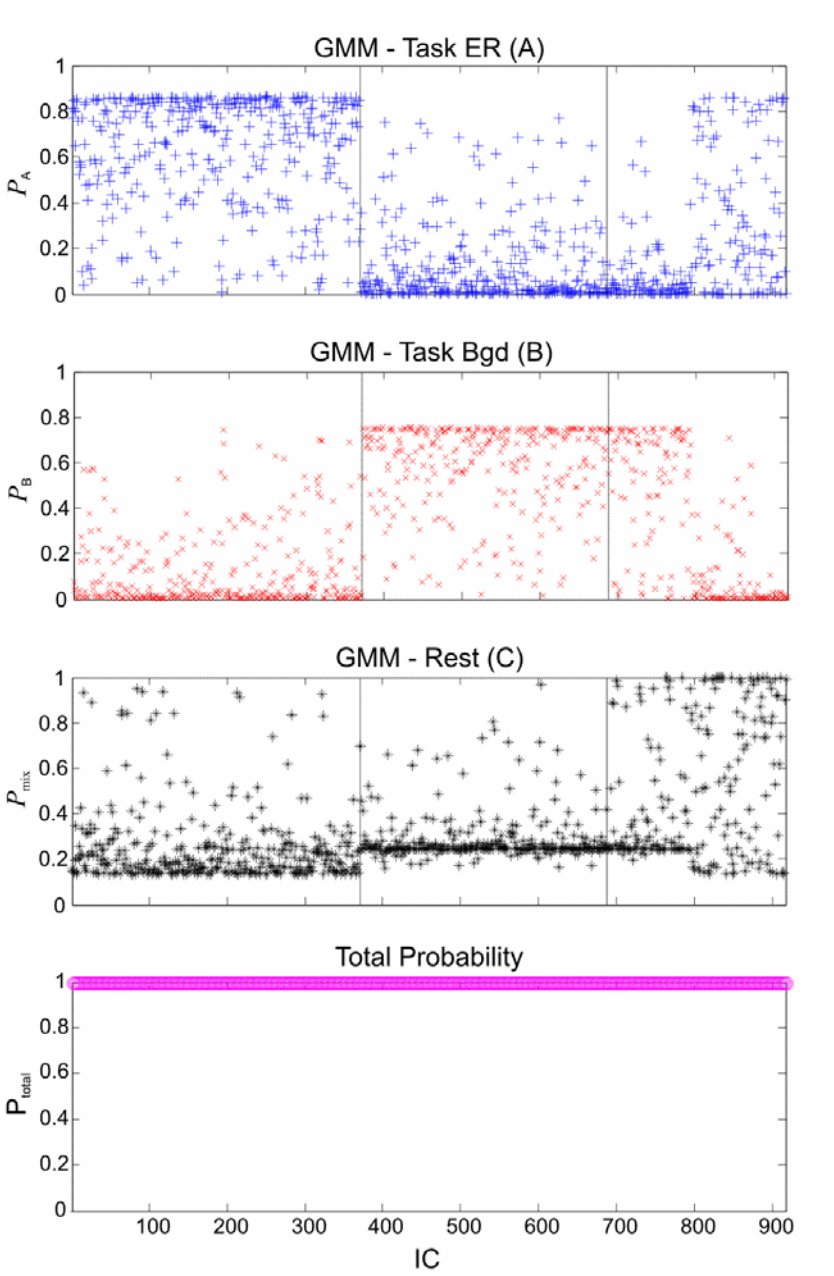

Figure 8-13. Normalised posterior probabilities for the 3 GMMs such that the probability for each data point adds up to one across the 3 classes.

The statistical error for the classification (based on a particular set of features) could then be derived by considering the maximum class probability for each data point representing one IC. For example, for the first data point (representing IC_1) P_A was 0.82, P_B was 0.08 and P_{mix} was 0.1, thus it was classified as belonging to process A, i.e. it was an ER task IC. From these values, the statistical error for classification, i.e. how distinct the ER, Background and Rest classes were based on the ICs features in that particular frequency band, could be computed. The interpretation (for class A only) is given in Table 8-1 (Linn, 2004).

	Actual condition	
Test result	**Belongs to class A**	**Does not belong to class A**
Classified as element of class A	True Positive	False Positive
Classified as element of class B or class C	False Negative	True Negative

Table 8-1. Definition of statistical error measures as applied to the 3-class problem.

The sensitivity of classification for class A was then defined as

$$\text{Sensitivity}_{class\ A} = 1 - \text{FNR}_{class\ A}, \tag{8.19}$$

where $\text{FNR}_{class\ A}$ is the false negative rate for class A given by

$$\text{FNR}_{class\ A} = \frac{\text{number of ICs that belong to class A misclassified as class B or C}}{\text{total number of ICs that belong to class A}}. \tag{8.20}$$

These indices for each class were portrayed in a confusion map. In the normalised map of Figure 8-14 the diagonals show the sensitivity of classification for each class. The off-diagonal terms of the first column represent the number of ICs that belong to A but are classified as either B (1st off-diagonal term) or C (2nd off-diagonal term), each divided by the total number of ICs that belong to A. Hence, the colour bar in this figure indicates the fraction of correctly or incorrectly classified ICs from the total number of ICs in one class (read column-wise). This decision was based on the maximum posterior probabilities across the three classes (from Figure 8-13).

From a neurophysiological perspective, the result in Figure 8-14 suggests that the ER and the Background brain activity could be distinguished very clearly using only the amplitude characterises of the brain sources in the slow wave band. 43% of the Rest slow wave amplitude features were distinct from those during task whereas 20% and 37% were not separable from the ER and Background features respectively. This indicates that the characteristics of the slow wave mechanism share essential similarities during rest and task but are distinct enough to be classified separately. This is in keeping with view that the default slow waves are consistently affecting underlying brain processes, and they are in turn affected by stimulation.

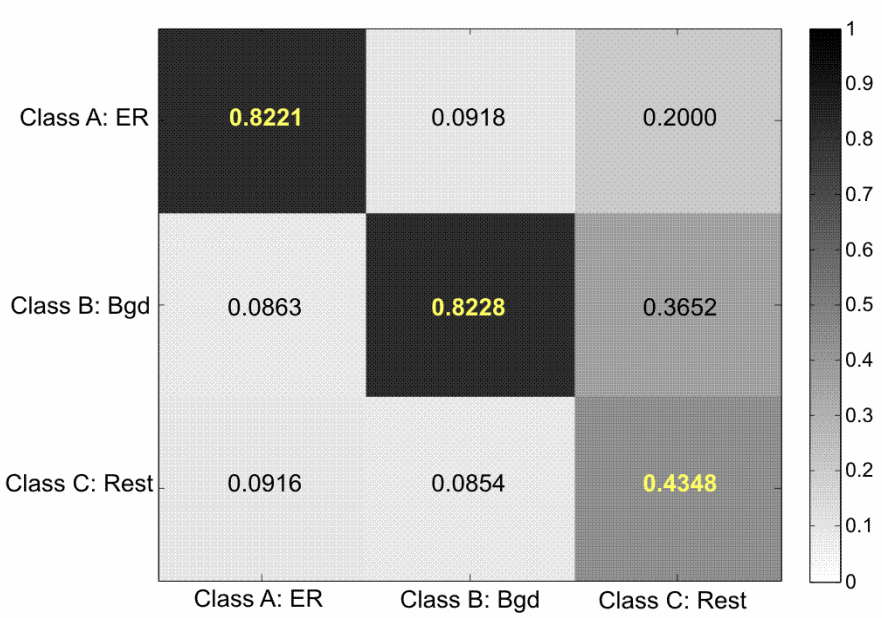

Figure 8-14. Confusion map for the classification based on slow wave amplitude ICs features. Diagonal values show the sensitivity of classification whereas the off-diagonal terms (column-wise) show the fraction of misclassified ICs for each class.

8.6.3 Test data

As explained earlier, neuroscale provides a *transformation* of the training data points onto the 2-D feature space. Therefore, a new set of test data can be mapped onto this space by simply modifying the parameters of the fixed RBF structure learnt in the training stage. As an example, the ICs extracted from 4 minutes of data recorded from three new participants during the Oddball Hard task environment were used. The Task ICs were taken together as one class, i.e. they were not previously classified into ER and Background by hierarchical clustering, and the Rest ICs were not ordered according to their frequency content. The AR and ID method was used to characterise the slow wave amplitude features of the ICs. This new set of input data points were first projected onto the 2-D space using the RBF structure learnt from the first ten participants (the training data), and the PDFs of this output were then characterised by projection onto the three GMMs obtained from the training process.

Results show that the Task ICs (1:70), although they were not pre-ordered into ER or Background, were clearly projected onto different GMMs as shown in Figure 8-15 (some are definitely classified as ER and some are definitely Background). Meanwhile, the Rest class overlapped with both ER and Background classes as expected. Classification of the test ICs based on the maximum posterior probability for each IC across the three classes gave a 3-class output, as shown in Figure 8-16 (b).

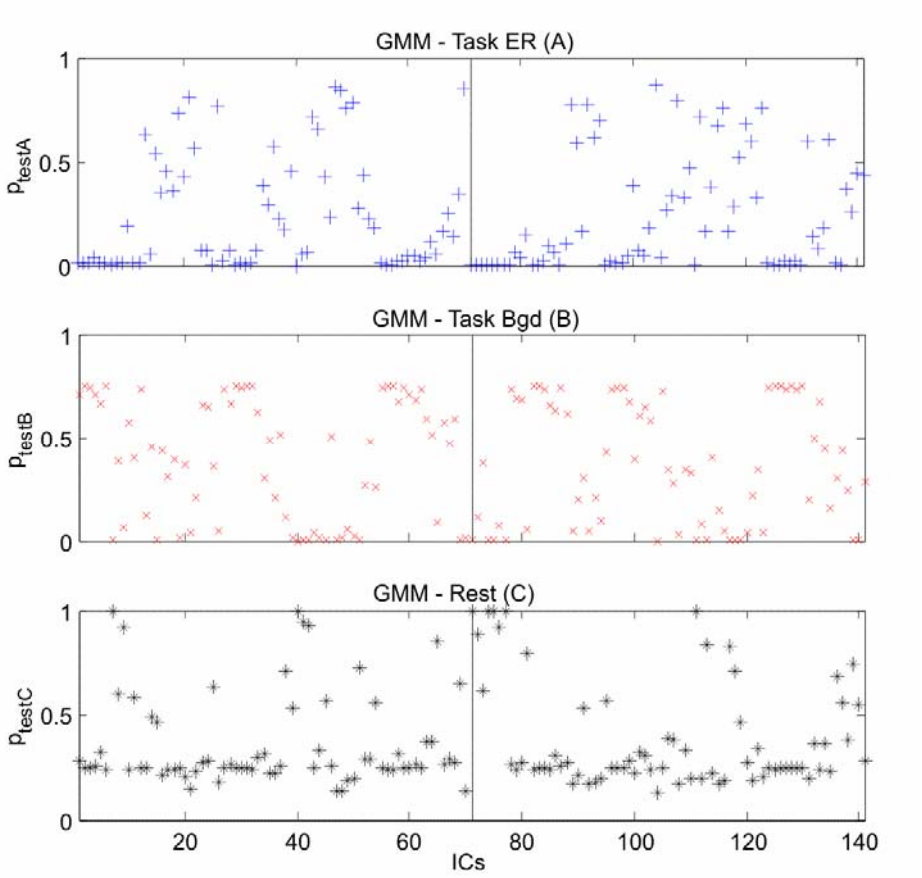

Figure 8-15. Probabilities characterising the neuroscale 2-D output for the test data when projected onto the three GMMs obtained from the training data.

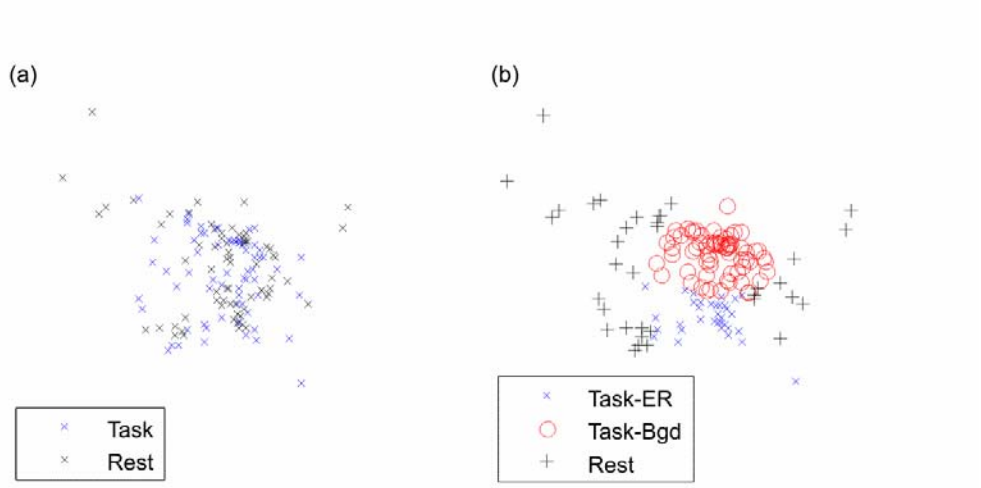

Figure 8-16. (a) The original clustering of the test data from neuroscale (141 points in 2-D space). (b) The classified data when projected onto the three GMMs obtained from the training data – classification based on the maximum probability of each data point across the three classes.

Figure 8-17 then shows the topographies of two ER, two Background and two Rest ICs from the test data which have been correctly classified by the trained GMMs. Note that the ER ICs

topographies show very clear P300 spatial distributions, whereas the Rest ICs show more parietal-occipital (alpha) and frontal activity as expected.

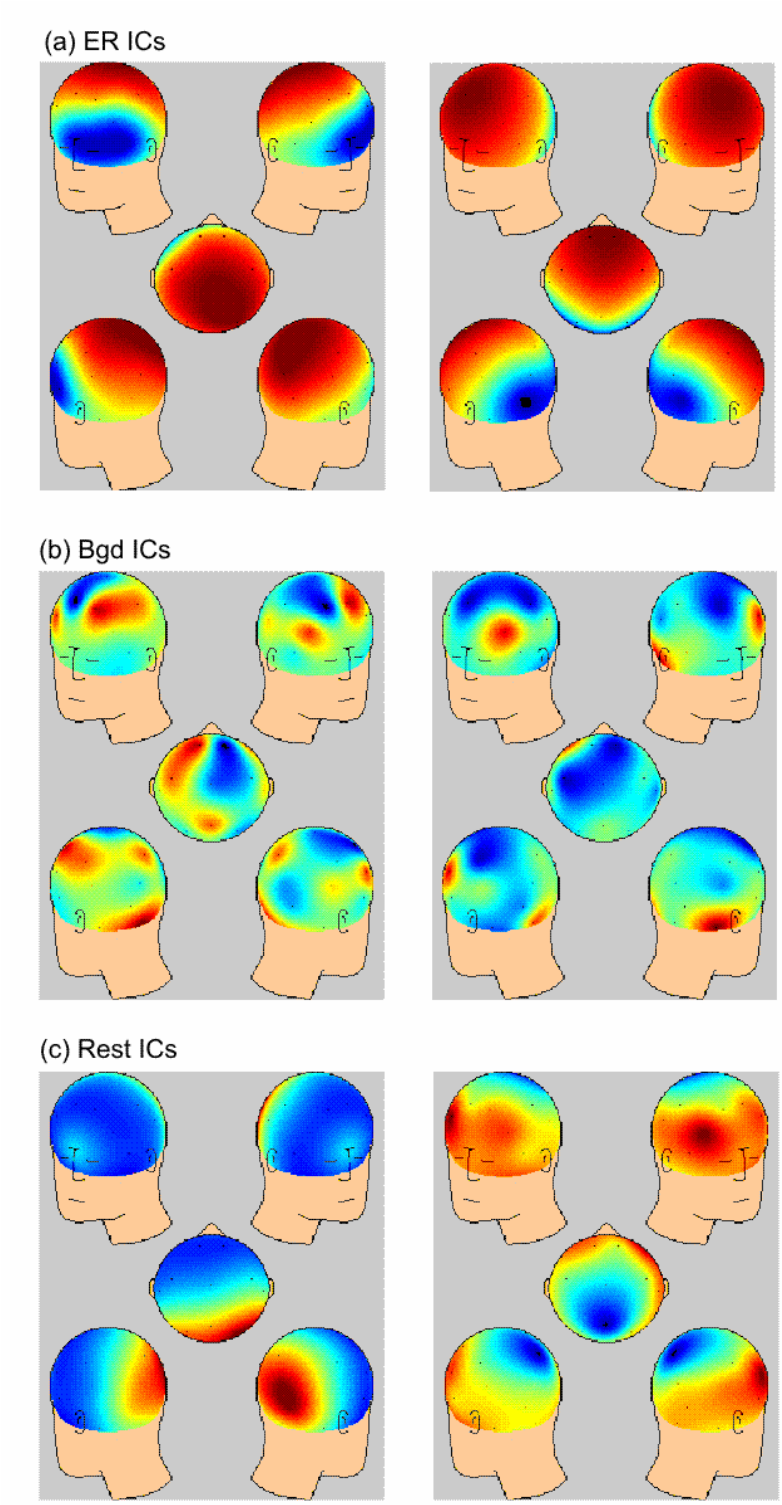

Figure 8-17. Topographies of two ER, two Background and two Rest correctly-classified ICs from the test data. Note that the ER topographies show very clear P300 spatial distributions, whereas the Rest ICs show more parietal-occipital (alpha) and frontal activity.

The methodology explained so far was employed on the whole dataset shown in Table 7-1. The data from two participants were unusable due to poor quality recordings, whilst one participant was unable to perform the tasks correctly (obtaining a 78.5% and 88% error rate during Go No-go and the Oddball Hard task respectively, and reported impatience and anxiety during the rest periods). Such performance would create outliers in the otherwise normal population and could potentially skew the final results; thus the dataset was eliminated. The remaining fourteen and six participants' recordings were used to form the training and test databanks respectively for each of the three task environments (SART – Rest, Oddball Easy – Rest and Oddball Hard – Rest), as shown in Table 8-2.

Task	**Condition**		
Go No-go (SART)	Task Block 1 (10 mins)	Rest (6 mins)	Task Block 2 (10 mins)
Oddball	Easy/Hard (8 mins)	Rest (6 mins)	Easy/Hard (8 mins)

Table 8-2. Task Environments. Note that for the Oddball task, the order of the Easy and Hard task blocks was counterbalanced across participants. The order of the two tasks was also counterbalanced.

For the Go No-go (SART) task, 5 minute data segments were considered, namely the first 5 minutes, the second 5 minutes and an overlap (2.5-7.5 minutes) for each task block. TDSEP-ICA and HC were then applied to each segment separately. Since the protocol remained the same throughout the task, the ICs extracted from the two task blocks were grouped together. For the rest condition, ICs were extracted from a 5 minute data segment (0.5 – 5.5 minutes into the rest block). This was carried out for every participant. The ICs of 14 participants were then grouped together, which rendered a total of 2300 ICs, (896 ER and 1077 Background task ICs as identified by HC, and 327 Rest ICs), forming the SART training databank. The ICs of the remaining 6 participants formed the SART test databank consisting of 317 ER and 305 Background task ICs, and 117 Rest ICs.

For the Oddball task, TDSEP and HC were applied to three 4-minute segments (1st 4 minutes, 2nd 4 minutes and an overlap - i.e. 2 to 6 minutes) consecutively, for the Easy and the Hard task blocks separately and for every participant. Across 14 participants this gave two databanks of 519 ER and 444 Background task ICs, and 501 ER and 462 Background task ICs for the Easy and Hard task conditions respectively, after HC. The Rest ICs were extracted from a 4-minute segment (1-5 minutes into the rest block), with a total of 321 Rest ICs across the 14 training participants. The data of the remaining 6 participants resulted in an Oddball Easy test databank of 183 ER and 162 Background task ICs, and 115 Rest ICs, and an Oddball Hard test databank of 160 ER and

185 Background task ICs, and 115 Rest ICs. Note that both the Easy and Hard task environments shared the same rest period, hence their databanks contained the same Rest ICs.

In the following section of this chapter the group results obtained are presented, analysed and discussed.

Section 2 - RESULTS

8.7. P300 Responses

Preliminary analysis investigated the P300 responses during the three task environments for the whole dataset (i.e. 20 participants). The data was first decomposed by TDSEP ICA which successfully isolated the three main types of P300 responses shown in Figure 8-18. Note that a robust P300 with a central distribution was elicited during the SART (a); during the Oddball task P300s with a frontal topography were elicited in response to distractor stimuli (indicating a dominant P3a subcomponent) shown in (b), whereas the targets generated P300s with a parietal focus (indicating a dominant P3b complex) shown in (c). For every recording (i.e. one participant, one task block), the artifactual components were removed, and the resultant ICs were then projected back onto the measurement space in order to investigate the coherent average of the responses for various stimuli and task conditions.

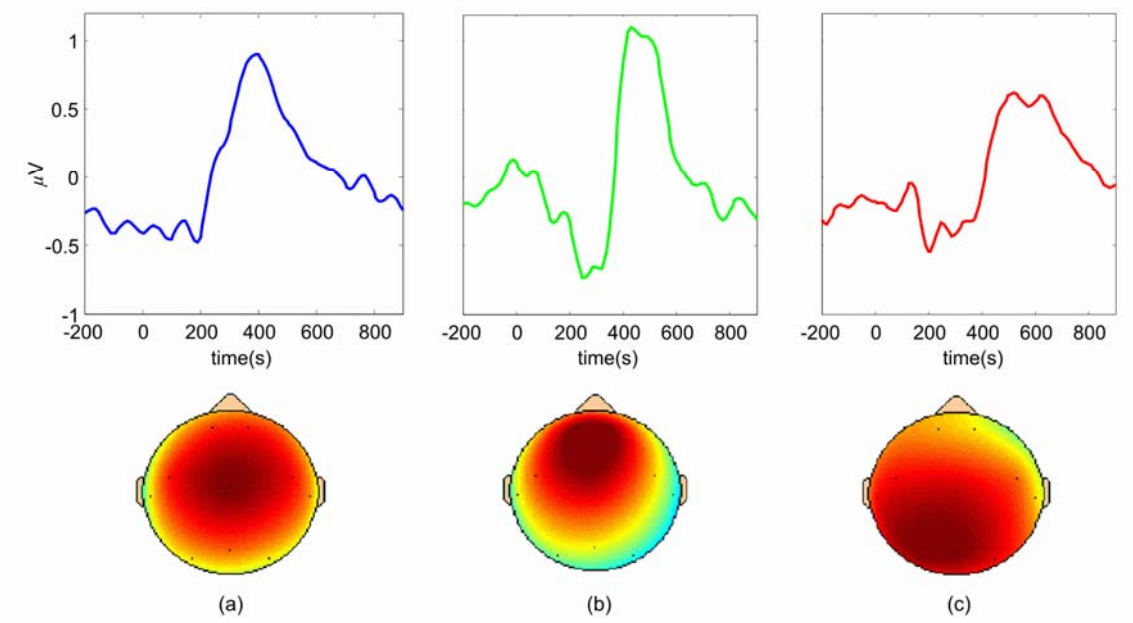

Figure 8-18. Three types of P300 responses extracted by TDSEP-ICA during the two tasks: (a) P300 with a central topography elicited during SART; (b) P300 response with a strong frontal focus elicited by distractor stimuli (c) and P300 for target stimuli with a parietal focus, for the Oddball task.

8.7.1. SART

The SART, being a relatively easy and repetitive task, provided robust P300 responses with a maximal central distribution as shown in Figure 8-19. The No-go and Go responses were compared by considering the largest positive-going peak (relative to the pre-stimulus baseline) within a latency window of 300 to 600 ms. The peak latency was measured from the time of stimulus onset. Paired *t*-test analyses for the amplitude of the No-go and Go responses yielded *p*-values below 0.05 for central and parietal channels as shown in Table 8-3. This implies that (as expected) the No-go stimuli, with 12% probability of occurrence, evoked significantly larger P300 amplitudes for both task blocks in central and central-parietal brain regions, a result that is in keeping with the literature (Katayama and Polich, 1996; Polich, 2007). For both task blocks, No-go responses generally exhibited longer latencies; however this effect was not always statistically significant (Table 8-3). The grand coherent average responses across the 20 participants for channels corresponding to C3, C4, Cz and Pz, for task blocks (TB) 1 and 2 are illustrated in Figure 8-19.

		TB1		**TB2**	
Channel		**Amplitude (μV)**	**Latency (ms)**	**Amplitude (μV)**	**Latency (ms)**
Cz	***t*(1,19)**	4.78	2.26	4.59	2.60
	***p*-value**	<0.001	0.051	0.001	0.029
	Go Mean ± Std	4.99 ± 1.97	387 ± 51.22	4.53 ± 1.84	389 ± 50.43
	No-go Mean ± Std	11.92 ± 4.39	437 ± 43.22	11.84 ± 5.07	449 ± 45.08
C3	***t*(1,19)**	4.79	2.14	3.97	2.42
	***p*-value**	<0.001	0.061	0.003	0.038
	Go Mean ± Std	4.07 ± 1.50	397 ± 45.96	3.27 ± 1.87	400 ± 45.46
	No-go Mean ± Std	7.99 ± 2.95	452 ± 57.89	7.41 ± 3.59	447 ± 36.22
C4	***t*(1,19)**	4.54	1.30	5.55	2.09
	***p*-value**	0.001	0.227	<0.001	0.066
	Go Mean ± Std	3.33 ± 1.72	418 ± 72.69	2.62 ± 1.31	391 ± 52.38
	No-go Mean ± Std	6.88 ± 2.58	459 ± 52.8	6.56 ± 2.54	447 ± 50.56
Pz	***t*(1,19)**	4.48	6.31	3.92	5.66
	***p*-value**	0.002	<0.001	0.004	<0.001
	Go Mean ± Std	4.42 ± 1.67	365 ± 19.01	3.78 ± 1.77	357 ± 18.89
	No-go Mean ± Std	7.89 ± 2.49	443 ± 37.73	7.60 ± 3.51	454 ± 42.74

Table 8-3. Paired *t*-test results (19 degrees of freedom) and the group's mean and standard deviation (Std) for the Go and No-go responses. The *p*-values <0.05 represent a significantly larger amplitude for the No-go responses during both task blocks. The latency is also generally longer for No-go P300s.

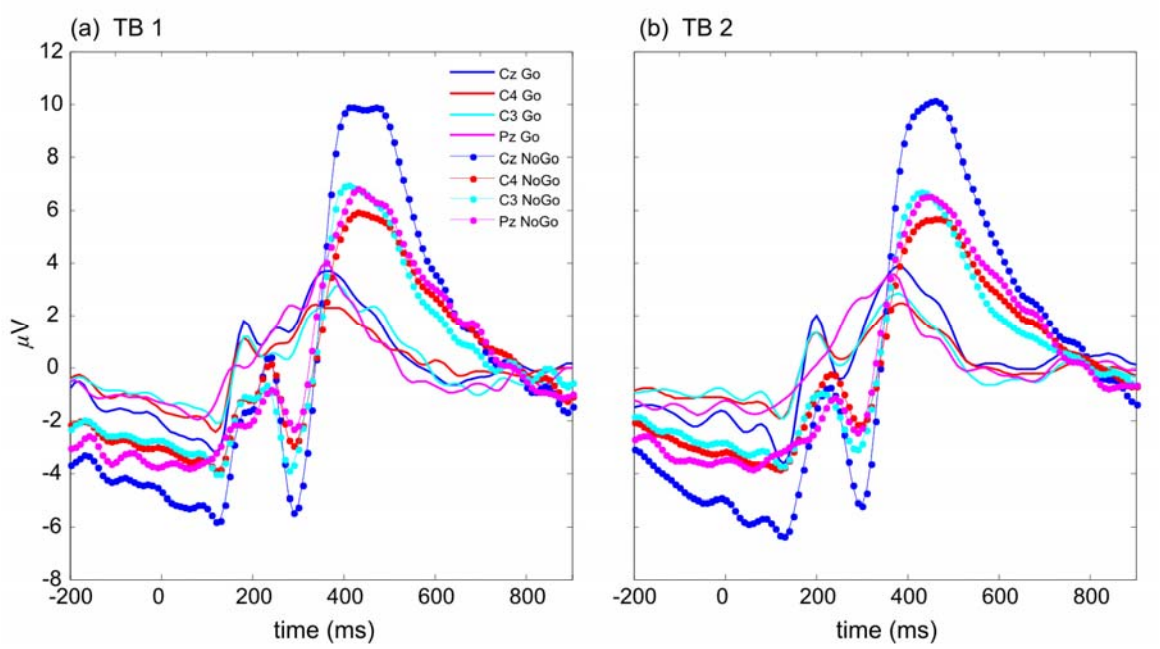

Figure 8-19. Grand coherent average across the 20 participants showing robust P300 responses during both SART task blocks.

8.7.2. Oddball Task

The group P300 responses elicited by the three stimuli – standard, distractor and target – during the Easy and Hard task conditions for selected frontal, central and parietal channels are illustrated in Figure 8-20. During the Easy task (when the perceptual discrimination difficulty between the standard and the target stimuli was low), the target P300s had a significantly higher amplitude in comparison to the Hard task condition. This is particularly evident in central and parietal areas where the P3b component is most prominent (Table 8-4). Moreover, on the central areas the target P300 exhibits significantly shorter latencies during the Easy task (Cz: $t(1,19) = -2.61$, p-value = 0.0287; C4: $t(1,19) = -2.22$, p-value = 0.0535; and C3: $t(1,19) = -3.39$; p-value = 0.0095). Meanwhile, the more frontal P300 subcomponent, the P3a, elicited by the distractor stimuli, showed significantly higher amplitude for the Hard task condition, as shown in Figure 8-20, whereas its latency varied very little across the two tasks. These effects suggest that distractor processing was engaged more strongly during the harder task, in order to increase focal attention for resource allocation operations and thus enhancing P3a responses, as clearly shown in the coherent average for the fronto-central channels (Ch8 and Ch18). No significant difference was found for the P300 elicited by the frequently occurring standard stimuli in both task conditions. These results replicate the findings by Comerchero and Polich (1999), and Hagen *et al*. (2006).

	Target: Easy vs Hard			
Channel	***t*(1,19)**	***p*-value**	**Group Mean ± Std (μV)**	
			Easy	**Hard**
Cz	6.22	<0.001	7.01 ± 2.87	5.15 ± 2.93
C3	4.23	0.036	5.13 ± 1.83	3.67 ± 2.46
C4	3.65	0.005	4.56 ± 2.28	3.59 ± 2.03
Pz	5.31	<0.001	8.85 ± 3.67	5.95 ± 3.24
	Distractor: Easy vs Hard			
Fz (right)	-3.17	0.011	2.78 ± 1.99	4.86 ± 2.45
Fz (left)	-4.61	0.001	2.79 ± 1.68	5.34 ± 2.46
FC (right)	-2.90	0.018	1.39 ± 1.58	2.70 ± 1.76
FC (left)	-2.84	0.019	1.74 ± 2.27	3.33 ± 1.73

Table 8-4. Paired *t*-test results, and the group mean and standard deviation for the amplitude of the Oddball P300 responses elicited during the Easy and Hard task conditions.

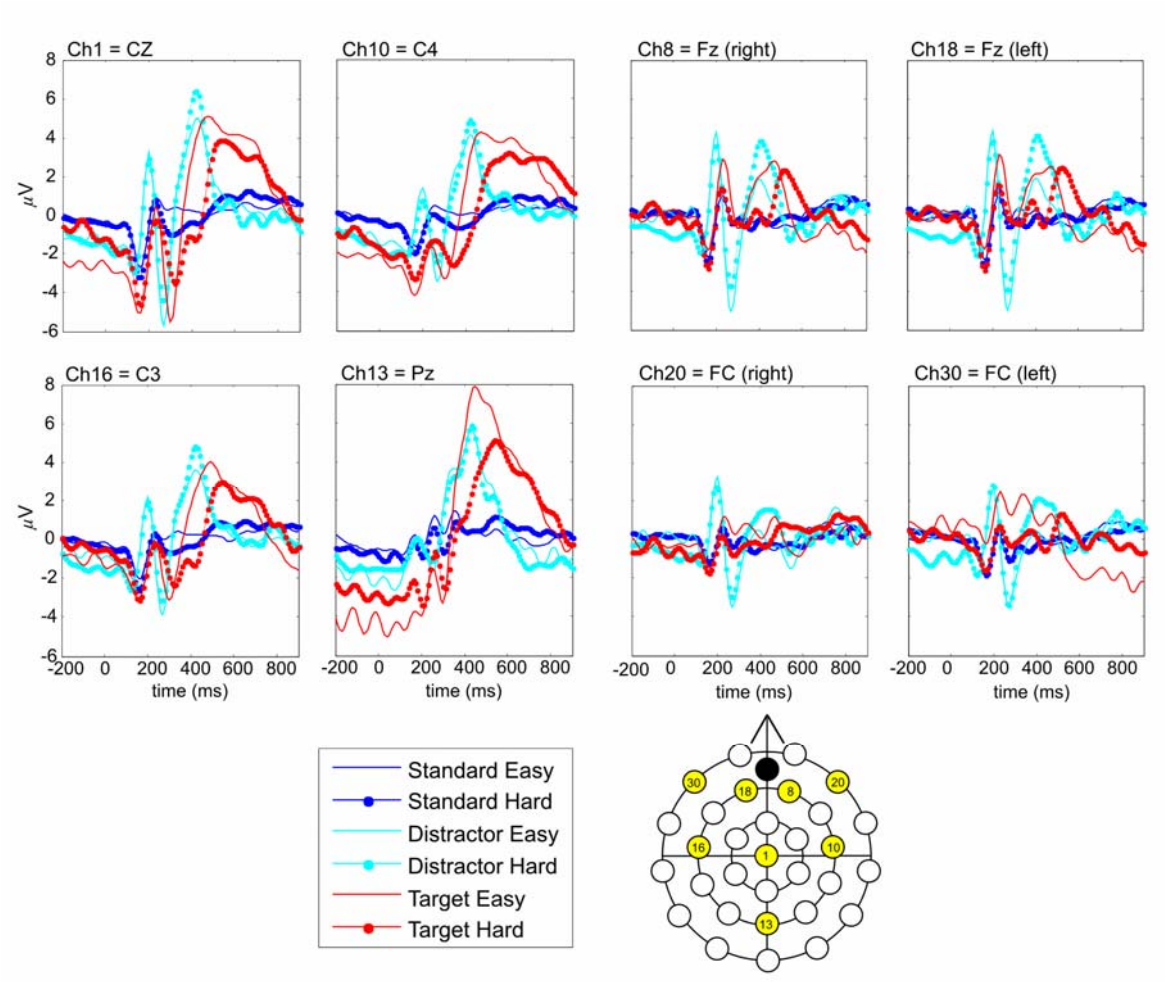

Figure 8-20. P300 responses for the three stimuli (standard, distractor and target) during Oddball Easy and Hard task conditions for 8 channels located in central, parietal, frontal and fronto-central areas.

8.8. Behavioural Data

Analysis of performance measures, namely reaction time (RT), error rates and false alarms, was carried out for both tasks. This was done in order to further assess whether the required task environments (with variable loading levels) have been created by the task protocols, and to determine how well participants carried out the experiment at hand.

8.8.1. SART

The mean and standard deviation of the global RT (i.e. RT across both task blocks) and the percentage error rate for every participant are shown in Figure 8-21. The error rates were derived from the number of false alarms, i.e. button presses to No-go responses; the number of misses to Go's was negligible. Across task blocks and participants the overall average RT and error rates were (440.99 ± 58.02) ms and (mean: 25.41, range: [4.55 48.19]) % respectively. Note that the robust P300's for the Go and No-go stimuli and the relatively low error rates indicate a high level of attention throughout the course of the task for most participants.

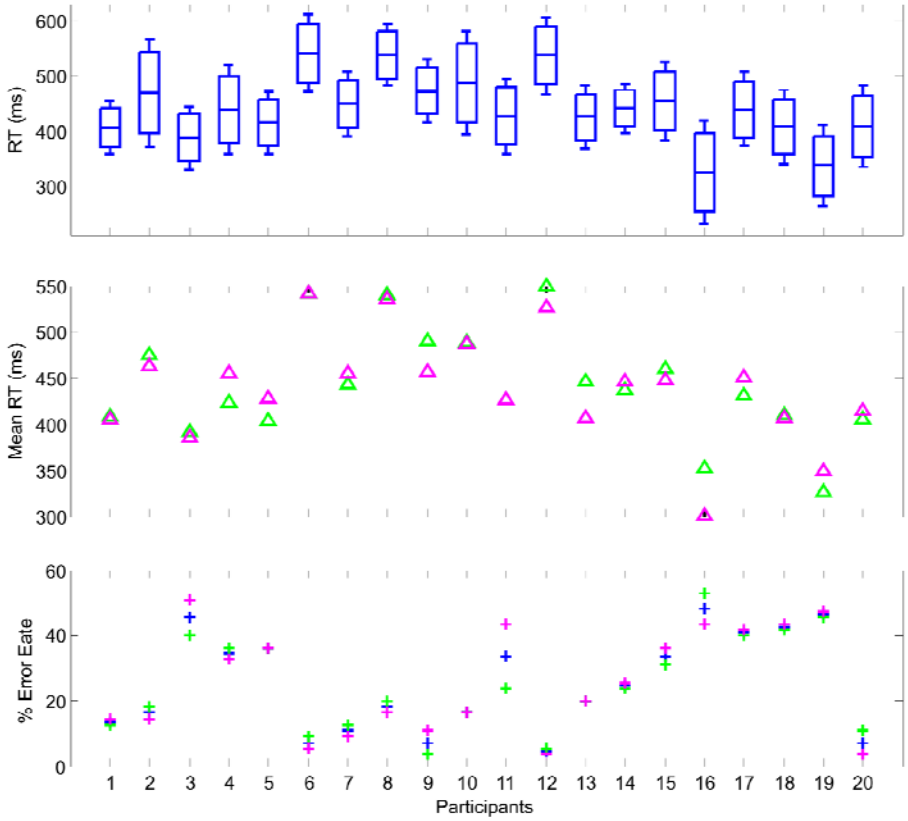

Figure 8-21. SART performance data: Mean and standard deviation for the global RT (across TB1 and TB2); the mean RT for TB1 (green) and TB2 (magenta); the percentage error rate (during TB1: green, TB2: magenta and their average: blue) for every participant.

Since the underlying aim of this work has been to assess the general influence of the slow waves on brain function, the variability in the RT across the entire 10 minute task blocks was investigated in order to observe whether this exhibited a slow wave pattern. Consequently, for every task block, a time series for the RT to hits (i.e. Go's) was formed. A cubic spline interpolation was then constructed for this time series in order to obtain an equally-sampled RT curve to compensate for the cases when a No-go stimulus was present (i.e. when no response was given), and its frequency response was calculated using the Welch method. It is important to note that this response was limited by the inter-stimulus interval: essentially, the time series had a sampling frequency of 1/1.2sec = 0.833 Hz, hence a maximum discernible frequency of 0.417 Hz. Nonetheless, the results in Figure 8-22(a) suggest that the RT variability exhibits slow wave fluctuations throughout the course of the task.

Since the frequency response of the RT variability was found to decay in a $1/f$ manner (Figure 8-22 (b)), the frequency-domain normalization approach was employed to cancel this trend and reveal predominant peaks in the power spectra. Following the procedure explained in Section 6.1.1, the normalization curve was obtained from the task data of three participants during 5-minute recordings within TB1, 5-minute recordings within TB2 and 5 minutes of rest data. The median frequency curve, across the three conditions and the three participants, was then used as the normalization curve. The RT variability curves of all participants were then normalized and their average obtained (as shown in Figure 8-22 (b), 2nd row). Here, specific VLF peaks previously masked by the $1/f$ trend are clearly visible, with a predominant peak around 0.2 Hz for both task blocks. This indicates that the RT was varying about every five seconds (i.e. approximately after every four stimuli) across the entire ten-minute task block.

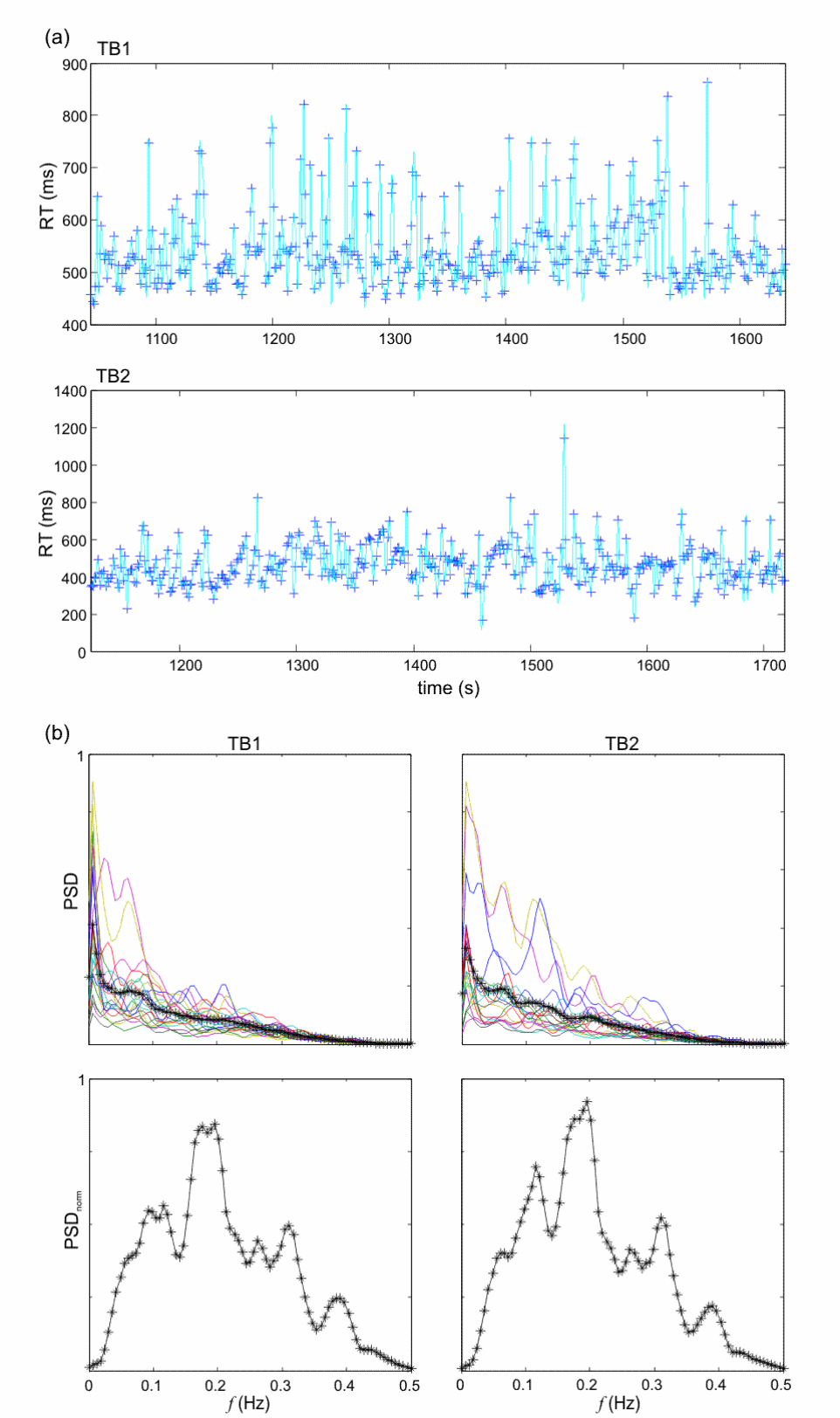

Figure 8-22. RT variability for the SART: (a) RT time series across the 10 minute task blocks – note the VLF variation in the time series (results of one participant shown as an example). (b) 1st row: The frequency response of this RT variability for all participants for TB1 and TB2; the average PSD across participants is shown by the (*-) curve. (b) 2nd row: The normalised average PSD curve shows predominant VLF peaks around 0.2 Hz.

8.8.2. Oddball Task

Mean RT, percentage error rate: misses to targets, and percentage of false alarms: hits to standard stimuli (since none of the participants responded to distractors) were computed for the Easy and Hard task blocks consecutively; the mean values across participants are shown in Table 8-5. Results show that when the target was very distinct from the standard stimuli, i.e. in the Easy condition, error rates were significantly smaller ($t(1,19) = 8.39$, p-value <0.001) and RT significantly shorter ($t(1,19) = 9.16$, p-value <0.001) than when the target was similar to the standard stimulus (Hard condition); this is also visible from Figure 8-23. This is because small standard-target perceptual differences demand more stimulus processing as previously shown in the literature (Comerchero and Polich, 1999; Hagen *et al*. 2006). Moreover, the percentage of false alarms with respect to standard stimuli was significantly larger for the Hard task ($t(1,19) = 3.53$, p-value <0.002). These results confirm the successful manipulation of graded task difficulty.

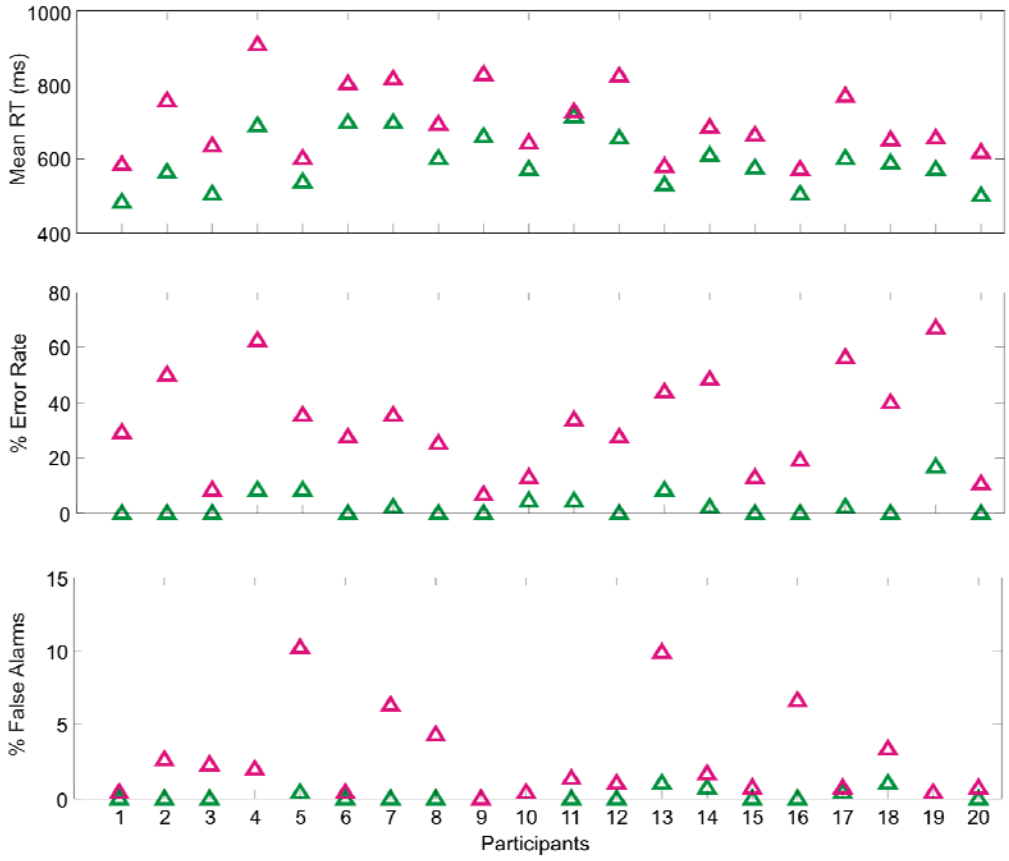

Figure 8-23. Mean RT, % Error rate (misses to targets) and % of false alarms (w.r.t. standard stimuli) for the Oddball task during the Easy (green) and Hard (magenta) task conditions.

		Oddball Easy	**Oddball Hard**
RT(ms)	**Mean ± Std**	592.18 ± 72.86	700.64 ± 98.29
	Max & Min values	[480.75 712.87]	[571.69 908.44]
Error Rate (%)	**Mean**	2.81	32.40
	Max & Min values	[0 16.67]	[6.25 66.67]
False Alarms (%)	**Mean**	0.30	2.73
	Max & Min values	[0 1.97]	[0 10.2]

Table 8-5. Mean of RT, % Error Rate and % False Alarms (w.r.t. standard stimuli) across participants for the Oddball Easy and Hard task conditions.

8.9. Multistage System Analysis Results

As seen in the previous sections, the P300 responses and performance results from the experimental protocols chosen replicated those found in the literature. Moreover, a task environment that gradually amplified the load on the brain has been successfully implemented. By using the multistage system designed in the previous section, the change that the brain's oscillators underwent in the three different task environments could be investigated. This was done by assessing how distinct the ICs were, i.e. how well they could be classified into Task-ER, Task-Background and Rest classes, when classification was based only on ICs' features in one specific frequency band.

Note that the results based on the AR model and ID method for feature extraction are shown here rather than on the features obtained from the amplitude and PDF moments of the instantaneous phase because the former provided more robust results. Nonetheless, comparable classification patterns were achieved from the first set of features, with weaker sensitivity of classification; some examples can be found in Appendix II (A). In order to ensure the AR model correctly captured the time series structure, the delta, theta and alpha amplitude or phase time series (each having an approximate bandwidth of 4 Hz) were downsampled to 12 Hz prior to model fitting. The slow wave band time series ($0<f<0.5$ Hz) were downsampled to 5 Hz.

8.9.1 Training Data

Figure 8-24 to Figure 8-29 show the classification results based on the ICs amplitude or phase features when filtered in the slow wave band during the three task environments for the training databank. Note the clear distinction between the ER and Background ICs features and the consistent overlap between Rest and Task classes. The sensitivity of classification for the Rest improves as the task difficulty increases from SART to Oddball Hard, (Slow wave amplitude

features: SART – 31.1%, Oddball Easy – 38.3%, Oddball Hard – 43.6%; Slow wave phase features: SART – 32.4%, Oddball Easy – 42.1%, Oddball Hard – 46.1%). This implies that the amplitude and phase in the slow wave band are undergoing enhanced changes from task to rest as the loading on the brain is increased. Moreover, the features of the Rest ICs with a predominant slow frequency content overlapped with those of the Background ICs, whereas those with a predominant theta and alpha frequency content overlapped with the ER ICs.

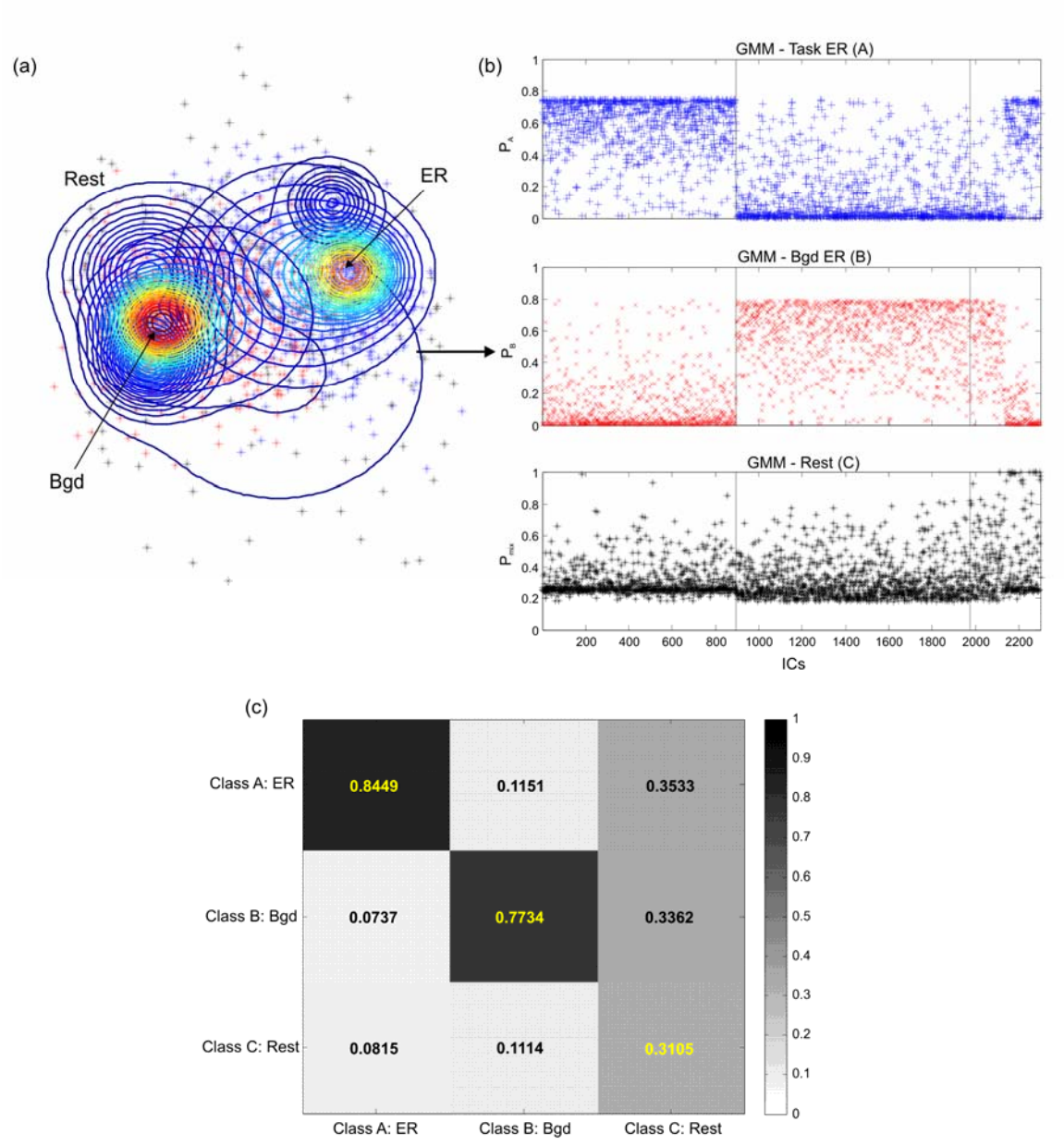

Figure 8-24. Training data classification results based on *Slow Wave Amplitude* features of the ICs for the SART task environment: (a) GMM contour plots for the neuroscale output, (b) Posterior probabilities from the GMMs of the three classes, (c) Confusion map showing sensitivity of classification on the diagonal.

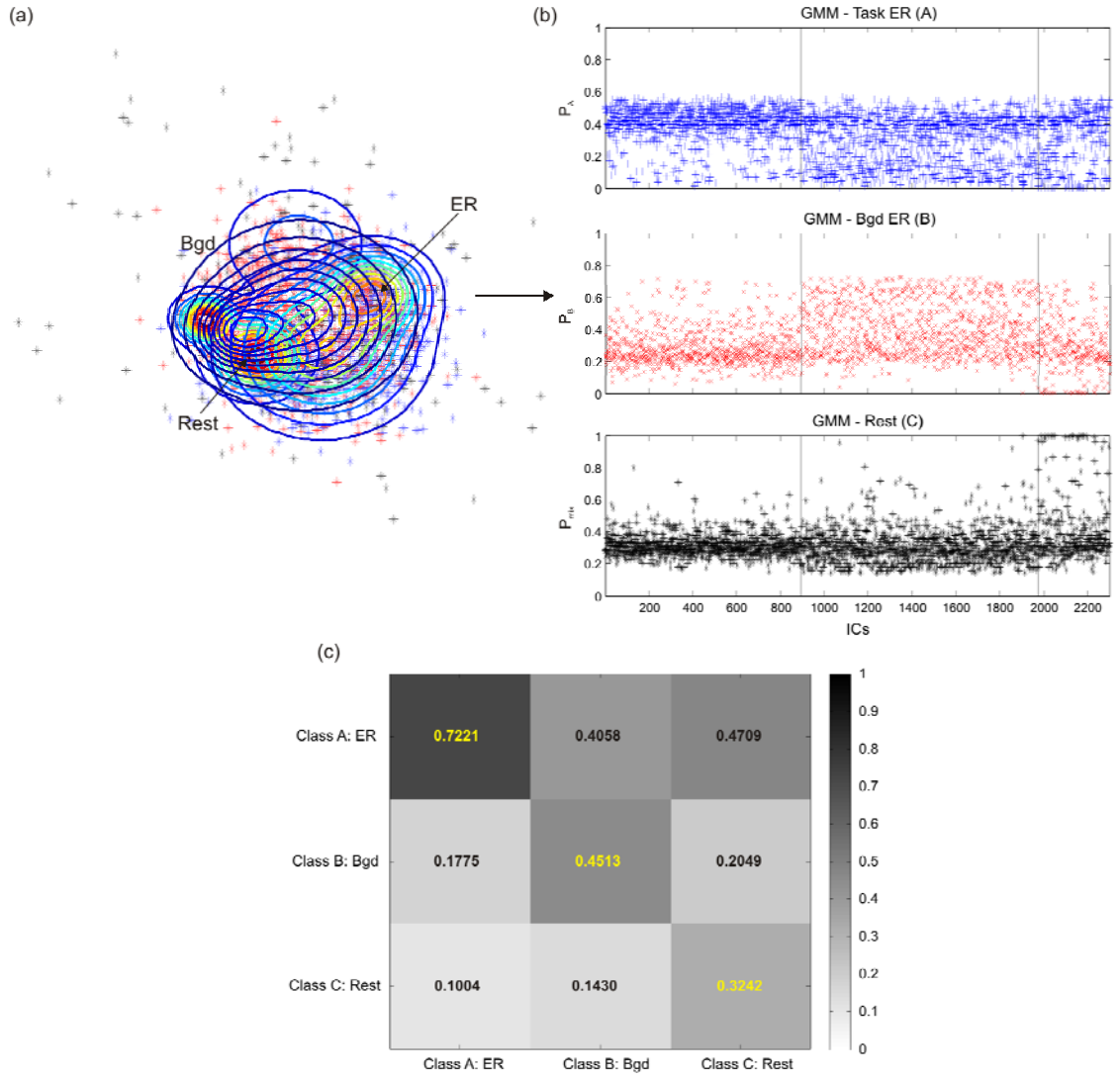

Figure 8-25. Training data classification results based on *Slow Wave Phase* features of the ICs for the SART task environment: (a) GMM contour plots for the neuroscale output, (b) Posterior probabilities from the GMMs of the three classes, (c) Confusion map showing sensitivity of classification on the diagonal.

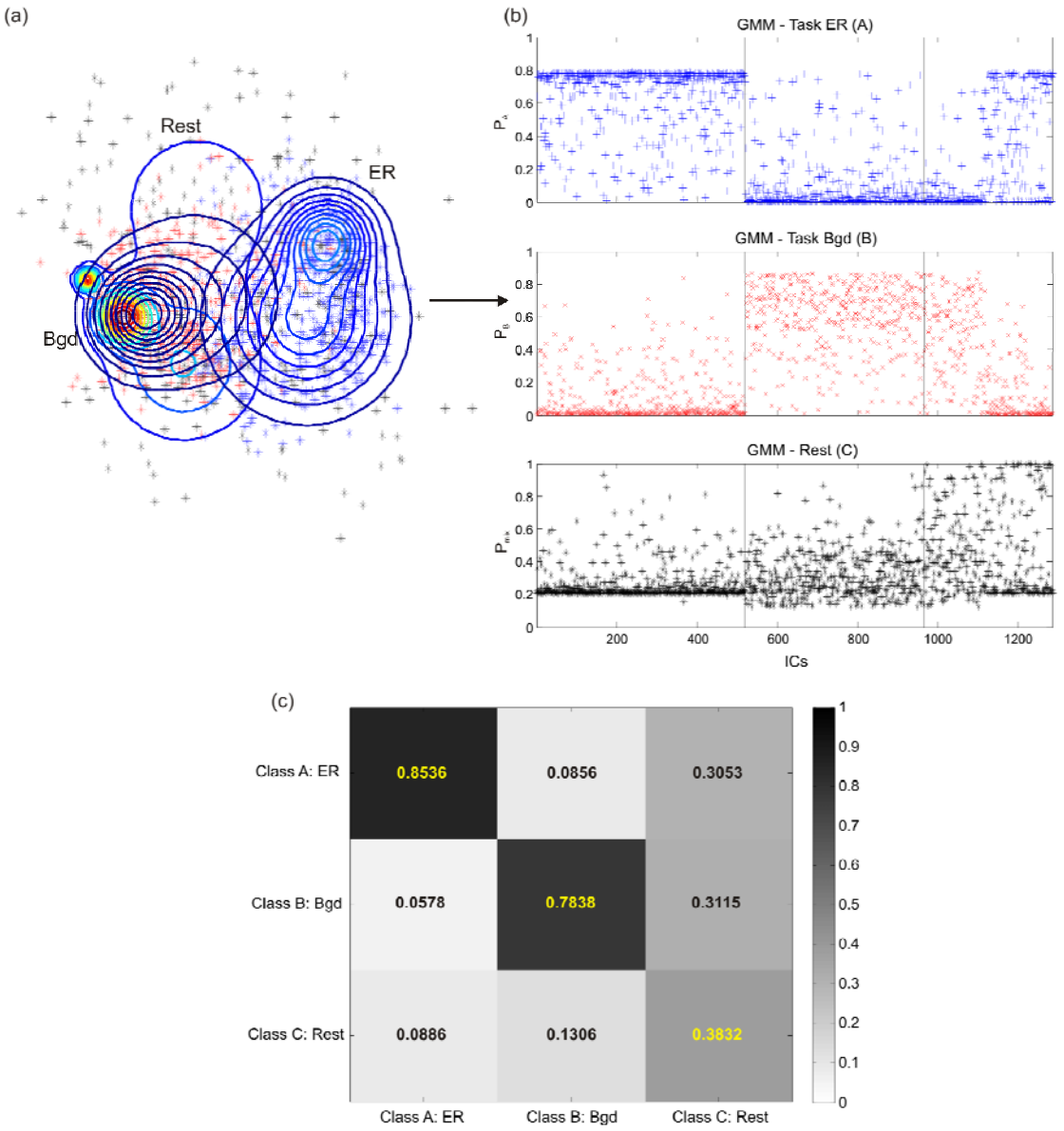

Figure 8-26. Training data classification results based on *Slow Wave Amplitude* features of the ICs for the Oddball Easy task environment: (a) GMM contour plots for the neuroscale output, (b) Posterior probabilities from the GMMs of the three classes, (c) Confusion map showing sensitivity of classification on the diagonal.

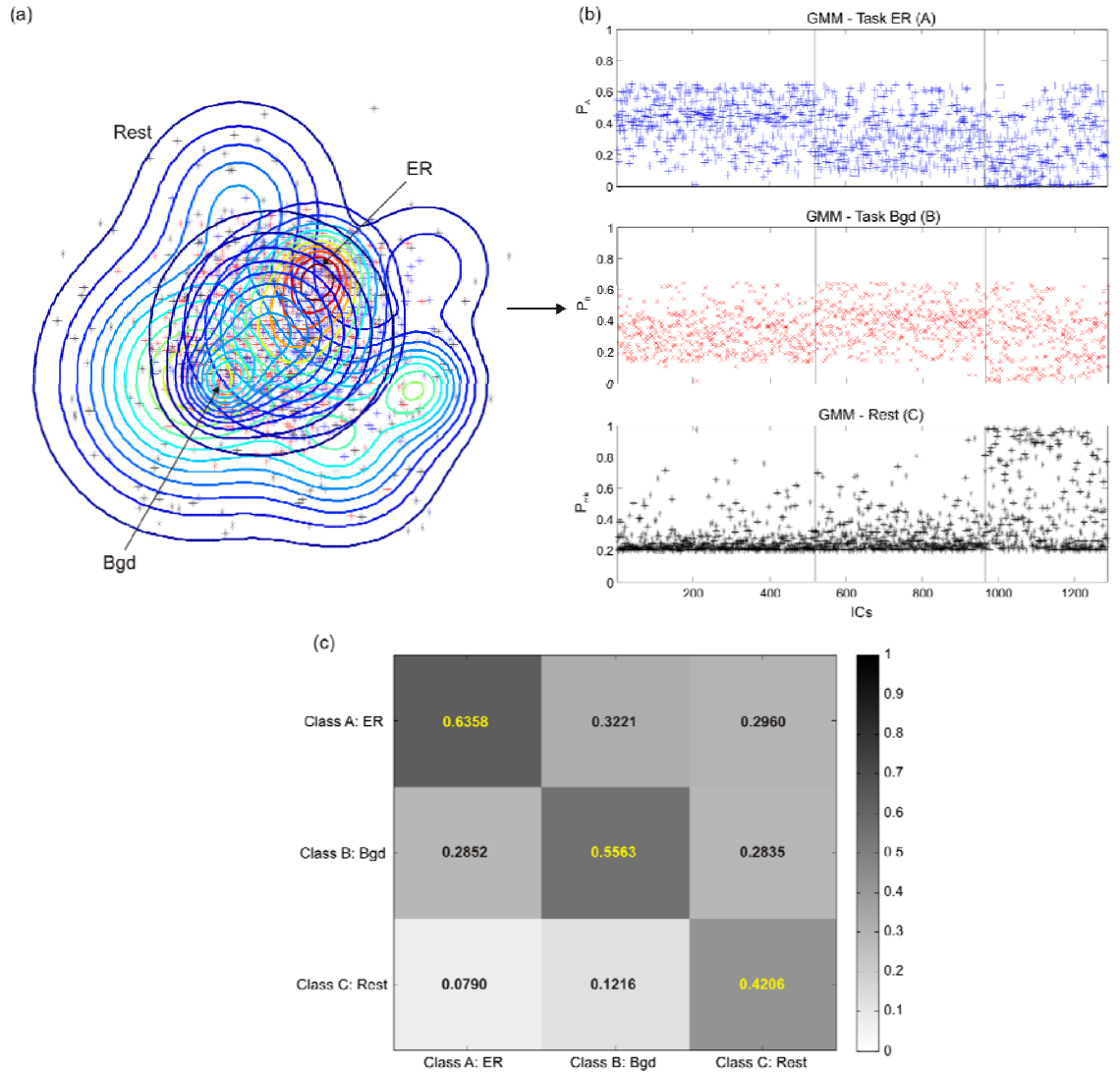

Figure 8-27. Training data classification results based on *Slow Wave Phase* features of the ICs for the Oddball Easy task environment: (a) GMM contour plots for the neuroscale output, (b) Posterior probabilities from the GMMs of the three classes, (c) Confusion map showing sensitivity of classification on the diagonal.

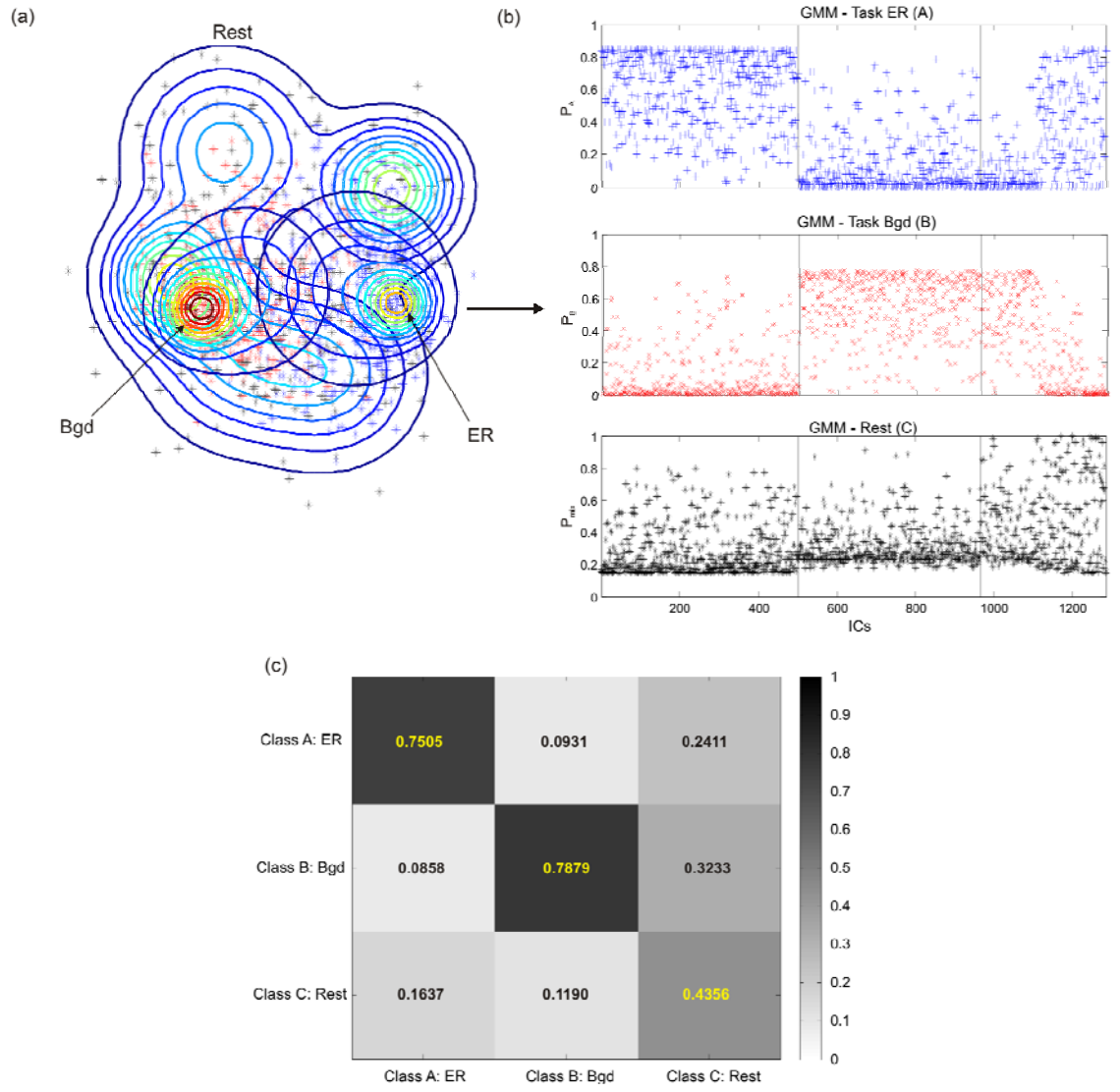

Figure 8-28. Training data classification results based on *Slow Wave Amplitude* features of the ICs for the Oddball Hard task environment: (a) GMM contour plots for the neuroscale output, (b) Posterior probabilities from the GMMs of the three classes, (c) Confusion map showing sensitivity of classification on the diagonal.

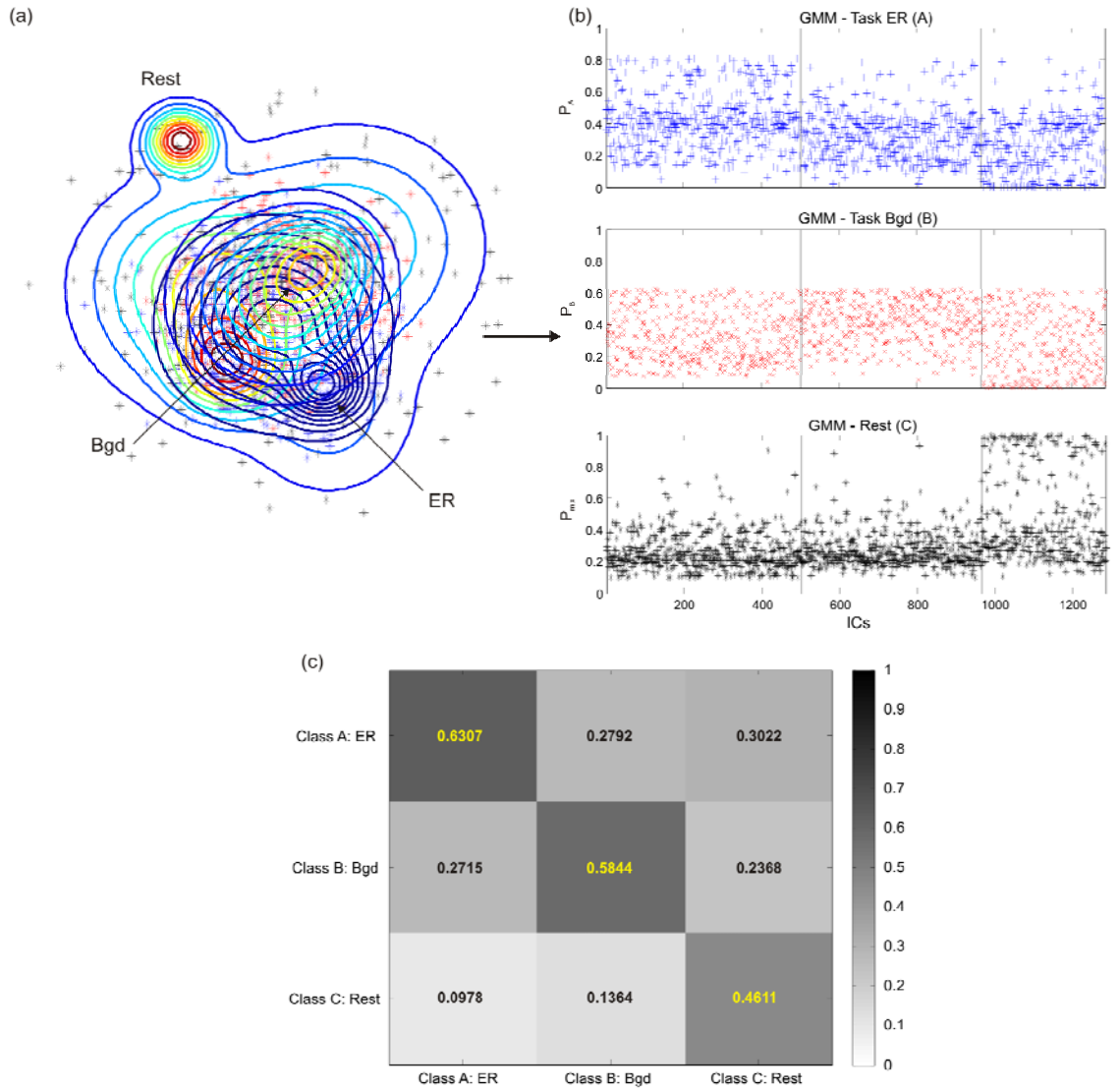

Figure 8-29. Training data classification results based on *Slow Wave Phase* features of the ICs for the Oddball Hard task environment: (a) GMM contour plots for the neuroscale output, (b) Posterior probabilities from the GMMs of the three classes, (c) Confusion map showing sensitivity of classification on the diagonal.

Figures 8-30 to 8-32 show training data classification results based on delta, theta and alpha features respectively for selected task environments (similar patterns were obtained for all three task environments, as shown in Appendix II (B)). Interestingly, for these frequency bands, the ER and Background task classes are not as separable as those for the slow wave band, whilst the Rest class is more distinct.

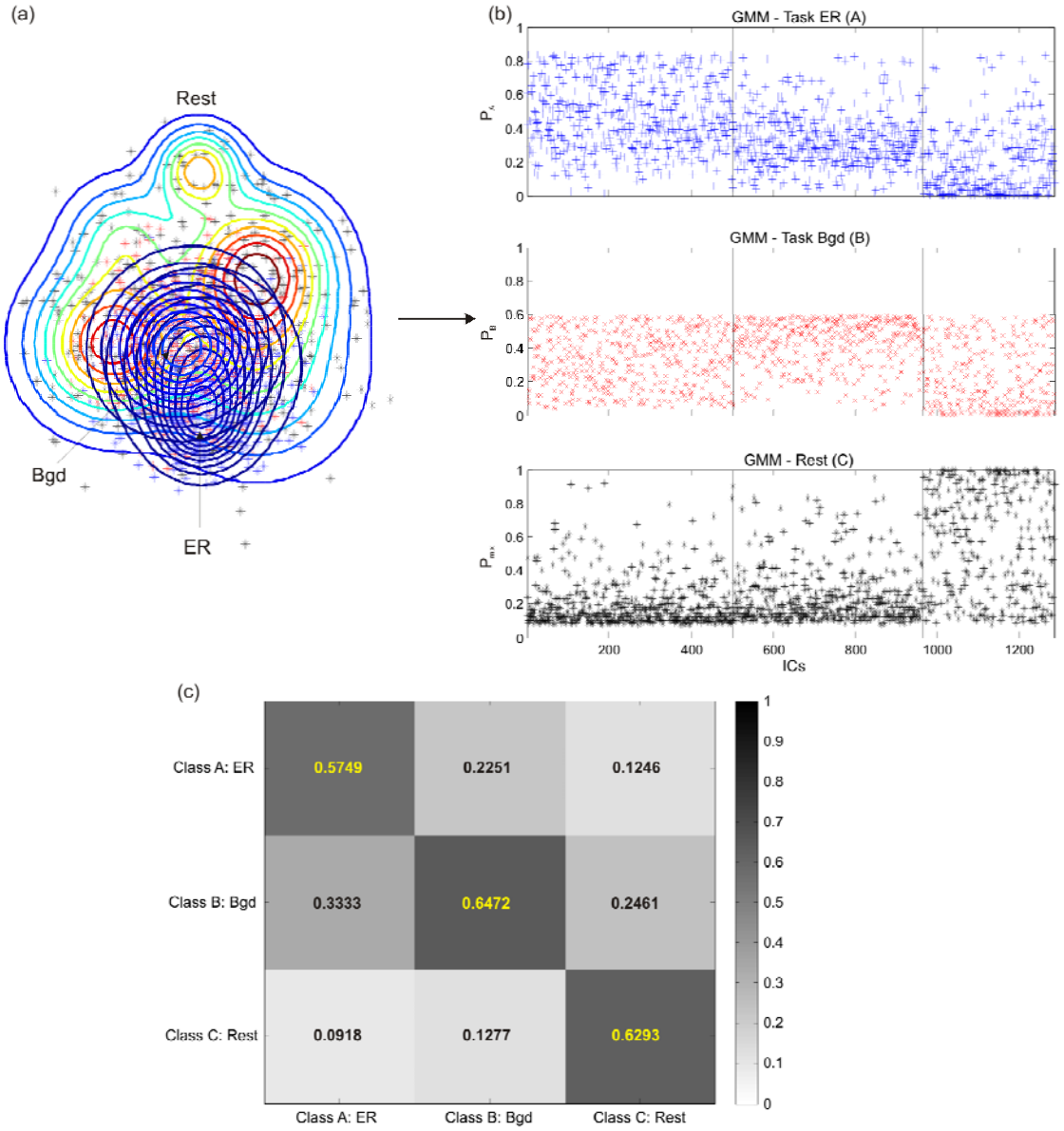

Figure 8-30. Training data classification results based on *Delta f-Band Amplitude* features of the ICs for the Oddball Hard task environment: (a) GMM contour plots for the neuroscale output, (b) Posterior probabilities from the GMMs of the three classes, (c) Confusion map showing sensitivity of classification on the diagonal.

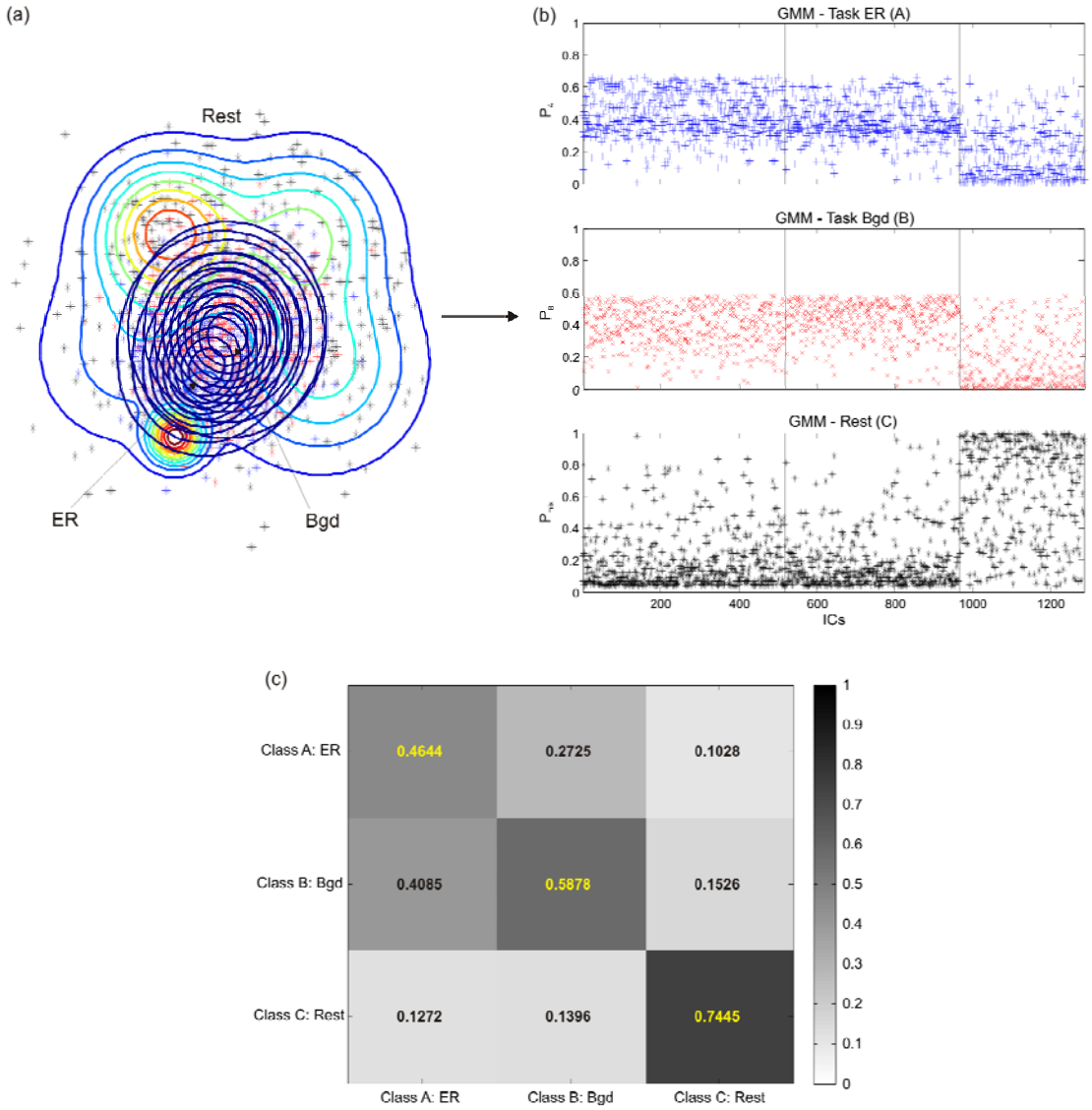

Figure 8-31. Training data classification results based on *Theta f-Band Phase* features of the ICs for the Oddball Easy task environment: (a) GMM contour plots for the neuroscale output, (b) Posterior probabilities from the GMMs of the three classes, (c) Confusion map showing sensitivity of classification on the diagonal.

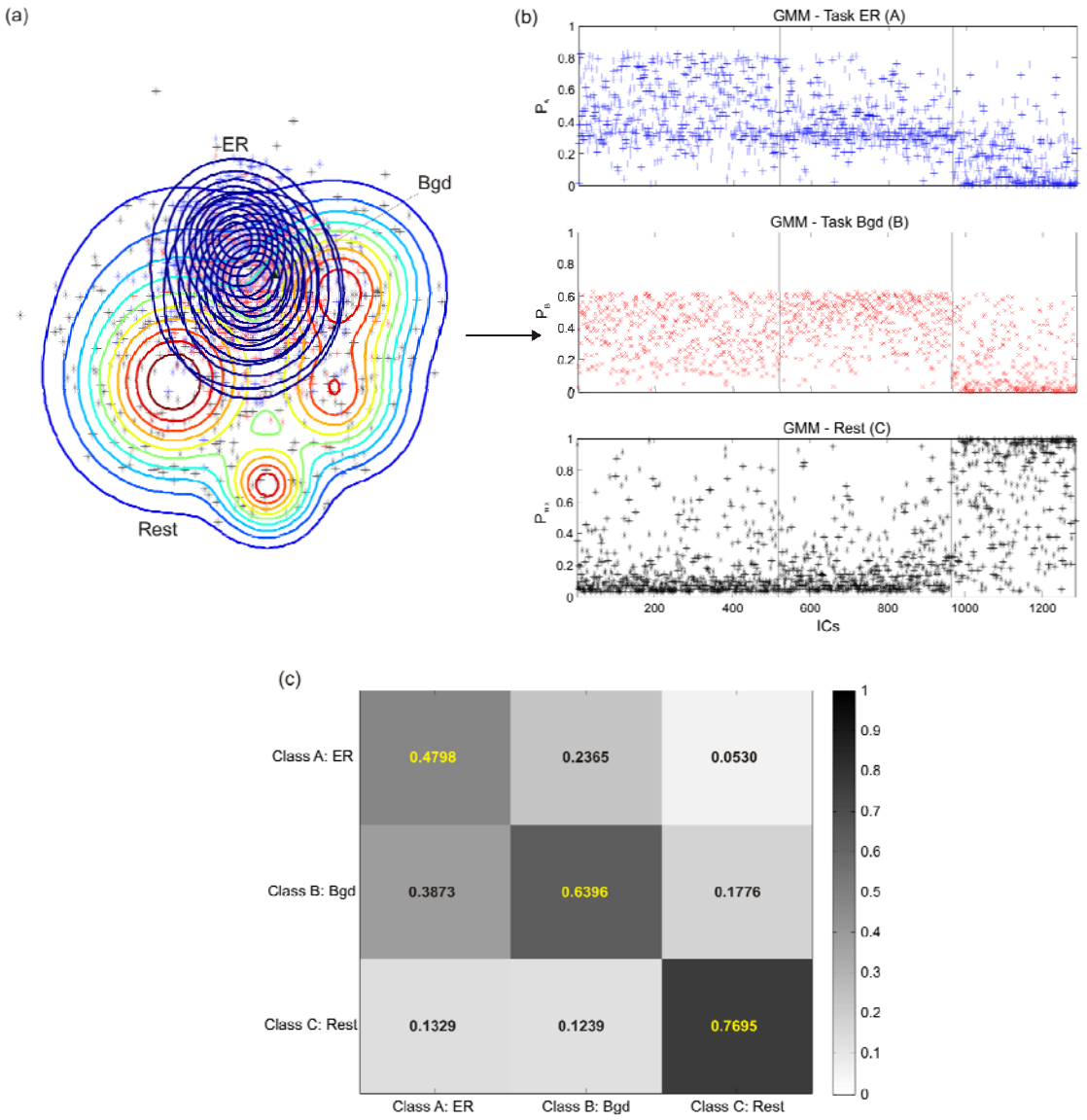

Figure 8-32. Training data classification results based on *Alpha f-Band Amplitude* features of the ICs for the Oddball Easy task environment: (a) GMM contour plots for the Neuroscale output, (b) Posterior probabilities from the GMMs of the three classes, (c) Confusion map showing sensitivity of classification on the diagonal.

The distinctive separability of the brain sources features during rest and task, particularly in the alpha *f*-band, comes as no surprise and has been well acknowledged in the literature (Herrmann and Knight, 2001; Ben-Simon *et al.*, 2008). The alpha oscillator is believed to act like a "stand-by" state or a "self-resonance" system that allows the brain to return more rapidly to goal-oriented cognitive functioning if and when required. When the primary visual cortex receives no or little input, it oscillates predominantly in the alpha range at a relatively high amplitude. In fact, as seen from these experiments, the most prominent activity in the EEG at rest is the ongoing alpha oscillatory component, which is thought to reflect cortical idling. This activity is desynchronised

by the presence of stimulation and the total alpha power is decreased (Herrmann and Knight, 2001). Furthermore, stimulation resets the randomly distributed phase of the alpha waves, leading to increased phase-locked alpha activity. This explains the very high sensitivity of classification for the Rest class during all task environments, for both amplitude and phase ICs features in the alpha *f*-band.

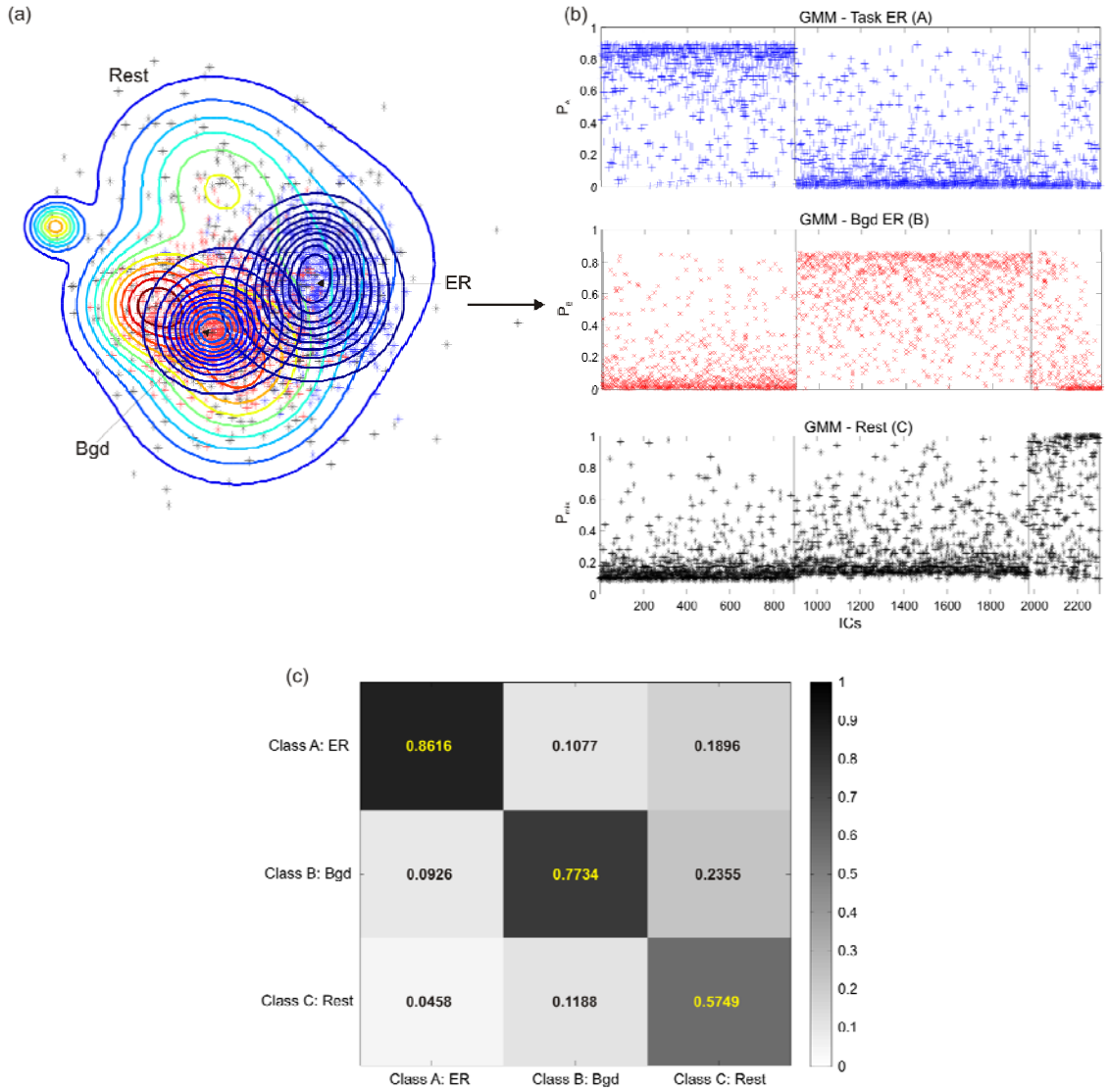

Figure 8-33. Training data classification results based on *All f-Bands Amplitude* features of the ICs for the SART task environment: (a) GMM contour plots for the Neuroscale output, (b) Posterior probabilities from the GMMs of the three classes, (c) Confusion map showing sensitivity of classification on the diagonal.

Finally, in order to get an overall picture of how the four oscillators were changing together during rest and task, the AR models of the amplitude of the four *f*-bands were concatenated and used in the classification method. The results shown in Figure 8-33 illustrate high sensitivity of classification for the three classes.

The sensitivity of classification for the training databank for the three task environments when using the characteristics of the amplitude or phase of the ICs in the four frequency bands is illustrated in Figure 8-34. Note the consistency of the results across different tasks, for both the amplitude and phase of the oscillators. The slow waves experience the highest level of overlap (lowest sensitivity) between the rest and task classes, whilst achieving the highest separation for the Task-ER and Task-Background classes in comparison to the other oscillators.

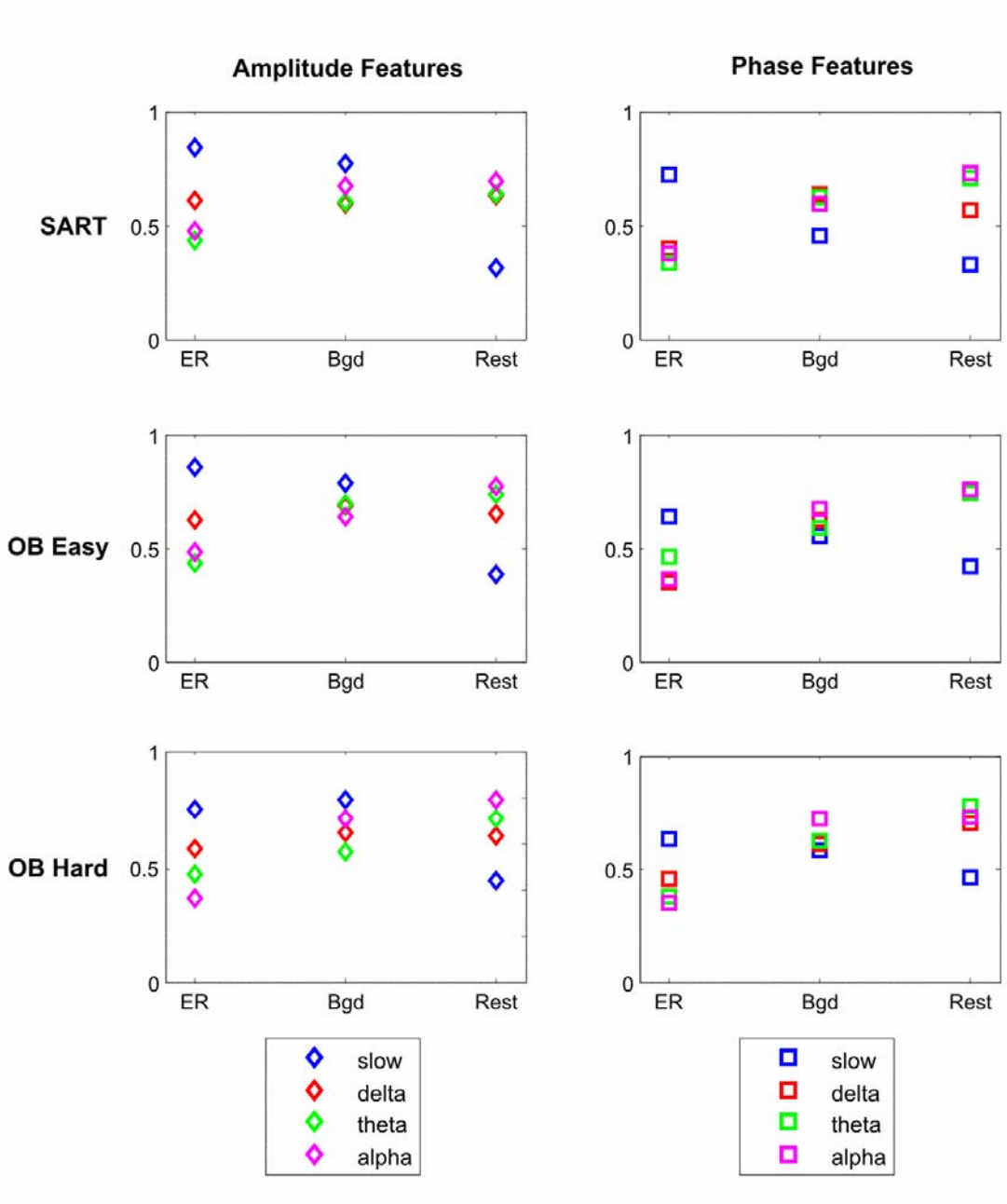

Figure 8-34. Training data sensitivity of classification for the three task conditions when using the characteristics of the amplitude or phase in the four frequency bands.

8.9.2 Test Data

As explained in Section 8.6.3, the test databank containing the ICs features (derived using the AR and ID method) of the remaining 6 participants was then mapped onto the 2-D feature space provided by the neuroscale output for the corresponding training databank (i.e. same task environment and frequency band). The PDFs of the 2-D output mapping were then characterised by projection onto the three corresponding training GMMs. Note that, as for the training data, the test data task ICs have been separated into ER and Background classes using the hierarchical clustering procedure described in Section 8.3, and the Rest ICs have also been ordered according to their frequency content (as explained in Section 8.4), prior to feature extraction and neuroscale mapping procedures.

Figure 8-35 shows an example of test data classification based on the slow wave amplitude features of the ICs for the SART task environment. The posterior probabilities after projection of the neuroscale 2-D output onto the 3 training GMMs (obtained from the training data of 14 participants based on SART slow wave amplitude features) very clearly distinguish the ER and Background classes. Moreover, a similar trend to that obtained for the training data is again shown for the Rest ICs: the features of those ICs with a predominant slow frequency content overlapped with the Background ICs, whereas those with a predominant theta and alpha frequency content overlapped with the ER ICs.

The neuroscale mapping and GMM projection procedures were repeated for the three task environments using the characteristics of the amplitude or phase of the test databank ICs in the four frequency bands, and the corresponding results for the sensitivity of classification are summarised in Figure 8-36. Although, as expected, the sensitivity values are lower than those obtained for the training data (shown in Figure 8-34), the two sets of results are comparable; for example, using the slow wave features, the ER and Background classes can be separated with the highest sensitivity in comparison to the other oscillators, whereas the alpha-based features show the greatest distinction between rest and task for all task environments. Interestingly, the test data also demonstrates a rise in the slow wave sensitivity (i.e. in the percentage of correct classification) for the Rest class as the task difficulty level increases (Slow wave amplitude features: SART – 24.2%, Oddball Easy – 26.6%, Oddball Hard – 29.5%; Slow wave phase features: SART – 22.2%, Oddball Easy – 24.8%, Oddball Hard – 32.4%).

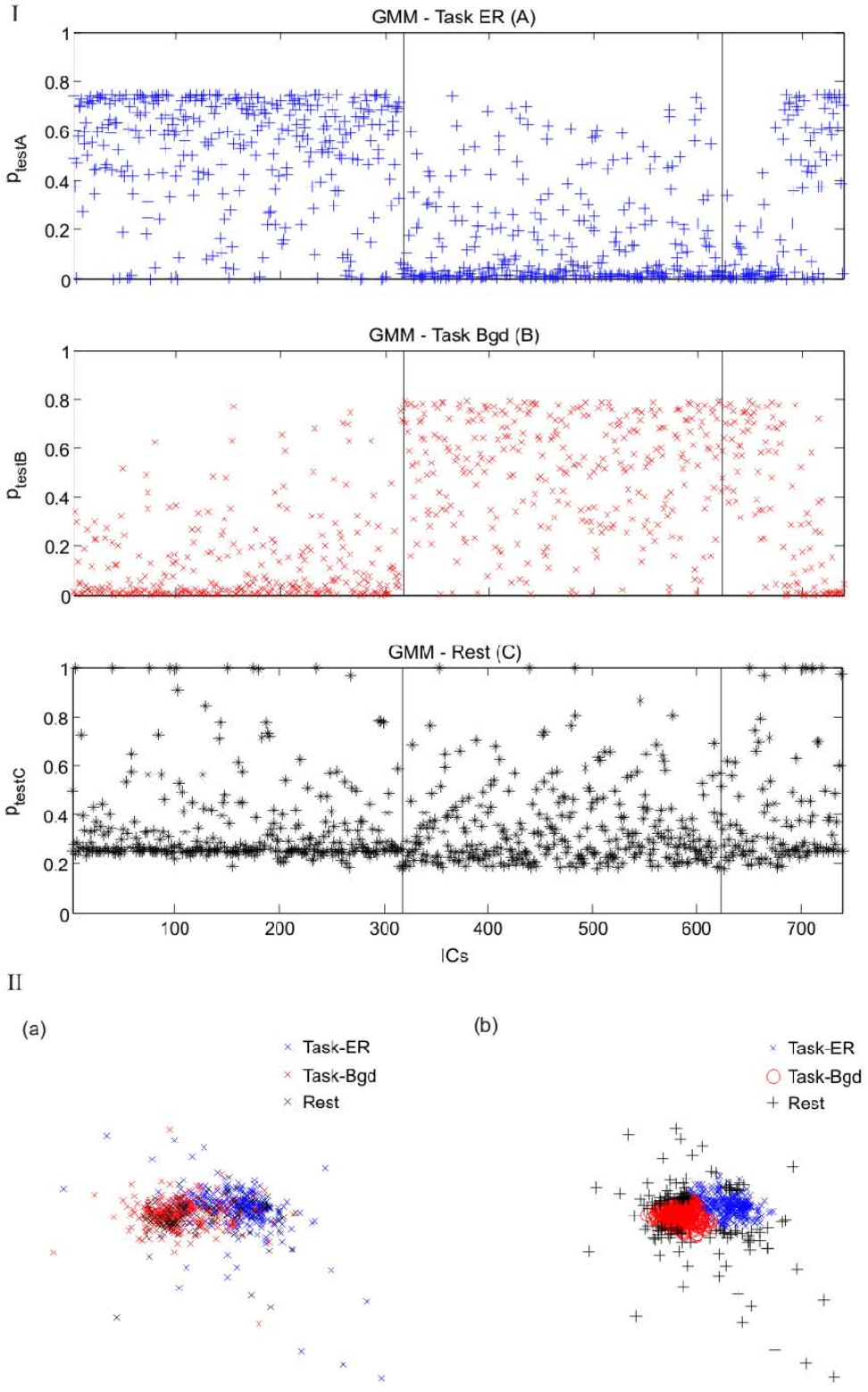

Figure 8-35. Test data classification of the *Slow Amplitude* features of the ICs for the SART task environment. I. Probabilities characterising the Neuroscale 2-D output mapping after projection onto the 3 GMMs obtained for the corresponding training data. II. (a) 2-D Neuroscale output; (b) Classified data after projection onto the training GMMs.

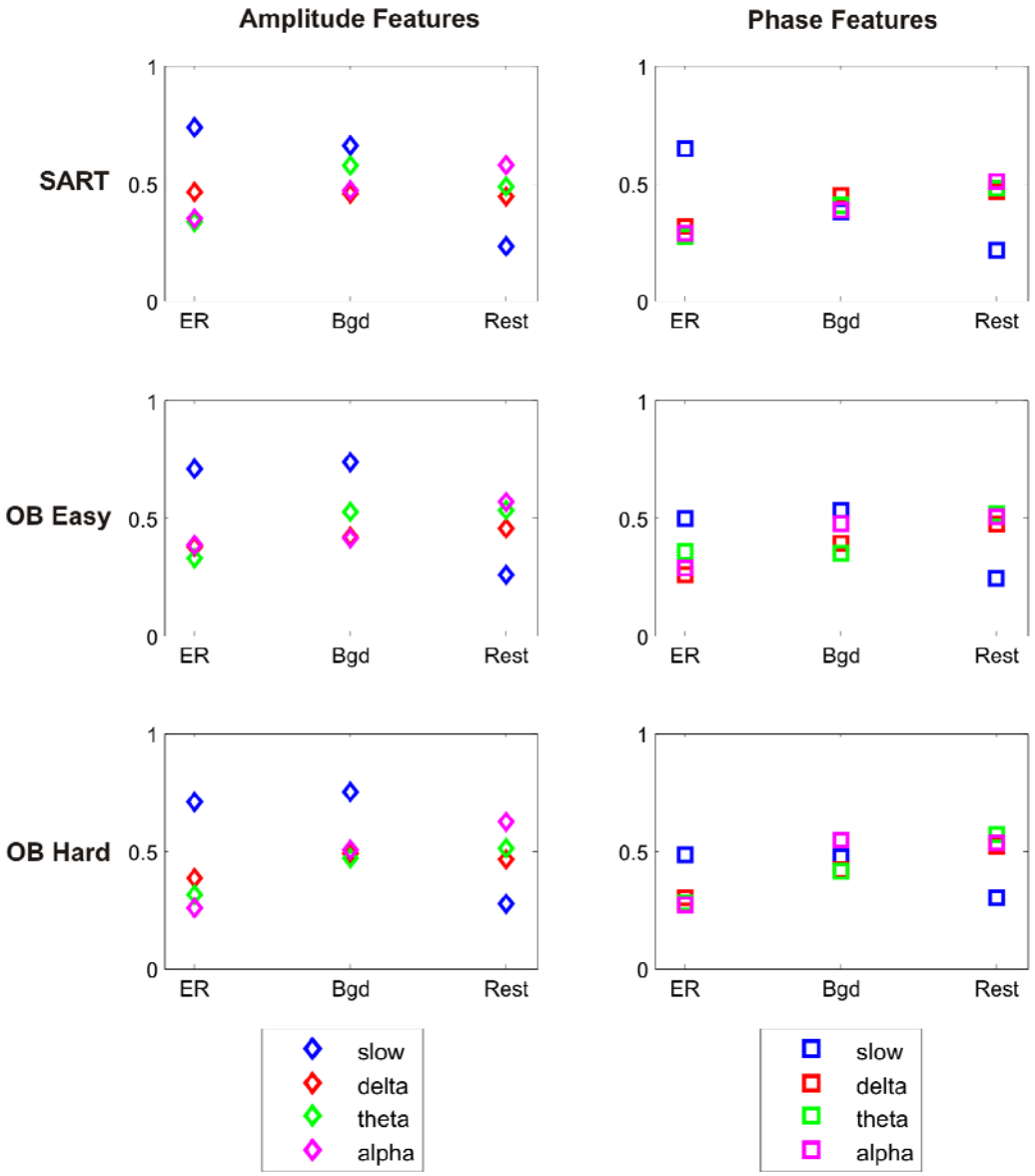

Figure 8-36. Test data sensitivity of classification for the three task conditions when using the characteristics of the amplitude or phase in the four frequency bands.

8.10. Investigating the Classification Results based on Slow Wave Features

Some of these results demonstrate that by using *only* the slow wave amplitude or phase features one can distinguish between three distinct types of brain activity. Hence, the slow wave oscillators are exhibiting *and/or* the slow wave mechanisms are causing considerable change in ER and background task activity, and between rest and task brain activity. Various questions arise from these observations, including:

(i) What specific changes are the slow waves undergoing?

(ii) Can these changes be quantified?

(iii) Where in the brain are these changes most prominent?

An attempt has been made to tackle these questions by considering the slow wave power and phase of these brain sources, and by projecting the classified sources onto the measurement space in order to investigate the topographies that arise from the three classes.

8.10.1. Slow Wave Power

For every task environment the slow wave power was calculated by considering the Task-ER, Task-Background and Rest ICs of all 20 participants (i.e. training and test databanks taken together), for each task environment. The average power during Rest and Task (ER and Background taken together) was then obtained by dividing the total power in each class with the number of Rest or Task ICs. This was done to compensate for the fact that the Rest and Task groups contained a different number of ICs.

	Task		
Average Power	**SART**	**Oddball Easy**	**Oddball Hard**
Task (P_T)	6.29×10^5 [1.03×10^4 3.84×10^7]	4.29×10^5 [6.23×10^3 8.92×10^6]	4.78×10^5 [7.65×10^3 1.12×10^7]
Rest (P_R)	1.15×10^6 [1.54×10^4 4.46×10^7]	6.87×10^5 [1.03×10^4 1.15×10^7]	6.87×10^5 [1.03×10^4 1.15×10^7]
Rest & Task (P_{RT})	8.90×10^5	5.58×10^5	5.82×10^5
% Diff = $(P_R-P_T)/P_{RT}$	**58.64**	**46.24**	**35.91**

Table 8-6. Average and [minimum maximum] power of the ICs during the three different task environments, and the percentage difference between Rest and Task power.

The average slow wave power during the tasks was always lower in comparison to that during Rest, with the biggest difference (58.6%) exhibited during the SART (this being the easiest, most rhythmic task) and the lowest difference (35.9%) experienced during the Oddball Hard task environment. Moreover, the average slow wave power during the Oddball Hard Task was 11% higher than that during the Easy task. The results shown in Table 8-6 suggest that the slow wave power is attenuated during goal-directed active processing, as predicted by the DMI hypothesis, and the change between rest and task varies with the level of task difficulty.

8.10.2. Slow Wave Phase

In order to characterize the structure of the instantaneous phase of each IC, the entropy was computed as a statistical measure of randomness. The ICs for all 20 participants (i.e. training and test databanks) were considered for this analysis. The results illustrated in Figure 8-37 show that the slow wave phase undergoes a change in structure in the three conditions. The phase of the ER ICs has a low entropy (high structure), whereas that for the Background ICs and the Rest ICs with a slow frequency morphology exhibit a much lower structure. The remaining of the Rest ICs, corresponding to those with a predominant high-delta, theta and alpha frequency content, experience low entropy levels. This partially explains the consistent overlap of the Rest ICs features with both ER and Background task classes in the results obtained from the classification procedure.

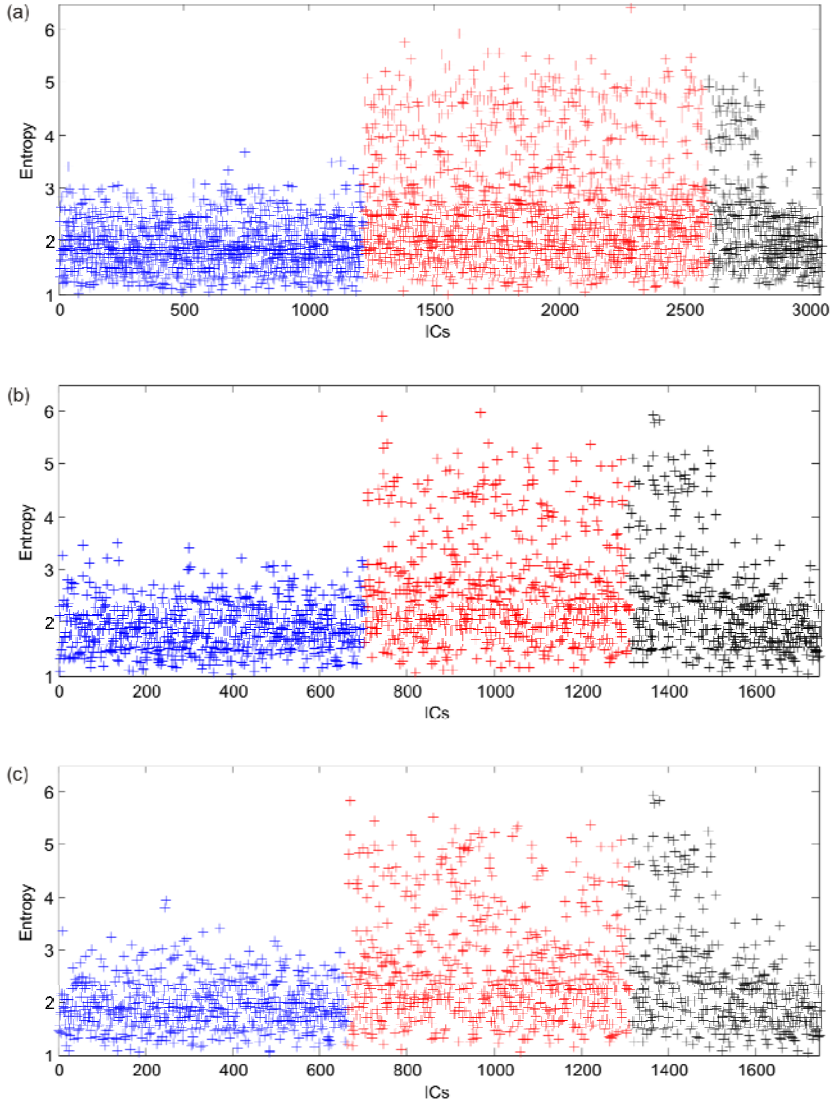

Figure 8-37. Entropy of the instantaneous slow wave phase of the ER (blue) Background (red) and Rest (green) ICs for (a) SART, (b) Oddball Easy and (c) Oddball Hard task environments.

8.10.3. Slow Wave Projections

Here, those ICs which have been correctly classified into the three classes based on slow wave amplitude features were selected and filtered in the frequency band ($0<f<0.5$ Hz). Since these ICs have been properly classified according to their slow wave features, they *must* exhibit significant changes in the slow wave band in three conditions (ER, Background and Rest), and therefore when filtered and back-projected onto the measurement space, they may provide some information on the location of the slow wave activity or relative changes during the three states. The training dataset ICs have been chosen for this purpose since the training set classification results were more robust. The slow wave projections during ER, Background and Rest conditions for each task environment are illustrated in Figures 8-38 to 8-40. The topographies represent the mean square power for each of the 25 channels of the projection.

Throughout the three task environments, the topography for the Background slow wave projection showed a central focus, whereas that for the Rest demonstrated an occipital focus with some frontal power. Meanwhile, the ER slow wave topography varied across tasks, from a left temporal-parietal focus (for the SART) to a more parietal-occipital focus (for the Oddball Hard).

Complexity of Projections

The slow wave projections' time-series of the ER, Background and Rest for different task environments (shown in Figures 8-38 to 8-40) were compared by means of a complexity measure described by James and Lowe (2000). This measure captures the temporal dynamics of the signals by means of dynamical embedding. Here, a matrix of delays (dimension 90) was constructed for 10-second time windows with 50% overlap along the 4-minute projections for each of the 25 channels. The number of system states, derived from the entropy of the normalised eigenvalues of the embedding matrix, was obtained as a measure of complexity of the underlying system. A brief description of this procedure is given below.

Let $\mathbf{X}_i$ be the embedding matrix for segment i (from channel j) consisting of m delay vectors. SVD is employed on $\mathbf{X}_i$ in order to obtain its eigenvalues, λ_i, which are then normalised such that

$$\hat{\lambda}_j^i = \lambda_j^i \Big/ \sum_{k=1}^{m} \lambda_k^i \ . \tag{8.21}$$

An entropy measure is then obtained by

$$H^i = -\sum_{k=1}^{m} \hat{\lambda}_k^i \log_2 \hat{\lambda}_k^i \ , \tag{8.22}$$

and the number of system states defined as:

$$\Omega^i = 2^{H^i}. \tag{8.23}$$

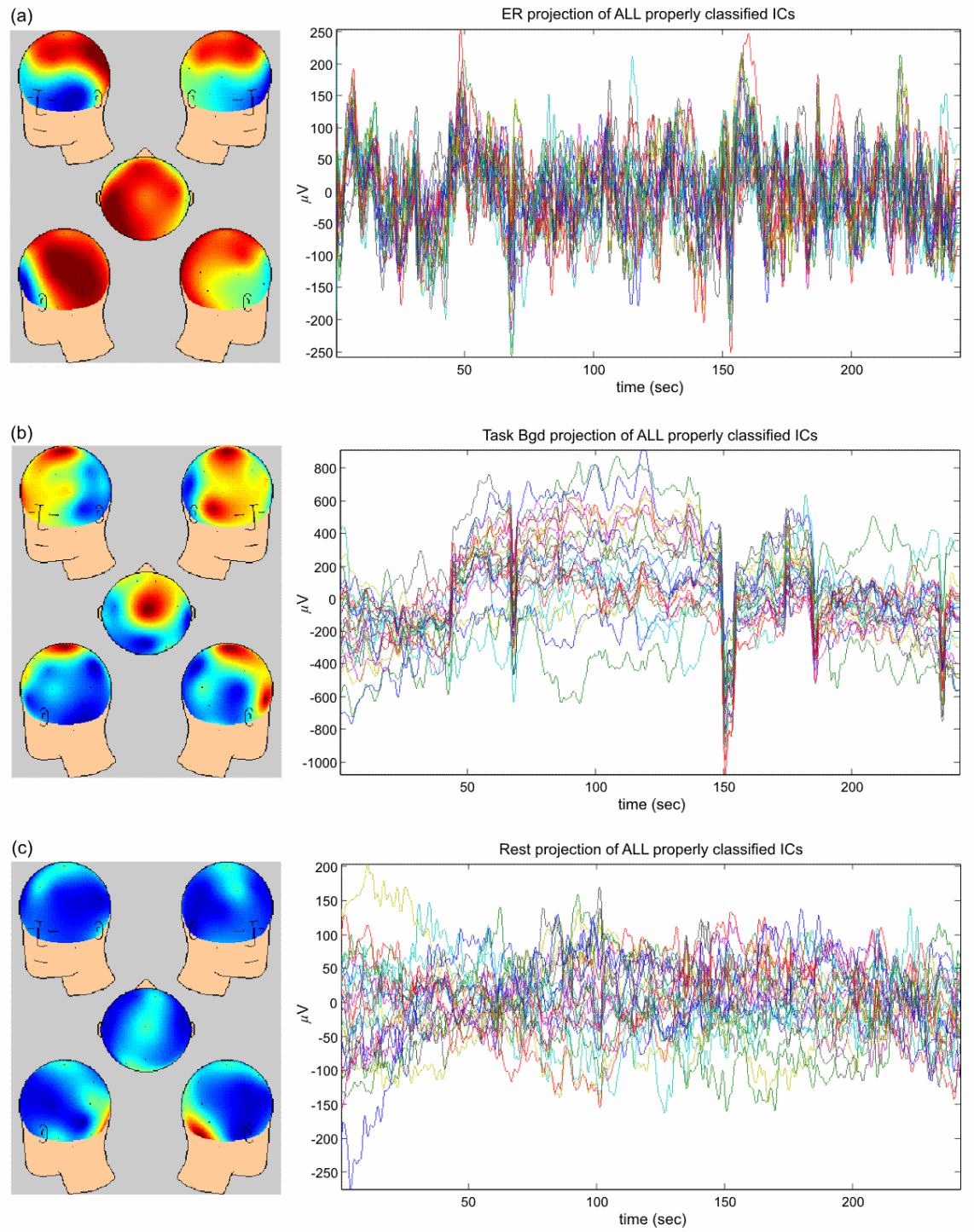

Figure 8-38. SART slow wave projections comprising all correctly classified ER (a), Background ICs (b) and Rest (c) ICs. The ICs have been filtered in the ($0<f<0.5$ Hz) band prior to back projection.

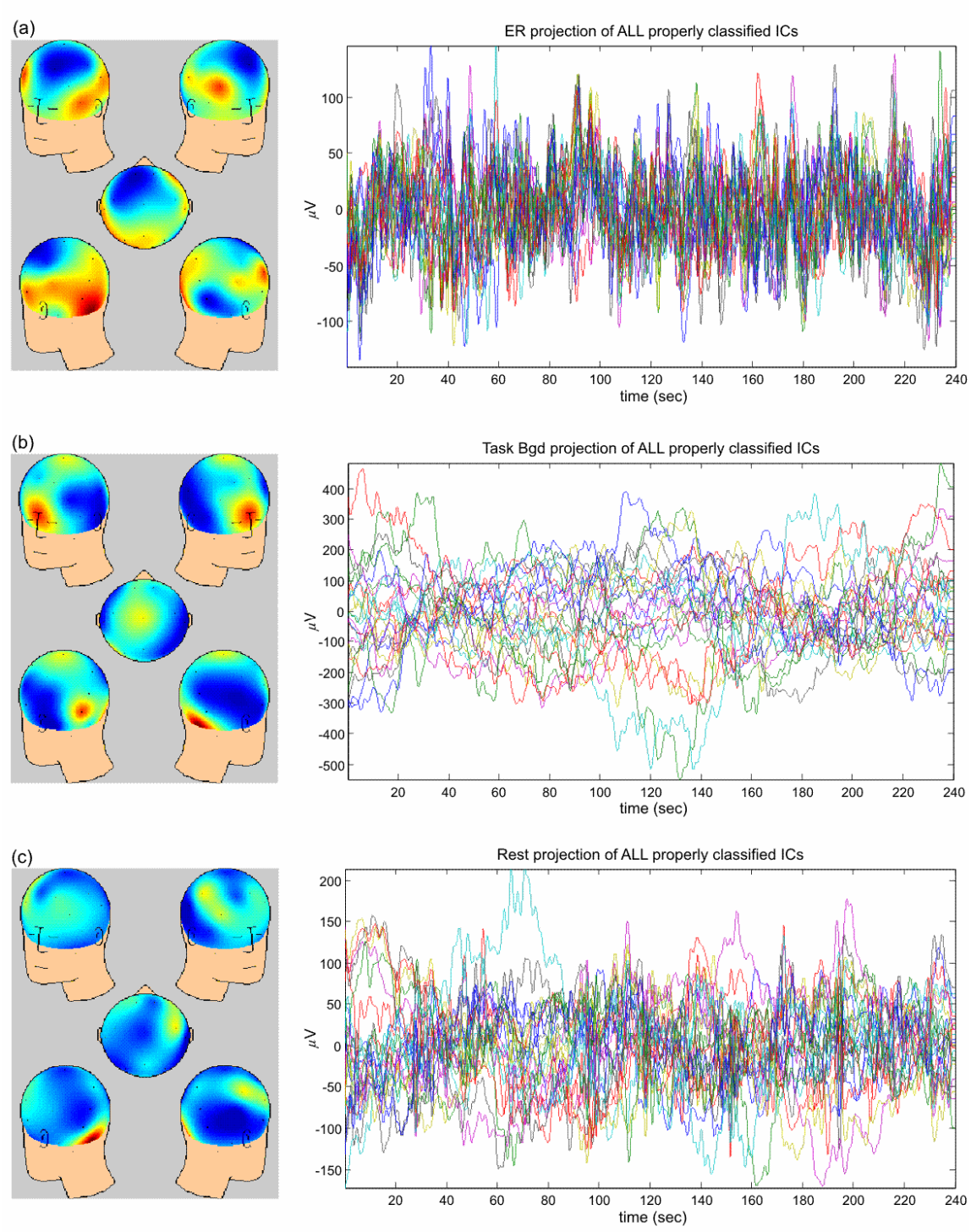

Figure 8-39. Oddball Easy slow wave projections comprising all correctly classified ER (a), Background ICs (b) and Rest (c) ICs. The ICs have been filtered in the ($0<f<0.5$ Hz) band prior to back projection.

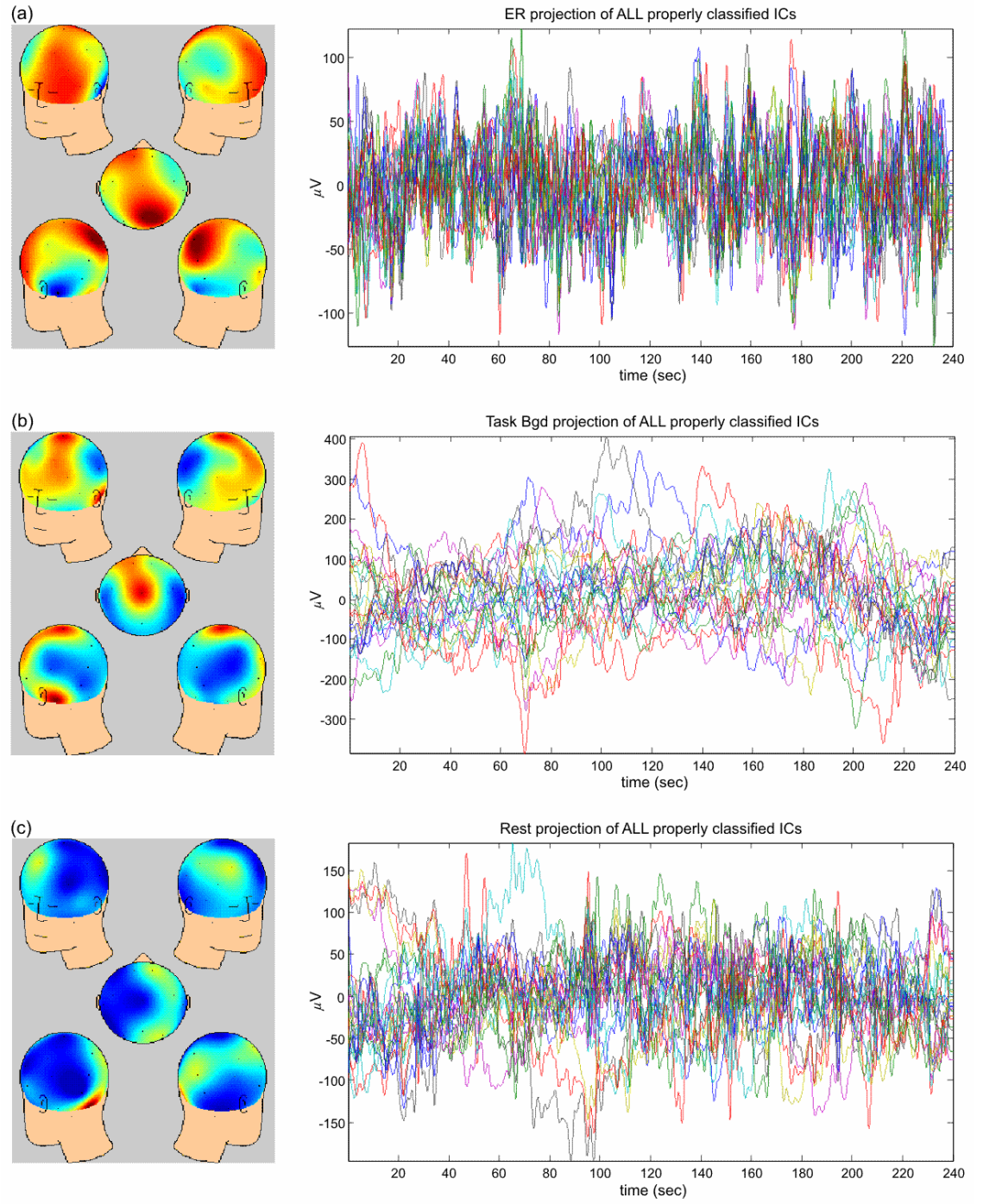

Figure 8-40. Oddball Hard slow wave projections comprising all correctly classified ER (a), Background ICs (b) and Rest (c) ICs. The ICs have been filtered in the ($0<f<0.5$ Hz) band prior to back projection.

The more information the projection contains, the higher is the number of system states required to describe it. Figure 8-41 shows the average complexity values across the 25 channels for ER, Background and Rest slow wave projections during the three task environments. In all cases, the Background projections have a sinusoidal morphology and therefore require a lower number of states to describe them – this is also visible from the waveforms in Figures 8-38 to 8-40 (b). The complexity of the Rest projections lies in between that of the Task-ER and Task-Background. This

is because, the rest recording, albeit the lack of time-locked activity to specific stimuli, still comprises a variety of brain activity. For example, Rothenberger (2009) suggests that the alpha component during rest represents a further neurophysiological correlate of the default mode network, which is related to a relaxed *but nonetheless* attentive state that allows some preparedness for changes (for example, to start task execution). Recall that throughout this work, rest activity has been further separated into three subclasses of brain sources, namely those with a predominantly slow, middle (high-delta and theta), and alpha frequency content. These, when filtered in the slow wave band ($0<f<0.5$ Hz) will all naturally have a different morphology, topography and a different level of complexity, mirroring distinct brain activities co-occurring during rest. In fact, when these three subclasses were projected separately onto the measurement space, three different topographies were obtained. The Rest topographies for the Oddball Easy task environment are shown as an example in Figure 8-42, which obviously add up to the total Rest topography of Figure 8-39 (c). Their complexity curves can be found in Figure 8-43.

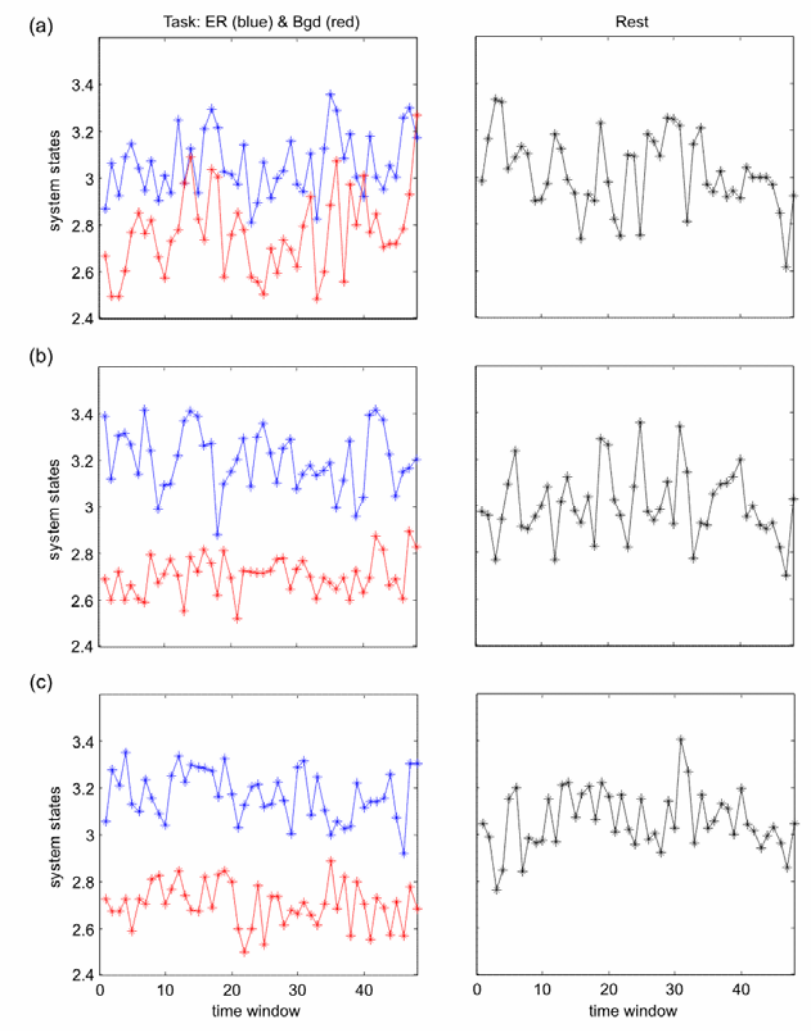

Figure 8-41. Complexity measure (number of system states) for the ER (blue), Background (red) and Rest (black) projections for (a) SART, (b) Oddball Easy and (c) Oddball Hard task environments. Traces show the average measure across the 25 channels for 10-second time windows with 50% overlap.

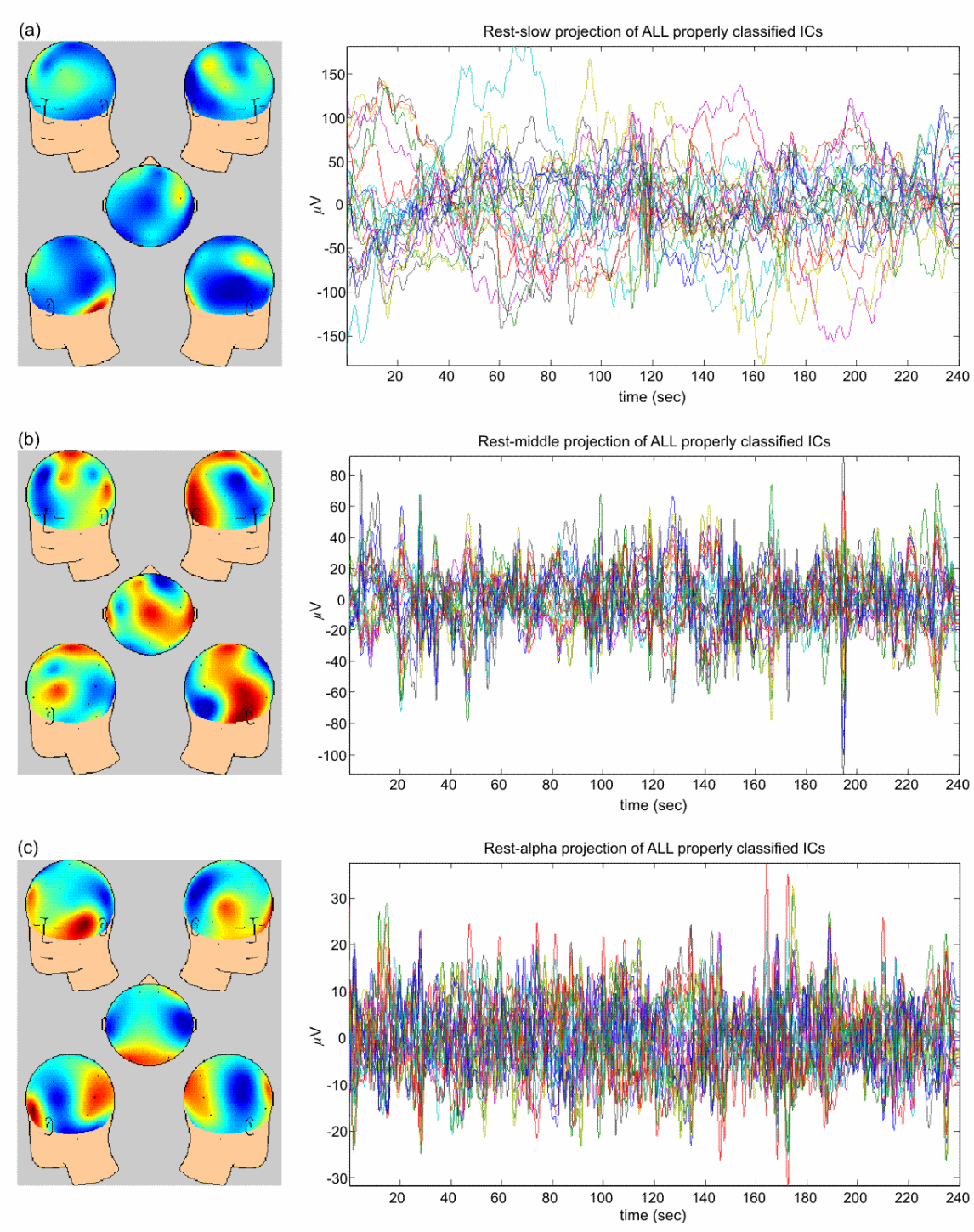

Figure 8-42. Oddball Easy slow wave projections comprising all the correctly classified Rest ICs with a predominantly slow: slow and low delta (a), middle: high delta and theta (b), and alpha (c) frequency content.

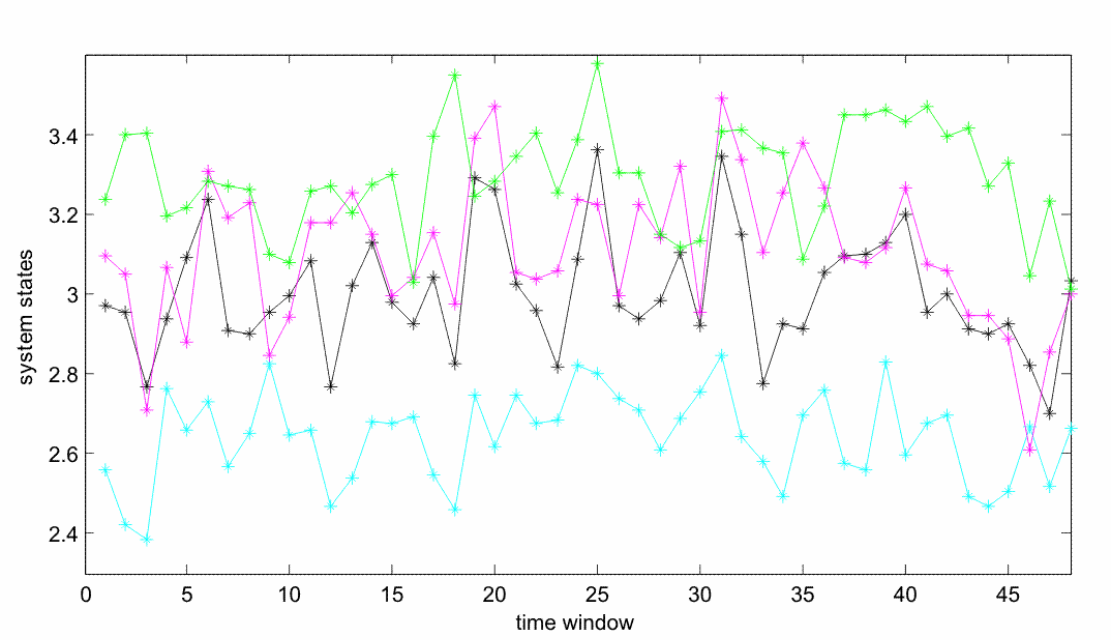

Figure 8-43. Complexity measure (number of system states) for the slow & low-delta (cyan), high-delta & theta (magenta), alpha (green) and combined (black) Rest projections for Oddball Easy task environment. Traces show the average measure across the 25 channels for 10-second time windows with 50% overlap.

Classification based on Projections

In order to further investigate the extent to which the ER, Background and Rest ICs, which have been correctly classified by the slow wave features, varied from a topographical perspective, the following test was carried out:

1. The topographies (i.e. columns of A) of the correctly classified ICs (based, for e.g. on the slow wave amplitude features) *only* were considered.
2. The power in the frontal, central, parietal and occipital regions were calculated for each topography (hence establishing a matrix of n correctly-classified ICs $\times 4$).
3. The Euclidean distances between the 4 power values of each topography with those of every other topography were obtained (hence forming an n square matrix of distances) as shown in Figure 8-44.

Three distinct classes are also visible in Figure 8-44, implying that those ICs which have been properly distinguished as ER, Background and Rest based only on the slow wave amplitude features, have also very clear distinct spatial profiles. The result for Oddball Easy task environment is shown as an example in Figure 8-44, (those for the other two task environments were similar). However, it is important to note here that, although this is a way of checking the slow wave classification results, it is not specifying exactly *where* the changes in the slow wave band are happening in the three brain states (since each column of the mixing matrix acts as a spatial filter for the corresponding IC rather than for its band-limited version).

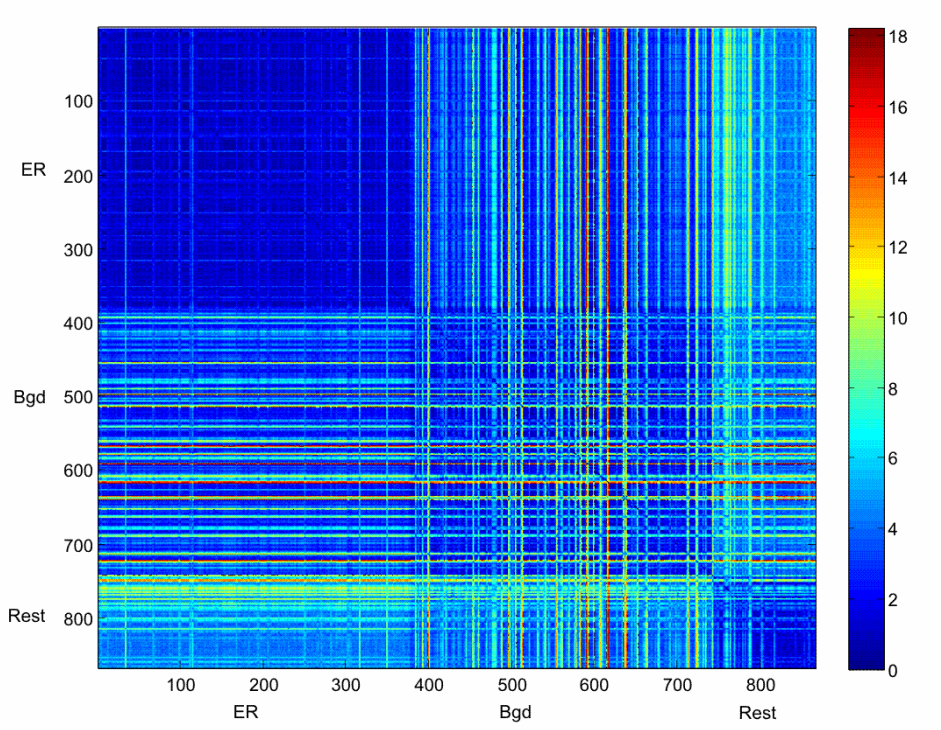

Figure 8-44. Euclidean distance matrix between the power in the frontal, central, parietal and occipital regions of the topographies of the correctly classified ICs (these ICs have been formerly classified based on the slow wave amplitude features) for the Oddball Easy task environment (shown as an example). Note the three distinct classes are clearly visible here (ER – 1:376; Background – 377:740; Rest – 741: 867).

8.11. Investigating the Relationship between Classification Results and Behavioural Data

The sensitivity values of the classification results obtained from the training data, based on band-limited IC features for different task environments, were correlated with behavioural data, namely reaction time, percentage error rate, and number of false alarms (the latter is only applicable to the Oddball task). This was done in order to assess whether the difference between the three brain states could be linked with performance throughout the course of the task. Recall that a high sensitivity of classification indicates that the *relative* change in the amplitude or phase features between brain sources related to task processing (ER), the Background brain sources during task and those during Rest, is significant enough for them to be classified separately. Significant correlation results are shown in Table 8-7, (the -- marks indicate no significant correlations, i.e. a *p*-value generally above 0.1). Note that the training dataset has been used for this purpose, since its classification results were more robust, and more data points were available (14 training rather than 6 test datasets) for computing the correlation coefficients and *p*-values.

For the slow wave features, the percentage of correct classification for the ER and Background classes was always negatively correlated with behavioural data (Figure 8-45), and there were more

significant correlations for the Oddball Hard task environment (i.e. for the hardest task). This implies that the lower the RT, percentage of error rates and number of false alarms, i.e. the better the participants' performance, the higher was the difference in the slow wave band between, for example, the ER brain state and the other (Background and Rest) states.

		Slow Amplitude Features			**Slow Phase Features**		
		ER	**Bgd**	**Rest**	**ER**	**Bgd**	**Rest**
SART	**RT**	--	--	--	--	--	R =-0.48 p = 0.08
OB Easy	**RT**	R = -0.50 p = 0.07	--	R = 0.60 p = 0.065	R = -0.57 p = 0.042	--	R = 0.45 p = 0.14
OB Hard	**RT**	R = -0.43 p = 0.09	R= -0.46 p = 0.103	R = 0.526 p = 0.053	--	--	R = 0.42 p = 0.101
	Error Rate	R = -0.46 p = 0.10	--	--	--	R = -0.55 p = 0.044	--
	False Alarms	--	R = -0.70 p = 0.005	--	--	R = -0.45 p = 0.09	--

		Delta Amplitude Features			**Delta Phase Features**		
		ER	**Bgd**	**Rest**	**ER**	**Bgd**	**Rest**
SART	**RT**	--	--	R = -0.58 p = 0.03	--	R =-0.45 p = 0.108	R = -0.45 p = 0.104
OB Easy	**Error Rate**	--	--		R = 0.70 p = 0.01	--	R = 0.60 p = 0.02
OB Hard	**False Alarms**	--	--	R = 0.62 p = 0.02	--	--	--

		Theta Amplitude Features			**Theta Phase Features**		
		ER	**Bgd**	**Rest**	**ER**	**Bgd**	**Rest**
SART	**RT**	--	R = -0.41 p = 0.105	--	--	--	--
	Error Rate	--	--	R = 0.60 p = 0.03	--	--	R = -0.54 p = 0.046
OB Easy	**RT**	--	--	R = 0.66 p = 0.01	R = 0.66 p = 0.01	--	--
	Error Rate	--	--	--	R = -0.56 p = 0.04	--	R = 0.41 p = 0.105
OB Hard	**RT**	R = -0.76 p = 0.002	--	--	--	--	--

		Alpha Amplitude Features			Alpha Phase Features		
		ER	**Bgd**	**Rest**	**ER**	**Bgd**	**Rest**
SART	**RT**	--	--	R = 0.58 p = 0.04	R = -058 p = 0.045	--	--
	Error Rate	--	--	R = 0.62 p = 0.02	--	--	--
OB Easy	**Error Rate**	R = -0.49 p = 0.07	--	R = 0.47 p = 0.09	--	--	--
OB Hard	**RT**	--	--	--		R = -0.51 p = 0.06	R = -0.62 p = 0.04
	Error Rate	R = -0.59 p = 0.027	--	R = 0.45 p = 0.102	--	--	--

		All-*f* Amplitude Features			All-*f* Phase Features		
		ER	**Bgd**	**Rest**	**ER**	**Bgd**	**Rest**
SART	**RT**	--	--	--	--	--	R = -0.61 p = 0.02
	Error Rate	--	--	--	R = -0.68 p = 0.008	--	R = 0.45 p = 0.105
OB Easy	**RT**	--	--	--	--	R = -0.55 p = 0.042	R = -0.54 p = 0.04
	Error Rate			R = 0.53 p = 0.05	--	--	--
OB Hard	**RT**	--	--	--	--	--	R = -0.65 p = 0.011
	Error Rate	--	--	R = -0.56 p = 0.04	R = 0.67 p = 0.01	--	--

Table 8-7. Correlations between the sensitivity of classification (ER, Background and Rest) and behavioural data (reaction time, % error rate and number of false alarms). The -- marks indicate no significant correlations, i.e. p-value generally above 0.1; R is the correlation coefficient.

Similar correlation results could be found for classification values based on amplitude or phase features in other frequency bands for the three task environments (Figures 8-45 and 8-46). However in some cases, namely (delta, phase features, Oddball Easy; theta, phase features, Oddball Easy; All-*f*, phase features, Oddball Hard), the percentage of correct classification in ER and Background was positively correlated with behavioural data (as shown in Table 8-7).

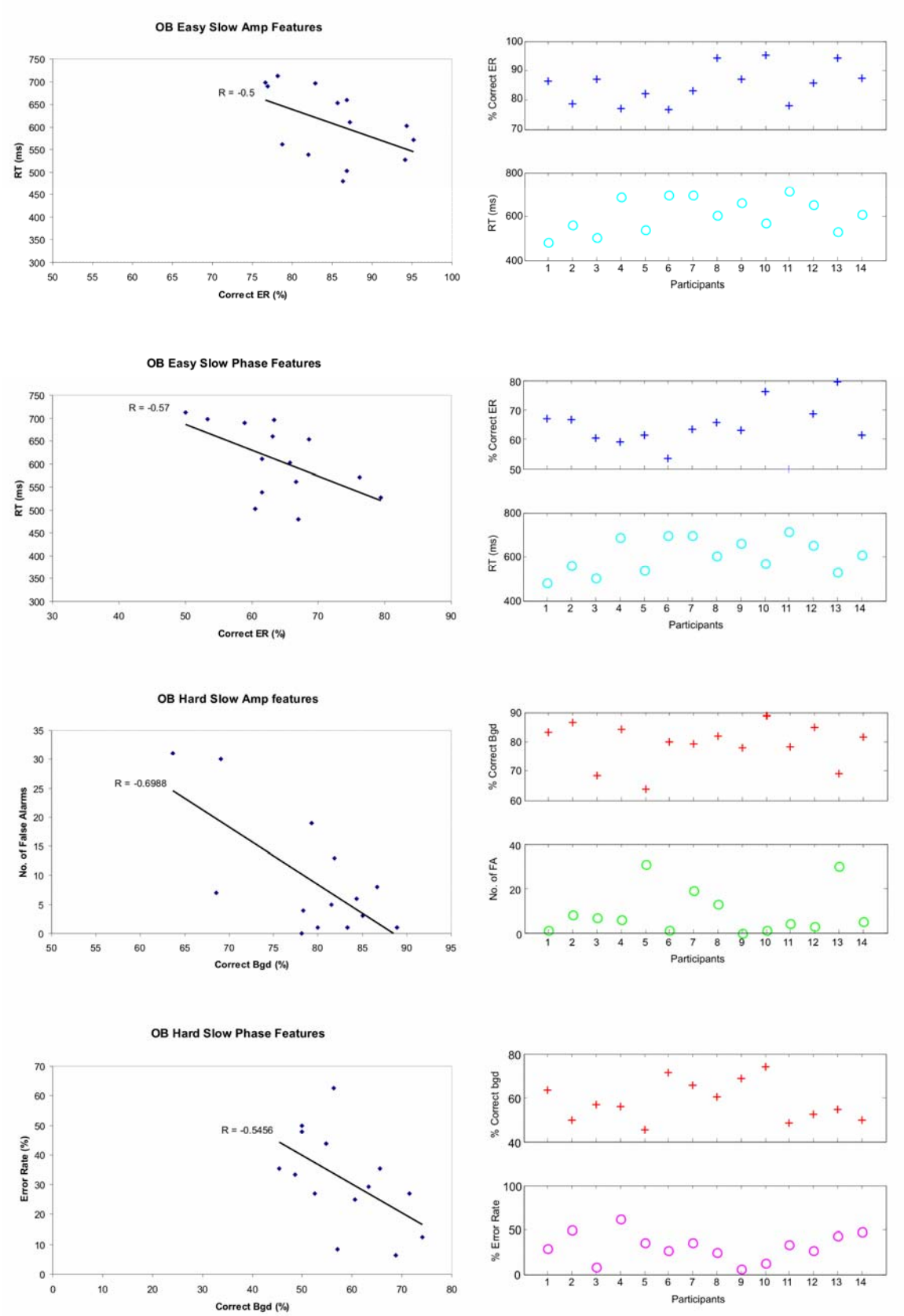

Figure 8-45. Sensitivity of classification based on the slow wave amplitude or phase features (for Oddball Easy and Hard task environments) is negatively correlated with behavioural data.

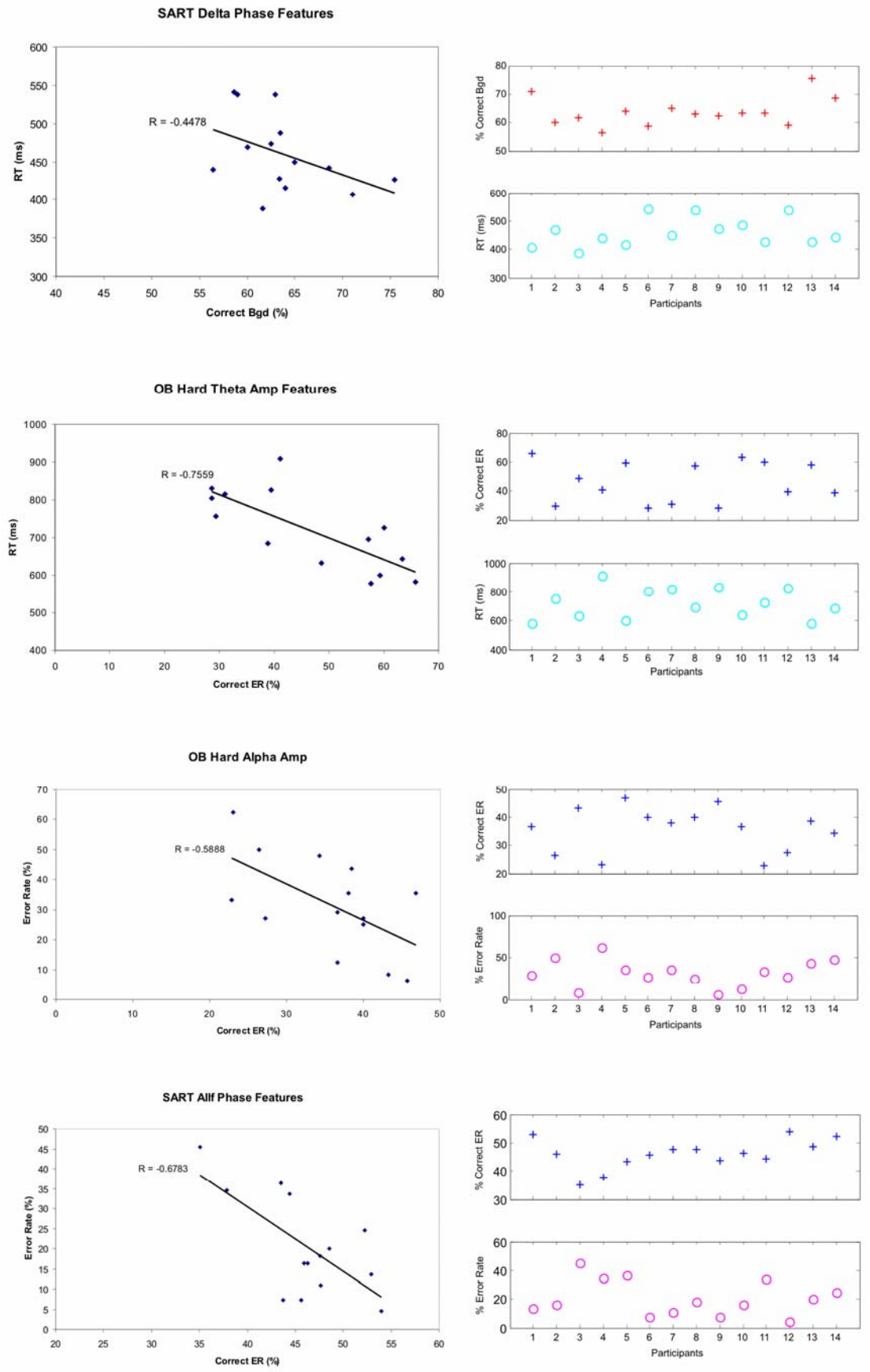

Figure 8-46 Sensitivity of classification based on delta, theta, alpha and All-*f* bands amplitude or phase features (for SART and Oddball Hard task environments) negatively correlated with behavioural data.

Some of the significant correlation results between the sensitivity of classification for the Rest and behavioural data are illustrated in Figures 8-47 and 8-48. This requires some interpretation because behavioural data is actually measured during the course of the task (in rest there is no response to stimuli). However, as previously explained, the classification results are a *differential* measure: they are indicating how distinct the band limited features are in the three different brain states. Therefore, the sensitivity of classification for the Rest is also reflecting what's happening during task; for instance, if the hypothesis is that during a task the slow waves are being taxed, then they will differ to those during rest, when the brain has "no load" imposed on it. This has been demonstrated in Section 8.9.1, where the sensitivity of the Rest classification was enhanced as task difficulty level was increased from SART to Oddball Hard task environments. This supports why behavioural data could also show correlations with the Rest classification sensitivity values.

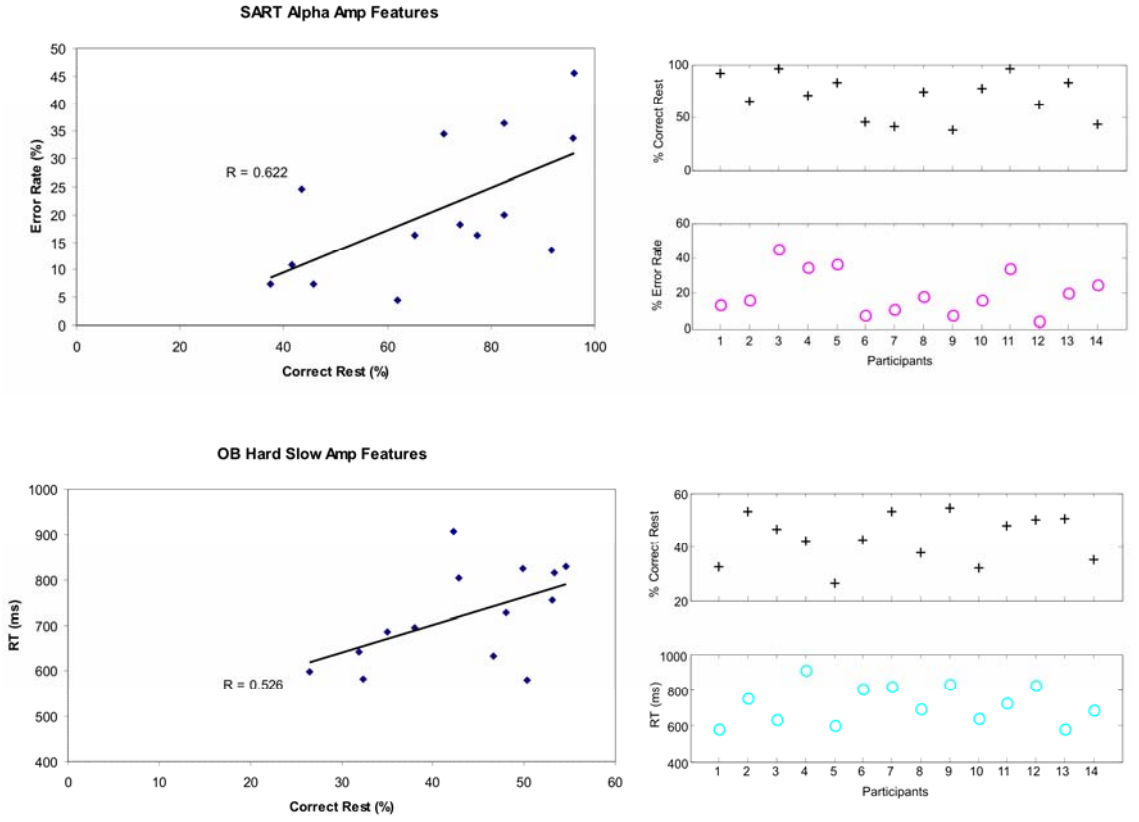

Figure 8-47. Sensitivity for the Rest classification based on slow and alpha amplitude features (for SART and Oddball Hard task environments) positively correlated with behavioural data.

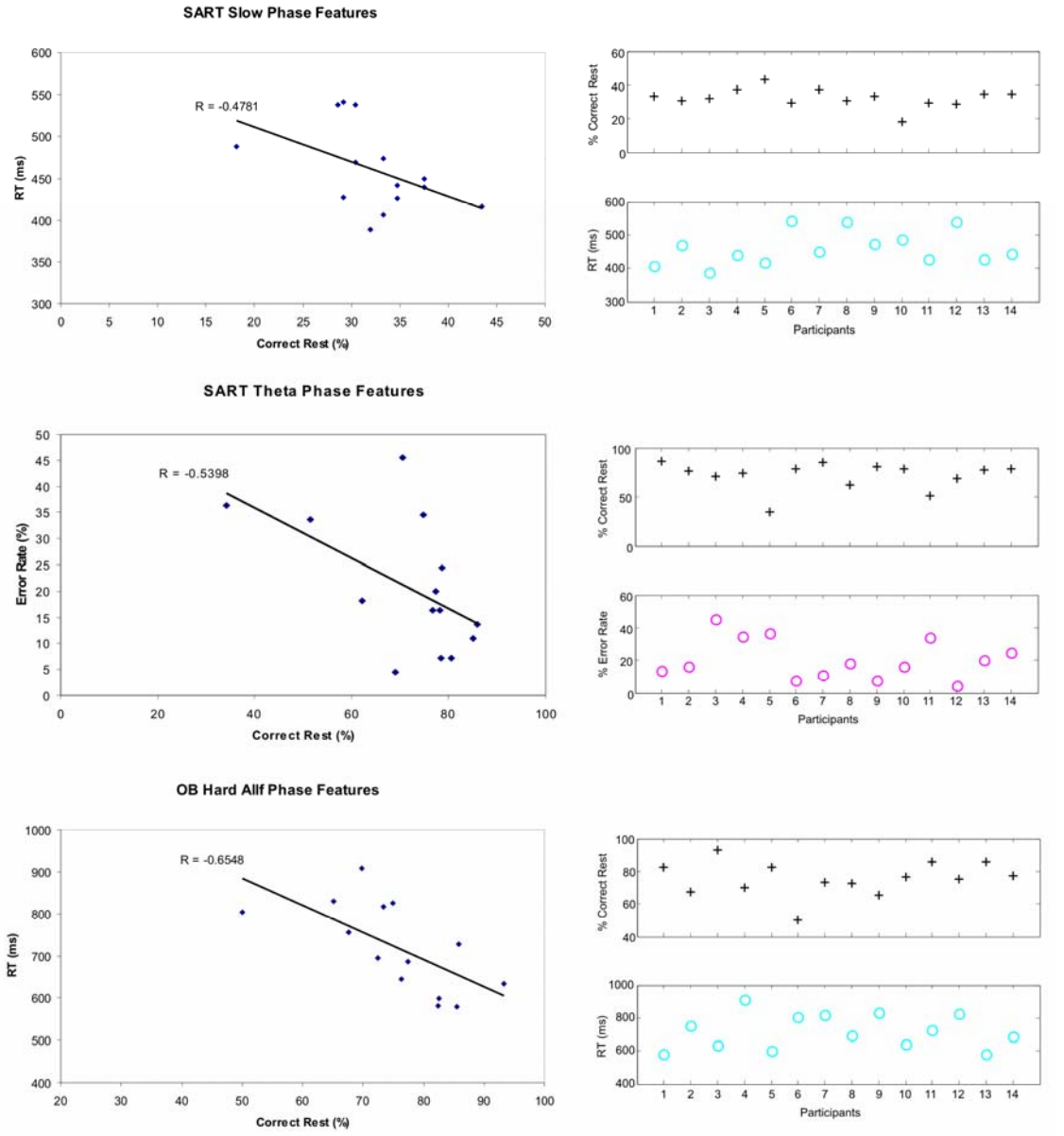

Figure 8-48. Sensitivity for the Rest classification based on slow, theta and All-*f* amplitude or phase features (for SART and Oddball Hard task environments) negatively correlated with behavioural data.

It is important to note here that the main aim of this work has been to investigate the slow waves, and despite the long recordings that have been used to obtain the classification results (which makes them robust), the number of participants (and hence the number of available performance data points) is small to perform reliable statistics on. Moreover, the work has been done on a normal, adult population (although some variability in the behavioural data is clearly visible). This implies that the interpretation of these correlation results needs to be made with caution, and the whole procedure merits further investigation on a clinical and control sample.

8.12. Summary

In this chapter, a methodology for investigating the measurable effects of the intrinsic slow waves in brain activity during periods of quiet wakefulness (rest), and whilst performing stimulus-based tasks of various difficulty levels has been developed. Here, the brain was envisaged as an oscillatory system onto which a graded load was imposed, which produced a variable output response. Particularly, the following questions have been raised: (i) How are the slow waves being affected at different loading levels? (ii) What differences are they undergoing or causing from when the brain is at rest? Furthermore, other frequency bands have also been considered, namely delta, theta and alpha, in keeping with the view that the brain comprises a system of oscillators working together at different levels of synchrony (Buzsáki and Draguhn, 2004). The experimental protocols used successfully elicited 'standard' P300 responses and the difficulty levels rendered expected variations in the P300s amplitude and latency, which were in keeping with the literature. The hypothesis underlying this work was that the slow waves provide a mechanism that modulates and perhaps even governs/controls underlying brain processes. Therefore, they may not appear in the data as distinct independent components, and information about their activity during different conditions (in various brain states) can be obtained by investigating all the relevant sources in the slow wave ($0<f<0.5$ Hz) band.

The multistage methodology developed can be summarised as follows. For each task environment:

(i) Divide the recordings into 4-5 minutes overlapping segments in order to accommodate the slow waves; employ a BSS algorithm (such as TDSEP-ICA) to denoise these segments and extract neurophysiologically meaningful brain sources (ICs).

(ii) Divide the brain sources during task into ER (related to task processing) and Background (ongoing brain activity) using hierarchical clustering based on the coherent average of the ICs.

(iii) Derive the ICs from resting-state recordings; these can be ordered (sub-optimally) according to their frequency content.

(iv) Repeat steps (i)-(iii) for all participants in order to form a databank of ER, Background and Rest ICs, (this is essentially the training databank).

(v) Filter the databank ICs in the four frequency bands of interest (slow, delta, theta and alpha) and obtain the instantaneous amplitude and phases for each (using the Hilbert transform).

(vi) Extract a set of amplitude and phase features of these time series for each filtered IC, using for example AR models.

(vii) Employ a neural network approach (here the Neuroscale algorithm was used) to classify these features based on a distance metric derived, for example, from the Itakura Distance between the AR model parameters.

(viii) Obtain Gaussian Mixture Models in order to track the classification probability in each of the three classes based on that particular set of features.
This classification marks variations in the frequency bands, i.e. in the four oscillators' amplitude or phase, during the three types of brain activity (ER, Background and Rest).

(ix) Perform further analysis on the ICs in order to quantify and localise these variations.

Since Neuroscale and GMMs derive a transformation (rather than a simple mapping) from the training data, a new batch of recordings can be treated as a test dataset, their features (obtained by following steps (i)-(vi)) can be projected onto the output of the training system, and the classification probabilities derived accordingly.

In this study, classification results show consistent variations between the brain sources during ER and Background task activity, and during Rest for all four oscillators. Particularly, using only the slow wave amplitude or phase features one can distinguish between the three distinct types of brain activity, and the sensitivity of classification is enhanced for higher task difficulty (from SART to Oddball Hard). Moreover, both the amplitude and phase of the ER and Background task brain sources are very different in the slow wave band. From the projections shown in Figures 8-38 to 8-40, this distinction could be due to the different morphology of these two types of task ICs. Meanwhile, the consistent overlap between the rest and task classes is consistent with the slow wave theoretical models found in the literature (Fox and Raichle, 2007; Sonuga Barke and Castellanos, 2007) – the slow wave mechanism that is affecting the brain sources and/or that is being affected by the different loadings during task does not operate in a binary fashion, i.e. it is not naturally turned "on" and "off" following a rest-to-task transition. Furthermore, results suggest that slow wave mechanisms share essential similarities in the two scenarios but are distinct enough to be classified separately. It is important to note here that these classification patterns are robust since they are derived from long datasets (48 minutes) of twenty (14 training and 6 test) control participants and are repeatable across the three task environments.

Specifically, slow wave power during different task environments was lower in comparison to the rest condition. This is in keeping with the DMI hypothesis since it shows that slow wave power is attenuated during task, with rest power being 58.6% (for SART), 46.2% (for Oddball Easy) and 35.9% (Oddball Hard) higher than task power. Hence, the level of attenuation of the slow waves drops as the task difficulty level is amplified. Moreover, the slow wave phase undergoes a change

in structure (entropy) in the three states; the phase of the ER and the Rest ICs with a predominant high-delta, theta and alpha frequency content had a much higher structure than that of the Rest ICs with slow and low-delta frequency content, and the Background ICs. Slow-wave projections of the classified ICs onto the measurement space showed interesting topographies and variations in their morphology and complexity for the three types of brain activity.

Lastly, the percentage of correct classification based on the slow wave features for the ER and Background classes was found to be negatively correlated with behavioural data, and there were more significant correlations for the Oddball Hard task environment, this being the most taxing of the three tasks. This indicates that the better the participants' performance (i.e. the lower the reaction time, percentage of error rates and number of false alarms) the greater was the difference in the slow wave band between, for instance, the Task-ER and the other (Task-Background and Rest) brain activity, hence the higher the sensitivity of classification. It would be interesting to test whether the same pattern would arise if the procedure had to be repeated on a larger dataset comprising a clinical group that is generally characterised by low performance measures (such as ADHD participants) and controls. Such a test could provide useful information on the relationship between brain electrical oscillations and behaviour, which is vital for the understanding of the behavioural patterns of children suffering from various psychiatric disorders (Rothenberger, 2009). Such a dataset was unobtainable for this work however.

The next chapter concludes this dissertation and presents suggestions for prospective future work on the investigation of the slow waves in brain signal recordings and their relation to neurobehavioral disorders.

Chapter 9

CONCLUSIONS AND FUTURE WORK

9.1. Conclusions

Existing work in the literature suggests that when the brain is supposedly at rest, a.k.a. being in its default mode of activity, spontaneous VLFOs (<0.5 Hz) consume two-thirds of its energy resources. These slow waves appear to be vital for functional and/or resting-state connectivity by allowing synchronisation between diverse neuronal networks (Fox *et al*., 2006; Fox and Raichle, 2007; Balduzzi, 2008). Their consistent presence during different resting states (such as periods of quiet wakefulness and sleep) and during task-related activity (Leistner *et al*., 2007; Helps *et al*., 2008; Monto *et al*., 2008) suggests an intrinsic, continuous process, which is required to maintain awareness of ourselves, of our surroundings and of the passage of time, almost independently of any activity we engage in (Fransson, 2006). Another possibility is that this spontaneous activity reflects dynamic modulations in the brain's internal representation of the intrinsic probabilistic model for foreseen events, which the brain develops and maintains over time (Fox *et al*., 2006). On the other hand, these VLFOs may be affecting performance during goal-directed activity by interrupting efficient information processing, resulting in periodic fluctuations in attention and performance (Sonuga-Barke and Castellanos, 2007). These theories raise several questions, including: are the VLFOs in brain activity, to a certain extent, insensitive to changes in perception, attention or any other internal task-oriented neuronal activity? Are they de-activated to some degree during task in order to facilitate focused attention, similar to the de-activation of the task-negative component of the default mode? Moreover, are event related components, such as the M100s and the P300s, being modulated by VLFOs such that all the brain processes oscillate in and out of synchrony because of the fluctuating neuronal activity baseline they provide? Finally, is the slow wave mechanism affecting or perhaps even governing underlying brain processing – analogous to the function of a heart's pacemaker – forming a basis which shapes our perception and behaviour to the outside world?

A vast amount of research is currently being undertaken to successfully address these questions and to tackle the corresponding challenges. As discussed in Chapter 3, VLF brain activity is notoriously difficult to study and one must ensure that such activity is entirely neuronal and is not the result of other physiological (respiratory, cardiac and vasomotion) processes (Auer, 2008) and/or a function of the data analysis procedure. A straightforward approach for investigating these intrinsic VLFOs is to specifically analyse the raw data in the frequency range below 0.5 Hz by standard FFT-based methods. However, this approach proves to be very long and cumbersome to apply on multi-dimensional systems, such as the 148-channel MEG, because the dense and noisy nature of the recordings makes the interpretation of the results highly subjective. Denoising by proper filtering methods or by BSS techniques is definitely required and even then, the extracted low frequency sources need to be subjectively classified as purely neuronal or artifactual. Moreover, since the premise is that this spontaneous VLF activity acts as a 'baseline' that underlies brain activity elicited by the task, it may not appear as 'oscillations' in the classical sense of having peaks in the power spectra of the EEG or MEG channels *per se*, or as separate independent processes following the demixing procedure.

The fundamental aim of this work has been to explore the slow wave mechanisms in EM brain signal recordings and investigate their contribution in brain function. Psychology and neuroscience literature continuously raises the need for discovering the origin of this neural activity, its purpose, and the best way to assess and quantify it (Fox *et al*., 2006; Fox and Raichle, 2007; Balduzzi, 2008, Rothenberger, 2009). Consequently, the first step in this research has been to look at existing work (both neuroimaging and electrophysiological studies), theories and hypothesis regarding the slow waves, one of which being the DMI hypothesis (Sonuga-Barke and Castellanos, 2007), which posits that the default mode slow waves undergo an attenuation in power during cognitive active processing. This theoretical model however does not take into account the phase of these slow waves, whilst ample work (on the origin of ER responses, for example) consider the notion of phase-reordering to be vital in explaining the way brain oscillators interact and neural networks react to input stimuli (Sauseng *et al*., 2007). Hence, this work needed to take into consideration *both* characteristics of these oscillations.

Next, it was important to understand the signal processing challenges that had to be overcome in analysing this VLF activity, which algorithms were readily available that could be exploited for this purpose, and what further methodologies had yet to be developed – an example being the normalisation filter to remove the intrinsic $1/f^{\gamma}$ trend, which psychologists were finding to be a hindrance when comparing the slow wave power with that of other higher frequency oscillators. Moreover, as explained earlier, one had to ensure that any noted slow wave effects

were not due to artifacts within the data, and that they were objectively interpreted. Standard BSS techniques could be employed for denoising purposes, as well as to achieve a closer representation of the underlying independent brain sources. The independent components following the BSS decomposition represent *estimates* of these sources, hence arriving at a thinner sphere of influence between the scalp recordings and the true signal generators.

However, the choice of the BSS technique which is best suited for the type of data at hand is crucial; for example, applying a spatial ICA algorithm, such as FastICA (Hyvärinen, 1999b), on the 148-channel MEG data potentially renders 148 ICs which need to be classified and interpreted, and slow wave information properly extracted from each. Using fewer channels may compromise the quality of the decomposition because standard ICA has only spatial information (from the sensor locations) to use in the separation process. In this work, state-of-the art variants of ICA, namely SC-ICA and ST-ICA, whereby source analysis is undertaken through the use of temporal or spatio-temporal information available in EM data, were proven to be more efficient for analysing such high density systems. The input data matrix leads to a meaningful decomposition from a single (or a few) recording channel(s) since the method of delays, which forms the basis of these two algorithms, creates a rich representation of the underlying mixture of brain processes.

For these reasons, SC-ICA was first employed to extract sources of interest underlying the MEG data (supplied by the University of Madrid) from single channels in selected scalp locations. The low-frequency functional and resting state connectivity were explored by means of phase synchronisation analysis between the brain sources derived from channels of interest. This presented a way of investigating significant interactions between band-limited slow wave sources, although the method was found to be too laborious for repetition on large datasets. Preliminary results showed variations in phase locking between ADHD and control groups and indicated a corresponding change in phase synchrony between the corresponding brain regions at periods of rest and when a task was being performed.

An alternative way for investigating the slow waves' modulatory effect on the brain processes in a robust manner was then achieved by means of a trial-by-trial procedure that was carried out on the same MEG data. This study proposed an objective method which looked for circumstantial evidence of the VLF activity; it exploited the well-defined nature of the evoked response processes and extracted 'clean' M100 time series by means of ST-ICA. This ensured that the inter-trial variations in the amplitude and latency of the responses could not be attributed to

physiological and/or environmental artifacts. Moreover, the frequency characteristics of these variations were found to be slightly variable across subjects (showing that it is unlikely for these effects to be artifactual), but they all fell within the frequency range of the intrinsic slow waves reported in fMRI BOLD imaging studies.

Next, a new experimental framework for investigating default mode brain activity in contrast with that during externally imposed cognitive tasks of various difficulty levels was developed in order to gain insight into the functional role of the slow waves persisting throughout in a more direct manner. In these experiments, the brain was envisaged as a system comprising a number of oscillators at varying frequencies (Rothenberger, 2009), onto which a graded load was imposed to yield a variable output response – the P300. EEG data were recorded from 23 healthy adult controls and a new multistage signal processing system was developed for its analysis. This comprised: (i) The application of BSS for denoising the data and extracting the underlying brain sources; (ii) Subspace analysis for the objective separation of the task ICs into brain sources related to stimulus processing (ER-ICs) and those related to background brain activity, based on hierarchical clustering; (iii) The extraction of features from the amplitude and phase of the ICs in different frequency bands. Note that here it was posited that the slow waves might not appear in the data as distinct brain sources (ICs), therefore information about their activity during different states was obtained by investigating all the brain sources in the slow wave ($0<f<0.5$ Hz) band. (iv) Classification of these features based on a neural network approach for pattern recognition using the Neuroscale algorithm and Gaussian Mixture Models. This provided a way of quantifying the changes that the slow waves (together with the delta, theta and alpha oscillators) underwent following a task-to-rest transition.

Results suggest that features of the slow wave mechanisms, such as their amplitude and phase, shared essential similarities during various rest and task conditions, but were distinct enough to be classified separately. Specifically, the slow wave power during different tasks of various difficulty levels was lower in comparison to the rest condition. This is in keeping with the DMI hypothesis since it showed that slow wave power was being attenuated during task, and the level of attenuation dropped as the task difficulty level was increased. Meanwhile, the slow wave phase underwent a change in structure (measured through entropy). Moreover, slow wave projections of the classified ICs onto the measurement space showed interesting topographies and variations in their complexity and structure for ER and background task activity, and for brain activity during rest. The level of cognitive attention (assessed by means of performance measures, namely reaction time, error rates and false alarms) exhibited significant correlations with the changes that the slow waves underwent between rest and task (assessed through the

sensitivity of classification based on the slow wave features). This points towards a relationship between slow electrical oscillations and behaviour, a link that has been explored in the works by Fox *et al.* (2007), Monto *et al.*, (2008) and Helps *et al.* (in press), and is fundamental for advances in the assessment of child psychiatric disorders (Rothenberger, 2009). These experiments and results provided a basis for testing and demonstrating that very low frequency oscillations in the EEG play a specific role in brain function and are far more than irrelevant noise. The original signal processing and neurophysiological contributions which resulted from this research are illustrated in Figure 9-1.

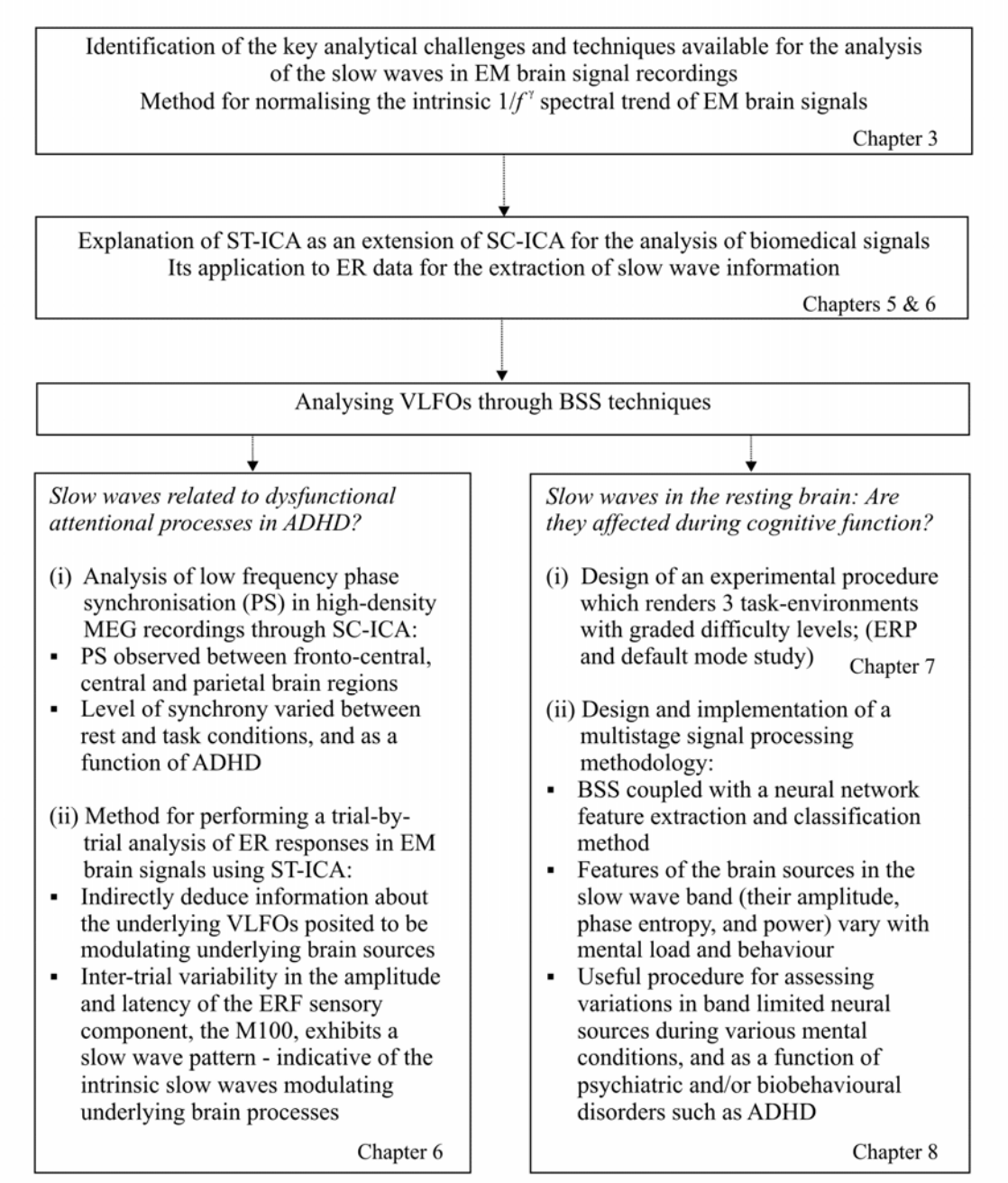

Figure 9-1. Summary of the original contributions of this research.

9.2. Future Work

As acknowledged in the first chapter of this work, the road to discovery of how the human brain generates cognition and behaviour, and the contribution of the slow waves towards this, is long and intricate. We are still somewhat at the beginning of this road, and although the findings that resulted from this work are promising, further research and development is clearly merited. In keeping with this research, the most viable approach seems to be one that incorporates psychology, neuroscience and engineering to: (i) advance the neurophysiological and psychological understanding of the slow wave mechanisms by formulating new theoretical models and hypothesis, and revising existing ones; (ii) improve current signal processing techniques, and develop new methodologies in order to test and challenge these hypothesis. Some prospective future work that would be highly beneficial to this field is outlined below.

9.2.1. Signal Processing Advances

Studies on coherent and phase synchronous structures are essential for investigating the active integration of distributed oscillators within the brain (Quian Quiroga *et al*., 2002; Pereda *et al*., 2005). These tools, when coupled carefully with BSS algorithms, can provide a reliable measure of brain areas interactions during various task environments. They could also aid in significantly identifying active seed regions (for example, in prefrontal areas and in the temporal and parietal cortex) in relation to the slow waves. An interesting addition to the multistage system developed in this work would be to establish a robust method for locating which areas of the brain are exhibiting the attenuation of power and/or the change in phase following the task-to-rest transition. Moreover, it would be useful to locate a slow wave network(s) of activity (by means of coherence or phase synchronisation measures) during rest and to examine how this is altered during tasks of various difficulty levels. As explained in Chapter 2, fMRI BOLD imaging studies revealed two diametrically opposed brain networks spanning regions that regularly experience task-related activations or deactivations; these networks demonstrate patterns of VLF correlations within their regions and anticorrelations with respect to the other network (Fox *et al*., 2005). Whether such patterns could be observed in the EM data remains open to investigation.

The novel application of ST-ICA for the extraction of ER brain processes from high density and noisy recordings in this work, demonstrate the potential of this newly-introduced algorithm as a spatio-temporal decomposition approach. However, further research is necessary on interpreting the extracted processes, each comprising *n* projected components (one per channel of interest), and on establishing ways for exploiting this information to assess the functional connectivity of various brain regions. Currently, the clustering of the spatio-temporal filters present in the

columns of the mixing matrix (learnt by FastICA) is performed manually based on the spectral characteristics of these filters. To this end, future work is required to develop an automated clustering method that makes use of the spatial, temporal and spectral modalities available in this framework.

Moreover, work in the literature shows that the phases of the brain oscillators carry crucial information about their dynamics (Buzsáki and Draguhn, 2004; Monto *et al*., 2008). This calls for the development of BSS strategies that base their separability criterion on the degree of significant phase locking between the sensor measurements for the extraction of underlying brain sources which are *maximally non-phase synchronous*.

9.2.2. Neurophysiologic and Psychological Advances

From this aspect, extensive clinical and control groups need to be recruited in order to assess variations in the slow waves (for example, by using the experimental framework developed in this work) as a function of neurological and biobehavioural disorders, such as epileptic seizures, ADHD, autism and schizophrenia, amongst others. Furthermore, the link between the findings obtained from EM and neuroimaging studies still needs to be established. This is because, as explained in Chapter 4, although the fMRI BOLD signal is closely linked to ongoing neuronal events in the brain's excitatory synapses, the actual relation between spontaneous BOLD activity and electrical/magnetic fluctuations measured by EEG and MEG remains to be determined (Huettel *et al*., 2004; Debener *et al*., 2006, Herrmann and Debener, 2008). Thus, for instance, direct comparisons between the 0.1 Hz fluctuations observed in the BOLD signals and the VLF activity patterns obtained in this work need to be considered with caution. Multimodal studies that include combined EEG, MEG and fMRI can provide a more solid understanding of the underlying neuronal dynamics, therefore providing additional insights into the presence and functionality of this intrinsic VLF activity.

Lastly, parallel advances in *both* domains are essential for broadening our understanding of the elaborate architecture of the human brain. This will pave the way for the prevention, accurate diagnosis and treatment of various psychiatric and neurobehavioural disorders.

Appendix I

FORMS FOR THE EEG EXPERIMENTS

1. Insurance and Research Governance Application Form
2. Ethics Form for the School of Psychology Ethics Committee
3. Risk Assessment Form
4. Participant Information Sheet
5. Consent Form for Research Participants – EEG experiment
6. Debriefing Statement for Research Participants – EEG Experiment
7. Barkley Adult ADHD Rating Scales
8. Demographics Questionnaire

Insurance and Research Governance Application for Projects Requiring Approval by Ethics Committee and Involving Research on Human Subjects, their tissues, organs or data, by Staff and/or Students of the University of Southampton

The project must not commence until insurance, ethics approval and sponsorship are obtained

PART A - PLEASE COMPLETE ALL QUESTIONS

1.

Ethics Submission Number: CD2

Title of Study: Very low frequency EEG-ERP recordings for testing the Default Mode Interference Hypothesis in a normal adult population

Start date: (02/02/2009) End date: (30/07/2009)

2.

Researcher's Details

Title: Miss Name: Charmaine Demanuele

University School: Psychology & Institute of Sound &Vibration Research

University Department/Division: Signal Processing & Control Group, ISVR,

Address: Tizard Building 13,
University of Southampton, Highfield,
Southampton, SO17 1BJ

Tel: 023 8059 4932 Email cd3@soton.ac.uk

3. Are student researchers involved with this project? Yes ☒ No ☐

4. Is the study based solely on questionnaires, or other research **not** involving invasive techniques or medicinal products? Yes ☒ No ☐

5.

Please estimate numbers of volunteers participating in the study:

	Adults	Minors *
Patients		
Healthy human volunteers	25	

* Minors under 18 years of age

Is this a Multi Centre Trial? Yes ☐ No ☒

If yes and the trial is sponsored by UoS or SUHT, or managed by UoS, please estimate numbers of volunteers participating in the study overall:

	Adults	Minors
Patients		
Healthy human volunteers		

6. Does the study involve invasive techniques? Yes ☐ No ☒

7.	Does the study involve the use of a medicinal product or the testing of a medical device?	Yes ☐ No ☒
	IF AN INVESTIGATIVE MEDICINAL PRODUCT IS INVOLVED Please indicate which phase category the study falls into	Phase 1, 2, 3, 4
8.	Who is the Research Sponsor?	School of Psychology & ISVR Rayleigh Scholarship
9.	Who is the Funder?	N/A
10.	**For Commercial trials only**, is an ABPI Indemnity being given?	Yes ☐ No ☐
	IF YES: the ABPI Indemnity form, preferably in triplicate, should be forwarded with this form for signature by an Authorised Signatory on behalf of the University.	
	Will any part of this study take place outside the UK?	Yes ☐ No ☒
	If Yes, in which country(ies)?	

PART B - PLEASE COMPLETE QUESTIONS AS APPLICABLE

11. **For Student projects** Student status: PG

Supervisor's Details	
Title: Professor	Name: Edmund Sonuga-Barke
University School	School of Psychology
University Department or Division	School of Psychology
Address:	University of Southampton
	Highfield,
	Southampton, SO17 1BJ
Tel: 023 8059 4604	Email ejb3@soton.ac.uk

12. **For multi site studies**

How many sites are involved? _____

Is Southampton the lead site? _____

Are any sites outside the UK? _____

Are contracts/site agreements in place? _____

13. **For studies involving the NHS Patients, staff or resources**

Is the study approved by the NHS Trust R+D office? Yes ☐ No ☐ Pending ☐

Is the study approved by NHS ethics committee? Yes ☐ No ☐ Pending ☐

14. **For Clinical Trials involving drugs, devices or clinical interventions** **Reference Number**

Is the study registered with the MHRA?	Yes ☐ No ☐	
Is the study registered on the European Clinical Trials (EudraCT) database?	Yes ☐ No ☐	
Is the study registered on the National Research Register (Clinical trials database)?	Yes ☐ No ☐	

	For studies using tissue samples	
15.	Are the tissue samples accessed via a licensed tissue bank?	Yes ☐ No ☐
	Are you seeking ethical approval for your study?	Yes ☐ No ☐
	For all studies, will the Applicant be responsible for:	
16.	Reporting amendments to the protocol	Yes ☒ No ☐
	Reporting adverse events and significant developments	Yes ☒ No ☐
	If No, who will be responsible?	

For Research Governance information, please contact:

Research Governance Office, Email: rgoinfo@soton.ac.uk Tel: 02380 598849

Website: http://www.resource1.soton.ac.uk/legalservices/rgo/index.html

For Insurance information, please contact:

Finance Department, Insurance Services, Email: insure@soton.ac.uk Tel: 02380 592417

Website http://www.soton.ac.uk/finance/insurance/index.html

Please send this form with all other supporting documents to:
Research Governance Office, University of Southampton, B37/4009, Highfield, Southampton SO17 1BJ or email to rgoinfo@soton.ac.uk.

Ethics Form

This ethics form submission is for working with humans

1. General Information

Study Title: Very low frequency EEG-ERP recordings for testing the Default Mode Interference Hypothesis in a normal adult population

Submitters:

Charmaine Demanuele
Dr Christopher James
Prof Edmund Sonuga-Barke

Advert for Psychobook:

N/A

How may you be contacted?

cd3@soton.ac.uk

Into which category does your research fall?

PhD Research

Supervisors

Dr Christopher James
Prof Edmund Sonaga-Barke

2. Study Protocol

Motivation
It has been suggested that the human brain is intrinsically organised into dynamic, anti-correlated functional networks (Fox et al., 2005).The aim of the researcher's work is to investigate the so-called default mode network (Broyd et al., in press) – which is active when the brain is apparently at rest – and networks of brain activity related to a given task, in electroencephalographic (EEG) recordings. Thus, it is required to collect EEG data during various rest and task conditions which will then be analysed using novel blind source separation techniques, in particular independent component analysis (ICA) (Hyvärinen et al., 2001).

Background
Functional magnetic resonance imaging (fMRI) studies of the brain have shown that brains of individuals undertaking no externally imposed cognitive tasks display patterns of spontaneous, intrinsic activity synchronised across widely distributed brain regions. This 'default mode' network is particularly observable during resting states and is associated with stimulus independent processes (Fransson, 2005). Spontaneous low frequency oscillations (LFOs) associated with this network are commonly attenuated during goal-directed tasks. However, they sometimes re-emerge during periods of task-related active processing, competing and interfering with goal-directed attention. This results in low frequency toggling between the task-independent (-negative) and task-positive components and presents a potential source of attention deficit during active task performance. This forms the basis of the default mode interference (DMI) hypothesis (Sonuga-Barke & Castellanos, 2007).

Event-related potentials (ERPs) are a basic, non-invasive method of neurophysiological investigation. The P300 is a well-studied late ERP component which is produced by a distributed network of brain processes associated with attention and memory operations (Polich, 2007). Oddball paradigms and Go No-go tasks are two ERP task-types particularly aimed at eliciting the P300 response which have been well tested and documented in the literature (Comerchero & Polich, 1998; Datta et al., 2007; Hagen et al, 2006; Katayama & Polich, 1996; Polich, 2007; Smallwood et al., 2008). The three-stimulus oddball paradigm involving a target, a standard stimulus and a distracter, where subjects respond to an infrequently occurring target stimulus, is often employed (Katayama & Polich, 1996). The perceptual discrimination difficulty between the target and the more frequently occurring standard stimuli can be varied to provide an easy or difficult task scenario – a high discrimination difficulty appears to engage frontal attentional mechanisms more strongly, producing large frontal/central P300 components (Comerchero & Polich, 1996; Hagen et al., 2006). On the other hand, the Go No-go sustained attention to response task (SART) requires the participant to respond to one stimulus type (go) and withhold a response to an infrequent stimulus (no-go) appearing in an unpredictable manner. The rhythmic nature of the task is designed to establish a relatively automatic, task-driven response (Datta et al., 2007). This has proved to be sensitive to the frequency of everyday action lapses in both traumatically brain injured patients and in healthy controls, and can thus be used to establish a measure for sustained attention (Smallwood et al., 2008).

This study will involve two separate sets of recordings, the first one based on the three stimulus oddball paradigm and the

second one based on the Go No-go task. In each recording, task blocks will then be separated by rest blocks for testing the DMI hypothesis.

Analysis

Data analysis will have two main approaches:

(a) Approaching the recordings as being blocks of task and rest EEG activity, hence differentiating between brain activity in the presence and absence of stimulation,

(b) Analysing the evoked potentials within the task blocks (ERP data),

both approaches taken in relation to the DMI hypothesis.

First, data analysis will be aimed at addressing questions such as: (i) Can the LFOs associated with the default network be identified within EEG recordings? (ii) Are distinct brain areas interacting during different rest and task conditions, forming a network of brain activity? (iii) Is there a change in this interaction with a switch from rest to task? Various ICA algorithms and techniques (Davies & James, 2007; Debener et al., 2005; Demanuele et al., 2008; Hyvärinen et al., 2001) will be employed to isolate neurophysiologically meaningful, low frequency brain sources in the presence of higher frequency brain activity and artifacts. Interaction between these sources will then be quantified by coherence and phase synchronisation measures. Coherence is a measure of the linear correlation of two signals as a function of frequency, whereas phase synchrony indicates whether the phase shift between the two signals is close to a constant over the specified time interval. These are widely used in the literature as vital mechanisms for dynamic integration of distributed oscillators within the brain (Lachaux et al., 1999; Quiroga et al., 2002).

Due to the nature of the tasks chosen for this study, ERP component measures such as P300 amplitude and latency could be exploited to formulate an index for the level of attention during tasks (Polich, 2007). This could then be compared and contrasted with brain networks' activation patterns obtained as described above. Particularly, the Go No-go SART task could be used to indicate the individual's capacity to maintain active attention control over the responses instead of being carried along with the regular pacing of the task (Datta et al., 2007; Smallwood et al., 2007). Hence, an index for sustained attention could be established by considering the mean value of P300 amplitude across the whole SART. Relationship between P300 amplitude and error rates could also be used for this purpose (Datta et al., 2007). Moreover, the modulation of the P300 response by the LFOs on a trial-by-trial basis leads to periodic amplitude fluctuations of the P300. This could be associated with fading in and out of attention caused by the intrusion of the task negative component during task blocks, which reduces the cognitive resources allocated for the task. The length of the experiment recordings is chosen to accommodate the long-period slow waves, and to be adequate to measure sustained attention.

References:

Broyd, S.J., Demanuele, C., Debener, S., Helps, S. K., James, C. J. and Sonuga-Barke, E.J.S. (2008). Default-mode brain dysfunction in mental disorders: a systematic review, *Neuroscience & Biobehavioral Reviews*. Article in Press.

Comerchero, M. D. and Polich, J. (1998). P3a, perceptual distinctiveness and stimulus modality, *Cognitive Brain Research*, 7, 41-48.

Datta, A., Cusack, R., Hawkins, K., Heutink, J., Rorden, C., Robertson, I.H., and Manly, T. (2007). The P300 as a marker of waning attention and error propensity, *Computational Intelligence and Neuroscience*, 9pgs.

Davies, M. E. and James, C. J. (2007). Source separation using single channel ICA, *Signal Processing*, 87, 1819-1832.

Debener, S., Makeig, S., Delorme, A. and Engel, A. K. (2005). What is novel in the novelty oddball paradigm? Functional significance of the novelty P3 event-related potential as revealed by independent component analysis, *Cognitive Brain Research*, 22, 309-321.

Demanuele, C., James, C.J., Capilla, A, Sonuga-Barke, E.J.S. (2008). Extracting event-related field components through space-time ICA: a study of MEG recordings from children with ADHD and controls, *4th European Congress for Medical and Biomedical Engineering, EMBEC 2008, Antwerp, Belgium; ECIFMBE Proceedings*, 22, 38-42.

Fox, M.D., Snyder, A. Z., Vincent, J. L., Corbetta, M., Van Essen, D.C. and Raichle, M.E.(2005). The human brain is intrinsically organized into dynamic, anticorrelated functional networks. *Procedings of the National Academy of Sciences of the United States of America*, 102, 9673-9678.

Fransson, P. (2005). Spontaneous low-frequency BOLD signal fluctuations: An fMRI investigation of the resting-state default mode of brain function hypothesis, *Human Brain Mapping*, 26(1), 15-29.

Hagen, G. F., Gatherwright, J. R., Lopez, B. A., and Polich, J. (2006). P3a from visual stimuli: task difficulty effects, *International Journal of Psychophysiology*, 59, 8-14.

Hyvärinen, A., Karhunen, J. and Oja, E. (2001). *Independent Component Analysis*, Wiley, New York.

Katayama, J. and Polich, J. (1996). P300, probability, and the three-tone paradigm, *Electroencephalography and Clinical Neurophysiology*, 100, 555-562.

Lachaux, J.-P., Rodriguez, E., Lutz, A., Martinerie, J. and Varela, F. J. (1999). Measuring Phase Synchrony in Brain Signals, *Human Brain Mapping*, 8, 194-208.

Polich, J. (2007). Updating P300: An integrative theory of P3a and P3b, *Clinical Neurophysiology*, 118, 2128-2148.

Quiroga, R. Q., Kraskov, A., Kreuz, T., and Grassberger, P. (2002). Performance of different synchronisation measures in real data: a case study on electroencephalographic signals, *Physical Review E*, 65, 041903, 14 pgs.

Smallwood, J., Beach, E., Schooler, J. W., and Handy, T. C., Going AWOL in the brain: Mind wandering reduces cortical analysis of external events, *Journal of Cognitive Neuroscience*, 20(3),458-469.

Sonuga-Barke, E. J. S., and Castellanos, F. X. (2007). Spontaneous attentional fluctuations in impaired states and pathological conditions: a neurobiological hypothesis, *Neuroscience Behavioral Review*, 31(7), 977-986.

What intervention/procedure will be used? (Briefly describe the design. Explain what the participants will experience, including the duration of any task/test).

Before the EEG recording, the Barkley Adult ADHD rating scales and demographics data attached hereunder (re: epileptic seizures incidents, head injuries, vision or hearing problems and the participants' use of medication or psychoactive substances) will be collected for every participant.

EEG Recording
The scalp direct-current (DC) EEG will be recorded using a Neuroscan Synamps2 70 channel EEG system[1] at 500 Hz, with a low-pass filter at 70 Hz. Participants will be fitted with an electrode cap (Easycap; Hersching, Germany) and EEG will be recorded from 68 equidistant Ag/AgCl electrodes, with the reference electrode attached to the nose. The electro-oculogram (EOG) will be recorded using electrodes below the left and right eye. Impedance for all electrodes will be kept below 5 kΩ. A high chloride, abrasive electrolyte gel will be used to achieve a DC-stable skin-gel contact that ensures stable operation of the Ag/AgCl electrodes[2].

Three-stimulus Oddball Task
Participants will be asked to complete a 22-minute three-stimulus oddball task, consisting of two 8-minute tasks blocks separated by a 6-minute rest block. In this task, the target stimulus (probability of occurrence = 0.12) will be a blue circle 4 cm in diameter, and the distracter stimulus (0.12) will be an 16 cm^2 square with black and white checkerboard pattern (1cm checks). The size of the standard stimuli will be systematically altered by using blue circle stimuli of 2.8 cm or 3.6 cm for the easy and hard task blocks respectively (0.76). This will increase error rates and response time across task conditions. The stimuli will be presented once every 1.2 seconds for a 250 ms duration, (i.e. 400 stimuli per task block). Stimuli presentations will be randomised and condition order counterbalanced across participants. Participants will be given a practice block consisting of 15 stimulus trails before each task condition. During the rest block participants will be asked to look at the monitor in a relaxed manner while focussing on a fixation cross at the centre of the screen in order to avoid extraneous movement.

Go No-go (SART) Task
The Go No-go SART task will consist of two 10-minute task blocks separated by a 6-minute rest block. During this task single, randomised digits from 1 to 9 will be presented on the computer screen at a regular, invariant rate. Participants will be asked to use the index finger of their preferred hand to press a single button for each digit as it appears, with the exception of the digit 3. Stimuli will be presented every 1.2 seconds for a 250 ms duration, implying a total of 500 stimuli per task block, among which 60 will be No-go stimuli (i.e. 12 % No-go stimuli). As for the previous task, during the rest block participants will be asked to focus at the fixation cross at the centre of the screen.

The order of the two tasks will be counterbalanced across participants. Throughout the recordings participants will be in a quiet room free from distractions and will be seated on a comfortable chair with the 17" LCD screen positioned approximately 60 cm away. They will be asked to avoid unnecessary head movements and to respond to the task at hand 'as quickly and accurately as possible'. After the first task participants are allowed to take a break until they feel ready to continue with the experiment.

[1] http://www.compumedics.com/ and http://www.neuroscan.com/

[2] Vanhatalo, S., Voipio, J., and Kaila, K. (2005). Full-band EEG (FbEEG): an emerging standard in electroencephalography, *Clinical Neurophysiology*, 116,1-8.

What measurement procedures will be used? Please attach copies of any questionnaires to be used or copy and paste the link to your online survey.

(a) The Barkley Adult ADHD rating scales, (b) Demographics questionnaire

3. Participants

About 25 postgraduate students from the University of Southampton.

How will they be identified, approached and recruited?

PhD students who are colleagues of the researcher will be approached and asked if they are interested and willing to patricipate in this study. It will be emphasised to participants that their participation is entirely voluntary, and if they decline to participate it will not affect their relationship with the ISVR or the School of Psychology in any way. Those who agree to make an appointment, will first be provided with the Participant Information Sheet upon their visit to the lab, detailing all aspects of the experimental procedure. Secondly, the experimenter will familiarise participants with the laboratory. If the participant is then happy to continue with the experiment, they will be asked to complete and sign a Consent Form (please see the attached documents).

How will you obtain the consent of participants?

Participants will be asked to sign a Consent Form after reading the Participant Information Sheet (attached).

Is there any reason to believe participants may not be able to give full informed consent? If yes, what steps do you propose to take to safeguard their interests?

No

If participants are under the responsibility of others (such as parents/carers, teachers or medical staff) have you obtained permission to approach the participants to take part in the study?

N/A

Detail any possible discomfort, inconvenience or other adverse effects the participants may experience, including after the study, and how this will be dealt with.

There are no risks involved in this study. An EEG system records electrical activity of the brain by means of scalp electrodes, and hence it is a completely non-invasive technique. However, the abrasive gel used to provide good attachment of the electrodes to the skin might create some discomfort, (although participants will be informed about this beforehand). The researcher will apply a small amount of gel to their skin (e.g. on their hand) before the experiment starts in order to test for any possible allergies. Moreover, they will be given wet-wipes and paper towels to clean their hair after the experiment.

How will it be made clear to participants that they may withdraw consent to participate at any time without penalty?

Participants will be informed in the Consent Form and in the Participant Information Sheet that they can withdraw from the study at any time and that their decision will not affect their legal rights or their treatment by the Institute/School.

Will the procedure involve deception of any sort?

No

How do you propose to debrief participants and/or provide them with information about the findings of the study?

Participants will be given a copy of the Debriefing Statement (attached) once the study is completed. Furthermore, participants will be informed that they have the option to contact the researcher for a summary of the research findings once the study is completed.

How will information obtained from or about participants be protected?

The data will be anonymous - each participant's file will be assigned a key-code which has no relation to the name, student number or other personal identification of the participant. EEG data will be coded and stored on a password-protected computer, and/or a password-protected hard-disk which will be locked in a filing cabinet in an academic office and to which only the researcher and the supervisors will have access. Coded questionnaires, consent forms and demographic information will be stored in a locked filing cabinet in an academic office.

4. Equipment Safety Check (A risk form must also be submitted)

Experimental apparatus employed must be approved for safety by Martin Hall. Has this approval been given?

Yes

5. Additional Checks

Do you intend to make a submission to the NHS Research Ethics Committee?
(certain projects may need NHS Ethical Approval, please check with your Supervisor)

No

Does this research involve work with children?

No

6. Technical Specifications

Please detail below any equipment required to carry out this research.

Equipment required:
Neuroscan Synamps 70 channel EEG system; and all equipment (electrogel etc) associated with EEG recording procedures;
A data acquisition computer;
3 LCD Computer screens: (Stimulus presentation monitor for the participants, Stimulus presentation monitor for the researcher; and EEG recording monitor);
Stimulus presentation program which will involve programming of markers during rest blocks and programming of the two tasks;
Neurscan software for Data acquisition;
Brain Vision Analyser Software for Data analysis;
Matlab Software for Data analysis.

School of Psychology Risk Assessment Form (As Part of the Ethics Submission Procedure)

Study Title

Very low frequency EEG-ERP recordings for testing the Default Mode Interference Hypothesis in a normal adult population

Brief outline of the study

This study investigates electrophysiological activity during periods of rest and during visual, stimuli-based tasks. EEG will be recorded for the whole duration of the experiment, using a Neuroscan Synamps2 70-channel EEG system. Participants will be fitted with an electrode cap (Easycap; Hersching, Germany) and EEG will be recorded from 68 equidistant Ag/AgCl electrodes with the reference electrode attached to the nose. Two electro-oculogram (EOG) electrodes will be attached beneath the left and right eye to record ocular activity. During the experiments participants will be seated on a chair positioned approximately 60cm away from a computer, LCD screen. Participants will be asked to perform two tasks each containing a resting period. In these resting periods, they will be asked to relax and focus on a fixation point presented in the centre of the screen. During the tasks they will be required to respond as quickly and accurately as possible to the visual stimuli presented.

The first task will be 22 minutes long, consisting of two 8-minute task blocks separated by a 6-minute rest block. The second task will consist of two 10-minute task blocks separated by a 6-minute rest block. The whole duration of the experiment is anticipated to be approximately 2 hours, which includes the completion of a demographics questionnaire, the Barkley Adult ADHD Rating Scales, and the cap fitting.

Location

Institute of Disorders of Impulse and Attention Lab, Room 3111, School of Psychology, University of Southampton.

Significant Hazards

EEG is a standard non-invasive technique and provided all the precautionary measures necessary are taken this procedure will not pose any significant hazards to any party involved in the experiment. All associated equipment will be sanitised using appropriate sanitisation procedures: there will be no cross-contamination of the electrogel, all equipment will be appropriately cleaned following every use, and the electrocap will be regularly sterilised.

In the unlikely event of an emergency concerning either the experimenter or the participant, the phone number and location of a first aid officer and the phone number of security will be clearly displayed within the laboratory. Furthermore, a landline will be available for use in emergencies within an adjacent office at all times.

Participants, who will be colleagues of the researcher and are therefore known by the researcher, will be given the option to perform the experiment during weekends or after normal working hours. In this case, a university security and a significant other

will be informed of the testing location and the approximate duration of the data collection session to ensure the safety of the both the researcher and participant.

Who might be exposed to the hazards?

This procedure does not pose a significant hazard to either the experimenter or the research participant, provided that all precautionary measures mentioned above are taken.

Existing control measures:

Control measures include cleaning and sterilisation products to sanitise all equipment associated with the EEG recording.

As stated above the phone number and location of a first aid officer and the phone number for University security will be clearly displayed at all times. A landline will be available for use at all times in case of emergency.

Are risks adequately controlled?

Yes all necessary precautionary measures will be taken to ensure the risks are adequately controlled for.

Participant Information Sheet – EEG Experiment

Study Title: Very low frequency EEG-ERP recordings for testing the Default Mode Interference Hypothesis in a normal adult population

Researcher: Charmaine Demanuele
PhD Student
School of Psychology and Institute of Sound and Vibration Research,
University of Southampton,
Highfield,
Southampton,
SO17 1BJ

Phone: 02380 594932
Email: cd3@soton.ac.uk

Ethics number: CD2

Dear Participant,

Please read this information carefully before deciding to take part in this research. If you are happy to participate you will be asked to sign a consent form.

What is the research about?
In this study we are recording the electrical brain activity during various rest and task conditions, through the use of an electroencephalogric (EEG) system. The aim of the experiment is to try and establish brain networks activation patterns during task-related activities as opposed to default mode activity, i.e. during rest, in the absence of external stimuli and goal-directed activity. This will be done in order to test the so-called Default Mode Interference Hypothesis.

Why have I been chosen?
You are being approached to take part in this study because we want to test this hypothesis on a sample of normal adult controls.

What will happen to me if I take part?
During the study, your electrical brain activity, i.e. your EEG, will be recorded whilst you perform various task blocks separated by periods of rest. Your participation will take approximately 2 hours. You will be fitted with an electrode cap, a reference electrode attached to the nose and two electro-oculogram electrodes (to measure eye activity). An electrolyte gel will be used to achieve good contact for the electrodes – this can be easily washed away after the experiment. Throughout the experiment, you will be sitting down in a quiet room on a comfortable chair and you will be asked to perform two stimulus-based, visual tasks each containing a resting period. In these resting periods, you will be asked to relax and focus on a fixation point presented in the centre of an LCD screen. During the tasks you will be required to respond as quickly and accurately as possible to the visual stimuli presented. In between the two tasks you will be given a break until you feel ready to proceed with the experiment. EEG will be recorded in all experimental sessions. Prior to the EEG recording, you will be asked to fill out a questionnaire assessing a variety of demographic factors and to complete the Barkley Adult ADHD rating scales.There will be no follow up visit. However you are given the opportunity to contact the researcher for more information about the findings of this study once it is completed.

Are there any benefits in my taking part?
There may be no specific benefit to you, other than getting knowledge about how electrical brain activity is recorded. However, since this is novel research work, your participation will help add to current knowledge in this field. Analysis of the data collected from this work could shed light on the cause of attention lapses experienced in several neurobehavioral disorders such as Attention Deficit/Hyperactivity Disorder (AD/HD).

Are there any risks involved?
There are no risks involved in this study. An EEG system records electrical activity of the brain by means of scalp electrodes, and hence it is a completely non-invasive technique. Before placing the electrodes on the scalp, nose and around the eyes, these sites will be gently cleaned with alcohol. Abrasive gel will also be used to provide good attachment of the electrodes to the skin. This might create some discomfort and you will be consulted first to ensure that you are comfortable with this procedure. You will be given wet-wipes and paper towels to clean your hair after the experiment.

Will my participation be confidential?
This research complies with the Data Protection Act and University Policy. The data will remain anonymous – your file will be assigned a key-code which has no relation to your name, student number or other personal identification. Collected data will be treated confidentially. It will be coded and stored on a password-protected computer to which only the researcher and the supervisors will have access.

What happens if I change my mind?
You can withdraw from the study at any time and your decision will not affect your legal rights or your treatment by the Institute/School.

What happens if something goes wrong?
If you have any concerns or complaints about this research, or if you have any questions about your right as a participant in this study, please contact: the researcher (cd3@soton.ac.uk) or the Chair of the Ethics Committee on:

Chair of the Ethics Committee
School of Psychology
University of Southampton
Southampton, SO17 1BJ.
Phone: (023) 8059 5578.

Where can I get more information?
If you would like any further information about this study, kindly contact the researcher (cd3@soton.ac.uk) or Dr. Christopher James (C.James@soton.ac.uk) and Prof Edmund Sonuga-Barke (ejb3@soton.ac.uk) who are supervising this study, and they will gladly answer any other queries that you may have.

Consent Form for Research Participants – EEG experiment

Very low frequency EEG-ERP recordings for testing the Default Mode Interference Hypothesis in a normal adult population

Information sheet

I am Charmaine Demanuele, a third year PhD student. My project is a collaboration between the School of Psychology and the Institute of Sound and Vibration Research (ISVR) at the University of Southampton. I am requesting your participation in a study for the recording of electrical brain activity during various rest and task conditions, through the use of an electroencephalogram (EEG) system. You will be fitted with an EEG electrode cap and your participation will take approximately 2 hours. Throughout the experiment, you will be sitting down in a quiet room on a comfortable chair and you will be asked to perform two stimulus-based, visual tasks each containing a resting period. In these resting periods, you will be asked to sit quietly and relax, while during the tasks you will be required to respond as quickly and accurately as possible to stimuli presented on an LCD screen. In between the two tasks you will be given a break until you feel ready to proceed with the experiment. Prior to the EEG recording, you will be asked to fill out a questionnaire assessing a variety of demographic factors and to complete the Barkley Adult ADHD rating scales. Personal information will not be released to or viewed by anyone other than researchers involved in this project. Results of this study will not include your name or any other identifying characteristics, and by doing such, confidentiality will be ensured.

Your participation is voluntary and you may withdraw your participation at any time. If you choose not to participate there will be no consequences to your grade or to your treatment as a student in the School of Psychology or in the ISVR. If you have any questions please ask them now, or contact Charmaine Demanuele at 023 8059 4932 or cd3@soton.ac.uk

Signature: _____ Date: _____

Charmaine Demanuele

Statement of Consent

I have read the above informed consent form. I understand that I may withdraw my consent and discontinue participation at any time without penalty or loss of benefit to myself. I understand that data collected as part of this research project will be treated confidentially, and that published results of this research project will maintain my confidentially. In signing this consent letter, I am not waiving my legal claims, rights, or remedies. A copy of this consent letter will be offered to me.

I give consent to participate in the above study.

Signature:_____ Date:_____

Name: _____(please print)

I understand that if I have questions about my rights as a participant in this research, or if I feel that I have been placed at risk, I can contact the Chair of the Ethics Committee, Department of Psychology, University of Southampton, Southampton, SO17 1BJ. Phone: (023) 8059 5578.

Debriefing Statement for Research Participants – EEG Experiment

Very low frequency EEG-ERP recordings for testing the Default Mode Interference Hypothesis in a normal adult population

The aim of this research was to investigate the default mode network(s) – i.e. the brain network that is active when the brain is apparently at rest – and networks of brain activity related to a given task, in electroencephalographic (EEG) recordings. The 'default mode' network is particularly observable during resting states and is associated with stimulus independent processes. Spontaneous low frequency oscillations associated with this network are commonly attenuated during goal-directed tasks. However they sometimes re-emerge during periods of task-related active processing, competing and interfering with goal-directed attention. This produces a potential source of attention deficit during active task performance, and could be the consequence of attention lapses experienced in several neurobehavioral disorders such as Attention Deficit/Hyperactivity Disorder (AD/HD). Analysis of your data will help our understanding of brain activity during different brain stimulation conditions, and in relation to the level of attention during specific tasks. Once again results of this study will not include your name or any other identifying characteristics. The experiment/research did not use deception. You may have a copy of the summary of the research findings once the project is completed.

If you have any further questions please contact Charmaine Demanuele at 023 8059 4932 or cd3@soton.ac.uk.

Thank you for your participation in this research.

Signature: _____ Date:_____

Name: _____

If you have questions about your rights as a participant in this research, or if you feel that you have been placed at risk, you may contact the Chair of the Ethics Committee, Department of Psychology, University of Southampton, Southampton, SO17 1BJ. Phone: (023) 8059 5578.

Barkley Adult ADHD Rating Scales

Subject code: [ ]

Please circle the response which best describes <u>your behaviour</u> over the past six months:

Frequency Code: 0=never
1=occasionally
2=often
3=very often

1. Fail to give close attention to details or make careless mistakes at work	0	1	2	3
2. Fidget with hands or feet or squirm in seat	0	1	2	3
3. Have difficulty sustaining attention in tasks or fun activities	0	1	2	3
4. Leave seat in situations where seating is expected	0	1	2	3
5. Don't listen when spoken to directly	0	1	2	3
6. Feel restless	0	1	2	3
7. Don't follow through on instructions and fail to finish work	0	1	2	3
8. Have difficulty engaging in leisure activities quietly	0	1	2	3
9. Have difficulty organizing tasks and activities	0	1	2	3
10. Feel "on the go" or "driven by a motor"	0	1	2	3
11. Avoid, dislike, or are reluctant to engage in work that requires sustained mental effort	0	1	2	3
12. Talk excessively	0	1	2	3
13. Lose things necessary for tasks and activities	0	1	2	3
14. Blurt out answers before questions have been completed	0	1	2	3
15. Easily distracted	0	1	2	3
16. Have difficulty awaiting turn	0	1	2	3
17. Forgetful in daily duties	0	1	2	3
18. Interrupt or intrude on others	0	1	2	3

Demographics Questionnaire

Subject code: [ ]

Dear Participant,

Please answer all questions listed below. If you have any questions about the following, please do not hesitate to ask the researcher.

Contact phone number: ……

Date of birth: ……

Sex (circle): **Male / Female**

Your handedness (circle): **Left / Right**

Please circle Yes or No to the following questions:

Have you consumed any product containing caffeine in the last two hours? **Yes/No**

Are you currently on any form of medication? **Yes/No**

If yes please specify:…….

Have you ever suffered an epileptic seizure? **Yes/No**

If yes please specify:…….

Have you ever suffered any serious head injuries or periods of unconsciousness? **Yes/No**

If yes please specify:…….

Do you have any vision problems? **Yes/No**

If yes please specify:…….

Do you have any hearing problems? **Yes/No**

If yes please specify:…….

Is English your first language? **Yes/No**

Have you used any psychoactive substance in the past 24 hours? **Yes/No**

Have you used any psychoactive substance more than once a month in the last 6 months? **Yes/No**

Appendix II

ADDITIONAL CLASSIFICATION RESULTS

(A) Classification based on the first set of features derived for the ER, Background and Rest ICs (as described in Chapter 8.5.1), namely the power in the instantaneous amplitude envelope and the 2nd to 4th order moments of the instantaneous phase (i.e. the variance, skewness and kurtosis) for each frequency band. The results below show some of the cases when the ICs were characterised by (i) the four features of the slow, delta, theta and alpha frequency bands (16 features from All *f*-bands), or (ii) the four features of the slow wave band. They were obtained by using 10 participants as training data.

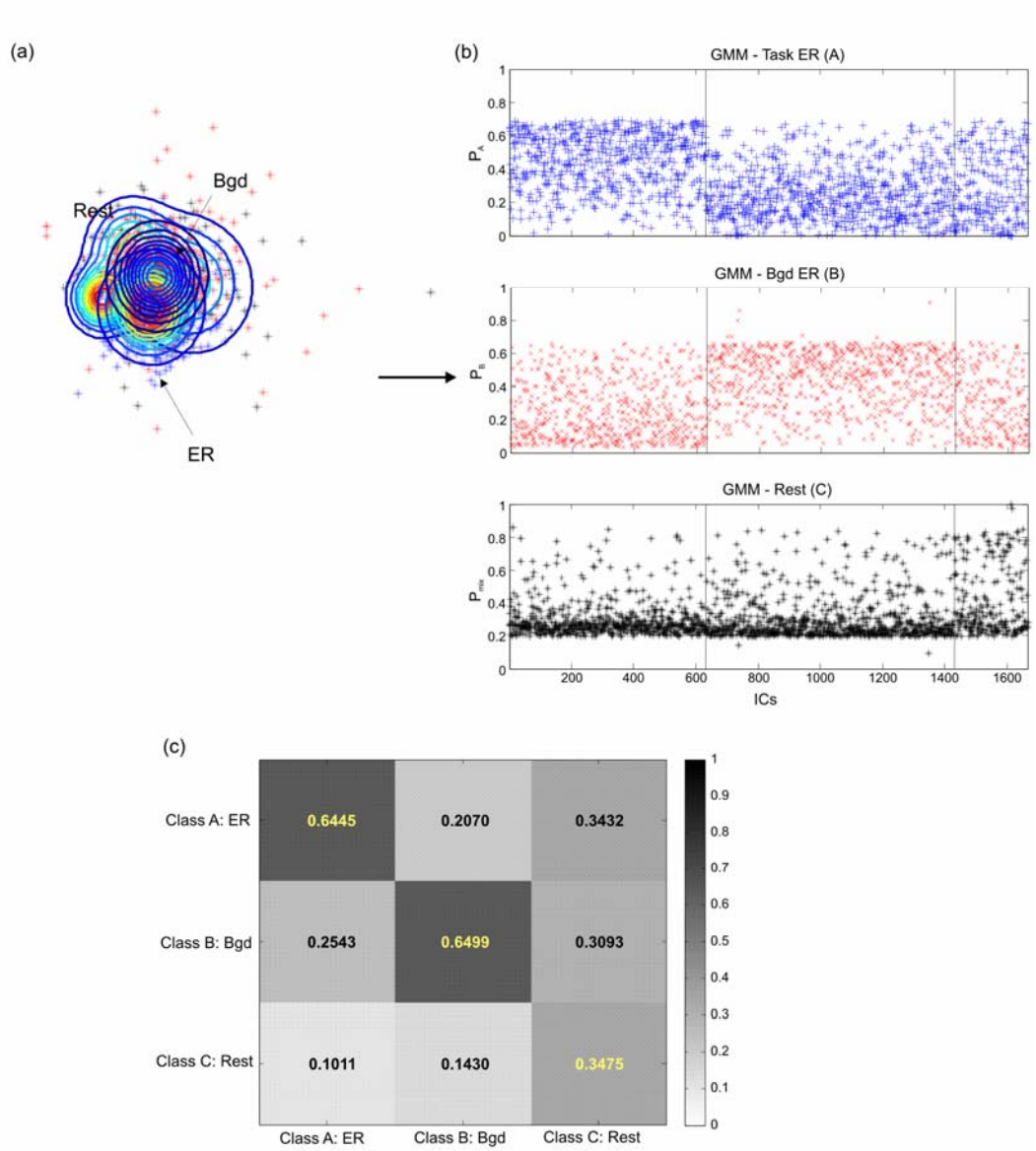

Figure II-1. Classification results based on 16 features (from All-*f* bands) of the ICs for the SART: (a) GMM contour plots for the neuroscale output, (b) Posterior probabilities from the GMMs of the three classes, (c) Confusion map showing sensitivity of classification on the diagonal.

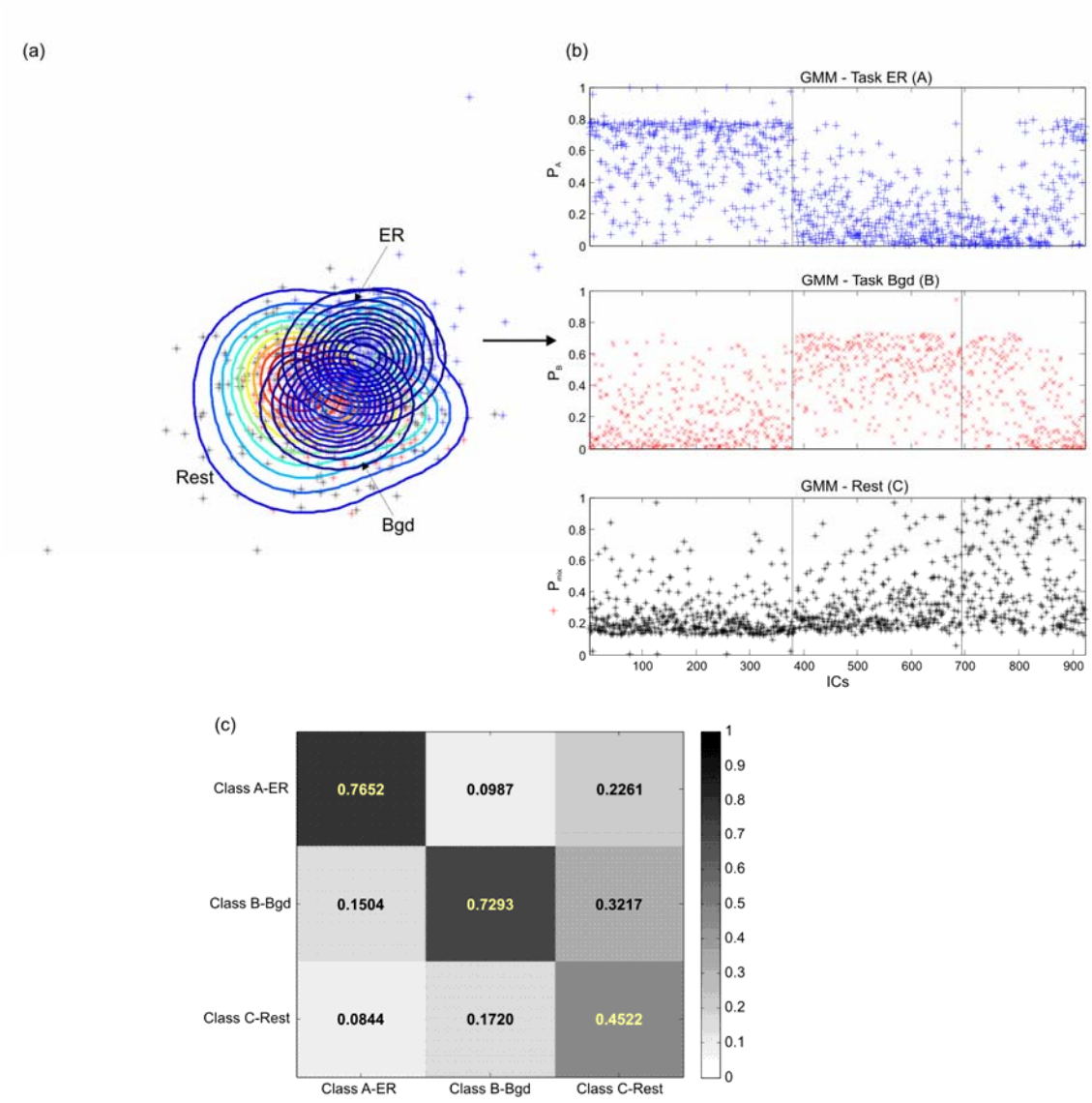

Figure II-2. Classification results based on 16 features (from All-*f* bands) of the ICs for the Oddball Easy task environment: (a) GMM contour plots for the neuroscale output, (b) Posterior probabilities from the GMMs of the three classes, (c) Confusion map showing sensitivity of classification on the diagonal.

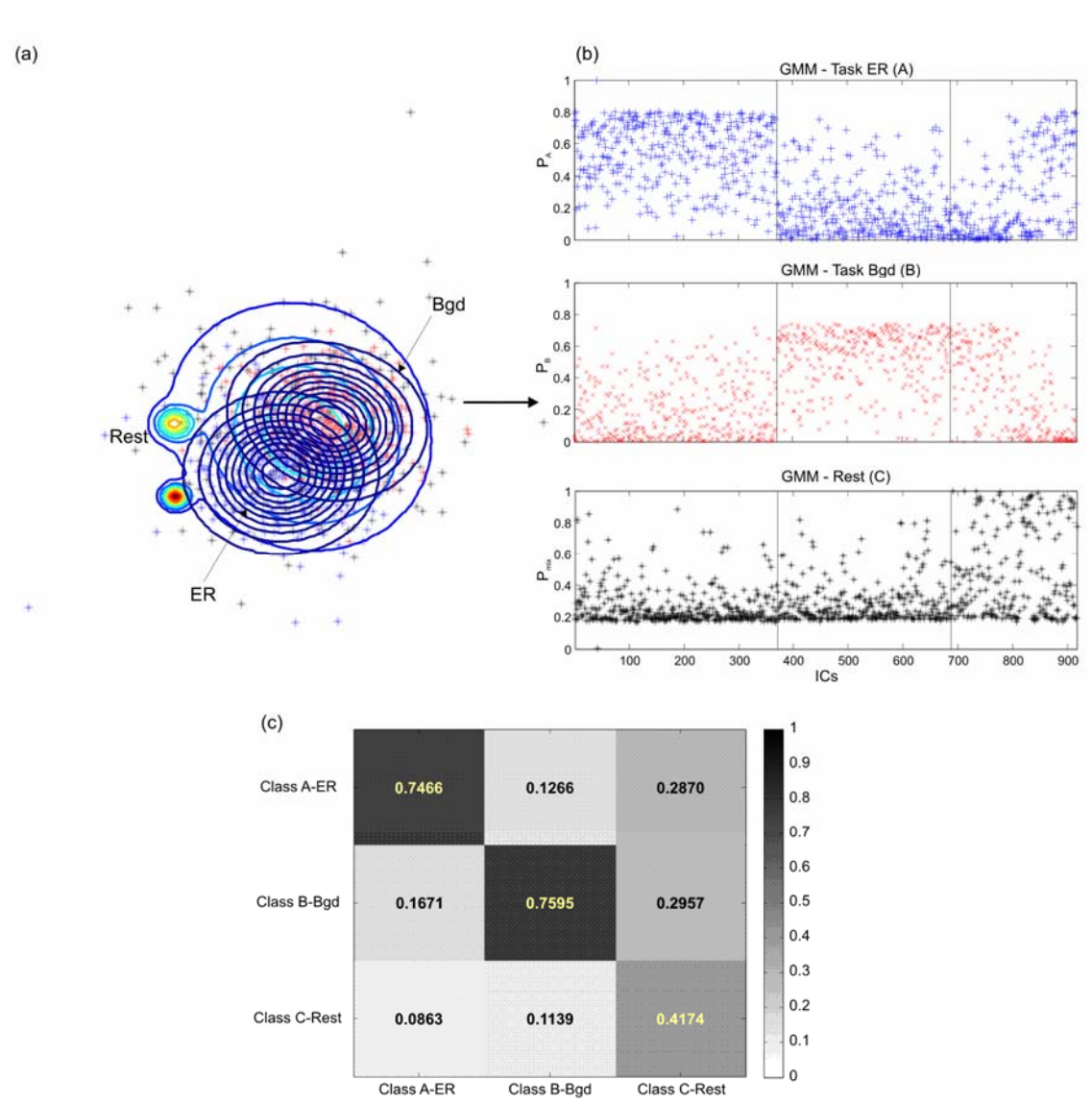

Figure II-3. Classification results based on 16 features (from All-*f* bands) of the ICs for the Oddball Hard task environment: (a) GMM contour plots for the neuroscale output, (b) Posterior probabilities from the GMMs of the three classes, (c) Confusion map showing sensitivity of classification on the diagonal.

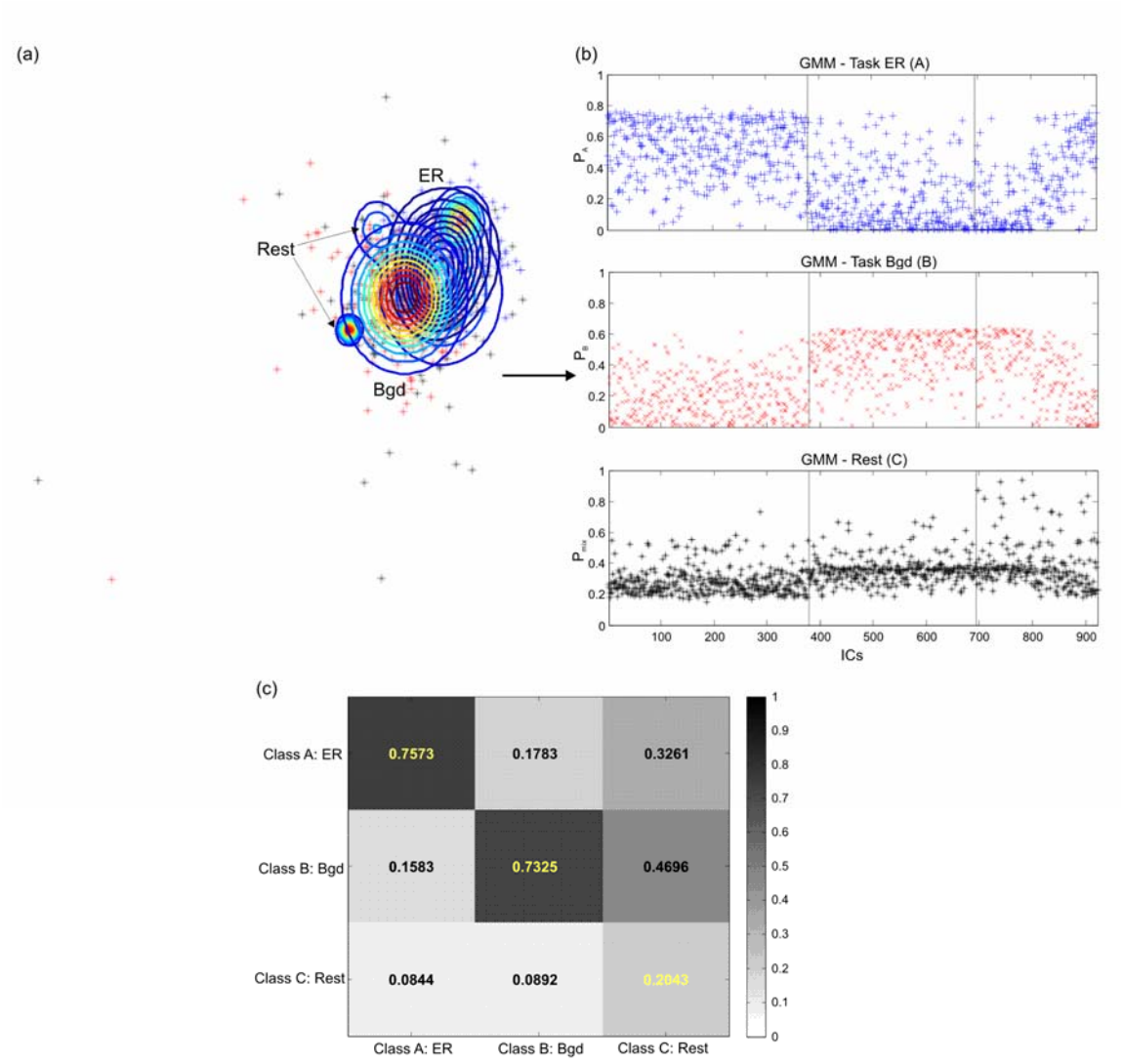

Figure II-4. Classification results based on 4 features (from slow wave band) of the ICs for the Oddball Easy task environment: (a) GMM contour plots for the neuroscale output, (b) Posterior probabilities from the GMMs of the three classes, (c) Confusion map showing sensitivity of classification on the diagonal.

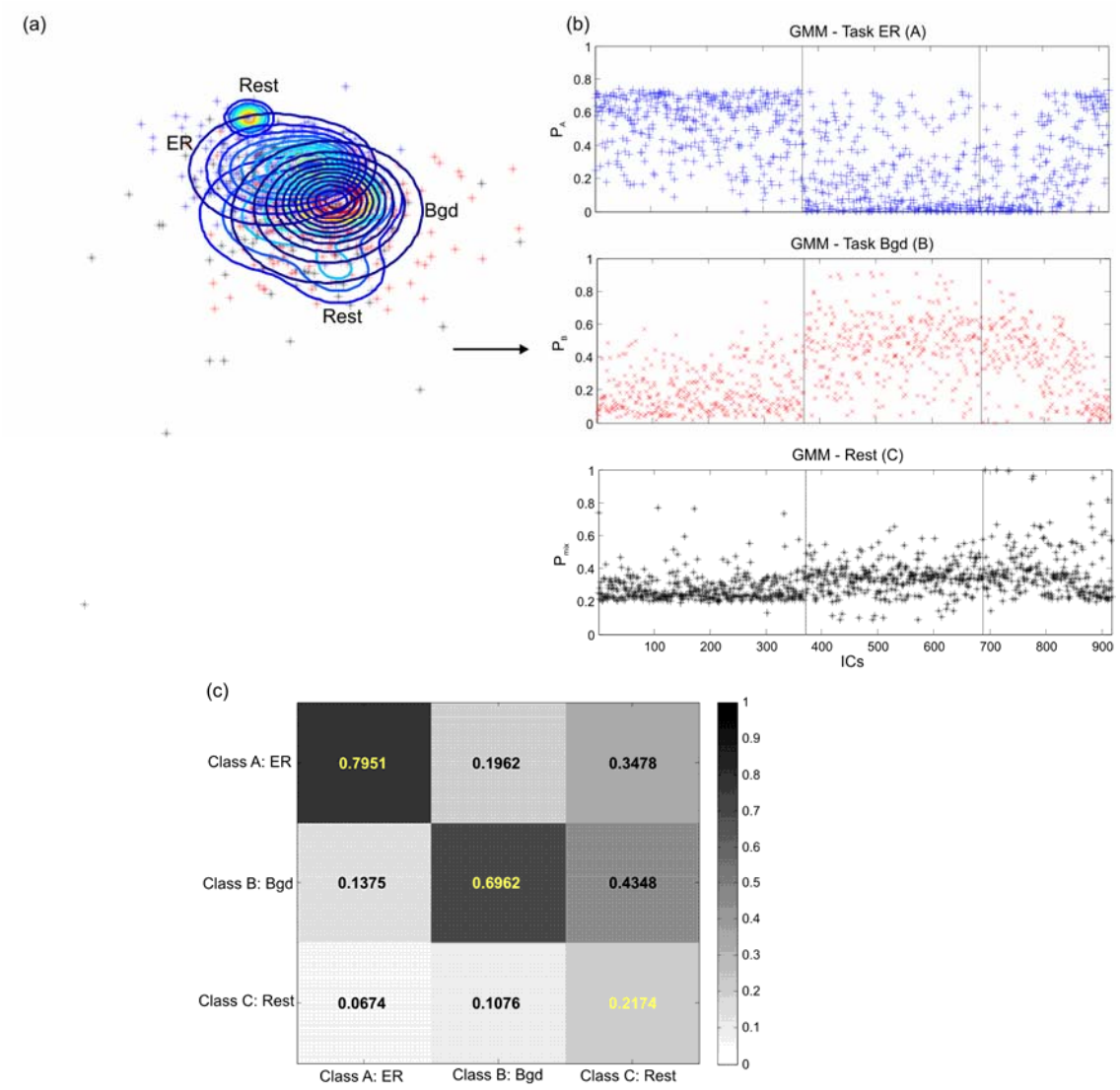

Figure II-5. Classification results based on the 4 features (from slow wave band) of the ICs for the Oddball Hard task environment: (a) GMM contour plots for the neuroscale output, (b) Posterior probabilities from the GMMs of the three classes, (c) Confusion map showing sensitivity of classification on the diagonal.

(B) The following plots illustrate further classification results based on the AR-ID method for different oscillators during various task environments. The results were based on the training data comprising the ICs of 14 participants, (similar to those shown in Chapter 8.9.1).

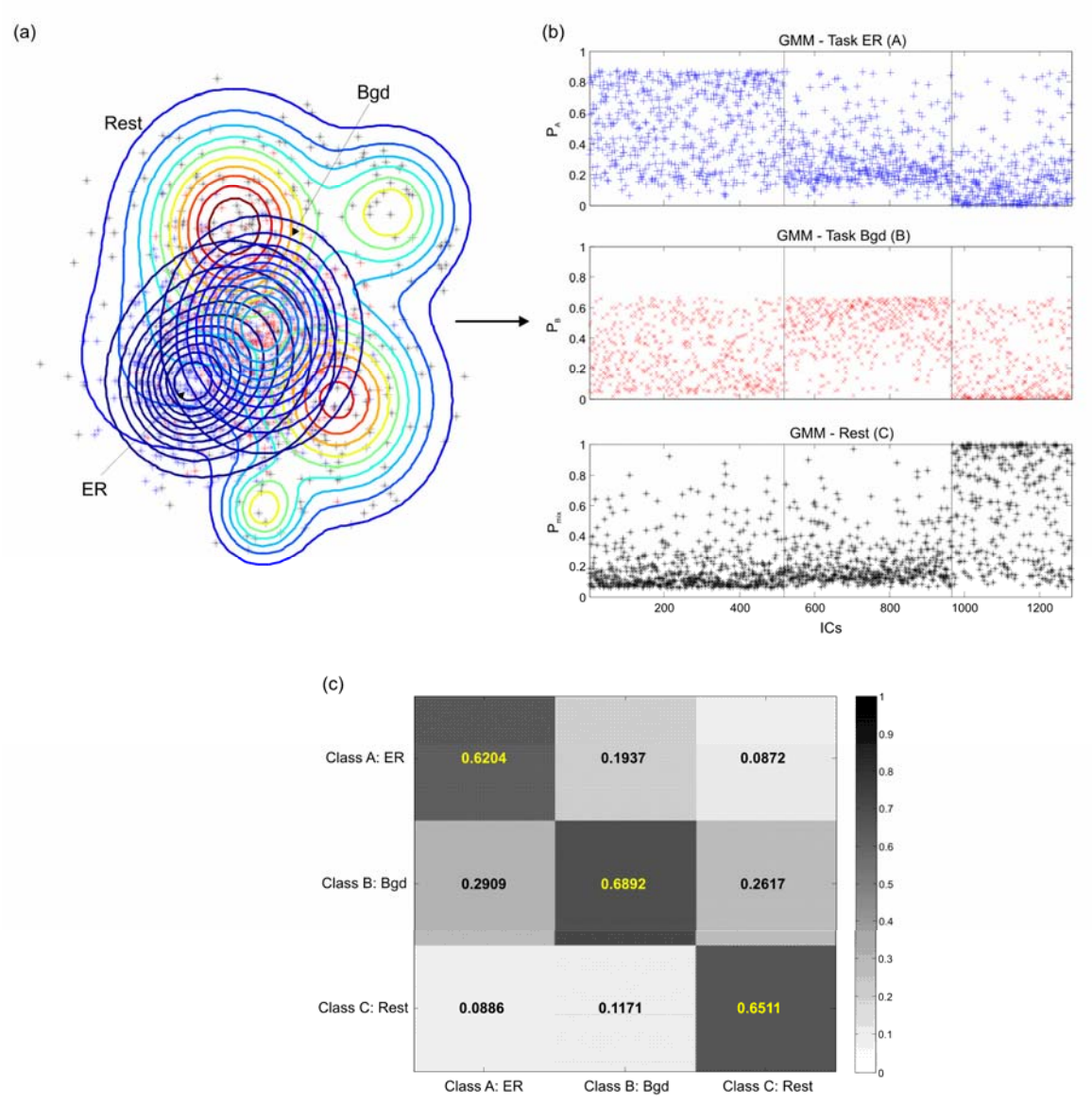

Figure II-6. Training data classification results based on *Delta f-Band Amplitude* features of the ICs for the Oddball Easy task environment: (a) GMM contour plots for the neuroscale output, (b) Posterior probabilities from the GMMs of the three classes, (c) Confusion map showing sensitivity of classification on the diagonal.

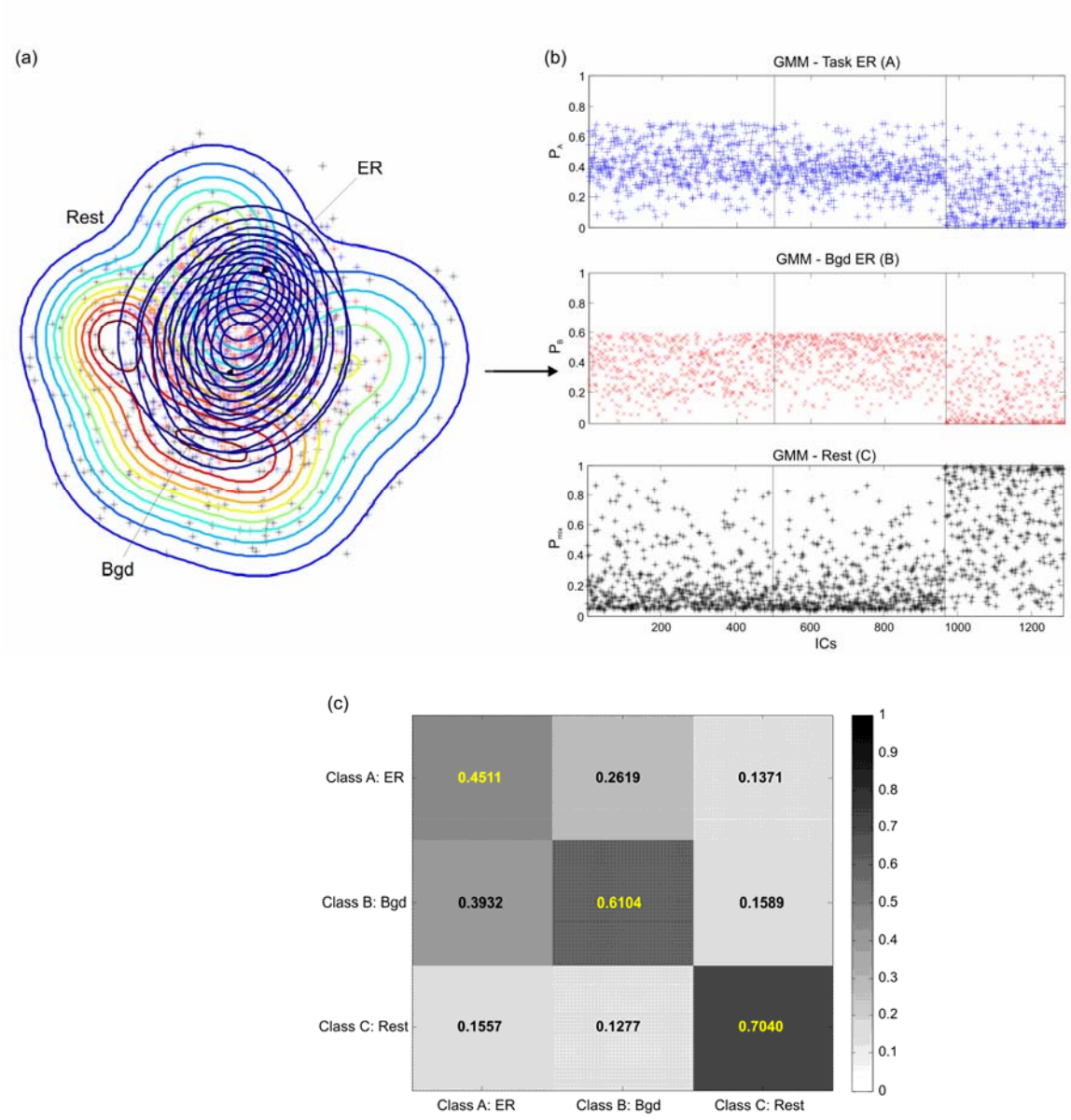

Figure II-7. Training data classification results based on *Delta f-Band Phase* features of the ICs for the Oddball Hard task environment: (a) GMM contour plots for the neuroscale output, (b) Posterior probabilities from the GMMs of the three classes, (c) Confusion map showing sensitivity of classification on the diagonal.

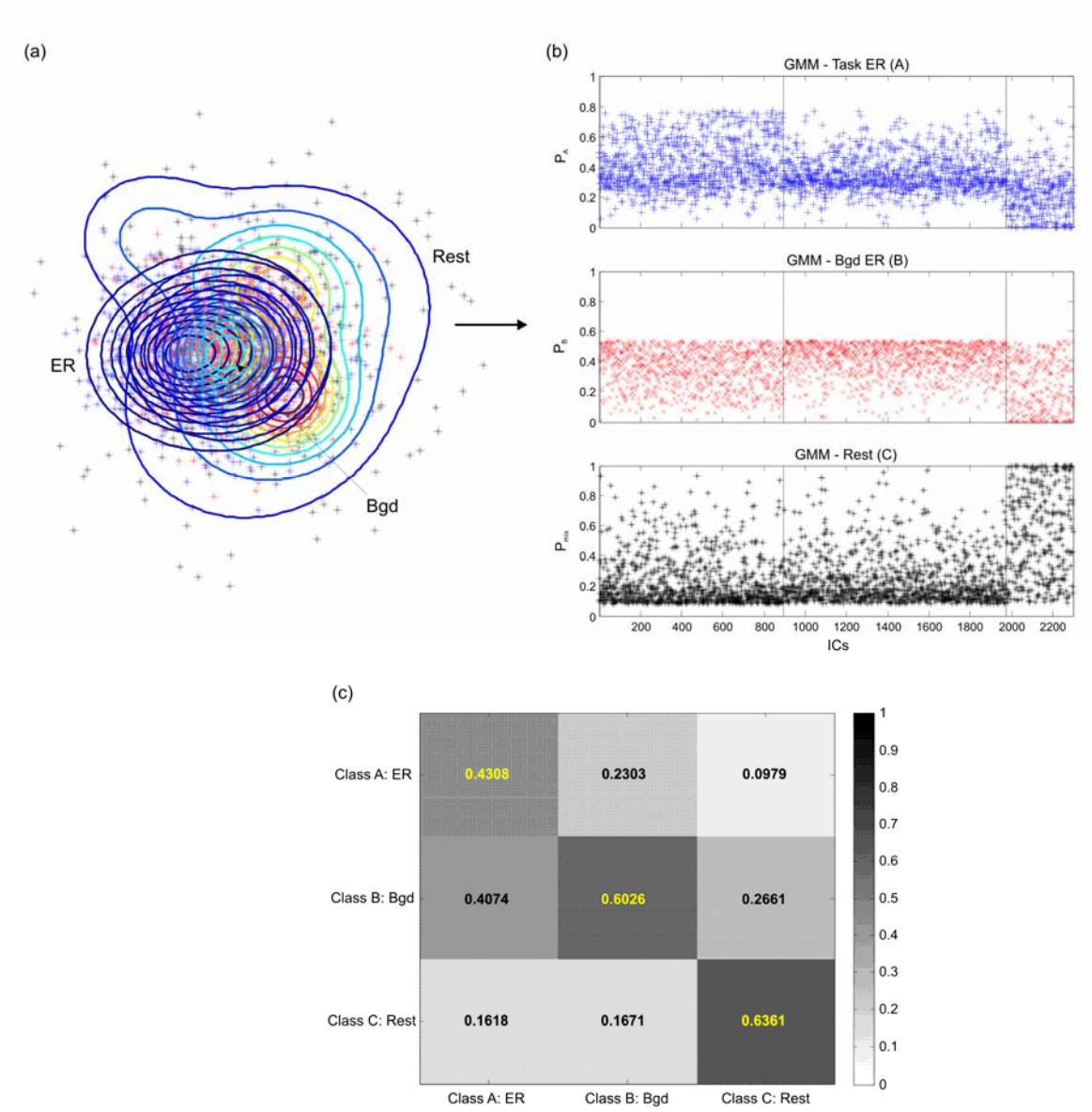

Figure II-8. Training data classification results based on *Theta f-Band Amplitude* features of the ICs for the SART task environment: (a) GMM contour plots for the neuroscale output, (b) Posterior probabilities from the GMMs of the three classes, (c) Confusion map showing sensitivity of classification on the diagonal.

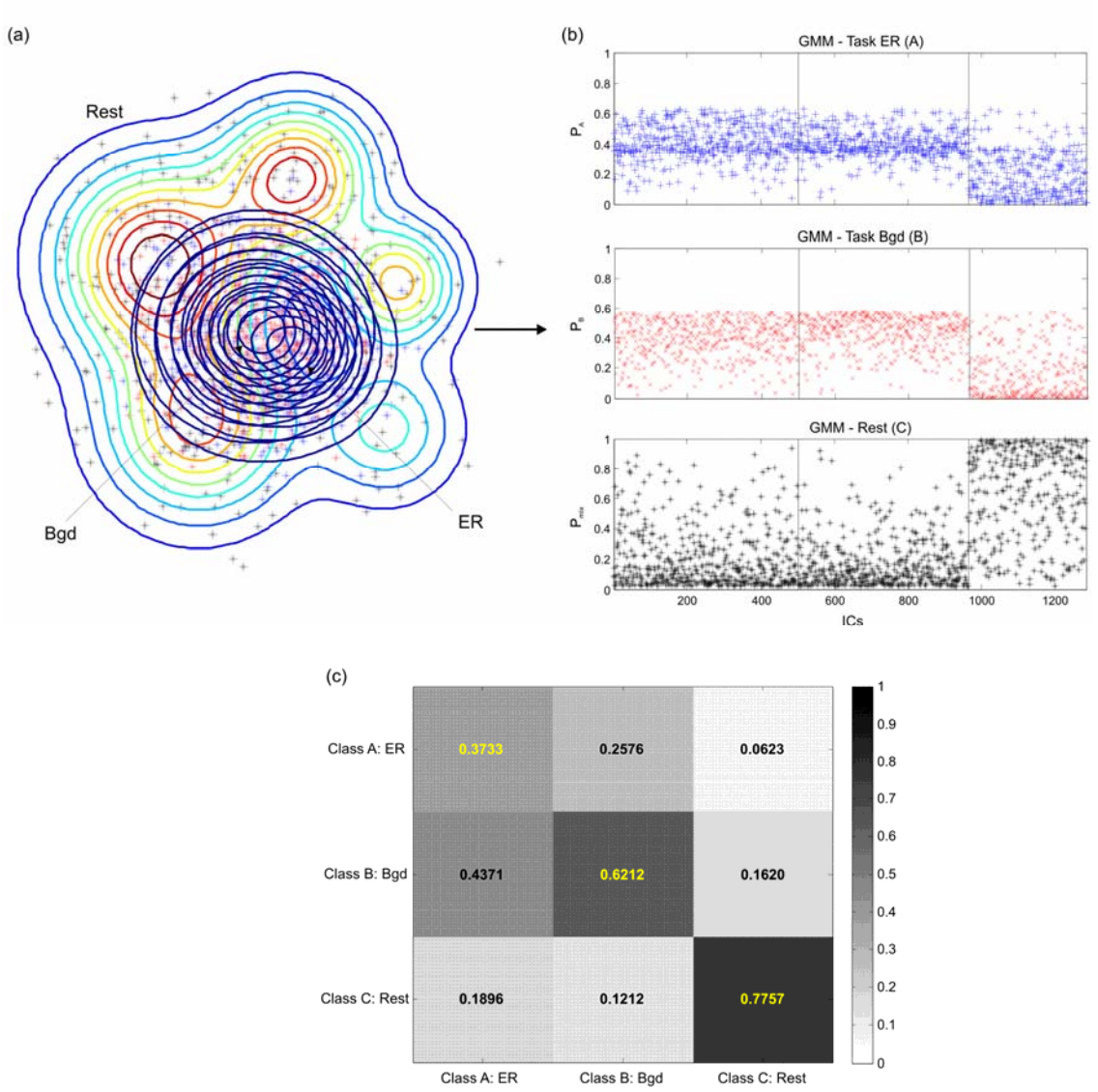

Figure II-9. Training data classification results based on *Theta f-Band Phase* features of the ICs for the Oddball Hard task environment: (a) GMM contour plots for the neuroscale output, (b) Posterior probabilities from the GMMs of the three classes, (c) Confusion map showing sensitivity of classification on the diagonal.

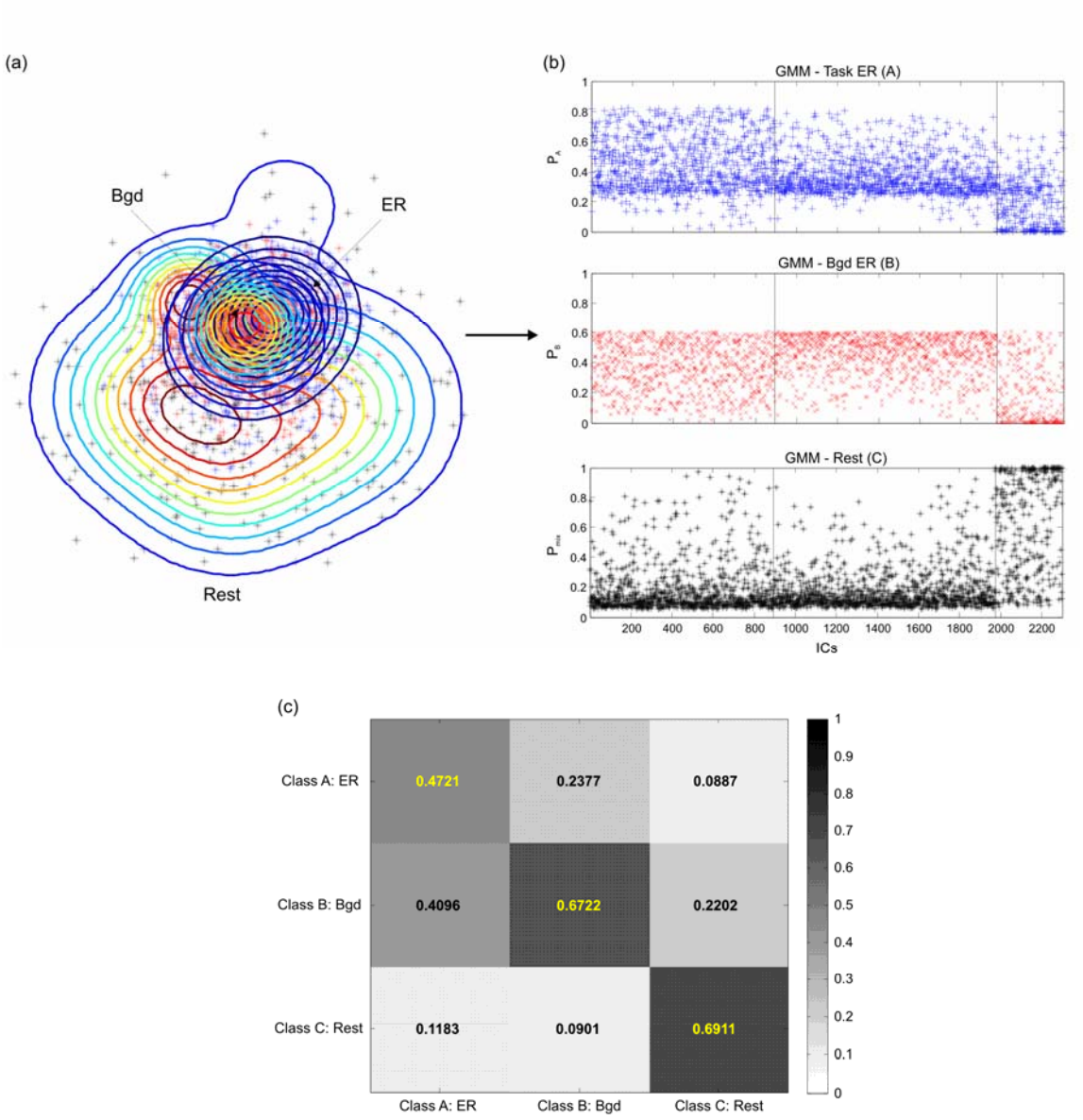

Figure II-10. Training data classification results based on *Alpha f-Band Amplitude* features of the ICs for the SART task environment: (a) GMM contour plots for the neuroscale output, (b) Posterior probabilities from the GMMs of the three classes, (c) Confusion map showing sensitivity of classification on the diagonal.

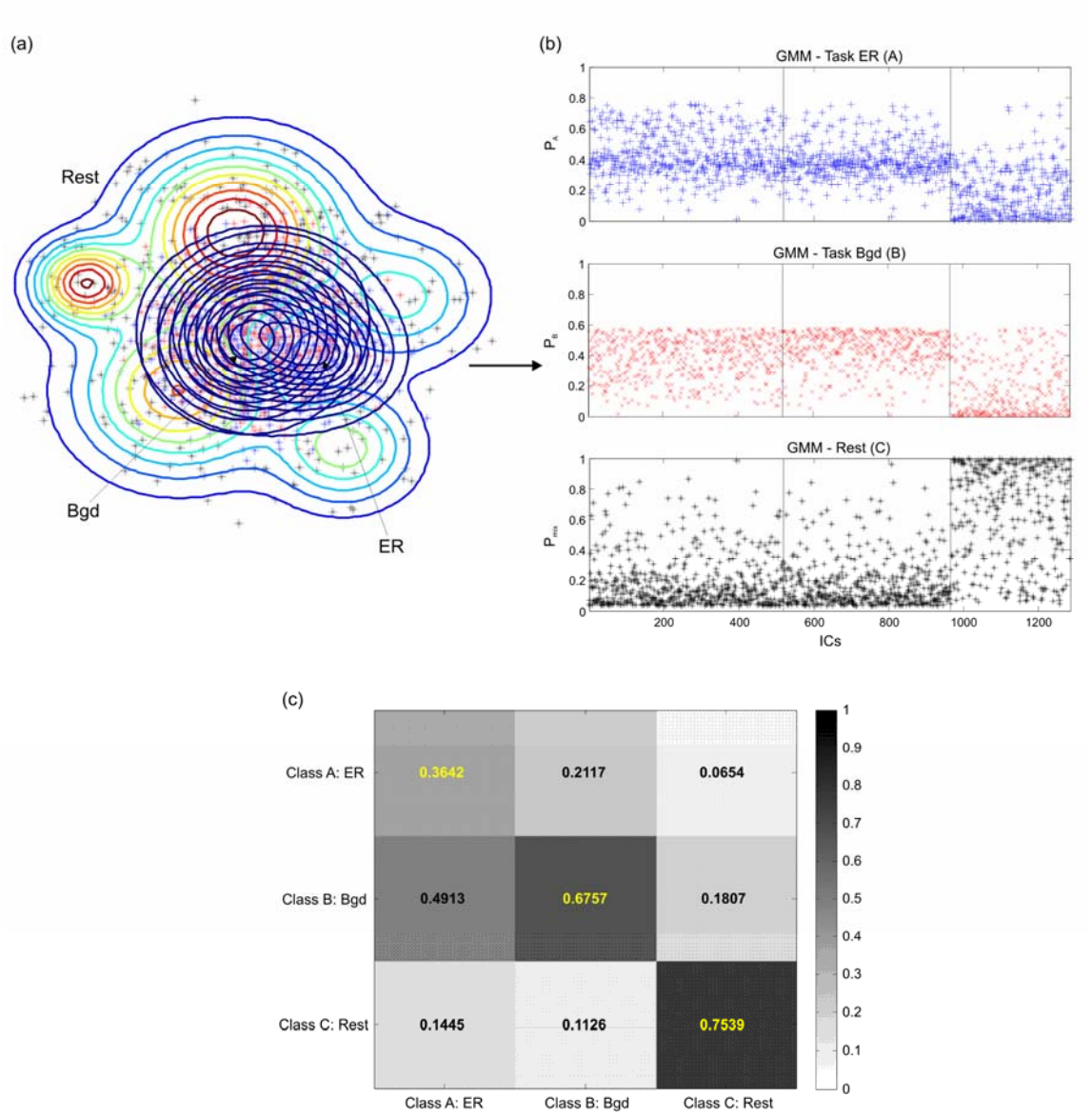

Figure II-11. Training data classification results based on *Alpha f-Band Phase* features of the ICs for the Oddball Easy task environment: (a) GMM contour plots for the neuroscale output, (b) Posterior probabilities from the GMMs of the three classes, (c) Confusion map showing sensitivity of classification on the diagonal.

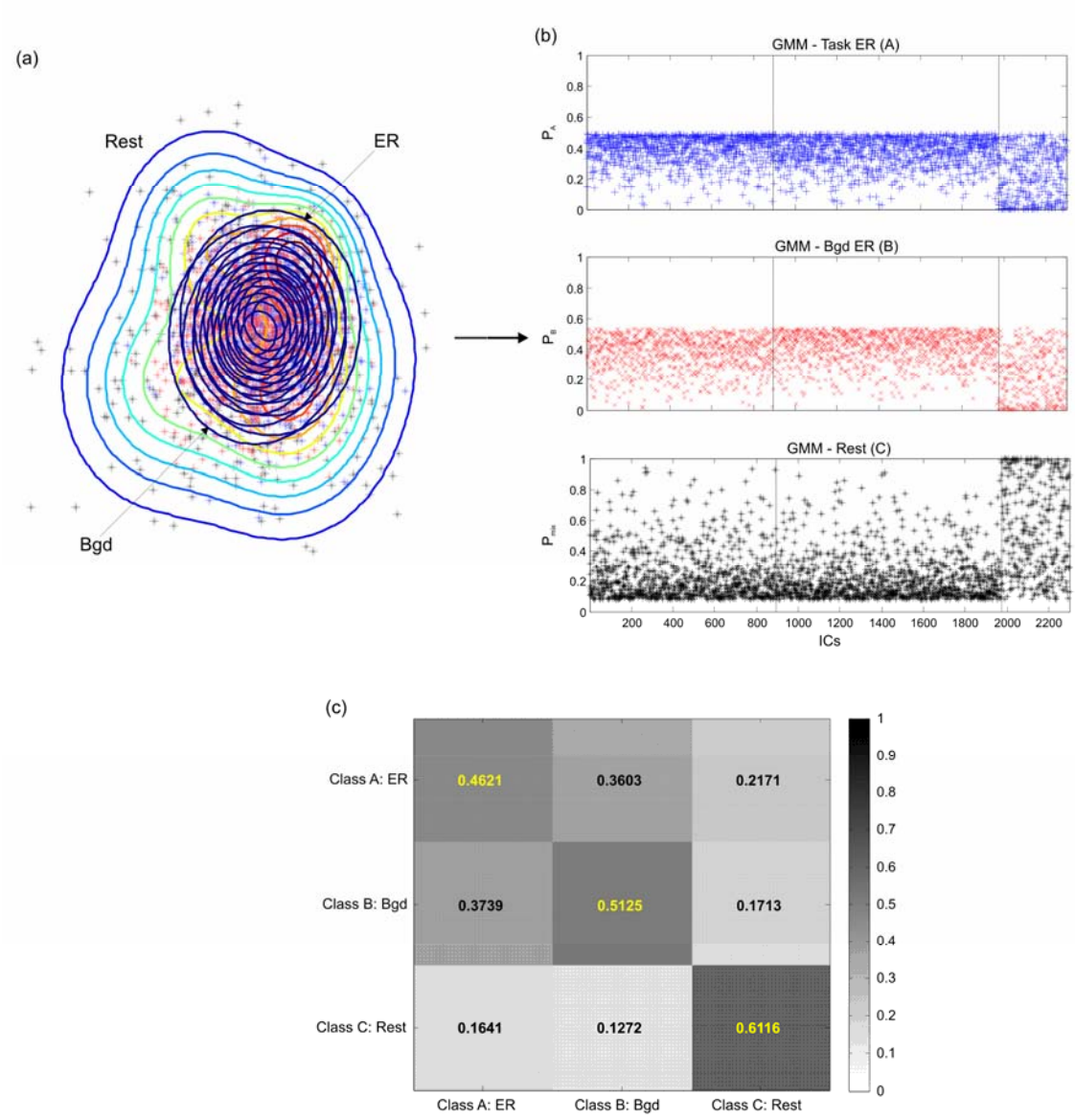

Figure II-12. Training data classification results based on *All f-Band Phase* features of the ICs for the SART task environment: (a) GMM contour plots for the neuroscale output, (b) Posterior probabilities from the GMMs of the three classes, (c) Confusion map showing sensitivity of classification on the diagonal.

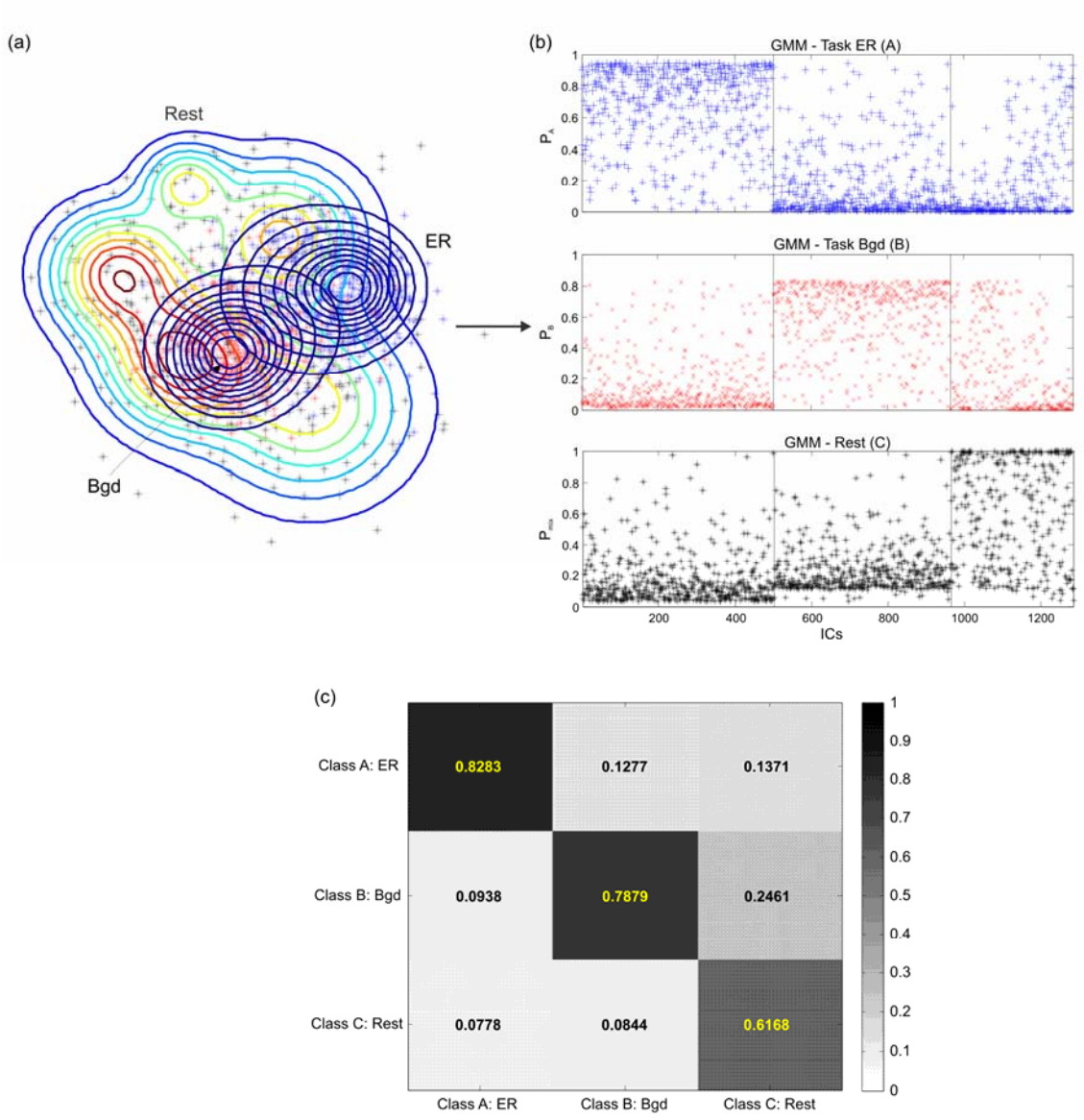

Figure II-13. Training data classification results based on *All f-Band Amplitude* features of the ICs for the Oddball Hard task environment: (a) GMM contour plots for the neuroscale output, (b) Posterior probabilities from the GMMs of the three classes, (c) Confusion map showing sensitivity of classification on the diagonal.

Appendix III

ACADEMIC ACTIVITIES THROUGHOUT THE PHD

- Faculty's Generic Skills Training Programme for Postgraduate Research Students
  - Introduction to Demonstrator Training – October 2006
  - Library Information Resource – October 2006
  - Research Methodology and Ethics – October 2006
  - Presenting your Research – March 2007
  - Project Management – March 2007
  - Technical Writing – April 2007

- Taught Modules
  - Biomedical Application of Signal Processing, Digital Signals and Systems, and Signal Processing (Masters Courses, ISVR, October 2006)
  - Adaptive Methods, Introduction to Random Signals (ISVR, 2007)

- Demonstrating Experience

  Demonstrating for undergraduates and master students at the University of Southampton, from October 2007 till January 2010:
  - Maths Tutorials
  - Signal Processing Labs

- Professional Experience
  - Followed training courses in *Public Engagement and Outreach Skills* and took part in several outreach activities for promoting biomedical engineering and neuroscience to school children, (Science Week organised by the University of Southampton, July 2007, March 2008 and March 2009, amongst others).
  - Was in the organisation committee of and chaired the 5th IEEE EMBS UK & Republic of Ireland Postgraduate Conference on Biomedical Engineering and Medical Physics, PGBIOMED'09, University of Oxford, UK, 12-14th July 2009.

References

Adrian, E.D. (1944). Brain rhythms. *Nature*, 153, 360-362.

Aihua, Z., and Yuhan, Z. (2005). Phase synchronization and support vector machines for recognition of mental tasks. *Proceedings of the 27th IEEE Engineering in Medicine and Biology Annual Conference, (EMBS'05)*, Shangai, China.

Al-Chalabi, A., Turner, M.R., Shane Delamont, R. (2006). *The Brain – A Beginner's Guide*. Oxford, England: Oneworld Publications.

American Psychiatric Association. (2000). *Diagnostic and Statistical Manual of Mental Disorders, 4th Edition, Text Revision, (DSM-IV-TR)*. Washington, DC: American Psychiatric Association.

Amin, M.G. and Belouchrani, A. (1998). Blind source separation based on time-frequency signal representations. *IEEE Transactions on Signal Processing*, 46, 2888-2897.

Andreou, P., Neale, B.M., Chen, W., Christiansen, H., Gabriels, I., Heise, A., Meidad, S., Muller, U.C., Uebel, H., Banaschewski, T., Manor, I., Oades, R., Roeyers, H., Rothenberger, A., Sham, P., Steinhausen, H.-C., Asherson, P. and Kuntsi, J. (2007). Reaction time performance in ADHD: improvement under fast-incentive condition and familial effects. *Psychological Medicine*, 37, 1703-1715.

Arieli, A., Sterkin, A., Grinvald, A., and Aertsen, A. (1996). Dynamics of ongoing activity: explanation of the large variability in evoked cortical responses. *Science*, 273, 1868-1871.

Astolfi, L., Cincotti, F., Mattia, D., Marciani, M.G., Baccala, L.A., de Vico Fallani, F., Salinari, S., Ursino, M., Zavaglia, M., and Babiloni, F. (2006). Assessing cortical functional connectivity by Partial Directed Coherence: simulations and application to read data. *IEEE Transactions on Biomedical Engineering*, 53, 1802-1812.

Auer, A.P. (2008). Spontaneous low-frequency blood oxygenation level-dependent fluctuations and functional connectivity analysis of the 'resting' brain. *Magnetic Resonance Imaging*, 26, 1055-1064.

Azouz, R. and Gray, C.M. (1999). Cellular mechanisms contributing to response variability of cortical neurons in vivo. *Journal of Neuroscience*, 19, 2209-2223.

Baccala, L.A. and Sameshima, K. (2001). Partial directed coherence: a new concept in neural structure determination. *Biological Cybernetics*, 84, 463-474.

Back, A.D. and Weigend, A.S. (1997). A first application of independent component analysis to extracting structure from stock returns. *International Journal on Neural Systems*, 8, 473-484.

Balduzzi, D., Riedner, B.A. and Tononi, G. (2008). A BOLD window into brain waves. *Proceedings of the National Academy of Sciences USA*, 105, 15641-15642.

Baloch, S.H., Krim, H. and Genton, M.G. (2005). Robust independent component analysis. *IEEE/SP Workshop on Statistical Signal Processing*, 61-64.

Banaschewski, T. and Brandeis, D. (2007). Annotation: What electrical brain activity tells us about brain functions that other techniques cannot tell us – A child psychiatric perspective. *Journal of Child Psychology and Psychiatry*, 48, 415-435.

Barratt, W. (2006). The Barratt simplified measure of social status (BSMSS) measuring SES. *Unpublished Manuscript*. Indiana State University, Terre Haute, Indiana.

Barry, R.J., Clarke, A.R., McCarthy, R. and Selikowitz, M. (2002). EEG coherence in attention-deficit/hyperactivity disorder: A comparative study of two DSM-IV types. *Clinical Neurophysiology*, 113, 579-585.

Barry, R.J., Johnstone, S.J. and Clarke, A.R. (2003). A review of electrophysiology in attention-deficit/hyperactivity disorder II. Event-related potentials. *Clinical Neurophysiology*, 114, 184-198.

Baudelet, C. and Gallez, B. (2005). Issues in the utility of blood oxygen level dependent MRI for the assessment of modulations in tumor oxygenation. *Current Medical Imaging Reviews*, 1, 229-243.

Baumgartner, C., Serles, W., Leutmezer, F., Pataraia, E., Aull, S., Czech, T., Pietrzyk, U., Relic, A. and Podreka, I. (1998). Pre-ictal SPECT in temporal lobe epilepsy: regional cerebral blood flow is increased prior to electroencephalography-seizure onset. *Journal of Nuclear Medicine*, 39, 978–982.

Bear, M., Connors, B. and Paradiso, M. (2001). *Neuroscience: Exploring the Brain*, 2nd Edition. USA: Lippincott Williams and Wilkins.

Bell, A.J. and Sejnowski, T.J. (1995). An information-maximization approach to blind source separation and blind deconvolution. Neural Computing, 7, 1129-1159.

Belouchrani, A., Abed-Meraim, K. and Cardoso, J.-F. (1997). A blind source separation technique using second-order statistics. *IEEE Transactions on Signal Processing*, 45, 434-444.

Ben-Simon, E., Podlipsky, I., Arieli, A., Zhdanov, A. and Hendler, T. (2008). Never resting brain: simultaneous representation of two alpha related processes in humans. *PLoS ONE*, 3(12):e3984, 9 pgs.

Bennington, J.Y. and Polich, J. (1999). Comparison of P300 from passive and active tasks for auditory and visual stimuli. *International Journal of Psychophysiology*, 34, 171-177.

Berger, H. (1929). Über das elektroenkephalogramm des menschen. *Archiv für Psychiatrie und Nervenkrankheiten*, 87, 527-570.

Beynon, J. and Snik, A.F.M. (2004). Use of the event-related P300 potential in cochlear implant subjects for the study of strategy-dependent speech processing. *International Journal of Audiology*, 43, S44-S47.

Birn, R.M., Diamond, J.B., Smith, M.A., and Bandettini, P.A. (2006). Separating respiratory-variation-related fluctuations from neuronal-activity-related fluctuations in fMRI. *NeuroImage*, 31, 1536-1548.

Bishop, C.M. (1995). *Neural Networks for Pattern Recognition*. New York: Oxford University Press Incorporation.

Biswal, B.B., Yetkin, F.Z., Haughton, V.M., and Hyde, J.S. (1995). Functional connectivity in the motor cortex of resting human brain using echo-planar MRI. *Magnetic Resonance in Medicine*, 34, 537-541.

Bledowski, C., Prvulovic, D., Hoechstetter, K., Scherg, M., Wibral, M., Goebel, R. and Linden, D.E.J. (2004). Localizing P300 generators in visual target and distractor processing: a combined event-related potential and functional magnetic resonance imaging study. *The Journal of Neuroscience*, 24, 9353-9360.

Broomhead, D.S. and King, G.P. (1986). Extracting qualitative dynamics from experimental data. *Physica*, 20D, 217-236.

Brown, G., Chadwick, O., Shaffer, D., Rutter, M., and Traub, M. (1981). A prospective study of children with head injuries: III Psychiatric sequelae. *Psychological Medicine*, 11, 63-78.

Broyd, S.J., Demanuele, C., Debener, S., Helps, S.K., James, C.J. and Sonuga-Barke, E.J.S. (2009). Default-mode brain dysfunction in mental disorders: A systematic review. *Neuroscience and Biobehavioral Reviews*, 33, 279-296.

Bruns, A. (2004). Fourier-, Hilbert- and wavelet-based signal analysis: are they really different approaches? *Journal of Neuroscience Methods*, 137, 321-332.

Buxton, R.B. (2009). *Introduction to Functional Magnetic Resonance Imaging Principles and Techniques*, 2nd Edition. New York: Cambridge University Press.

Buzsáki, G. and Draguhn, A. (2004). Neuronal oscillations in cortical networks. *Science*, 304, 1926-1929.

Campanella, S., Montedoro, C., Streel, E., Verbanck, P. and Rosier, V. (2006). Early visual components (P100 and N170) are disrupted in chronic schizophrenic patients: an event-related potentials study. *Clinical Neurophysiology*, 36, 71-78.

Cardoso, J.-F. (1998). Multidimensional independent components analysis. *Proceedings of IEEE International Conference on Acoustics, Speech and Signal Processing, (ICASSP'98)*, Seattle, WA, 1941-1944.

Castellanos, F.X., Sonuga-Barke, E.J.S., Scheres, A., Di Martino, A., Hyde, C., and Walters, J. (2005). Varieties of attention-deficit/hyperactivity disorder-related intra-individual variability. *Biological Psychiatry*, 57, 1416-1423.

Castellanos, F. X., Margulies, D.S., Clare Kelly, A. M., Uddin,, L.Q., Ghaffari, M., Kirsch, A., Shaw, D., Shehzad, Z., Di Martino, A., Biswal, B., Sonuga-Barke, E.J.S., Rotrosen, J., Adler, L.A. and Milham, M.P. (2008). Cingulate-precuneus interactions: a new focus of dysfunction in adult attention deficit/hyperactivity disorder. *Biological Psychiatry*, 63, 332-337.

Chavez, M., Besserve, M., Adam, C. and Martinerie, J. (2006). Towards a proper estimation of phase synchrony from time series. *Journal of Neuroscience Methods*, 154, 149-160.

Cho, B.H., Lee, J.M., Ku, J.H., Jang, D.P., Kim, J. S., Kim, I.Y., Lee, J.H. and Kim, S.I. (2002). Attention enhancement system using virtual reality and EEG biofeedback, *Proceedings of the IEEE Virtual Reality*, 2002.

Cichocki, A. and Belouchrani, A. (2001). Source separation of temporally correlated sources using bank of band pass filters. *Proceedings of the International Conference on Independent Component Analysis and Blind Signal Separation, (ICA'01)*, San Diego, CA, 173-178.

Clarke, A.R., Barry, R. J., McCarthy, R. and Selikowitz, M. (2001). Excess beta activity in children with attention-deficit/hyperactivity disorder: an atypical electrophysiological group. *Psychiatry Research*, 103, 205-218.

Clarke, A.R., Barry, R.J., McCarthy, R., Selikowitz, M., Clarke, D.C. and Croft, R.J. (2003). Effects of stimulant medication on children with attention-deficit/hyperactivity disorder and excessive beta activity in their EEG. *Clinical Neurophysiology*, 114, 1729-1737.

Comani, S., Mantini, D., Pennesi, P., Lagatta, A. and Cancellieri, G. (2004). Independent component analysis: fetal signal reconstruction from magnetocardiographic recording. *Computer Methods and Programs in Biomedicine*, 75, 163-177.

Comerchero, M. D. and Polich, J. (1998). P3a, perceptual distinctiveness and stimulus modality. *Cognitive Brain Research*, 7, 41-48.

Comerchero, M. D. and Polich, J. (1999). P3a and P3b from typical auditory and visual stimuli. *Clinical Neurophysiology*, 110, 24-30.

Comings, D.E., Chen, T.J.H., Blum, K., Mengucci, J. F., Blum, S. H. and Meshkin, B. (2005). Neuromagnetic interactions and aberrant behavioural comorbidity of ADHD: dispelling myths. *Theoretical Biology and Medical Modelling*, 2.

Comon P. (1994). Independent component analysis, a new concept? *Signal Processing*, 36, 287–314.

Darvas, F., Pantazis, D., Kucukaltun-Yildirim E. and Leahy, R.M. (2004). Mapping human brain function with MEG and EEG: methods and validation. *Neuroimage*, 23, S289-99.

Datta, A., Cusack, R., Hawkins, K., Heutink, J., Rorden, C., Robertson, I.H., and Manly, T. (2007). The P300 as a marker of waning attention and error propensity. *Computational Intelligence and Neuroscience*, 9 pgs.

Davies, M.E. and James, C.J. (2007). Source separation using single channel ICA. *Signal Processing*, 87, 1819-1832.

Davies, M., James, C.J. and Wang, S. (2007). Space-time ICA and EM brain signals. *Proceedings of the 7th International Conference on Independent Component Analysis and Signal Separation, (ICA'07)*, London, UK, pp. 577-584.

Debener, S., Makeig, S., Delorme, A. and Engel, A. K. (2005). What is novel in the novelty oddball paradigm? Functional significance of the novelty P3 event-related potential as revealed by independent component analysis. *Cognitive Brain Research,* 22, 309-32.

Debener, S., Ullsperger, M., Siegel, M., Fiehler, K., von Cramon, D.Y. and Engel, A.K. (2006). Single-trial EEG/fMRI reveals the dynamics of cognitive function. *Trends in Cognitive Sciences*, 10, 558-563.

Delorme,A., Makeig, S., Fabre-Thorpe, M. and Sejnowski, T. (2002). From single-trail EEG to brain area dynamics. Neurocomputing, 44-46, 1057-1064.

Delorme, A. and Makeig, S. (2004). EEGLAB: an open source toolbox for analysis of single-trial EEG dynamics including ICA. *Journal of Neuroscience Methods*, 134, 9-21.

Di Martino, A., Ghaffari, M., Curchack, J., Reiss, P., Hyde, C., Vannucci, M., Petkova, E., Klein, D. and Castellanos, F. (2008). Decomposing intra-subject variability in children with attention-deficit/hyperactivity disorder. *Biological Psychiatry*, 64, 607-614.

Elekta Neuromag® MEG System Description, NM21761B-A. (2006). http://www.elekta.com/healthcare_us_elekta_neuromag.php

Ellison, P.A.T. and Semrud-Clikeman, M. (2007). *Child Neuropsychology*. New York: Springer.

Elsner, J.B. (2007). Granger causality and Atlantic Hurricanes, *Tellus*, 59A.

Estrada, E., Nazeran, H., Behbehani, K., Burk, J. and Lucas, E. (2005). Itakura distance: a useful similarity measure between EEG and EOG signals in computer-aided classification of sleep stages. *In the 27th IEEE Engineering in Medicine and Biology Annual Conference (EMBS)*, Shanghai, China, 1189-1192.

Everitt, B. (1993). *Cluster Analysis*, 3rd Edition. New York: Edward Arnold.

Feig, E. and Winograd, S. (1992). Fast algorithms for the discrete cosine transform. *IEEE Transactions on Signal Processing*, 40, 2174-2193.

Fergusson, D., Horwood, L. and Lynskey, M. (1994). The childhoods of multiple problem adolescents: A 15-year longitudinal study. *Australian and New Zealand Journal of Psychiatry*, 35, 1123-1140.

Fisch, B. (1999). *Fisch and Spehlmann's EEG Primer: Basic Principles of Digital and Analog EEG*. Amsterdam: Elsevier Science B.V.

Fiser, J., Chiu, C. and Weliky, M. (2004). Small modulation of ongoing cortical dynamics by sensory input during natural vision. *Nature*, 431, 573-578.

Flandrin, P. (2004). Empirical mode decomposition as a filter bank. *IEEE Signal Processing Letters*, 11, 112-114.

Fox, M.D., Snyder, A.Z., Vincent, J.L., Corbetta, M., Van Essen, D.C. and Raichle, M.E. (2005). The human brain is intrinsically organized into dynamic, anticorrelated functional networks. *Proceedings of the National Academy of Sciences of the United States of America*, 102, 9673-9678.

Fox, M.D., Snyder, A.Z., Zacks, J.M. and Raichle, M.E. (2006). Coherent spontaneous activity accounts for trial-to-trial variability in human evoked brain responses. *Nature Neuroscience*, 9, 23-25.

Fox, M.D. and Raichle, M.E. (2007). Spontaneous fluctuations in brain activity observed with functional magnetic resonance imaging. *Nature Neuroscience Reviews*, 8, 700-711.

Fox, M., Snyder, A., Vincent, J. and Raichle, M.E. (2007). Intrinsic fluctuations within cortical systems account for intertrial variability in human behavior. *Neuron*, 56, 171-184.

Franaszczuk, P. J. and Bergey, G. K. (1998). Application of Directed Transfer Function method to mesial and lateral onset temporal lobe seizures. *Brain Topography*, 11, 13-21.

Franc, V. and Hlaváč, V. (2004). *Statistical pattern recognition toolbox for MATLAB® – User's Guide*. Czech Technical University Prague.

Freeman, W.J. (1988). Strange attractors that govern mammalian brain dynamics shown by trajectories of electroencephalographic (EEG) potential. *IEEE Transactions on Circuits and Systems*, 35, 781-783.

Freeman, W.J., Holmes, M.D., Burke, B.C. and Vanhatalo, S. (2003). Spatial spectra of scalp EEG and EMG from awake humans. *Clinical Neurophysiology*, 114, 1053-1068.

Fransson, P. (2005). Spontaneous low-frequency BOLD signal fluctuations: an fMRI investigation of the resting-state default mode of brain function hypothesis. *Human Brain Mapping*, 26, 15-29.

Fransson, P. (2006). How default is the default mode of brain function? Further evidence from intrinsic BOLD signal fluctuations. *Neuropsychologia*, 44, 2836-2845.

Gautama, T. and Van Hulle, M.M. (2003). Surrogate-based test for Granger Causality. *IEEE XIII Workshop on Neural Networks for Signal Processing*, 799-808.

Georgopoulos, A.P., Karageorgiou, E., Leuthold, A.C., Lewis, S.M., Lynch, J.K., Alonso, A.A., Aslam, Z., Carpenter, A.F., Georgopoulos, A., Hemmy, L.S., Koutlas, I.G., Langheim, F.J.P., Riley McCarten, J., McPherson, S.E., Pardo, J.V., Pardo, P.J., Parry, G.J., Rottunda, S.J., Segal, B.M., Sponheim, S.R., Stanwyck, J.J., Stephane, M. and Westermeyer, J.J. (2007). Synchronous neural interactions assessed by magnetoencephalography: a functional biomarker for brain disorders. *Journal of Neural Engineering*, 4, 349-355.

Gokcay, A., Celebisoy, N., Gokcay, F., Ekmekci, O. and Ulku, A. (2003). Visual evoked potential in children with occipital lobe epilepsies. *Official Journal of the Japanese Society of Child Neurology: Brain and Development*, 25, 268-271.

Gramatikov, B. and Georgiev, I. (1995). Wavelets as alternative to short-time fourier transform in signal-averaged electrocardiography. *Medical and Biological Engineering and Computing*, 33, 482-487.

Gupta, D., James, C.J. and Gray, W. (2008). De-noising epileptic EEG using ICA and phase synchrony. *Proceedings of the 4th IET International Conference on Advances in Medical, Signal and Information Processing, (MEDSIP'08)*, Sta. Margherita Ligure, Italy.

Hagen, G.F., Gatherwright, J.R., Lopez, B.A. and Polich, J. (2006). P3a from visual stimuli: task difficulty effects. *International Journal of Psychophysiology*, 59, 8-14.

Hansenne, M. (2000). The P300 event-related potential II. Interindividual variability and clinical application in psychopathology. *Clinical Neurophysiology*, 30, 211-231.

Hayes, M.H. (1996). *Statistical Digital Signal Processing and Modeling*, USA: Wiley.

He, B.J., Snyder, A.Z., Zempel, J.M., Smyth, M.D. and Raichle, M. (2008). Electrophysiological correlates of the brain's intrinsic large-scale functional architecture. *Proceedings of the National Academy of Sciences USA*, 105, 16039–16044.

Heinrich, H., Moll, G.H., Dickhaus, H., Kolev, V., Yordanova, J. and Rothenberger, A. (2001). Time-on-task analysis using wavelet networks in an event-related potential study on attention-deficit hyperactivity disorder. *Clinical Neurophysiology*, 112, 1280-1287.

Helps, S., James, C., Debener, S., Karl, A. and Sonuga-Barke, E.J.S. (2008). Very low frequency EEG oscillations and the resting brain in young adults: a preliminary study of localization, stability and association with symptoms of inattention. *Journal of Neural Transmission*, 115, 279-285.

Helps, S.K., Broyd, S.J., James, C.J., Karl, A. and Sonuga-Barke, E.J.S. (in press). The attenuation of very low frequency brain oscillations in transitions from a rest state to active attention. *Journal of Psychophysiology*.

Helps, S.K., Broyd, S.J., James, C.J., Karl, A., Chen, W. and Sonuga-Barke, E.J.S. (2010). Altered spontaneous low frequency brain activity in Attention Deficit/Hyperactivity Disorder. *Brain Research*.

Hennighausen, E., Heil, M., and Rösler, F. (1993). A correction method for DC drift artefacts. *Electroencephalography and Clinical Neurophysiology*, 89, 199-204.

Herrmann, C.S. and Knight, R.T. (2001). Mechanisms of human attention: event-related potentials and oscillations. *Neuroscience and Biobehavioural Reviews*, 25, 465-476.

Herrmann, C. S. and Demiralp, T. (2005). Human EEG gamma oscillations in neuropsychiatric disorders. *Clinical Neurophysiology*, 116, 2719-2733.

Herrmann, C.S. and Debener, S. (2008). Simultaneous recording of EEG and BOLD responses: a historical perspective. *International Journal of Psychophysiology*, 67, 161-168.

Hesse, W., Moller, E., Arnold, M. and Schack, B. (2003). The use of time-variant EEG Granger causality for inspecting directed interdependencies of neural assemblies. *Journal of Neuroscience Methods*, 124, 27-44.

Hillyard, S.A. and Anllo-Vento, L. (1998). Event-related brain potentials in the study of visual selective attention. *Proceedings of the National Academy of Science USA*, 95, 781-787.

Hillyard, S.A. and Kutas, M. (2002). Event-related potentials and magnetic fields in the human brain. In: Davis, L.K., Charney, D., Coyle, J.T., Nemeroff, C.B., (Eds.), *Neuropsychopharmacology: The Fifth Generation of Progress*. USA: Lippincott Williams and Wilkins, 427: 439.

Hollingshead, A. B. (1975). Four factor index of social status. Unpublished manuscript, Department of Sociology, Yale University, New Haven, Connecticut.

Hong, B., Acharya, S., Gao, S. and Thakor, N.V. (2005). Transient phase synchrony of independent components underlying scalp EEG. *Proceedings of the 27th IEEE Engineering in Medicine and Biology Annual Conference*, *(EMBS'05)*, Shangai, China.

Hong, B., Acharya, S., Ku, Y., Gao, S. and Thakor, N.V. (2006). Measurement of dynamic coupling of independent EEG components from cognitive tasks. *International Journal of Bioelectromagnetism*, 8, VII/1 - VII/7.

Horowitz, B. (2003). The elusive concept of brain connectivity. *NeuroImage*, 19, 466-470.

Huang, N.E., Shen, Z., Long, S.R., Wu, M.C., Shih, H.H., Zheng, Q., Yen, N.C., Tung, C.C. and Liu, H.H. (1998). The empirical mode decomposition and the Hilbert spectrum for nonlinear and non-stationary time series analysis. *Proceedings of the Royal Society of London A*, 454, 903-995.

Huettel, S.A., McKeown, M.J., Song, A.W., Hart, S., Spencer, D.D., Allison, T. and McCarthy, G. (2004). Linking hemodynamic and electrophysiological measures of brain activity: evidence from functional MRI and intracranial field potentials. *Cerebral Cortex*, 14, 165-173.

Hurtado, J.M., Rubchinsky, L.L. and Sigvardt, K.A (2004). Statistical method for detection of phase-locking episodes in neural oscillations. *Journal of Neurophysiology*, 91, 1883-1898.

Hyvärinen, A. (1999a). The fixed point algorithm and maximum likelihood estimation of independent component analysis. *Neural Processing Letters*, 10, 1-5.

Hyvärinen, A. (1999b). Fast and robust fixed-point algorithms for independent component analysis. *IEEE Transactions on Neural Networks*, 10, 626-34.

Hyvärinen A., and Oja, E. (2000). Independent component analysis: algorithms and applications. *Neural Networks*, 13, 411-430.

Hyvärinen, A., Hoyer, P.O. and Inki, M. (2001). Topographic independent component analysis. *Neural Computation*, 13, 1527-1558.

Hyvärinen, A., Karhunen, J. and Oja, E. (2001). *Independent Component Analysis*. New York: Wiley.

Itakura, F. (1975). Minimum prediction residual principle applied to speech recognition. *IEEE Transactions on Acoustics, Speech and Signal Processing*, 23, 67-72.

James, C.J. and Lowe, D. (2000). Using dynamical embedding to isolate seizure components in the ictal EEG. *IEE Proceedings on Science, Measurement & Technology*, 147, 315-320.

James, C.J. and Lowe, D. (2001). Single channel analysis of electromagnetic brain signals through ICA in a dynamical systems framework. *Proceedings of the 23rd IEEE Engineering in Medicine and Biology Annual International Conference*, *(EMBS'01)*, Turkey, 1974-1977.

James, C.J. and Lowe, D. (2003). Extracting multisource brain activity from a single electromagnetic channel. *Artificial Intelligence in Medicine*, 28, 89-104.

James, C.J. and Gibson, O.J. (2005). Temporally Constrained ICA: An application to artifact rejection in electromagnetic brain signal analysis. *IEEE Transactions on Biomedical Engineering*, 50, 1108-1116.

James, C.J., and Hesse, C.W. (2005). Independent component analysis for biomedical signals. *Physiological Measurement*, 26, 15-39.

James, C.J., Gibson, O.J. and Davies, M. (2006). On the analysis of single versus multiple channels of electromagnetic brain signals. *Artificial Intelligence in Medicine*, 37, 131-143

James, C.J., Abasolo, D. and Gupta, D. (2007). Space-time ICA versus Ensemble ICA for ictal EEG analysis with component differentiation via Lempel-Ziv complexity. *Proceedings of the 29th IEEE Engineering in Medicine and Biology Annual International Conference*, *(EMBS'09)*, Lyon, France, 5473-5476.

James, C.J. (2008). Contrasting spatial, temporal and spatio-temporal ICA applied to ictal EEG recordings. *Proceedings of the 30th IEEE Engineering in Medicine and Biology Annual International Conference*, *(EMBS'08)*, Vancouver, Canada, 3336-3339.

James, C.J. and Davies, M.E. (2008). A fast algorithm for automated independent process separation from single channel biomedical signal recordings: FastIPA. *Proceedings of the International Conference on Medical Signal and Information Processing*, *(MEDSIP'08)*, Sta Margerita Ligure, Italy.

James, C.J. and Demanuele, C. (2009). On spatio-temporal component selection in space-time independent component analysis: An application to ictal EEG. *Proceedings of the 31st IEEE Engineering in Medicine and Biology Annual International Conference*, *(EMBS'09)*, Minnesota, USA.

Jasper, H.H. (1958). The 10-20 electrode system of the International Federation. *Electroencephalography and Clinical Neurophysiology*, 10, 371-5.

Jeon, Y.-W. and Polich, J. (2001). P3a from a passive visual stimulus task. *Clinical Neurophysiology*, 112, 2202-2208.

Jeon, Y.-W. and Polich, J. (2003). Meta-analysis of P300 and schizophrenia: Patients, paradigms, and practical implications. *Psychophysiology*, 40, 684-701.

Jerger, K., Netoff, T., Fransis, J., Sauer, T., Pecora, L., Weinstein, S. L. and Schiff, S. J. (2001). Early seizure detection. *Journal of Clinical Neurophysiology*, 18, 259-68.

Jiménez-González, A. and James, C.J. (2009). Extracting sources from noisy abdominal phonograms: a single-channel blind source separation method. *Medical and Biological Engineering and Computing*, 47, 655-664.

Johnson, J.B. (1925). The Schottky effect in low frequency circuits. *Physical Review*, 26, 71-85.

Johnson, K.A., Kelly, S.P., Bellgrove, M.A., Barry, E., Cox, M., Gill, M., and Robertson, I.H. (2007). Response variability in attention-deficit/hyperactivity disorder: evidence of neuropsychological heterogeneity. *Neuropsychologia*, 45, 630-638.

Johnstone, S.J., Barry, R.J. and Dimoska, A. (2003). Event-related slow-wave activity in two subtypes of attention-deficit/hyperactivity disorder. *Clinical Neurophysiology*, 114, 504-514.

Jung, T.-P., Makeig, S., Westerfield, M., Townsend, J., Courchesne, E. and Sejnowski, T.J. (2001a). Analysis and visualization of single-trial event-related potentials. *Human Brain Mapping*, 14, 166-185.

Jung, T.-P., Makeig, S., Mckeown M. and Bell, A.J. (2001b). Imaging brain dynamics using independent component analysis. *Proceedings of the IEEE*, 89, 1107-1121.

Jonkman, L. M., Kemner, C., Verbaten, M.N., Koelega, H.S., Camfferman, G., Gaag, R.J., Buitelaar, J.K., and van Engeland, H. (1997). Event-related potentials and performance of attention-deficit hyperactivity disorder: children and normal controls in auditory and visual selective attention tasks. *Biological Psychiatry*, 41, 595-611.

Jonkman, L., Kenemans, J., Kemner, C., Verbaten, M., and van Engeland, H. (2004). Dipole source localization of event-related brain activity indicative of an early visual selective attention deficit in ADHD children. *Journal of Clinical Neurophysiology*, 115, 1537-1549.

Kaplan, D.T. (1995). Nonlinearity and nonstationarity: The use of surrogate data in interpreting fluctuations in Heart Rate. *Proceedings of the 3rd Annual Workshop on Computer Applications of Blood Pressure and Heart Rate Signals*, Florence, Italy.

Karakas, S., Erzengin, O.U. and Başar, E. (2000). The generis of human event-related responses explained through the theory of oscillatory neural assemblies. *Neuroscience Letters*, 285, 45-48.

Karayanidis, F., Robaey, P., Bourassa, M., De Koning, D., Geoffroy, G. and Pelletier, G. (2000). ERP differences in visual attention processing between ADHD and control boys in the absence of performance differences. *Psychophysiology*, 37, 319-333.

Katayama, J. and Polich, J. (1996). P300, probability, and the three-tone paradigm. *Electroencephalography and Clinical Neurophysiology*, 100, 555-562.

Keshner, M.S. (1982). 1/*f* Noise. *Proceedings of the IEEE*, 70, 212-218.

Khader, P., Schicke, T., Röder, B. and Rösler, F. (2008). On the relationship between slow cortical potentials and BOLD signal changes in humans. *International Journal of Psychophysiology*, 67, 252-261.

Klein, A., Sauer, T., Jedynak, A. and Skrandies, W. (2006). Conventional and wavelet coherence applied to sensory-evoked electrical brain activity. *IEEE Transactions on Biomedical Engineering*, 53, 266-272.

Kobayashi, K., James, C.J., Nakahori, T., Akiyama, T. and Gotman, J. (1999). Isolation of epileptiform discharges from unaveraged EEG by independent component analysis. *Clinical Neurophysiology*, 110, 1755-1763.

Kobayashi, M. and Musha, T. (1982). 1/*f* Fluctuation of Heartbeat Period. *IEEE Transactions on Biomedical Engineering*, 29, 456-457.

Kolev, V. and Yordanova, J. (1997). Analysis of phase-locking is informative for studying event-related EEG activity. *Biological Cybernetics*, 76, 229-235.

Kolev, V., Demiralp, T., Yordanova, J., Ademoglu, A. and Isoglu-Alkaç, Ŭ. (1997). Time-frequency analysis reveals multiple functional components during oddball P300. *Cognitive Neuroscience and Neuropsychology*, 8, 2061-2065.

Kong, X., Goel, V. and Thakor, N. (1995). Quantification of injury-related EEG signal changes using Itakura distance measure. *Proceedings of the IEEE International Conference on Acoustics Speech and Signal Processing, (ICASSP'95)*, Detroit, MI, USA, 2947-2950.

Lachaux, J.-P. Rodriguez, E., Lutz, A., Martinerie, J. and Varela, F.J. (1999). Measuring Phase Synchrony in Brain Signals. *Human Brain Mapping*, 8, 194-208.

Laufs, H., Krakow, K., Sterzer, P., Eger, E., Beyerle, A., Salek-Haddadi, A. and Kleinschmidt, A. (2003). Electroencephalographic signatures of attentional and cognitive default modes in spontaneous brain activity at rest. *Proceedings of the National Academy of Science USA*, 100, 11053-11058.

Leistner, S., Sander, T., Burghoff, M., Curio, G., Trahms, L. and Mackert, B.-M. (2007). Combined MEG and EEG methodology for non-invasive recording of infraslow activity in the human cortex. *Clinical Neurophysiology*, 118, 2774-2780.

Le Van Quyen, M., Foucher, J., Lachaux, J.-P., Rodriguez, E.O., Lutz, A., Martinerie, J. and Varela, F. J. (2001). Comparison of Hilbert transform and wavelets methods for analysis of neural synchrony. *Journal of Neuroscience Methods*, 111, 83-98.

Levin, K.H. and Lüders, H.O. (2000). *Comprehensive Clinical Neurophysiology*. USA: W.B. Saunders Company.

Li, Y., Cichocki, A., Amari, S.-I., Shishkin, S., Cao, J. and Gu, F. (2003). A sparse representation and its applications in blind source separation. *Neural Information Processing Systems Foundation*, online papers: http://books.nips.cc/papers/files/nips16/NIPS2003_AA31.pdf

Li, Y., Cichocki, A. and Amari, S.-I. (2006). Blind estimation of channel parameters and source components for EEG signals: a sparse factorisation approach. *IEEE Transactions on Neural Networks*, 17,419-431.

Linn, S. (2004). A new conceptual approach to teaching the interpretation of clinical tests. *Journal of Statistics Education*, 12(3).

Liu, X., Qi, H., Wang, S. and Wan, M. (2006). Wavelet-based estimation of EEG coherence during Chinese stroop task. *Computers in Biology and Medicine*, 36, 1303-1315.

Londei, A., Ausilio, A.D., Basso, D., Sestieri, C., Del Gratta, C., Romani, G.L. and Belardinelli, M.O. (2007). Brain network for passive word listening as evaluated with ICA and Granger causality. *Brain Research Bulletin*, 72, 284-292.

Lowe, D. (1993). Novel "topographic" nonlinear feature extraction using radial basis functions for concentration coding in the 'artificial nose'. *Proceedings of the 3rd IEE International Conference on Artificial Neural Networks*, London.

Lowe, D. and Tipping, M.E. (1996). Feed-forward neural networks and topographic mappings for exploratory data analysis. *Neural Computing and Applications*, 4, 83-95.

Lowe, D. and Tipping, M.E. (1997). NeuroScale: Novel topographic feature extraction using RBF networks, in: Mozer, M., Jordan, M. and Petsche, T. (Eds.) *Advances in Neural Information Processing Systems*, vol. 9, Cambridge: MIT Press.

Martinez, W.L. and Martinez, A.R. (2002). *Computational Statistics Handbook with MATLAB®*. USA: Chapman & Hall/CRC.

Max, J. E., Schachar, R. J., Levin, H. S., Ewing-Cobbs, L., Chapman, S. B., Dennis, M., Suanders, A. and Landis, J. (2005). Predictors of attention-deficit/hyperactivity disorder within 6 months after pediatric traumatic brain injury. *Journal of the American Academy of Child Adolescent Psychiatry*, 44, 1032-1040.

Makeig, S., Jung, T.-P., Bell, A. J., Ghahremani, D. and Sejnowski, J. (1997). Blind separation of auditory event-related brain responses into independent components. *Neurobiology*, 94, 10979-10984.

Makeig, S., Westerfield, M., Townsend, J., Jung, T.-P., Courchesne, E. and Sejnowski T.J. (1999a). Functionally independent components of early event-related potentials in a visual spatial attention task. *Philosophical Transactions of the Royal Society of London Series B-Biological Sciences*, 354, 1135-1144.

Makeig, S., Westerfield, M., Jung, T.-P. Covington, J. Townsend, J. Sejnowski, T. J. and Courchesne, E. (1999b). Functionally independent components of the later positive ERP during visual-spatial attention. *The Journal of Neuroscience*, 19, 2665-2680.

Mäkinen, V.T., May, P.J. and Tiitinen, H. (2004). Spectral characterisation of ongoing and auditory event-related brain processes. *Neurology and Clinical Neurophysiology*, 104, 5 pgs.

Malmivuo, J. and Plonsey, R. (1995). *Bioelectromagnetism – Principles and Applications of Bioelectric and Biomagnetic Fields*. New York: Oxford University Press.

Mantini, D., Hild II, K.E., Alleva, G. and Comani, S. (2006). Performance comparison of independent component analysis algorithms for fetal cardiac signal reconstruction: a study on synthetic fMCG data. *Physics in Medicine and Biology*, 51, 1033-1046.

McKeown, M.J., Makeig, S., Brown, G.G., Jung, T.-P., Kindermann, S.S., and Sejnowski, T.J. (1998). Analysis of fMRI by blind separation into independent spatial components. *Human Brain Mapping*, 6, 60-188.

Meinecke, F.C., Zeihe, A., Kurths, J. and Müller, K.-R. (2005). Measuring phase synchronisation of superimposed signals. *Physical Review Letters*, 94, 4 pgs.

di Michela, F., Prichep, L., John, E.R. and Chabot, R.J. (2005). The neurophysiology of attention-deficit/hyperactivity disorder. *International Journal of Psychophysiology*, 58, 81-93.

Milanesi, M., James, C.J., Martini, N., Gemignani, A., Menicucci, D., Ghelarducci B., and Landini, L. (2008). Late positive event-related potentials enhancement through independent component analysis clustering. *Proceedings of the 4th IET International Conference on Advances in Medical, Signal and Information Processing, (MEDSIP'08)*, Sta Margherita Ligure, Italy.

Modarres-Zadeh, M., Xu, X., Jaromczyk, A., and Senders, S. (2005). A neuro-behavioural test and algorithms for screening and evaluating therapy in ADHD. *Proceedings of the 27th IEEE Engineering in Medicine and Biology Annual Conference*, *(EMBS'05)*, Shanghai, China.

Monto, S., Palva, S., Voipio, J. and Palva, J.M. (2008). Very slow EEG fluctuations predict the dynamics of stimulus detection and oscillation amplitudes in humans. *Journal of Neuroscience*, 28, 8268–8272.

Mormann, F., Lehnertz, K., David, P. and Elger, C.E. (2000). Mean phase coherence as a measure for phase synchronisation and its application to the EEG of epilepsy patients. *Physica D*, 144, 358-369.

Mulas, F., Capilla, A., Fernández, S., Etchepareborda, M.C., Campo, P., Maestú, F., Fernández, A., Castellanos, F.X. and Ortiz, T. (2006). Shifting-related brain magnetic activity in attention-deficit/hyperactivity disorder. *Biological Psychiatry*, 59, 373-379.

Mulert, C. and Lemieux, L. (Eds.) (2010). *EEG–fMRI Physiological Basis, Technique and Applications*. Berlin Heidelberg: Springer-Verlag.

Müller, K.-R., Vigario, R., Meinecke, F. and Ziehe, A. (2004). Blind source separation techniques for decomposing event-related brain signals. *International Journal of Bifurcation and Chaos*, 14, 773-791.

Nabney, I.T. (2004). *NETLAB Algorithms for Pattern Recognition*. London: Springer.

Nakagawa, S., Ueno, S. and Imada, T. (1999). Measurements and source estimation of extremely low frequency brain magnetic fields in a short-term memory task by a whole-head neurogradiometer. *IEEE Transactions on Magnetics*, 35, 4130-4132.

Nass, R.D. (2005). Evaluation and assessment issues in the diagnosis of attention deficit hyperactivity disorder. *Seminars in Pediatric Neurology*, 12, 200-216.

Netoff, T.I. and Schiff, S.J. (2002). Decreased neuronal synchronization during experimental seizures. *The Journal of Neuroscience*, 22, 7297-7307.

Neumaier, A. and Schneider, T. (2001). Estimation of parameters and eigenmodes of multivariate autoregressive models. *ACM Transactions on Mathematical Software*, 27, 27-57.

Niedermeyer, E. (2005). Ultrafast EEG activities and their significance. *Clinical EEG and Neuroscience*, 36, 257-262.

Nolte, G., Ziehe, A., Meinecke, F. and Muller, K.-R. (2005). Analysing coupled brain sources: distinguishing true from spurious interaction. *Neural Information Processing Systems Foundation*, online papers: http://books.nips.cc/papers/files/nips18/NIPS2005_0534.pdf

Nunez, P.L. and Silberstein, R.B. (2000). On the relationship of synaptic activity to macroscopic measurements: Does co-registration of EEG with fMRI make sense? *Brain Topography*, 13, 79-96.

Ozdag, M., Yorbik, O., Ulas, U., Hamamcioglu, K. and Vural, O. (2004). Effect of methylphenidate on auditory event related potential in boys with attention deficit hyperactivity disorder. *International Journal of Pediatric Otorhinolaryngology*, 68, 1267-1272.

Paetau, R. (2002). Magnetoencephalography in pediatric neuroimaging. *Developmental Science*, 5, 361-370.

Penttonen, M. and Buzsáki, G. (2003). Natural logarithmic relationship between brain oscillators. *Thalamus and Related Systems*, 2, 145-152

Perchet, C., Revol, O., Fourneret, O., Mauguiere, F. and Garcia-Larrea, L. (2001). Attention shift and anticipatory mechanisms in hyperactive children: An ERP study using Posner paradigm. *Biological Psychiatry*, 50, 44-57.

Petsche, H., Etlinger, S.C. and Filz, O. (1996). Brain electrical mechanism of bilingual speech management: an initial investigation. *Electroencephalography Clinical Neurophysiology*, 86, 145-159.

Pereda, E., Quiroga R. Q. and Bhattacharya, J. (2005). Nonlinear multivariate analysis of neurophysiological signals. *Progress in Neurobiology*, 77, 1-37.

Piccione, F., Giorgi, F. and Tonin, P. (2006). P300-based brain computer interface: Reliability and performance in healthy and paralysed participants. *Clinical Neurophysiology*, 117, 531-537.

Pikovsky, A., Rosenblum, M. and Kurths, J. (2002). *Synchronization: A Universal Concept in Nonlinear Science*. New York: Cambridge University Press.

Polanczyk, G., de Lima, M.S., Horta, B.L., Biederman, J. and Rohde, L.A. (2007). The worldwide prevalence of ADHD: a systematic review and metaregression analysis. *American Journal of Psychiatry*, 164, 942-948.

Polich, J. (2007). Updating P300: An integrative theory of P3a and P3b. *Clinical Neurophysiology*, 118, 2128-2148.

Poupard, L., Sartene, R. and Mathieu, M. (1996). Slow rhythms of the EEG. *Proceedings of the 18th IEEE Engineering in Medicine and Biology Society Annual International Conference*, *(EMBS'96)*, Amsterdam, The Netherlands.

Quian Quiroga, R., Kraskov, A., Kreuz, T., and Grassberger, P. (2002). Performance of different synchronisation measures in real data: a case study on electroencephalographic signals. *Physical Review E*, 65, 14 pgs.

Rama, P., Carlson, S., Kekoni, J. and Hamalainen, H. (1995). A spatial oculomotor memory-task performance produces a task-related slow-shift in human electroencephalography. *Electroencephalography and Clinical Neurophysiology*, 94, 371-380.

Reynolds, C. R. and Kamphaus, R.W. (1992). *Behaviour Assessment System for Children* (BASC), Circle Pines: American Guidance Services (Ags).

Reynolds, C.R. and Kamphaus, R.W. (2004). *BASC: Sistema de Evaluación de la Conducta en Niños y Adolescentes*, (Spanish Adaptation), Madrid: TEA.

Rilling, G., Flandrin, P. and Gonçalvès, P. (2003). On empirical mode decomposition and its algorithms. *Proceedings of the IEEE Workshop on Applications of Signal Processing*, *(EURASIP'03)*, 5 pgs.

Rosenblum, M.G., Pikovsky, A.S. and Kurths, J. (1996). Phase synchronization of chaotic oscillators. *Physical Review Letters*, 76, 1804-1807.

Rothenberger, A. (2009). Brain oscillations forever – neurophysiology in future research of child psychiatric problems. *The Journal of Child Psychology and Psychiatry*, 50, 79-86.

Ruckin, D.S., Canoune, H., Johnson, R. and Ritter, W. (1990). Working memory and preparation elicit different patterns of slow wave event-related brain potentials. *Psychobiology*, 32, 399-410.

Sauseng, P., Klimesch, W., Gruber, W.R., Hanslmayr, S., Freunberger, R., and Doppelmayr, M. (2007). Are event-related potential components generated by phase resetting of brain oscillations? A critical discussion. *Neuroscience*, 146, 1435-1444.

Schack, B. and Krause, W. (1996). Instantaneous coherence as a sensible parameter for considering human information processing. *Proceedings of the 13th IEEE International Conference on Pattern Recognition*, *(ICPR'96)*, Vienna, Austria.

Schelter, B., Winterhalder, M., Eichler, M., Peifer, M., Hellwig, B., Guschlbauer, B., Lucking, C.H., Dahlhaus, R. and Timmer, J. (2006). Testing for directed influences among neural signals using partial directed coherence. *Journal of Neuroscience Methods*, 152, 210-219.

Schneider, T. and Neumaier, A. (2001). ARFIT – A Matlab package for the estimation of parameters and eigenmodes of multivariate autoregressive models. *ACM Transactions on Mathematical Software*, 27, 58-65.

Semrud-Clikeman, M., Pliszka, S. and Lotti, M. (2008). Executive functioning in children with attention-deficit/hyperactivity disorder: combined type with and without a stimulant medication history. *Neuropsychology*, 22, 329–340.

Shen, M., Li, X. and Zhang, X. (2002). The time-varying coherent analysis of medical signals. *Proceedings of the 5th International Conference on Signal Processing, (ICSP'02)*, 1528-1531.

Shlens, J. (2003). A tutorial on principal component analysis: derivation, discussion and singular value decomposition. 16 pgs. http://neurobot.bio.auth.gr/Tutorials/Documents/pca_paper_tut_2.pdf

Shmuel, A. and Leopold, D.A. (2008). Neuronal correlated of spontaneous fluctuations in fMRI signals in monkey visual cortex: implications for functional connectivity at rest. *Human Brain Mapping*, 29, 751-61.

Smallwood, J., Beach, E., Schooler, J.W. and Handy, T.C. (2007). Going AWOL in the brain: Mind wandering reduces cortical analysis of external events. *Journal of Cognitive Neuroscience*, 20, 458-469.

Solanto, M.V. (2002). Dopamine dysfunction in AD/HD: integrating clinical and basic neuroscience research. *Behavioural Brain Research*, 130, 65-71.

Song, L., Gysels, E. and Gordon, E. (2005). Phase synchrony rate for the recognition of motor imagery in brain-computer interface. *Proceedings of the Conference on Advances in Neural Information Processing Systems 18, (NIPS'05)*, Vancouver, Canada.

Sonuga-Barke, E.J.S. (2003). The dual pathway model of AD/HD: An elaboration of neuro-developmental characteristics. *Neuroscience and Behavioural Reviews*, 27, 593-604.

Sonuga-Barke E.J.S. and Castellanos, F.X. (2007). Spontaneous attentional fluctuations in impaired states and pathological conditions: a neurobiological hypothesis. *Neuroscience and Biobehavioral Reviews*, 31, 977-986.

Spenser, K.M., Nestor, P.G., Niznikiewicz, M.A., Salisbury, D.F., Shenton, M.E. and McCarley, R.W. (2003). Abnormal neural synchrony in schizophrenia. *Journal of Neuroscience*, 23, 7404-7411.

Srinivasan, R. (1999). Methods to improve the spatial resolution of EEG. *International Journal of Bioelectromagnetism*, 1, 102-111.

Steriade, M., Nunez A. and Amzica, F. (1993). A novel slow (<1 Hz) oscillation of neocortical neurons in vivo: depolarizing and hyperpolarizing components. *Neuroscience*, 13, 3252-3265.

Stone, J.V. (2004). *Independent Component Analysis: A Tutorial Introduction*. USA: MIT Press.

Stone, J.V. (2005). Independent Component Analysis. In *The Encyclopaedia of Statistics in Behavioral Science*. BS Everitt and DC Howell (Eds.), Chichester: Wiley, 2, 907-912.

Sweeney-Reed, C. M. (2007). *Analysis of Synchronisation in the Electroencephalogram*. Doctor of Philosophy Thesis, Cybernetics, School of Systems Engineering, University of Reading, 2007.

Takens, F. (1981). Dynamical systems and turbulence. In *Lecture Notes in Mathematics*. D.A. Rand, and L.S. Young, (Eds.), Berlin: Springer, 898, 366-381.

Tallon-Baudry, C., Bertrand, O. and Fischer, C. (2001). Oscillatory synchrony between human extrastriate areas during visual short-term memory maintenance. *The Journal of Neuroscience*. 21, RC177:1-5.

Taner, M.T., Koehler, F. and Sheriff, R.E. (1979). Complex seismic trace analysis. *Geophysics*. 44, 1041:1063.

Tass, P., Rosenblum, M.G., Weule, J., Kurths, J., Pikovsky, A., Volkmann, J., Schnitzler, A. and Freund, H.-J. (1998). Detection of *n*:*m* phase locking from noisy data: Application to magneto-encephalography. *Physical Review Letters*, 81, 3291-3294.

Taylor, E.A. and Sonuga-Barke, E.J.S. (2008). Disorders of Attention and Activity. In: *Rutter's Child & Adolescent Psychiatry*. Rutter, M., Bishop, D., Pine, D., Scott, S., Stevenson, J.S., Taylor, E.A., Thapar, A., (Eds.), 5th Edition. UK: Wiley-Blackwell, 521-542.

Tcheslavski, G.V. (2005). *Coherence and Phase Synchrony Analysis of Electroencephalogram*, Dr. of Philosophy Thesis, Virginia Polytechnic Institute and State University, Blacksburg Virginia.

Tcheslavski, G.V. and (Louis) Beex, A.A. (2006). Phase synchrony and coherence analysis of EEG as tools to discriminate between children with and without attention deficit disorder. *Biomedical Signal Processing and Control*, 1, 151-161.

The MathWorks Incorporation (1984-2007). *Cluster Analysis* (Statistics Toolbox™), Documentation on Hierarchical Clustering.

Torkkola, K. (1999). Blind separation for audio signals: Are we there yet? *Proceedings of the International Workshop on Independent Component Analysis and Blind Separation of Signals*, *(ICA'99)*, Aussois, France.

Uddin, L.Q., Clare Kelly, A.M., Biswal, B., Margulies, D.S., Shehzad, Z., Shawc, D., Ghaffari, M., Rotrosen, J., Adler, L.A., Castellanos, F.X. and Milham, M.P. (2008). Network homogeneity reveals decreased integrity of default-mode network in ADHD. *Journal of Neuroscience Methods*, 169, 249-254.

Ulmer, S. and Jansen, O. (Eds.) (2010). *fMRI Basics and Clinical Applications*. Berlin Heidelberg: Springer-Verlag.

Varela, F., Lachaux, J.-P., Rodriguez, E. and Martinerie, J. (2001). The brainweb: Phase synchronisation and large-scale integration. *Nature Reviews: Neuroscience*, 2, 228-239.

Vanhatalo, S., Palva, J.M., Holmes, M.D., Miller, J.W., Voipio, J. and Kaila, K. (2004). Infraslow oscillations modulate excitability and interictal epileptic activity in the human cortex during sleep. *Neuroscience*, 101, 5053-5057.

Vanhatalo, S., Voipio, J. and Kaila, K. (2005). Full-band EEG (FbEEG): An emerging standard in electroencephalography. *International Federation of Clinical Neurophysiology*, 116, 1-8.

Vigario, R., Jousmaki, V., Hamalainen, M., Hari, R. and Oja, E. (1998). Independent component approach for identification of artifacts in magnetoencephalographic recordings. In *Advances in Neural Information Processing Systems*. MIT Press, 229-235.

Vigario, R., Sarela, J., Jousmaki, V., Hamalainen, M., and Oja, E. (2000). Independent component approach to the analysis of EEG and MEG recordings. *IEEE Transactions on Biomedical Engineering*, 47, 589-593.

Wang, S. and James, C.J. (2007). Extracting rhythmic brain activity for brain-computer interfacing through constrained independent component analysis. *Computational Intelligence and Neuroscience*, (ID41468), 9 pgs.

Wang, Y., Hang, B., Gao, X. and Gao, S. (2006). Phase synchrony measurement in motor cortex for classifying single-trial EEG during motor imagery. *Proceedings of the 28th IEEE Engineering in Medicine and Biology Annual International Conference*, *(EMBS'06)*, New York, USA.

Wechsler, D. (2005). WISC - IV - *Escala de inteligencia de Wechsler para niños* (Spanish Adaptation). Madrid: TEA.

Weiss, S. and Mueller, H. (2003). The contribution of EEG coherence to the investigation of language. *Brain Language*, 85, 325-343.

Welch, P.D. (1967). The use of Fast Fourier Transform for the estimation of power spectra: A method based on time averaging over short, modified periodograms. *IEEE Transactions on Audio Electroacoustics*, 15, 70-73.

White, K.R. (1982). The relation between socioeconomic status and academic achievement. *Psychological Bulletin*, 91, 461-481.

Whiting, S., Ning, T. and Bronzino, J.D. (1989). Data length effects on the coherence estimate of EEG. *Proceedings of the 15th IEEE Engineering in Medicine and Biology Annual International Conference, (EMBS'89)*, Boston, USA.

Wienbruch, C., Paul, I., Bauer S. and Kivelitz, H. (2005). The influence of methylphenidate on the power spectrum of ADHD children – a MEG study. *BMC Psychiatry,* 5:29, 16 pgs.

Winterhalder, M., Schelter, B., Hesse, W., Schwab, K., Leistritz, L., Klan, D., Bauer, R., Timmer J., and Witte, H. (2005). Comparison of linear signal processing techniques to infer directed interactions in multivariate neural systems. *Signal Processing*, 85, 2137-2160.

Wodka, E.L., Mahone, E.M., Blankner, J.G., Gidley Larson, J.C., Fotedar, S., Denckla, M., Mostofsky, S.H. (2007). Evidence that response inhibition is a primary deficit in ADHD. *Journal of Clinical and Experimental Neuropsychology*, 29, 345-356.

Woon, W.L. and Lowe, D. (2004). Can we learn anything from single-channel unaveraged MEG data? *Neural Computing and Applications*, 13, 360-368.

Wornell, G. W. (1993). Wavelet-based representations for the 1/*f* family of fractal processes. *Proceedings of the IEEE*, 81, 1428-1450.

Yamaguchi, C. (2003). Fourier and wavelet analyses of normal and epileptic electroencephalogram (EEG). *Proceedings of the 1st International IEEE EMBS Conference on Neural Engineering*, Capri Island, Italy

Ye, S. and Hu, J. (2005). Ill-posed MEG inverse solution based on deterministic regularization theory framework. *Proceedings of the International Conference on Neural Networks and Brain*, *(ICNN&B'05)*, Beijing, China, pp. 144-146.

Yordanova, J., Devrim, M., Kolev, V., Ademoglu, A. and Demiralp, T. (2000). Muliple time-frequency components account for the complex functional reactivity of P300. *Cognitive Neuorscience*, 5, 1097-1103.

Yordanova, J., Heinrich, H., Kolev., V. and Rothenberger, A. (2006). Increased event-related theta activity as a psychological marker of comorbidity in children with tics and attention-deficit/hyperactivity disorder. *NeuroImage*, 32, 940-955.

Young, H., Baum, R., Cremerius, U., Herholz, K., Hoekstra, O., Lammertsma, A.A., Pruim, J., Price, P. and on behalf of the European Organization for Research and Treatment of Cancer (EORTC) PET Study Group, (1999). Measurement of clinical and subclinical tumour response using [18F]-fluorodeoxyglucose and positron emission tomography: review and 1999 EORTC recommendations. *European Journal of Cancer*, 35, 1773–1782.

Zarzoso, V. and Comon, P. (2007). Comparative speed analysis of FastICA. *Proceedings of the 7th International Conference on Independent Component Analysis and Signal Separation*, *(ICA'07)*, London, UK, pp. 293-300.

Ziehe A. and Müller, K.-R. (1998). TDSEP – an efficient algorithm for blind separation using time structure. *Proceedings of the International Conference on Artificial Neural Networks*, *(ICANN'98)*, pp. 675-680.

Zhan, Y., Halliday, D., Jiang, P., Liu, X. and Feng, J. (2006). Detecting time-dependent coherence between non-stationary electrophysiological signals – a combined statistical and time-frequency approach. *Journal of Neuroscience Methods*, 156, 322-332.

Zylowska, L., Ackerman, D.L., Yang, M.H., Futrell, J.L., Horton, N.L., Sigi Hale, T., Pataki, C. and Smalley, S.L. (2000). Mindfulness meditation training in adults and adolescents with ADHD: a feasibility study. *Journal of Attention Disorders*, 11, 737-46.